Retrospective Registration of Tomographic Brain Images

J.B. Antoine Maintz

Colofon

This book was typeset by the author using LaTeX 2_ε. The main body of the text was set using a 10 points Bookman font. Float captions are rendered in Avant-garde. Both fonts are © Adobe Systems Incorporated. Images were included formatted as encapsulated Postscript (™ Adobe Systems Incorporated). The final output was converted to Postscript and transfered to film for printing.

Cover image: *Suimen* (Water Surface) by Jun Oi.
The image is an autostereogram, and is therefore a beautiful example of registration, with the two images to register hidden in one picture. Permission for reproduction has been granted by the artist, and by Viz Communications Inc.
© 1994 Jun Oi. This image was originally published in *Super Stereogram* by Cadence Books, San Francisco.

ISBN 90–393–1227–3

Retrospective Registration of Tomographic Brain Images

Retrospectieve Registratie
van Tomografische Hersenbeelden

(met een samenvatting in het Nederlands)

PROEFSCHRIFT
TER VERKRIJGING VAN DE GRAAD VAN DOCTOR AAN DE UNIVERSITEIT UTRECHT
OP GEZAG VAN DE RECTOR MAGNIFICUS, PROF. DR J.A. VAN GINKEL,
INGEVOLGE HET BESLUIT VAN HET COLLEGE VAN DECANEN IN HET OPENBAAR TE
VERDEDIGEN OP DINSDAG 10 DECEMBER 1996 DES MIDDAGS TE 4:15

DOOR

Josephus Bernard Antoine Maintz

Geboren op 18 juni 1969 te Doetinchem

Promotor: Prof. dr ir M.A. Viergever
Faculteit der Geneeskunde
Universiteit Utrecht
Copromotor: Dr P.A. van den Elsen
Faculteit der Wiskunde en Informatica
Universiteit Utrecht

This thesis was published with financial support from the Corporate Technology group of Philips Medical Systems Nederland B.V., the Nationaal Epilepsie Fonds – De Macht van het Kleine, Amersham Cygne, Picker International Inc./P.I. Benelux, and ADAC.

This work was carried out in the framework of the research program “3D Computer Vision”, supported by the Netherlands ministries of Education & Science and Economics Affairs through a SPIN grant, and by the industrial companies Philips Medical Systems, KEMA, Shell Research, and ADAC.

Contents

On the "authentic" historic perspective:
Stravinsky changed Mozart.
Esa-Pekka Salonen.

Chapter 1

Introduction and Summary

The development of medical imaging apparatus has truly soared in the past decades. Nowadays, the clinician can employ a vast array of specialized imaging techniques supporting the diagnostic and treatment track. For various reasons, more than one image is often acquired of the same anatomy, either *monomodally* or *multimodally*. In the monomodal case, only one imaging apparatus is used. Several monomodal images of the same anatomy are, *e.g.*, used in growth monitoring, in comparison of rest and stress conditions, in comparison of ictal and interictal conditions, and in vascular imaging. When there is a need to surpass the limits set by a single imaging device, multimodal images can be acquired. Multimodal imagery can be used, *e.g.*, to extend knowledge on anatomy (by combining anatomical modalities such as CT[1] and MRI[2]), or to link physiological and anatomical information (by combining an anatomical modality with a functional modality such as SPECT[3] or PET[4]).

It is by no means trivial to use all of the available image information to its maximum extent. This thesis addresses the highly specialized research area of integration of different images of the same anatomy. More exactly, we focus on the problem of *registration* of the image data involved, *i.e.*, finding the correct geometrical transformation that brings one image in precise spatial correspondence with another image. Registration is a necessary pre-processing step in many instances where information from several images is to be combined. For example, an image of an epileptic brain, constructed by subtracting functional images of

[1] Computed tomography.
[2] Magnetic resonance imaging.
[3] Single photon emission computed tomography.
[4] Positron emission tomography.

the brain in ictal and interictal condition, is only meaningful if the two original images involved are properly registered. Another example is the projection of meaningful visual information into the ocular of an operating microscope during surgery, *e.g.*, indicative of the surgical target and of vascular structures that are paramount not to be damaged. Needless to say, the displayed information must be accurately registered with the anatomy visible through the microscope.

The state-of-the-art concerning registration algorithms is heavily application dependent. In some applications, a clinically acceptable stage has apparently been reached, but in others, *e.g.*, those that require elastic transformations to be found based on sparse or degraded spatial information, the stage is still that of debating the existence and uniqueness of a solution. In the area concering the validation of registration algorithms, very little research has so far been conducted, which can be ascribed accredited to the fact that clinical registrations come without a "gold standard" for reference. The purpose of this thesis is twofold: first, to survey recent methodologies as concerns medical registration and their verification. Second, to develop and investigate new methods specifically designed for registration of tomographic images of the brain.

In chapter 2 we survey existing literature on medical image registration, and classify a large number of recent papers according to a scheme based on nine criteria. A notable dichotomy of existing registration methods is *extrinsic* versus *intrinsic*, *i.e.*, the division of methods according to the nature of the information used: either patient related (intrinsic), or based on foreign objects introduced into the image (extrinsic). It can be observed that the major application areas of registration currently are neurosurgery, radiation therapy, and orthopedic surgery.

The following chapters detail parts of our research on registration of human brain images carried out in the past four years. In chapter 3 we present a method to register CT and MR images based on the *ridgeness* of the skull bone structure. CT and MR registration is useful especially in the areas of neurosurgery and radiotherapy planning. The concept of a *ridge* is first transfered to image structure in an intuitive manner, then in a more formal mathematical way. *Ridgeness* is defined in terms of geometric invariants, the concept of which will be introduced. To tackle the problem of the ill-posed differentiation of sampled images, we briefly outline the concept of *scale space* with a focus on computing derivatives by means of Gaussian convolution. A number of ridgeness operators is formulated, and they are examined as concerns their practical behavior. Finally, CT-MR registration is performed by optimizing the cross-correlation of extracted ridgeness images. Experiments are carried out on two pairs of CT and MR images, and the registration results are shown to be

accurate by visual inspection and by visual comparison to a registration based on skin markers attached to the patients.

Chapter 4 expands on the methods outlined in the previous chapter. Next to the ridge operators, a number of operators extracting edges and various other geometrical entities are defined. Their performance as relating to CT-MR registration is examined extensively by experimentation. The best registration results (as defined by visual inspection, comparison to marker-based registration, and robustness) were obtained using the gradient magnitude edgeness extracting operator. The operator itself performed best at a low scale (in the order of a voxel width), which is indicative of the fact that local differential operations may perform just as well as differentiation using expensive Gaussian convolution. In chapter 6, we therefore make use of a morphological gradient operator.

In chapter 5 we focus on a specific monomodal problem: the registration of HMPAO SPECT images. This registration problem features especially in computing SPECT subtraction images, for instance the difference images of rest and stress conditions. We address more than the registration problem, and include image grey scaling (an issue which must be addressed when subtracting two SPECT images), and address visualization issues. We aim at detailing all of the image technology necessary in the post-acquisition clinical track using registered images. The registration problem addressed in this chapter makes no use of the mathematics developed in the previous chapters: since the images to be registered are very much alike, the grey values themselves can be used adequately to find a registration. Good registration results were obtained, as validated by visual inspection and by reference to marker-based registration. The latter registration was based on markers designed specifically for this project: they cannot be detected in the clinically relevant images, and therefore do not disturb the clinical track of events, nor influence our grey value based registrations.

In the final chapter (6), we turn back to multimodal applications, in a more general manner than before: besides CT and MR images, SPECT and PET images are included. The registration of MR to SPECT or PET images is especially useful for providing an anatomical frame of reference (obtained from the MR data) to the functional data. We make use of operators defined in the field of *mathematical morphology* to extract anatomically related structures from two multimodal images, and use those structures as input for a cross-correlation optimizing algorithm. By using morphology, we are able to “focus” our operators on typically relevant anatomy such as the skin or cortex. We apply the developed methods to clinically acquired images, and validate the results by visual inspection, by comparison to registration obtained by invasive and skin markers, and by

cross-comparison to previously developed methods. In the case of CT to MR registration a cadaver study is used for additional verification. The results are promising, although not yet suitable for automated routine clinical applications in the registrations that involve functional images. In the studies where clinically relevant CT and MR images were used, the results are good and reliable.

To write a reference, you must have the work you're referring to in front of you. Do not rely on your memory. Do not rely on your memory. Just in case the idea ever occured to you, do not rely on your memory.
Mary-claire van Leunen (1992), *A handbook for scholars.*

Chapter 2

A Survey of Medical Image Registration

Abstract

The purpose of this chapter is to present a survey of recent publications concerning medical image registration techniques. These publications will be classified according to a model based on nine salient criteria, the main dichotomy of which is extrinsic *versus* intrinsic *methods The statistics of the classification show definite trends in the evolving registration techniques, which will be discussed. At this moment, the bulk of interesting intrinsic methods is either based on segmented points or surfaces, or on techniques endeavoring to use the full information content of the images involved.*

2.1 Introduction

Within the current clinical setting, medical imaging is a vital component of a large number of applications. Such applications occur throughout the clinical track of events; not only within clinical diagnostis settings, but prominently so in the area of planning, consummation, and evaluation of surgical and radiotherapeutical procedures. The imaging modalities employed can be divided into two global categories: *anatomical* and *functional*. Anatomical modalities, *i.e.*, depicting primarily morphology, include X-ray, CT (computed tomography[1]), MRI (magnetic resonance imaging[2]), US (ultrasound[3]), portal images, and (video) sequences obtained by various catheter "scopes", *e.g.*, by laparoscopy or laryngoscopy. Some prominent derivative techniques are so detached from the original modalities that they appear under a separate name, *e.g.*, MRA (magnetic resonance angiography), DSA (digital subtraction angiography, derived from X-ray), CTA (computed tomography angiography), and *Doppler* (derived from US, referring to the Doppler effect measured). Functional modalities, *i.e.*, depicting primarily information on the metabolism of the underlying anatomy, include (planar) scintigraphy, SPECT (single photon emission computed tomography[4]), PET (positron emission tomography.[5]), which together make up the *nuclear medicine* imaging modalities, and fMRI (functional MRI). With a little imagination, spatially sparse techniques like, EEG (electro encephalography), and MEG (magneto encephalography) can also be named functional *imaging* techniques. Many more functional modalities can be named, but these are either little used, or still in the pre-clinical research stage, *e.g.*, pMRI (perfusion MRI), fCT (functional CT), EIT (electrical impedance tomography), and MRE (magnetic resonance elastography).

Since information gained from two images acquired in the clinical track of events is usually of a complementary nature, proper *integration* of useful data obtained from the separate images is often desired. A first step in this integration process is to bring the modalities involved into spatial alignment, a procedure referred to as *registration*. After registration, a *fusion* step is required for the integrated display of the data involved. Unfortunately, the terms *registration* and *fusion*, as well as *matching*, *integration*, *correlation*, and others, appear polysemously in literature, either referring to a single step or to the whole of the modality inte-

[1] Also formerly and popularly CAT, computed axial tomography.
[2] Also referred to as NMR, nuclear magnetic resonance, spin imaging, and various other names.
[3] Also echo(graphy).
[4] Also SPET, single photon emission tomography.
[5] SPECT and PET together are sometimes referred to as ECAT (emission computerized axial tomography).

gration process. In this chapter, only the definitions of registration and fusion as defined above will be used.

An eminent example of the use of registering different modalities can be found in the area of epilepsy surgery. Patients may undergo various MR, CT, and DSA studies for anatomical reference; ictal and interictal SPECT studies; MEG and extra and/or intra-cranial (subdural or depth) EEG, as well as ^{18}FDG and/or ^{11}C-Flumazenil PET studies. Registration of the images from practically any combination will benefit the surgeon. A second example concerns radiotherapy treatment, where both CT and MR can be employed. The former is needed to accurately compute the radiation dose, while the latter is usually better suited for delineation of tumor tissue.

Besides multimodality registration, important application areas exist in mono-modality registration. Examples include treatment verification by comparison of pre- and post-intervention images, comparison of ictal and inter-ictal (during and between seizures) SPECT images, and growth monitoring, *e.g.*, using time series of MR scans on tumors, or X-ray time series on specific bones. Because of the high degree of similarity between these images, solving the registration is usually an order of magnitude easier than in the multimodality applications.

This chapter aims to provide a survey of recent literature concerning medical image registration. Because of the sheer volume of available papers, the material presented is by necessity heavily condensed, and –except for a few interesting and "classic" cases– no papers written before 1993 are referred to. Concerning publications pre-dating 1993, we refer the reader to review papers such as van den Elsen, Pol & Viergever (1993) and Maurer, McCrory, & Fitzpatrick (1993). No complete review papers of a later date exist to our knowledge, except for the field of computer aided surgery[6]. To narrow the field of available publications in such a way does not, however, impede us in reaching our primary goal, which is to paint a comprehensive picture of current medical image registration methods.

2.2 Classification of registration methods

The classification of registration methods used in this chapter is based on the criteria formulated by van den Elsen, Pol & and Viergever (1993). A version considerably augmented and detailed is presented. Nine basic criteria are used,

[6](Lavallée 1996)

each of which is again subdivided on one or two levels. The nine criteria and primary subdivisions are:

- **I.** Dimensionality
- **II.** Nature of registration basis
  - **a.** Extrinsic
  - **b.** Intrinsic
  - **c.** Non-image based
- **III.** Nature of transformation
  - **a.** Rigid
  - **b.** Affine
  - **c.** Projective
  - **d.** Curved
- **IV.** Domain of transformation
- **V.** Interaction
- **VI.** Optimization procedure
- **VII.** Modalities involved
  - **a.** Monomodal
  - **b.** Multimodal
  - **c.** Modality to model
  - **d.** Patient to modality
- **VIII.** Subject
  - **a.** Intrasubject
  - **b.** Intersubject
  - **c.** Atlas
- **IX.** Object

A registration procedure can always be decomposed into three major pillars: the *problem statement*, the *registration paradigm*, and the *optimization procedure*. The problem statement and the choice of paradigm and optimization procedure together provide a unique classification according to the nine criteria mentioned. Although pillars and criteria are heavily intertwined and have many cross-influences, it can be said that the problem statement determines the classification according to criteria **VII**, **VIII**, and **IX**, and has a direct bearing on the criteria **I** and **III**. The paradigm influences the criteria **II**, **III**, **IV**, and **V** most directly, while the optimization procedure influences criterion **V** and controls **VI**. It is often helpful to remember the three pillars are independent, since many papers do not describe them as such, often presenting problem statement, paradigm, and optimization procedure in a compounded way.

In the following sections, we will discuss the separate criteria in more detail.

2.3 Dimensionality

I. Dimensionality

a. Spatial dimensions only:

1. 2D/2D
2. 2D/3D
3. 3D/3D

b. Time series (more than two images), with spatial dimensions:

1. 2D/2D
2. 2D/3D
3. 3D/3D

2.3.1 Spatial registration methods

The main division here is whether all dimensions are spatial, or that time is an added dimension. In either case, the problem can be further categorized depending on the number of spatial dimensions involved. Most current papers focus on the *3D/3D* registration of two images (no time involved). *3D/3D* registration normally applies to the registration of two tomographic datasets, or the registration of a single tomographic image to any spatially defined information, *e.g.*, a vector obtained from EEG data. *2D/2D* registration may apply to separate slices from tomographic data, or intrinsically 2D images like portal images. Compared to *3D/3D* registration, *2D/2D* registration is less complex by an order of magnitude both where the number of parameters and the volume of the data are concerned, so obtaining a registration is in many cases easier and faster than in the *3D/3D* case. We reserve *2D/3D* registration for the direct alignment of spatial data to projective data, (*e.g.*, a pre-operative CT image to an intra-operative X-ray image), or the alignment a single tomographic slice to spatial data. Some applications register multiple 2D projection images to a 3D image, but since a usual preprocessing step is to construct a 3D image from the 2D projection images, such applications are best categorized as *3D/3D* applications. Since most *2D/3D* applications concern intra-operative procedures within the operating theater, they are heavily time-constrained and consequently have a strong focus on speed issues connected to the computation of the paradigm and the optimization. The majority of applications outside the operating theater and radiotherapy setting allow for off-line registration, so speed issues need only be addressed as constrained by clinical routine.

2.3.2 Registration of time series

Time series of images are acquired for various reasons, such as monitoring of bone growth in children (long time interval), monitoring of tumor growth (medium interval), post-operative monitoring of healing (short interval), or observing the passing of an injected bolus trough a vessel tree (ultra-short interval). If two images need to be compared, registration will be necessary except in instances of ultra-short time series, where the patient does not leave the scanner between the acquisition of two images. The same observations as for spatial-only registrations apply.

2.4 Nature of registration basis

II. Nature of registration basis

- **a.** Extrinsic
  1. Invasive
     - **A.** Stereotactic frame
     - **B.** Fiducials (screw markers)
  2. Non-invasive
     - **A.** Mould, frame, dental adapter, *etc.*
     - **B.** Fiducials (skin markers)
- **b.** Intrinsic
  1. Landmark based
     - **A.** Anatomical
     - **B.** Geometrical
  2. Segmentation based
     - **A.** Rigid models (points, curves, surfaces)
     - **B.** Deformable models (snakes, nets)
  3. Voxel property based
     - **A.** Reduction to scalars/vectors (moments, principal axes)
     - **B.** Using full image content
- **c.** Non-image based (calibrated coordinate systems)

2.4.1 Extrinsic registration methods

Image based registration can be divided into *extrinsic*, *i.e.*, based on foreign objects introduced into the imaged space, and *intrinsic* methods, *i.e.*, based on the image information as generated by the patient.

Extrinsic methods rely on artificial objects attached to the patient, objects which are designed to be well visible and accurately detectable in all of the pertinent modalities. As such, the registration of the acquired images is comparatively easy, fast, can usually be automated, and, since the registration parameters can often be computed explicitly, has no need for complex optimization algorithms. The main drawbacks of extrinsic registration are the prospective character, *i.e.*, provisions must be made in the pre-acquisition phase, and the often invasive character of the marker objects. Non-invasive markers can be used, but as a rule are less accurate. A commonly used fiducial object is a *stereotactic frame*[7] screwed rigidly to the patient's outer skull table, a device which until recently provided the best "gold standard" for registration accuracy. Such frames are used for localization and guidance purposes in neurosurgery. Since neurosurgery is one of the main application areas of registration, the use of a stereotactic frame in the registration task does not add an additional invasive strain to the patient. However, the mounting of a frame for the sole purpose of registration is not permissible. Sometimes other invasive objects are used, such as screw-mounted markers[8], but usually non-invasive marking devices are reverted to. Most popular amongst these are markers glued to the skin[9], but larger devices that can be fitted snugly to the patient, like individualized foam moulds,

[7](Lunsford 1988, Vandermeulen 1991, Lemieux, Kitchen, Hughes & Thomas 1994, Lemieux & Jagoe 1994, Strother, Anderson, Xu, Liow, Bonar & Rottenberg 1994, Hemler, van den Elsen, Sumanaweera, Napel, Drace & Adler 1995, Vandermeulen, Collignon, Michiels, Bosmans, Suetens, Marchal, Timmens, van den Elsen, Viergever, Ehricke, Hentschel & Graumann 1995, Peters, Davey, Munger, Comeau, Evans & Olivier 1996)

[8](Gall & Verhey 1993, Leung Lam, ten Haken, McShan & Thornton 1993, Maurer, McCrory & Fitzpatrick 1993, Li, Pelizzari & Chen 1994, Maurer, Aboutanos, Dawant, Gadamsetty, Margolin, Maciunas & Fitzpatrick 1994, Maurer, Fitzpatrick, Galloway, Wang, Maciunas & Allen 1995, Maurer, Aboutanos, Dawant, Margolin, Maciunas & Fitzpatrick 1995, Simon, O'Toole, Blackwell, Morgan, DiGioia & Kanade 1995, Ellis, Toksvig-Larsen, Marcacci, Caramella & Fadda 1996)

[9](Evans, Marrett, Torrescorzo, Ku & Collins 1991, Maguire, Noz, Rusinek, Jaeger, Kramer, Sanger & Smith 1991, Malison, Miller, Greene, McCarthy, Charney & Innis 1993, Wang, Fitzpatrick, Maurer & Maciunas 1994, Wahl, Quint, Cieslak, Aisen, Koeppe & Meyer 1993, Bucholz, Smith, Henderson & McDurmont 1994, Li, Pelizzari & Chen 1994, Edwards, Hawkes, Hill, Jewell, Spink, Strong & Gleeson 1995, Edwards, Hill, Hawkes, Spink, Colchester, Strong & Gleeson 1995, Leslie, Borys, McDonald, Dupont & Peterdy 1995, Stapleton, Caldwell, Ehrlich, Leonhardt, Black & Yaffe 1995, Wang, Fitzpatrick & Maurer 1995, Fuchs, Wischmann, Neumann, Weese, Zylka, Sabczynski, Kuhn, Buzug, Schmitz & Gieles 1996)

head holder frames, and dental adapters have also been used, although they are little reported on in recent literature[10].

Since extrinsic methods by definition cannot include patient related image information, the nature of the registration transformation is often restricted to be rigid (translations and rotations only). Furthermore, if they are to be used with images of low (spatial) information content such as EEG or MEG, a calibrated video image or spatial measurements are often necessary to provide spatial information for basing the registration on. Because of the rigid-transformation constraint, and various practical considerations, use of extrinsic 3D/3D methods is largely limited to brain and orthopedic[11] imaging, although markers can often be used in projective (2D) imaging of any body area. Non-rigid transformations can in some cases be obtained using markers, *e.g.*, in studies of animal heart motion, where markers can be implanted into the cardiac wall.

2.4.2 Intrinsic registration methods

Intrinsic methods rely on patient generated image content only. Registration can be based on a limited set of identified salient points *(landmarks)*, on the alignment of segmented binary structures *(segmentation based)*, most commonly object surfaces, or directly onto measures computed from the image grey values *(voxel property based)*.

2.4.2.1 Landmark based registration methods

Landmarks can be *anatomical*, *i.e.*, salient and accurately locatable points of the morphology of the visible anatomy, usually identified interactively by the user[12], or *geometrical*, *i.e.*, points at the locus of the optimum of some geometric property, *e.g.*, local curvature extrema, corners, *etc*, generally localized in

[10](Greitz, Bergström, Boëthius, Kingsley & Ribbe 1980, Laitinen, Liliequist, Fagerlund & Eriksson 1985, Schad, Boesecke, Schlegel, Hartmann, Sturm, Strauss & Lorenz 1987, Hawkes, Hill & Bracey 1992, Evans, Marrett, Collins & Peters 1989, Evans et al. 1991)

[11](Simon, O'Toole, Blackwell, Morgan, DiGioia & Kanade 1995, Ellis et al. 1996)

[12](Evans et al. 1989, Evans et al. 1991, Hill, Hawkes, Crossman, Gleeson, Cox, Bracey, Strong & Graves 1991, Hill, Hawkes & Hardingham 1991, Maguire et al. 1991, Zubal, Zhang & Duncan 1991, Henri, Cukiert, Collins, Olivier & Peters 1992, Bijhold 1993, Ding, Shalev & Gluchev 1993, Fright & Linney 1993, Gluhchev & Shalev 1993, Hill, Hawkes, Hussain, Green, Ruff & Robinson 1993, Morris, Muswick, Ellert, Steagall, Goyer & Semple 1993, Neelin, Crossman, Hawkes, Ma & Evans 1993, Wahl et al. 1993, Ge, Fitzpatrick, Votaw, Gadamsetty, Maciunas, Kessler & Margolin 1994, Harmon, Vayda, Erlandson, Taren & Ross 1994, Moseley & Munro 1994, Pietrzyk, Herholz, Fink, Jacobs, Mielke, Slansky, Würker & Heis 1994, Strother et al. 1994, Edwards, Hawkes, Hill, Jewell, Spink,

an automatic fashion[13]. Technically, the identification of landmark points is a segmentation procedure, but we reserve the classification *segmentation based* registration for methods relating to segmentation of structures of higher order, *i.e.*, curves, surfaces, and volumes. Landmark based registration is versatile in the sense that it –at least in theory– can be applied to any image, no matter what the object or subject is. Landmark based methods are mostly used to find rigid or affine transformations. If the sets of points are large enough, they can theoretically be used for more complex transformations. Anatomical landmarks are also often used in combination with an entirely different registration basis[14]: methods that rely on optimization of a parameter space that is not quasi-convex are prone to sometimes get stuck in local optima, possibly resulting in a large mismatch. By constraining the search space according to anatomical landmarks, such mismatches are unlikely to occur. Moreover, the search procedure can be sped up considerably. A drawback is that user interaction is usually required for the identification of the landmarks.

In landmark based registration, the set of identified points is sparse compared to the original image content, which makes for relatively fast optimization procedures. Such algorithms optimize measures such as the average distance (L_2 norm) between each landmark and its closest counterpart (the *Procrustean* metric), or iterated minimal landmark distances. For the optimization of the latter measure the *Iterative closest point* (ICP) algorithm[15] and derived methods are popular. Its popularity can be accredited to its versatility –it can be used for point sets, and implicitly and explicitly defined curves, surfaces and volumes–, computational speed, and ease of implementation. The Procrustean optimum can sometimes be computed, using *e.g.*, Arun's method (1987), but is more commonly searched for using general optimization techniques. Such

Strong & Gleeson 1995, Edwards, Hill, Hawkes, Spink, Colchester, Strong & Gleeson 1995, Ge, Fitzpatrick, Kessler, Jeske-Janicka & Margolin 1995, Hamadeh, Sautot & Cinquin 1995, Hamadeh, Sautot, Lavallée & Cinquin 1995, Leslie et al. 1995, Meyer, Leichtman, Brunberg, Wahl & Quint 1995, McParland & Kumaradas 1995, Soltys, Beard, Carrasco, Mukherji & Rosenman 1995, Savi, Gilardi, Rizzo, Pepi, Landoni, Rossetti, Lucignani, Bartorelli & Fazio 1995, Stapleton et al. 1995, Vandermeulen et al. 1995, Zubal, Spencer, Khurseed Imam, Smith, Wisniewski & Hoffer 1995, Christensen, Kane, Marsh & Vannier 1996, Evans, Strong, Colchester, Zhao & Holton-Tainter 1996, Evans, Collins, Neelin & Marrett 1996, Erbe, Kriete, Jödicke, Deinsberger & Böker 1996, Fang, Raghavan & Richtsmeier 1996, Peters et al. 1996, Rubinstein, Karger, Pietrzyk, Siegal, Gomori & Chisin 1996)

[13](He, Maublant, Cauvin & Veyre 1991, Fontana, Crovetto, Bergognoni & Casali 1993, Ault & Siegel 1994, Eilertsen, Skretting & Tennvassas 1994, Thirion 1994, Ault & Siegel 1995, Uenohara & Kanade 1995, Amit & Kong 1996, Chua & Jarvis 1996, Thirion 1996*a*)

[14](Evans et al. 1989, Evans et al. 1991, Wahl et al. 1993, Moseley & Munro 1994, Hamadeh, Sautot, Lavallée & Cinquin 1995, McParland & Kumaradas 1995, Zubal et al. 1995, Christensen et al. 1996, Evans, Strong, Colchester, Zhao & Holton-Tainter 1996)

[15](Besl & McKay 1992)

techniques are referred to in section 2.7. Yet other methods perform landmark registration by testing a number of likely transformation hypotheses, which can, *e.g.*, be formulated by aligning three randomly picked points from each point set involved. Common optimization methods here are quasi-exhaustive searches, graph matching and dynamic programming approaches.

2.4.2.2 Segmentation based registration methods

Segmentation based registration methods can be *rigid model based*[16], where anatomically the same structures (mostly surfaces) are extracted from both im-

[16](Chen, Pelizzari, Chen, Cooper & Levin 1987, Levin, Pelizzari, Chen, Chen & Cooper 1988, Guéziec & Ayache 1992, Jiang, Robb & Holton 1992, Ayache, Guéziec, Thirion, Gourdon & Knoplioch 1993, Collignon, Géraud, Vandermeulen, Suetens & Marchal 1993, Fritsch 1993, Gee, Reivicj & Bajcsy 1993, Gee, Barillot, le Bricquer, Haynor & Bajcsy 1994, Gee, le Bricquer & Barillot 1995, Gee, le Bricquer, Barillot, Haynor & Bajcsy 1995, Gee & Haynor 1996, Gilhuijs & van Herk 1993, Hill, Hawkes, Harrison & Ruff 1993, Kittler, Christmas & Petrou 1993, Miller, Christensen, Amit & Grenander 1993, Rusinek, Tsui, Levy, Noz & de Leon 1993, Tsui, Rusinek, van Gelder & Lebedev 1993, Turkington, Jaszczak, Pelizzari, Harris, MacFall, M. & Coleman 1993, Zhao, Young & Ginsberg 1993, Collignon, Vandermeulen, Suetens, Marchal, Baert & Oosterlinck 1994, Ettinger, Grimson, Lozano-Pérez, Wells III, White & Kikinis 1994, Ettinger, Grimson & Lozano-Pérez 1994, Feldmar & Ayache 1994, Fritsch, Pizer, Morse, Eberly & Liu 1994, Fritsch, Pizer, Chaney, Liu, Raghavan & Shah 1994, Grimson, Lozano-Pérez, Wells, Ettinger, White & Kikinis 1994, Grimson, Lozano-Pérez, Wells III, Ettinger, White & Kikinis 1994*a*, Grimson, Lozano-Pérez, Wells III, Ettinger, White & Kikinis 1994*b*, Hemler, Sumanaweera, Pichumani, van den Elsen, Napel & Adler 1994, Hemler, Sumanaweera, Pichumani, van den Elsen, Napel, Drace & Adler 1994, Huang & Cohen 1994, Hata, Suzuki, Dohi, Iseki, Takakura & Hashimoto 1994, Henderson, Smith & Bucholz 1994, van Herk & Kooy 1994, Kanatani 1994, Krattenthaler, Mayer & Zeiler 1994, Kooy, van Herk, Barnes, Alexander III, Dunbar, Tarbell, Mulkern, Holupka & Loeffler 1994, Lavallée, Sautot, Troccaz, Cinquin & Merloz 1994, Liu, Pizer, Eberly, Morse, Rosenman, Chaney, Bullitt & Carrasco 1994, Maurer et al. 1994, Mendonça, Campilho & Nunes 1994, Péria, François-Joubert, Lavallée, Champleboux, Cinquin & Grand 1994, Philips 1994, Petti, Kessler, Fleming & Pitluck 1994, Simon, Hebert & Kanade 1994, Serra & Berthod 1994, Szelinsky & Lavallée 1994, Szeliski & Lavallée 1994, Scott, Macapinlac, Divgi, Zhang, Kalaigian, Pentlow, Hilton, Graham, Sgouros, Pelizzari, Chen, Schlom, Goldsmith & Larson 1994, Strother et al. 1994, Staib & Xianzhang 1994, Taneja, Holton, Camp & Robb 1994, Wang, Toro, Zeffiro & Hallett 1994, Zuk, Atkins & Booth 1994, Ardekani, Braun, Hutton, Kanno & Ida 1995, Andersson, Sundin & Valind 1995, Andersson 1995, Betting & Feldmar 1995, Betting, Feldmar, Ayache & Devernay 1995, Burel, Henocq & Catros 1995, Christmas, Kittler & Petrou 1995, Feldmar, Ayache & Betting 1995, Grimson, Ettinger, White, Gleason, Lozano-Pérez, Wells III & Kikinis 1995, Henri, Colchester, Zhao, Hawkes, Hill & Evans 1995, Hemler, van den Elsen, Sumanaweera, Napel, Drace & Adler 1995, Hemler, Sumanaweera, van den Elsen, Napel & Adler 1995, Hemler, Napel, Sumanaweera, Pichumani, van den Elsen, Martin, Drace & Adler 1995, Hamadeh, Sautot & Cinquin 1995, Hamadeh, Sautot, Lavallée & Cinquin 1995, Hamadeh, Lavallée, Szeliski, Cinquin & Péria 1995, Kruggel & Bartenstein 1995, Lavallée & Szeliski 1995, Leszczynski, Loose & Dunscombe 1995, Maurer, Aboutanos, Dawant, Margolin, Maciunas & Fitzpatrick 1995, Pellot, Bloch, Sureda, Herment, Sigelle, Horain & Long 1995, Pallotta, Gilardi, Bettinardi, Rizzo, Landoni, Striano, Masi & Fazio 1995, Pajdla & van Gool 1995, Pennec & Thirion 1995, Ryan, Erickson, Levin, Pelizzari, MacDonald & Dohrmann 1995, Rizzo, Gilardi, Prinster, Grassi, Scotti, Cerutti & Fazio 1995, Si-

ages to be registered, and used as sole input for the alignment procedure. They can also be *deformable model based*[17], where an extracted structure (also mostly surfaces, and curves) from one image is elastically deformed to fit the second image. The *rigid model based* approaches are probably the most popular methods currently in clinical use. Their popularity relative to other approaches is probably for a large part due to the success of the "head-hat" method as introduced by Pelizzari and co-workers[18], which relies on the segmentation of the skin surface from CT, MR and PET images of the head. Since the segmentation task is fairly easy to perform, and the computational complexity relatively low, the method has remained popular, and many follow-up papers aimed at automating the segmentation step, improving the optimization performance, or otherwise extending the method have been published. Another popularity cause is the fast *Chamfer matching* technique for alignment of binary structures by means of a distance transform, introduced by Borgefors (1988). A drawback of segmentation based methods is that the registration accuracy is limited to the accuracy of the segmentation step. In theory, segmentation based registration is applicable to images of many areas of the body, yet in practice the application areas have largely been limited to neuroimaging and orthopedic imaging. The methods are commonly automated but for the segmentation step, which is performed semi-automatically most of the times.

With *deformable models* however, the optimization criterion is different: it is always locally defined and computed, and the deformation is constrained by elastic modeling constraints (by a regularization term) imposed onto the segmented curve or surface. Deformable curves appear in literature as *snakes* or

mon, O'Toole, Blackwell, Morgan, DiGioia & Kanade 1995, Simon, Hebert & Kanade 1995, Serra & Berthod 1995, Scott, Macapinlac, Zhang, Daghighian, Montemayor, Kalaigian, Sgouros, Graham, Kolbert, Yeh, Lai, Goldsmith & Larson 1995, Sull & Ahuja 1995, Troccaz, Laieb, Vassal, Menguy, Cinquin, Bolla & Giraud 1995, Turkington, Hoffman, Jaszczak, MacFall, Harris, Kilts, Pelizzari & Coleman 1995, Vassal, Troccaz, Laieb, Cinquin, Bolla & Berland 1995, Vandermeulen et al. 1995, Xiao & Jackson 1995, Zubal et al. 1995, Declerc, Feldmar, Betting & Goris 1996, Evans, Strong, Colchester, Zhao & Holton-Tainter 1996, Ettinger, Grimson, Leventon, Kikinis, Gugino, Cote, Karapelou, Aglio, Shenton, Potts & Alexander 1996, Feldmar & Ayache 1996, Grimson, Ettinger, White, Lozano-Pérez, Wells III & Kikinis 1996, Gilhuijs, van den Ven & van Herk 1996, Ge, Maurer & Fitzpatrick 1996, Goris, Declerck, Feldmar & Ayache 1996, Hemler, Sumanaweera, van den Elsen, Napel & Adler 1996, Jain, Zhong & Lakshmanan 1996, Lavallée, Troccaz, Sautot, Mazier, Cinquin, Merloz & Chirossel 1996, Lavallée, Szeliski & Brunie 1996, Qian, Mitsa & Hoffman 1996, Szeliski & Lavallée 1996, Wang, Cheng, Collins & Hanson 1996)

[17](Bajcsy, Lieberson & Reivich 1983, Guéziec 1993, Taubin 1993, Davatzikos & Prince 1994, MacDonald, Avis & Evans 1994, Sandor & Leahy 1994, Tom, Efstratiadis & Katsaggelos 1994, Bronielsen 1995, Bainville, Champledoux, Cinquin, Dessenne, Hamadeh, Troccaz, Lavallée, Péria, Sautot & Szeliski 1995, Mangin, Tupin, Bloch, Rougetet, Régis & López-krahe 1995, Sandor & Leahy 1995, Thirion 1995, Cuisenaire, Thiran, Macq, Michel, de Volder & Marquès 1996, Davatzikos, Prince & Bryan 1996, Davatzikos 1996, McInerney & Terzopoulos 1996, Thirion 1996*b*)

[18](Chen et al. 1987, Levin et al. 1988, Pelizzari, Chen, Spelbring, Weichselbaum & Chen 1989, Chen & Pelizzari 1989)

active contours; 3D deformable models are sometimes referred to as *nets*. To ease the physical modeling, the data structure of deformable models is not commonly a point set. Instead, it is often represented using localized functions such as splines. The deformation process is always done iteratively, small deformations at a time. Deformable model approaches are based on a *template model* that needs to be defined in one image. After this, two types of approaches can be identified: the template is either deformed to match a segmented structure in the second image[19], or the second image is used *unsegmented*[20]. In the latter case, the fit criterion of the template can be, *e.g.*, to lie on an edge region in the second image. Opposed to registration based on extracted rigid models, which is mainly suited for intrasubject registration, deformable models are in theory very well suited for intersubject and atlas[21] registration, as well as for registration of a template obtained from a patient to a mathematically defined general model of the templated anatomy. A drawback of deformable models is that they often need a good initial position in order to properly converge, which is generally realized by (rigid) pre-registration of the images involved. Another disadvantage is that the local deformation of the template can be unpredictably erratic if the target structure differs sufficiently from the template structure. A typical error is that the deformable model matches the anatomy perfectly, except in the one interesting image area where a large tumor growth has appeared. In intrasubject matching of, *e.g.*, the cortical surface, this may result in entire gyri being missed or misplaced. The solution may lie in locally adapting the elasticity constraints[22]. Deformable models are best suited to find local curved transformations between images, and less so for finding (global) rigid or affine transformations. They can be used on almost any anatomical area or modality, and are usually automated but for the segmentation step. In the current literature the major applications are registration of bone contours obtained from CT[23], and cortical registration of MR images[24]. Deformable models are ideally suited for the former application, as the bone contours are easily extracted from the CT, and there are often no other contours near that disturb the proper deformation convergence. The latter application is important because if a cortical registration between two brains can be found, a segmentation of one cortex can

[19](Taubin 1993, Davatzikos & Prince 1994, Sandor & Leahy 1994, Tom et al. 1994, Bro-nielsen 1995, Bainville et al. 1995, Sandor & Leahy 1995, Thirion 1995, Cuisenaire et al. 1996, Davatzikos et al. 1996, Davatzikos 1996, Thirion 1996*b*)

[20](Bajcsy et al. 1983, Guéziec 1993, MacDonald et al. 1994)

[21]Intersubject and atlas registration is covered in section2.9.

[22](Bro-nielsen 1995, Little, Hill & Hawkes 1996)

[23]*e.g.*, see (Fang et al. 1996)

[24](Bajcsy et al. 1983, Davatzikos & Prince 1994, MacDonald et al. 1994, Sandor & Leahy 1994, Sandor & Leahy 1995, Thirion 1995, Cuisenaire et al. 1996, Davatzikos et al. 1996, Davatzikos 1996, Thirion 1996*b*)

be instantly transfered to the other.

2.4.2.3 Voxel property based registration methods

The *voxel property based* registration methods stand apart from the other intrinsic methods[25] by the fact that they operate directly on the image grey values, without prior data reduction by the user or segmentation. There are two distinct approaches: the first is to immediately *reduce* the image grey value content to a representative set of scalars and orientations, the second is to use the full image content throughout the registration process.

Principal axes and moments based methods are the prime examples of *reductive* registration methods. Within these methods the image center of gravity and its principal orientations (principal axes) are computed from the image zeroth and first order moments. Registration is then performed by aligning the center of gravity and the principal orientations[26]. Sometimes, higher order moments are also computed and used in the process. The result is usually not very accurate, and the method is not equipped to handle differences in scanned volume well, although some authors attempt to remedy this latter problem. Despite its drawbacks, principal axes methods are widely used in registration problems that require no high accuracy, because of the automatic and very fast nature of its use, and the easy implementation. The method is used primarily in the realignment of scintigraphic cardiac studies (even intersubject)[27], and as a coarse pre-registration in various other registration areas[28]. Moment based methods also appear as hybridly classified registration methods that use segmented or binarized image data for input. In many applications, pre-segmentation is mandatory in order for moment based methods to produce acceptable results.

Voxel property based methods using the full image content are the most interesting methods researched currently. Theoretically, these are the most flexible of registration methods, since they –unlike all other methods mentioned– do not start with reducing the grey valued image to relatively sparse extracted information, but use all of the available information throughout the registration process.

[25] Except some instances of geometric landmark registration.

[26] (Alpert, Bradshaw, Kennedy & Correia 1990, Banerjee & Toga 1994, Ettinger, Grimson, Lozano-Pérez, Wells III, White & Kikinis 1994, Ettinger, Grimson & Lozano-Pérez 1994, Pavía, Ros, Catafau, Lomeña & Setoain 1994, Wang & Fallone 1994, Slomka, Hurwitz, Stephenson & Cradduck 1995, Dong & Boyer 1996, Wang, Volkow, Levy, Fowler, Logan, Alexoff, Hitzemann & Schyler 1996)

[27] (Slomka et al. 1995)

[28] (Banerjee & Toga 1994, Ettinger, Grimson, Lozano-Pérez, Wells III, White & Kikinis 1994, Ettinger, Grimson & Lozano-Pérez 1994, Pavía et al. 1994, Slomka et al. 1995, Dong & Boyer 1996)

Although voxel property based methods have been around a long time, their use in extensive 3D/3D clinical applications has been limited by the considerable computational costs. An increasing clinical call for accurate and retrospective registration, along with the development of ever-faster computers with large internal memories, have enabled full-image-content methods to be used in clinical practice, although they have not yet been introduced in time-constrained applications such as intra-operative 2D/3D registration. Methods using the full image content can be applied in almost any medical application area, using any type of transformation. However, such a statement is largely merited by the fact that "full-image-content based" is a very gross classifier. The real versatility of a method can only be established on an individual basis. Many recent papers report on applications that are tailored for rigid or affine global registration of 3D images of the head. Nearly all presented methods are automatic, although hybrid approaches (*e.g.*, including an interactive landmark based preregistration) are being suggested[29]. While the methods theoretically support curved transformations and intersubject registration, we have encountered only few publications on this.

As concerns full-image-content based voxel property registration methods, literature reports on the following paradigms being used ($*$ = most likely restricted to monomodal applications)

- Cross-correlation (of original images or extracted feature images)[30].
- Fourier domain based cross-correlation, and phase-only correlation[31].
- Minimization of variance of intensity ratios[32].

[29](Studholme, Hill & Hawkes 1996)

[30](Junck, Moen, Hutchins, Brown & Kuhl 1990, Bacharach, Douglas, Carson, Kalkowski, Freedman, Perrone-Filardi & Bonow 1993, Bettinardi, Gilardi, Lucignani, Landoni, Rizzo, Striano & Fazio 1993, van den Elsen & Viergever 1993, Hill 1993, Hua & Fram 1993, Münch & Rüegsegger 1993, Radcliffe, Rajapakshe & Shalev 1993, Banerjee & Toga 1994, Collins, Neelin, Peters & Evans 1994, Collins, Peters & Evans 1994, van den Elsen 1994, van den Elsen, Pol, Sumanaweera, Hemler, Napel & Adler 1994, Lemieux, Jagoe, Fish, Kitchen & Thomas 1994, Moseley & Munro 1994, Maintz, van den Elsen & Viergever 1994, Maintz, van den Elsen & Viergever 1996*b*, Pavía et al. 1994, Radcliffe, Rajapakshe & Shalev 1994, Andersson 1995, Andersson et al. 1995, Cideciyan 1995, Collins, Evans, Holmes & Peters 1995, van den Elsen, Maintz, Pol & Viergever 1995, Hemler, van den Elsen, Sumanaweera, Napel, Drace & Adler 1995, McParland & Kumaradas 1995, Maintz, van den Elsen & Viergever 1995, Perault, Wampach & Liehn 1995, Studholme, Hill & Hawkes 1995*b*, Studholme, Hill & Hawkes 1995*a*, Dong & Boyer 1996, Gottesfeld Brown & Boult 1996, Hristov & Fallone 1996, Lehmann, Goerke, Schmitt, Kaupp & Repges 1996, Maintz, van den Elsen & Viergever 1996*a*)

[31](de Castro & Morandi 1987, Leclerc & Benchimol 1987, Chen 1993, Lehmann et al. 1996, Shekarforoush, Berthod & Zerubia 1996, Wang, Reinstein, Hanley & Meek 1996)

[32](Hill 1993, Hill, Hawkes, Harrison & Ruff 1993, Woods, Maziotta & Cherry 1993, Ardekani, Braun, Kanno & Hutton 1994, Studholme et al. 1995*b*, Studholme et al. 1995*a*, Zuo, Jiang, Buff, Mahon & Wong 1996)

- Minimization of variance of grey values within segments[33].
* Minimization of the histogram entropy of difference images[34].
- Histogram clustering and minimization of histogram dispersion[35].
- Maximization of mutual information (relative entropy) of the histogram[36].
* Maximization of zero crossings in difference images (Stochastic sign change (SSC), and Deterministic sign change (DSC) criterion)[37].
* Cepstral echo filtering[38].
* Determination of the optic flow field[39].
* Minimization of the absolute or squared intensity differences[40].
* Matching local low-order Taylor expansions determined by the image grey values[41].
- Implicitly using surface registration by interpreting a 3D image as an instance of a surface in 4D space[42].

2.4.3 Non-image based registration

It seems paradoxical that registration of multimodal images can be *non-image based*, but it is possible if the imaging coordinate systems of the two scanners

[33](Cox & de Jager 1994, Ardekani et al. 1995)
[34](Buzug & Weese 1996)
[35](Hill 1993, Hill, Studholme & Hawkes 1994, Hill & Hawkes 1994, Collignon, Vandermeulen, Suetens & Marchal 1995, Hawkes, Ruff, Hill, Studholme, Edwards & Wong 1995, Studholme et al. 1995*b*, Studholme et al. 1995*a*, Lehmann et al. 1996)
[36](Collignon, Maes, Delaere, Vandermeulen, Suetens & Marchal 1995, Viola & Wells III 1995, Viola 1995, Wells III, Viola & Kikinis 1995, Maes, Collignon, Vandermeulen, Marchal & Suetens 1996, Pokrandt 1996, Studholme et al. 1996, Viola, Schraudolph & Sejnowski 1996, Wells III, Viola, Atsumi, Nakajima & Kikinis 1996)
[37](Venot, Golmard, Lebruchec, Pronzato, Walter, Frij & Roucayrol 1983, Venot, Lebruchec & Roucayrol 1984, Venot & Leclerc 1984, Hua & Fram 1993, Hoh, Dahlbom, Harris, Choi, Hawkins, Phelps & Maddahi 1993, Venot, Pronzato & Walter 1994, Perault et al. 1995, Bani-Hashemi, Krishnan & Samaddar 1996)
[38](Bandari, Xiang & Little 1994)
[39](Barber, Tindale, Hunt, Mayes & Sagar 1995, Meunier, Guimond, Janicki, Imbert & Soucy 1996)
[40](Hoh et al. 1993, Lange, O'Tuama & Treves 1993, Zhao et al. 1993, Moseley & Munro 1994, Yeung, Yeo, Liou & Bani-Hashemi 1994, Christensen, Rabbitt, Miller, Joshi, Grenander, Coogan & van Essen 1995, Christensen, Miller, Marsh & Vannier 1995, Haller, Christensen, Joshi, Miller & Vannier 1995, Hajnal, Saeed, Oatridge, Williams, Young & Bydder 1995, Hajnal, Saeed, Soar, Oatridge, Young & Bydder 1995, Jacq & Roux 1995, Kruggel & Bartenstein 1995, Slomka et al. 1995, Unser, Thévenaz, Lee & Ruttimann 1995, Christensen et al. 1996, Eberl, Kanno, Fulton, Ryan, Hutton & Fulham 1996, Haller, Christensen, Joshi, Newcomer, Miller, Csernansky & Vannier 1996)
[41](Shields, Barber & Sheriff 1993)
[42](Feldmar, Malandain, Declerck & Ayache 1996)

involved are somehow calibrated to each other. This usually necessitates the scanners to be brought in to the same physical location, and the assumption that the patient remain motionless between both acquisitions. These are prohibitive prerequisites in nearly all applications, but they can be sufficiently met in applications involving the use of ultrasound[43]. Since ultrasound systems can come as hand-held devices that are equipped with a spatial (optical) localization system, they are easily calibrated, and can be used while the patient is immobilized on the CT, MR or operating gantry. The technique of calibrated coordinate systems is also often used in registering the position of surgical tools mounted on a robot arm to images[44].

2.5 Nature and domain of the transformation

III. Nature of transformation

- **a.** Rigid
- **b.** Affine
- **c.** Projective
- **d.** Curved

IV. Domain of transformation

- **a.** Local
- **b.** Global

2.5.1 Nature of the transformation

An image coordinate transformation is called *rigid*, when only translations and rotations[45] are allowed. If the transformation maps parallel lines onto parallel

[43](Hata et al. 1994, Péria, Chevalier, François-Joubert, Caravel, Dalsoglio, Lavallée & Cinquin 1995, Erbe et al. 1996)

[44]For instance (Potamianos, Davies & Hibberd 1995, Peters et al. 1996). See computer aided surgery literature (Lavallée 1996) for more complete references.

[45]and, technically, reflections, but this is disregarded in our formulation, since they do not apply to the general medical image registration problem.

lines it is called *affine*. If it maps lines onto lines, it is called *projective*. Finally, if it maps lines onto curves, it is called *curved* or *elastic*. Each type of transformation contains as special cases the ones described before it, *e.g.*, the rigid transformation is a special kind of affine transformation. A composition of more than one transformation can be categorized as a single transformation of the most complex type in the composition, *e.g.*, a composition of a projective and an affine transformation is a projective transformation, and a composition of rigid transformations is again a rigid transformation.

A rigid or affine 3D transformation can be described using a single constant matrix (a) equation: $y_i = a_{ij}x_j$, where x and y are the old and new coordinate vectors. In the rigid case, this equation is constrained as:

$$\begin{pmatrix} y_1 \\ y_2 \\ y_3 \\ 1 \end{pmatrix} = \left(\begin{array}{ccc|c} & r & & t \\ \hline 0 & 0 & 0 & 1 \end{array}\right) \begin{pmatrix} x_1 \\ x_2 \\ x_3 \\ 1 \end{pmatrix},$$

where t is an arbitrary translation vector, and r is a 3×3 rotation matrix defined by:

$$r_{il} = r^{(1)}_{ij} r^{(2)}_{jk} r^{(3)}_{kl}, \qquad r^{(1)} = \begin{pmatrix} 1 & 0 & 0 \\ 0 & \cos\alpha_1 & -\sin\alpha_1 \\ 0 & \sin\alpha_1 & \cos\alpha_1 \end{pmatrix},$$

$$r^{(2)} = \begin{pmatrix} \cos\alpha_2 & 0 & \sin\alpha_2 \\ 0 & 1 & 0 \\ -\sin\alpha_2 & 0 & \cos\alpha_2 \end{pmatrix}, \quad r^{(3)} = \begin{pmatrix} \cos\alpha_3 & -\sin\alpha_3 & 0 \\ \sin\alpha_3 & \cos\alpha_3 & 0 \\ 0 & 0 & 1 \end{pmatrix},$$

i.e., $r^{(i)}$ rotates the image around axis i by an angle α_i. In the affine case, r is unrestricted. In the projective case, we can only use a constant matrix representation if employing homogeneous coordinates: $y_i = u_i/u_4, u_i = a_{ij}x_j$, where a is an arbitrary 4×4 constant matrix. Curved transformations cannot in general be represented using constant matrices. Most applications represent curved transformations in terms of a local *vector displacement* (disparity) field: $y_i = x_i + t_i(x)$, or as polynomial transformations in terms of the old coordinates.

2.5.2 Domain of the transformation

A transformation is called *global* if it applies to the entire image, and *local* if subsections of the image each have their own transformations defined. Figure 2.1 shows examples of all transformation types mentioned.

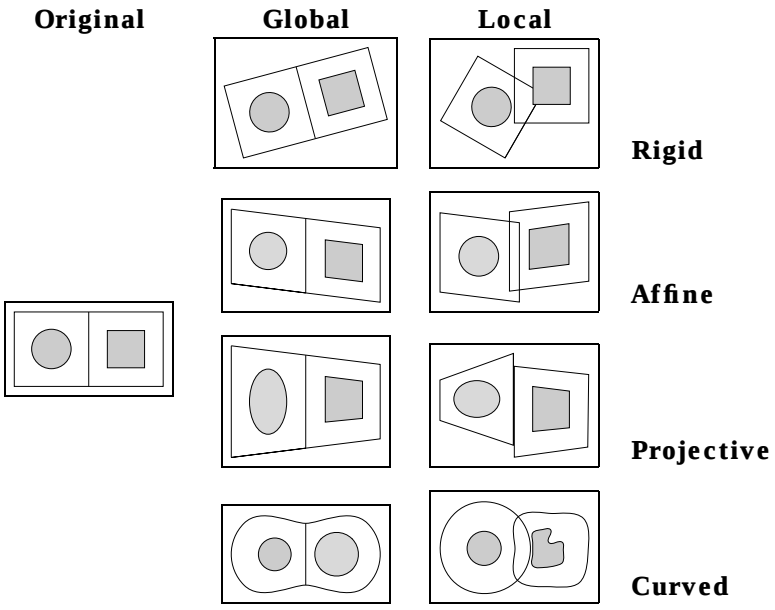

Figure 2.1 Examples of 2D transformations.

2.5.3 General transformation observations

Local transformations are seldom used directly, because they may violate the local continuity and bijectiveness of the transformations, which impairs straightforward image resampling when applying the transformation to the image. The term *local transformation* is reserved for transformations that are composites of *at least* two transformations determined on sub-images that cannot be generally described as a global transformation. Hence, a *single* transformation computed on some volume of interest of an image, is a *global* transformation, except that "global" now refers to the new image, which is a sub-image of the original. This definition, perhaps confusingly, does not impair a global transformation to be computed locally, *e.g.*, some applications compute a global rigid transformation of an image of the entire head based on computations done in the area of the facial surface only. Local rigid, affine, and projective transformations occur only rarely in the literature, although local rigid transformations may appear embedded in local curved transformations[46]. Some problems that are intrinsically locally rigid (such as the individual vertebrae in an image of the spinal column)

[46](Bro-nielsen 1995, Little et al. 1996)

are in registration tasks often solved by splitting the image in images meeting the global rigid body constraint.

In recently published registration papers, as a rule, rigid and affine transformations are global, and curved transformations are local. This makes sense, given the physical model underlying the curved transformation type, and given that the rigid body constraint is –globally, or in well defined sub-images– approximately met in many common medical images. Affine transformations are typically used in instances of rigid body movement where the image scaling factors are unknown or suspected to be incorrect, (notably in MR images because of geometric distortions). The projective transformation type has no real physical basis in image registration except for *2D/3D* registration, but is sometimes used as a "constrained-elastic" transformation when a fully elastic transformation behaves inadequately or has too many parameters to solve for. The projective transformation is not always used in *2D/3D* applications: even though projections will always figure in the problem, the transformation itself is not necessarily projective but may be rigid, if it applies to the 3D image prior to its projection to the 2D image.

Since local information of the anatomy is essential to provide an accurate local curved transformation, applications are nearly always *intrinsic*, mostly *deformable model based* or *using the full image content*, and mostly semi-automatic, requiring a user-identified initialization. They appear almost solely using anatomical images (CT, MR) of the head, and are excellently suited for intersubject and image to atlas registration. Many methods require a pre-registration (initialization) using a rigid or affine transformation.

The global rigid transformation is used most frequently in registration applications. It is popular because in many common medical images the rigid body constraint is, at least to a good approximation, satisfied. Furthermore, it has relatively few parameters to be determined, and many registration techniques are not equipped to supply a more complex transformation. The most common application area is the human head.

2.6 Interaction

V. Interaction

a. Interactive

1. Initialization supplied
2. No initialization supplied

b. Semi-automatic

1. User initializing
2. User steering/correcting
3. Both

c. Automatic

Concerning registration algorithms, three levels of interaction can be recognized. *Automatic*, where the user only supplies the algorithm with the image data and possibly information on the image acquisition. *Interactive*, where the user does the registration himself, assisted by software supplying a visual or numerical impression of the current transformation, and possibly an initial transformation guess. *Semi-automatic*, where the interaction required can be of two different natures: the user needs to *initialize* the algorithm, *e.g.*, by segmenting the data, or *steer* the algorithm, *e.g.*, by rejecting or accepting suggested registration hypotheses.

Many authors strive for fully automated algorithms, but it can be discussed whether this is wished for in *all* current clinical applications. The argument is that many current methods have a trade-off between minimal interaction and speed, accuracy, or robustness. Some methods would doubtlessly benefit if the user were "kept in the loop", steering the optimization, narrowing search space, or rejecting mismatches. On the other hand, many methods spent over 90% of their computation time examining registrations at a resolution level that would hardly benefit from human intervention. If they perform robustly, such methods are better left automated. Furthermore, many applications require registration algorithms to operate objectively, and thus allow no human interaction. Human interaction also complicates the validation of registration methods, inasmuch as it is a parameter not easily quantified or controlled.

Extrinsic methods are often easily *automated*, since the marker objects are designed to be well visible and detectable in the images involved[47]. Sometimes users are required to roughly point out the marker region, or supply a seed point located in the marker (*semi-automatic*). Of the *intrinsic* methods, the *anatomical landmark* and *segmentation based* methods are commonly *semi-automatic (user initializing)*, and the *geometrical landmark* and *voxel property based* methods are

[47] see, *e.g.*, (Wang et al. 1995)

usually *automated*. Fully *interactive* methods are reported on very little in the recent literature[48]. Perhaps, like many methods that rely primarily on the proper use of good visualization software, they are considered trivial.

2.7 Optimization procedure

VI. Optimization procedure

a. Parameters computed

b. Parameters searched for

The parameters that make up the registration transformation can either be *computed* directly, *i.e.*, determined in an explicit fashion from the available data, or *searched for*, *i.e.*, determined by finding an optimum of some function defined on the parameter space. In the former case, the manner of computation is completely determined by the paradigm. The only general remark we can make is that the use of *computation* methods is restricted almost completely to applications relying on very sparse information, *e.g.*, small point sets[49]. In the case of *searching* optimization methods, most registration methods are able to formulate the paradigm in a standard mathematical function of the transformation parameters to be optimized. This function attempts to quantify the similarity as dictated by the paradigm between two images given a certain transformation. Such functions are generally less complex in monomodal registration applications, since the similarity is more straightforward to define. Hopefully, the similarity function is well-behaved (quasi-convex) so one of the standard and well-documented optimization techniques can be used. Popular techniques are Powell's method[50], the Downhill Simplex method[51], Brent's

[48](Morris et al. 1993, Pietrzyk et al. 1994, Soltys et al. 1995)

[49]see, *e.g.*, (Arun, Huang & Blostein 1987, Hill, Hawkes, Crossman, Gleeson, Cox, Bracey, Strong & Graves 1991, Hill, Hawkes, Hussain, Green, Ruff & Robinson 1993)

[50](Levin et al. 1988, Hill, Hawkes & Hardingham 1991, Tsui et al. 1993, Ettinger, Grimson, Lozano-Pérez, Wells III, White & Kikinis 1994, Ettinger, Grimson & Lozano-Pérez 1994, Hata et al. 1994, van Herk & Kooy 1994, Kooy et al. 1994, Lemieux, Jagoe, Fish, Kitchen & Thomas 1994, Andersson 1995, Andersson et al. 1995, Collignon, Maes, Delaere, Vandermeulen, Suetens & Marchal 1995, Leszczynski et al. 1995, Bani-Hashemi et al. 1996, Gilhuijs et al. 1996, Gottesfeld Brown & Boult 1996, Maes et al. 1996)

[51](Hill, Hawkes & Hardingham 1991, Gilhuijs & van Herk 1993, Hill, Hawkes, Harrison & Ruff 1993, Hoh et al. 1993, Leung Lam et al. 1993, van Herk & Kooy 1994, Kooy et al. 1994, Li, Pelizzari & Chen 1994, Meyer et al. 1995, Slomka et al. 1995, Eberl et al. 1996)

method and series of one-dimensional searches[52], Levenberg-Marquardt optimization[53], Newton-Raphson iteration[54], stochastic search methods[55], gradient descent methods[56], genetic methods[57], simulated annealing[58], geometric hashing[59], and quasi-exhaustive search methods[60]. Many of these methods are documented in (Press, Teukolsky, Vetterling & Flannery 1992). Frequent additions are multi-resolution (*e.g.*, pyramid) and multi-scale approaches to speed up convergence, to reduce the number of transformations to be examined (which is especially important in the quasi-exhaustive search methods) and to avoid local minima. Some registration methods employ non-standard optimization methods that are designed specifically for the similarity function at hand, such as the ICP algorithm[61], created for *rigid model* based registration. Many applications use more than one optimization technique, frequently a fast but coarse technique followed by an accurate yet slow one.

2.8 Modalities involved in the registration

Note: The lists of modalities below, in exception, are not meant to be theoretically complete, but give the modality instances encountered in recent literature.

VII. Modalities involved

[52](Bacharach et al. 1993, Münch & Rüegsegger 1993, Ault & Siegel 1994, Petti et al. 1994, Ault & Siegel 1995, Ardekani et al. 1995, McParland & Kumaradas 1995, Hristov & Fallone 1996)

[53](Taubin 1993, Hemler, Sumanaweera, Pichumani, van den Elsen, Napel & Adler 1994, Hemler, Sumanaweera, Pichumani, van den Elsen, Napel, Drace & Adler 1994, Szelinsky & Lavallée 1994, Szeliski & Lavallée 1994, Bainville et al. 1995, Hamadeh, Sautot & Cinquin 1995, Hamadeh, Sautot, Lavallée & Cinquin 1995, Lavallée & Szeliski 1995, Unser et al. 1995, Lavallée, Szeliski & Brunie 1996, Szeliski & Lavallée 1996)

[54](Fright & Linney 1993, Woods et al. 1993, Zuo et al. 1996)

[55](Miller et al. 1993, Viola & Wells III 1995, Viola 1995, Wells III et al. 1995, Viola et al. 1996, Wells III et al. 1996)

[56](Zuk et al. 1994, Perault et al. 1995, Buzug & Weese 1996, Christensen et al. 1996, Cuisenaire et al. 1996)

[57](Hill, Hawkes, Harrison & Ruff 1993, Hill et al. 1994, Hill & Hawkes 1994, Staib & Xianzhang 1994, Kruggel & Bartenstein 1995, Cross, Wilson & Hancock 1996)

[58](Liu et al. 1994)

[59](Guéziec & Ayache 1992, Ayache et al. 1993, Pajdla & van Gool 1995)

[60](Bettinardi et al. 1993, van den Elsen & Viergever 1993, Hua & Fram 1993, Cox & de Jager 1994, van den Elsen 1994, van den Elsen et al. 1994, Mendonça et al. 1994, Maintz et al. 1994, Maintz, van den Elsen & Viergever 1996*b*, van den Elsen et al. 1995, Maintz et al. 1995, Dong & Boyer 1996, Maintz, van den Elsen & Viergever 1996*a*)

[61](Besl & McKay 1992, Simon et al. 1994, Feldmar & Ayache 1994, Maurer, Aboutanos, Dawant, Margolin, Maciunas & Fitzpatrick 1995, Pajdla & van Gool 1995, Simon, Hebert & Kanade 1995, Betting & Feldmar 1995, Betting et al. 1995, Cuchet, Knoplioch, Dormont & Marsault 1995, Feldmar et al. 1995, Ellis et al. 1996, Feldmar et al. 1996, Feldmar & Ayache 1996, Goris et al. 1996)

a. Monomodal

1. Auto-radiographic
2. CT or CTA
3. MR
4. PET
5. Portal
6. SPECT
7. US
8. Video
9. X-ray or DSA

b. Multimodal

1. CT—MR
2. CT—PET
3. CT—SPECT
4. DSA—MR
5. PET—MR
6. PET—US
7. SPECT—MR
8. SPECT—US
9. TMS[62]—MR
10. US—CT
11. US—MR
12. X-ray—CT
13. X-ray—MR
14. X-ray—portal
15. X-ray—US
16. Video—CT
17. Video—MR

c. Modality to model

1. CT

[62]Transcranial magnetic stimulation.

2. MR
3. SPECT
4. X-ray

d. Patient to modality

1. CT
2. MR
3. PET
4. Portal
5. X-ray

Four classes of registration tasks can be recognized based on the modalities that are involved. In *monomodal* applications, the images to be registered belong to the same modality, as opposed to *multimodal* registration tasks, where the images to be registered stem from two different modalities. In *modality to model* and *patient to modality* registration only one image is involved and the other "modality" is either a model or the patient himself. Hence we use the term "modality" in a loose sense, not only applying to acquired images, but also to mathematical models of anatomy or physiology, and even to the patient himself. Such inclusions are necessary to properly type-cast the four categories according to the actual registration task to be solved. At a first glance, this classification may seem paradoxical; *patient to modality* may seem a registration task appearing in any application. However, the classification is disjunct and closed if only the *actual coordinate systems that need to be related are considered , i.e.,* the coordinate systems referring to the actual modalities named in the *problem statement.* For example:

- For diagnostic purposes, two myocardial SPECT images are acquired of the patient, under rest and stress conditions. Their registration is a monomodal application.
- To relate an area of dysfunction to anatomy, a PET image is registered to an MR image. This is a multimodal application.
- To register an MR to a PET image, a PET image image is first *simulated* from the MR image, and the real and simulated PET images are registered. This is still a multimodal application.
- An example of modality to model is the registration of an MR brain image to a mathematically defined compartimental model of gross brain structures.

- In radiotherapy treatment, the patient can be positioned with the aid of registration of in-position X-ray simulator images to a pre-treatment anatomical image. Although the registration task is performed using only the images acquired, the actual task of patient positioning is clearly an example of *patient to modality* registration.

The *patient to modality* registration tasks appear almost exclusively in intraoperative[63] and radiotherapy[64] applications. *Modality to model* can be applied in gathering statistics on tissue morphology (*e.g.*, for finding anomalies relative to normalized structures), and to segmentation tasks[65]. *Monomodal* tasks are well suited for growth monitoring, intervention verification, rest-stress comparisons, ictal-interictal comparisons, subtraction imaging (also DSA, CTA), and many other applications. The applications of multimodal registration are abundant and diverse, predominantly diagnostic in nature. A coarse division would be into *anatomical-anatomical* registration, where images showing different aspects of tissue morphology are combined, and *functional-anatomical*, where tissue metabolism and its spatial location relative to anatomical structures are related[66].

2.9 Subject

VIII. Subject

a. Intrasubject

[63](Bucholz et al. 1994, Harmon et al. 1994, Henderson et al. 1994, Lemieux, Jagoe, Fish, Kitchen & Thomas 1994, Lavallée et al. 1994, Lea, Watkins, Mills, Peshkin, Kienzle III & Stulberg 1994, Li, Pelizzari & Chen 1994, Simon et al. 1994, Wang, Toro, Zeffiro & Hallett 1994, Betting et al. 1995, Betting & Feldmar 1995, Bainville et al. 1995, Cuchet et al. 1995, Edwards, Hawkes, Hill, Jewell, Spink, Strong & Gleeson 1995, Edwards, Hill, Hawkes, Spink, Colchester, Strong & Gleeson 1995, Hamadeh, Sautot, Lavallée & Cinquin 1995, Hamadeh, Lavallée, Szeliski, Cinquin & Péria 1995, Lea, Santos-munné & Peshkin 1995, Lea, Watkins, Mills, Peshkin, Kienzle III & Stulberg 1995, Maurer, Fitzpatrick, Galloway, Wang, Maciunas & Allen 1995, Miaux, Guermazi, Gossot, Bourrier, Angoulvant, Kahiroune, Turki & Bouché 1995, Ryan et al. 1995, Simon, O'Toole, Blackwell, Morgan, DiGioia & Kanade 1995, Simon, Hebert & Kanade 1995, Evans, Strong, Colchester, Zhao & Holton-Tainter 1996, Fuchs et al. 1996, Lavallée, Troccaz, Sautot, Mazier, Cinquin, Merloz & Chirossel 1996, Lavallée 1996, Peters et al. 1996)

[64](Bijhold 1993, Gall & Verhey 1993, Leung Lam et al. 1993, Troccaz et al. 1995, Vassal et al. 1995, Gilhuijs et al. 1996)

[65](Bajcsy et al. 1983, Rizzo et al. 1995, Amit & Kong 1996, Cuisenaire et al. 1996, Jain et al. 1996)

[66]References to monomodal and multimodal applications will be given in the *object* section, since they are numerous, and moreover many papers are not specific to one of the four application categories.

b. Intersubject

c. Atlas

When all of the images involved in a registration task are acquired of a single patient, we refer to it as *intrasubject* registration. If the registration is accomplished using two images of different patients (or a patient and a model), this is referred to as *intersubject* registration. If one image is acquired from a single patient, and the other image is somehow constructed from an image information database obtained using imaging of many subjects, we name it *atlas* registration. In literature, many instances of registration of a patient image to an image of a "normal" subject is termed atlas registration. Although this definition is as good as ours, we refer to this type of registration as *intersubject*, to keep the class distinctions clear. *Intrasubject* registration is by far the most common of the three, used in almost any type of diagnostic and interventional procedure. *Intersubject*[67] and *atlas* registration[68] appear mostly in *3D/3D MR or CT brain image* applications. The nature of the registration transformation is mostly *curved*; these applications are always *intrinsic*, either *segmentation based* or *voxel property based, using the full image content*. A proper (manual) initialization is frequently desired. Some applications use *rigid* transforms, but their application is limited. Others use *anatomical landmarks* for a deformation basis of a *curved* transformation; unfortunately such applications often require the transformation in large image areas to be interpolated from the nearest landmark transformations, which may prove unreliable. The use of *intersubject* and *atlas* matching can notably be found in the areas of gathering statistics on the size and shape of specific structures, finding (accordingly) anomalous structures, and transferring segmentations from one image to another.

2.10 Object

IX. Object

[67](Bajcsy et al. 1983, Gee et al. 1993, Miller et al. 1993, Szeliski & Lavallée 1994, Szelinsky & Lavallée 1994, Sandor & Leahy 1994, Collins et al. 1995, Ge et al. 1995, Haller et al. 1995, Sandor & Leahy 1995, Thirion 1995, Amit & Kong 1996, Declerc et al. 1996, Fang et al. 1996, Gee & Haynor 1996, Haller et al. 1996, Thirion 1996*b*)

[68](Collins, Neelin, Peters & Evans 1994, Collins, Peters & Evans 1994, Davatzikos & Prince 1994, MacDonald et al. 1994, Barber et al. 1995, Christensen, Rabbitt, Miller, Joshi, Grenander, Coogan & van Essen 1995, Christensen, Miller, Marsh & Vannier 1995, Slomka et al. 1995, Christensen et al. 1996, Cuisenaire et al. 1996, Davatzikos et al. 1996, Feldmar et al. 1996)

a. Head

1. Brain or skull
2. Eye
3. Dental

b. Thorax

1. Entire
2. Cardiac
3. Breast

c. Abdomen

1. General
2. Kidney
3. Liver

d. Pelvis and perineum

e. Limbs

1. General
2. Femur
3. Humerus
4. Hand

f. Spine and vertebrae

The above list is, again, not theoretically complete, but composed of those imaging areas encountered in recent literature. Almost all reviewed papers will be cited in this section[69], focussing on the paradigm used. We will break down this section according to the areas mentioned in the list. Hopefully this will give an idea of the specific approaches and trends associated with each image area. Since many papers concern global head registration (177 out of over 300 reviewed papers), this subsection will be further divided according to the modalities involved. *Note that many papers may have more than one application area, even though they only demonstrate a registration method in one area.* This implies that some areas, *e.g.*, CT-SPECT registration, appear to have been poorly examined, while in fact good methods have been developed in other areas that are

[69]The reader is warned that readability was not foremost in our minds at the time of writing. Rather, this section serves a reference purpose.

instantly or easily transfered to the problem at hand. Many general papers do not detail a specific medical registration application. Such papers are mentioned at the end of this section.

2.10.1 Registration of head images

Many possible registration tasks can be defined on images of the human head, including all types of monomodal, multimodal, model, and patient registration of a plethora of image modalities in various diagnostic and interventionist settings. This makes for the prevalence of papers concerned with registration of images of the head, possibly along with the fact that the head can be considered a rigid body in many applications, while such a constraint cannot be met in many thoracic, abdominal, pelvic, and spinal images.

2.10.1.1 Monomodal applications: CT

Intrasubject 3D CT registration was performed by Guéziec and Ayache[70] by registering "crest lines" (extremal lines of the principal curvature) of surfaces. This technique was later adapted by Thirion[71], using only the extremal points of the crest lines. Van Herk[72] and Xiao[73] employed *surfaces* for registration by Chamfer matching, a technique which uses a pre-computed distance map for fast computation of the distance between two surfaces[74]. Liu[75] also used a Chamfer-like technique, employing *cores* instead of surfaces, with a full scale-space distance metric. A core can be defined as a multi-scale instance of a medial axis, *i.e.*, a structure, supported by a quench-like function, that runs "in the middle" of some perceived object. Petti[76] performed registration by maximizing the overlap, or, more precisely, by minimizing the "exclusive or" (XOR) overlap of *segmented* solid structures. Finally, Lemieux[77] studied the accuracy of *frame-based* registration relative to the accuracy of *marker* detection.

[70](Guéziec & Ayache 1992, Ayache et al. 1993, Guéziec 1993)
[71](Thirion 1994, Thirion 1996*a*)
[72](van Herk & Kooy 1994)
[73](Xiao & Jackson 1995)
[74](Borgefors 1988)
[75](Liu et al. 1994)
[76](Petti et al. 1994)
[77](Lemieux, Kitchen, Hughes & Thomas 1994, Lemieux & Jagoe 1994)

3D morphing of CT skulls was performed by Christensen[78], who *elastically* morphed infants skulls to an *atlas* by locally minimizing the intensity difference, after an initial *rigid* alignment based on *anatomical landmarks*. Fang[79] performed interspecies morphing of the skull based on *anatomical landmarks*, between human and macaque skulls.

Local elastic 3D intrasubject CTA registration was performed by Bani-Hashemi[80] and Yeung[81], by extending methods used in DSA to 3D. The former used the DSC criterion, while the latter searches for a matching voxel by finding the voxel closest (in the squared sense) in grey value.

2.10.1.2 Monomodal applications: rigid and affine MR registration

Fully interactive rigid registration methods are described by Morris[82] and Pietrzyk[83]. Alpert[84] registers by alignment of the *principal axes* and the center of gravity. Ettinger[85] also uses these for a pre-registration, but then refines the transformation using a semi-automatically extracted intra-cranial *surface* with a Gaussian weighted distance function. Approximately the same method is implemented by Rusinek[86], which does not weigh the distance, but supplies an *affine* instead of a rigid transformation. Their method is (an extension of) the well-known "head-hat" *surface* matching technique, minimizing the squared distance between two segmented (skin) surfaces, originally presented by Pelizzari and co-workers, including Levin[87], who documented its use on the current application. *Rigid surface* based Chamfer matching was used by Jiang[88] on *manually segmented surfaces*, and extended by Zuk[89], who added hierarchical surface point sampling. Various *surface based* methods using Besl's[90] ICP algorithm were implemented by Feldmar. In (Feldmar & Ayache 1994), ICP was used directly on *segmented surfaces* to find an *affine* transformation. In (Feldmar &

[78](Christensen et al. 1996)
[79](Fang et al. 1996)
[80](Bani-Hashemi et al. 1996)
[81](Yeung et al. 1994)
[82](Morris et al. 1993)
[83](Pietrzyk et al. 1994)
[84](Alpert et al. 1990)
[85](Ettinger, Grimson, Lozano-Pérez, Wells III, White & Kikinis 1994, Ettinger, Grimson & Lozano-Pérez 1994)
[86](Rusinek et al. 1993)
[87](Levin et al. 1988)
[88](Jiang, Holton & Robb 1992, Jiang, Robb & Holton 1992)
[89](Zuk et al. 1994)
[90](Besl & McKay 1992)

Ayache 1996) the segmented surface was elaborated to an 8D structure: not only the spatial coordinates were used in the cost (distance) function computation, but also the surface normals and the principal curvatures. In (Feldmar et al. 1996) the 'surface' needed no segmentation, since the entire 3D image was considered to be a surface in 4D (spatial coordinates plus intensity) space.

Rigid registration based on *segmented curves* was done by Guéziec[91], by using the crest lines of a surface, which was extracted by using a *deformable model*. Thirion[92] also employed crest lines, but used only their curvature-extremal *points* in the registration process. Pennec[93] examined the precision of this method.

Collignon[94] performed *rigid* registration by using *segmentation*: each set is segmented using K-means clustering, and the registration is performed by minimizing the "fuzziness" between corresponding segments. He later used clustering of the joint histogram of the images to find the transformation in a *full image content* based method. Hill[95] used a similar method based on minimizing the histogram dispersion using the third order moment of the histogram. Other *full image content* based methods were proposed by Hajnal and Bandari. The former[96] performed *rigid* registration by minimizing the squared intensity differences in the brain, which needs to be segmented first. The latter[97] finds translation between the images to be registered by gluing them together and regarding the compound as a time series. The second image is then registered to the first by finding the occurrence of the cepstral echo of the first image in the time series. Finally, Collignon[98] and Maes[99] (*rigid* transformations), simultaneously with Viola[100] (*affine* and higher order transformations) used maximization of the mutual information, *i.e.*, the relative entropy, of the joint histogram to achieve registration.

Several methods, amongst which *frame* and *mould* based registration, head-hat *segmented surface* registration, *anatomical landmark* based methods, and ratios of voxel variance based methods, where compared by Strother[101].

[91](Guéziec 1993)
[92](Thirion 1994, Thirion 1996*a*)
[93](Pennec & Thirion 1995)
[94](Collignon et al. 1994)
[95](Hill et al. 1994, Hill & Hawkes 1994)
[96](Hajnal, Saeed, Oatridge, Williams, Young & Bydder 1995, Hajnal, Saeed, Soar, Oatridge, Young & Bydder 1995)
[97](Bandari et al. 1994)
[98](Collignon, Maes, Delaere, Vandermeulen, Suetens & Marchal 1995)
[99](Maes et al. 1996)
[100](Viola & Wells III 1995, Viola 1995, Viola et al. 1996)
[101](Strother et al. 1994)

2.10.1.3 Monomodal applications: curved MR registration

Elastic deformation of segmented curves or surfaces to corresponding structures was performed on two-dimensional slices by Nakazawa[102], where the correct slices needed to be selected *manually*. The same approach, except fully in *three dimensions* was followed by Christensen and Haller[103], using a fluid model morphing, Davatzikos[104], using elastic deformation of the brain and ventricular surface, Sandor[105], using elastic deformation of morphologically smoothed Marr-Hildreth edges, MacDonald[106], and Thirion[107], using elastic deformations using *demons*, where demons are particles than can either push or pull, depending on what side of the boundary they are on.

Collins[108] performed *curved* registration by local optimization of the cross-correlation based on intensity and gradient values extracted at several scales of resolution. Ge[109] employed *user defined* cortical traces and sub-cortical *landmarks*, and interpolated the curved transformation in undefined areas. Gee[110] used Bayesian modeling applied to various *segmented* structures. Kruggel[111] performed *elastic* registration by minimizing the local squared intensity differences, after an initial global Chamfer matching. Finally, Miller[112] performed *curved* registration by using multi-valued MR images, (T1 weighted, T2 weighted, segment values, *etc.*) by minimizing the squared distance error and the elastic energy.

2.10.1.4 Monomodal applications: PET

All of the encountered PET—PET registration methods of brain images are *3D* and *rigid*, excepting Unser, who provides an *affine* registration. Pietrzyk[113] designed a fully *interactive* method using graphical tools, *e.g.*, rendering, cut-planes, edges, *etc.* Zuk[114] does Chamfer matching, improved with hierarchical

[102](Nakazawa & Saito 1994)
[103](Christensen, Miller, Marsh & Vannier 1995, Haller et al. 1995, Haller et al. 1996)
[104](Davatzikos & Prince 1994, Davatzikos et al. 1996, Davatzikos 1996)
[105](Sandor & Leahy 1994, Sandor & Leahy 1995)
[106](MacDonald et al. 1994)
[107](Thirion 1995, Thirion 1996*b*)
[108](Collins, Neelin, Peters & Evans 1994, Collins, Peters & Evans 1994, Collins et al. 1995)
[109](Ge et al. 1995)
[110](Gee et al. 1993, Gee et al. 1994, Gee, le Bricquer & Barillot 1995, Gee & Haynor 1996)
[111](Kruggel & Bartenstein 1995)
[112](Miller et al. 1993)
[113](Pietrzyk et al. 1994)
[114](Zuk et al. 1994)

data sampling, on *segmented* surfaces. The remaining methods are *Full image content* based: Andersson[115] registers by optimizing the cross-correlation values in image ares near edges, where edges are defined by thresholding gradient images of the Gaussian filtered original. Eberl[116] and Unser[117] find the optimal transformation by optimizing the SAD (sum of absolute differences of intensity values). Finally, Hoh[118] also uses the SAD, and compares it to results obtained by optimizing the SSC criterion.

2.10.1.5 Monomodal applications: SPECT

The method of Eberl[119] from the previous section, using the SAD, also applies to SPECT registration. A similar *3D rigid, using full image content* method, based on minimizing the sum of squared intensity differences, was suggested by Lange[120]. Other *full image content* based methods were implemented by Barber, Junck, Maintz, Meunier, and Pavía. Barber[121] finds an *global affine* transformation by minimizing the optic flow field. Meunier also uses minimizes the optic flow field, but finds a *local curved* transformation. For a pre-registration, he uses the optic flow method global *rigidly*. Junck[122] finds 2D *rigid* transformations by optimizing the cross-correlation. Also, the image midline in transversal images is found by optimizing the correlation between the left and mirrored right part of the image. Maintz[123] and Pavía[124] also directly use the cross-correlation, but in a *3D rigid* manner. The former uses an hierarchical approach to optimization, the latter employs a pre-registration using principal axes. Zubal[125] uses the head-hat method on *segmented surfaces*, possibly combined with *user defined anatomical landmarks* to find a *3D rigid* transformation. *3D rigid* methods based solely on *user defined anatomical landmarks* are compared with methods based on *external markers* (both *automatically* and *semi-automatically* detected) by Leslie[126]. Finally, two *interactive 3D rigid* methods are reported on: Rubinstein[127], who

[115](Andersson 1995)
[116](Eberl et al. 1996)
[117](Unser et al. 1995)
[118](Hoh et al. 1993)
[119](Eberl et al. 1996)
[120](Lange et al. 1993)
[121](Barber et al. 1995)
[122](Junck et al. 1990)
[123](Maintz, Beekman, de Bruin, van den Elsen, van Rijk & Viergever 1996)
[124](Pavía et al. 1994)
[125](Zubal et al. 1995)
[126](Leslie et al. 1995)
[127](Rubinstein et al. 1996)

uses *anatomical landmarks*, and Stapleton[128], where the user defines the Talairach coordinate system by pointing out the midline, the AP (anterior-posterior) center line, and the OM (orbitomeatal) line, in the latter case aided by a single lead marker.

2.10.1.6 Monomodal applications: portal images

Since portal imaging appears exclusively in radiotherapy treatment settings (in fact, a portal image is obtained by measuring the transmission of the radiation beam, and hence is a 2D image), applications are only found in this specific field. Only three method instances were found: Dong[129] and Hristov[130] find respectively a *global affine* and a *global rigid* transformation by optimizing the cross-correlation. Radcliffe[131] uses basically the same method, but speeds it up by using pseudo-correlation, which limits the computations to randomly selected small regions.

2.10.1.7 Monomodal applications: DSA

Venot[132] introduced the DSC criterion for finding a *rigid global* registration of the X-ray images involved in DSA. Hua[133] compared the registration performance of DSC on original images, DSC on grey-valued edge images, and of cross-correlation optimization. Leclerc[134] used generalized cross-correlation for finding a *local curved* transformation, in a *computed* way by implementation in a Fourier transfer-function setting. Cox[135], finally, performed *local curved* registration by locally minimizing the intensity variance.

2.10.1.8 Other monomodal applications

Shields[136] registered *2D time series* of US carotid images in an *affine* way by locally matching the first order image grey value Taylor expansion, and vali-

[128](Stapleton et al. 1995)
[129](Dong & Boyer 1996)
[130](Hristov & Fallone 1996)
[131](Radcliffe et al. 1993, Radcliffe et al. 1994)
[132](Venot et al. 1983, Venot et al. 1984, Venot & Leclerc 1984)
[133](Hua & Fram 1993)
[134](Leclerc & Benchimol 1987)
[135](Cox & de Jager 1994)
[136](Shields et al. 1993)

dated the transformation by checking cross-correlation values. Zhao[137] *affinely* registered slices of auto-radiographic imagery (scintigraphic images of cadaver slices), by minimizing displacement of *manually segmented* contours, or directly by minimizing the intensity value differences between images.

2.10.1.9 Multimodal applications: CT—MR

Unless otherwise stated, all of the registrations in this section supply *global rigid* transformations.

Hill[138] used *user identified* anatomical landmarks, to *compute* the transformation. *Identified landmarks*, either *anatomical* or *externally marked*, were also used by Maguire[139], but coarsely, since the *affine* transformation was based on optimizing the cross-correlation in areas around the landmarks. Other *full image content* based methods using cross-correlation were proposed by van den Elsen[140], using the entire image, where the CT grey values are remapped in a local linear fashion to improve correspondence with the MR image, and van den Elsen[141] and Maintz[142], optimizing cross-correlation of ridgeness images extracted from the original modalities. Maintz later[143] included optimization of edgeness cross-correlation and compared them.

Wang[144] and Maurer[145] used *invasive fiducial markers*, and compared them to *segmented surface* registration[146]. Maurer also integrated the two methods into a single one[147].

Other *segmented surface* based methods were implemented by Ge, Hemler, Jiang, Levin, Petti, Taneja, van Herk, and Kooy. Ge[148] used an ICP variation for the

[137](Zhao et al. 1993)
[138](Hill, Hawkes, Crossman, Gleeson, Cox, Bracey, Strong & Graves 1991, Hill, Hawkes, Hussain, Green, Ruff & Robinson 1993)
[139](Maguire et al. 1991)
[140](van den Elsen et al. 1994)
[141](van den Elsen & Viergever 1993, van den Elsen 1994, van den Elsen et al. 1995)
[142](Maintz et al. 1994, Maintz, van den Elsen & Viergever 1996*b*)
[143](Maintz et al. 1995, Maintz, van den Elsen & Viergever 1996*a*)
[144](Wang, Fitzpatrick, Maurer & Maciunas 1994, Wang et al. 1995)
[145](Maurer et al. 1993, Maurer, Fitzpatrick, Galloway, Wang, Maciunas & Allen 1995)
[146](Maurer et al. 1994)
[147](Maurer, Aboutanos, Dawant, Margolin, Maciunas & Fitzpatrick 1995)
[148](Ge et al. 1996)

optimization. Hemler[149] used an automatically extracted surface with manual correction. Levin[150] used the head-hat method. Jiang[151] and Taneja[152] used the Chamfer matching technique, which was also used by van Herk[153], and Kooy[154], except in their case the surface segmentation was *automated*. Petti[155] found an *affine* transformation by minimizing the "exclusive or" overlap of segmented solids. One author implemented a non-surface based *segmentation* based method: Collignon[156] proposed the minimization of "fuzziness" in corresponding segments found by K-means clustering of the original images.

Various authors used *surface based* registrations in comparisons to other methods. Hemler[157] compared it to a *frame* based method, and optimization of the cross-correlation of remapped grey values. Vandermeulen[158] compared surface based methods to *frame* based and *anatomical landmark* based methods. Hill[159] compared surface based registration and registration by minimizing the variance of intensity ratios.

Besides the above mentioned cross-correlation methods, other *full image content* based methods were proposed by Collignon, Maes, and Wells. Collignon[160] used clustering of the joint histogram to find the optimal transformation. He also implemented optimizing the mutual information of the joint histogram,[161] a method also used by Maes,[162] and Wells[163].

West[164] compared many (13) *intrinsic* registration methods using a large image database with a "gold" registration standard obtained using *invasive fiducial markers*.

[149](Hemler, Sumanaweera, Pichumani, van den Elsen, Napel & Adler 1994, Hemler, Sumanaweera, Pichumani, van den Elsen, Napel, Drace & Adler 1994, Hemler, Sumanaweera, van den Elsen, Napel & Adler 1995, Hemler, Napel, Sumanaweera, Pichumani, van den Elsen, Martin, Drace & Adler 1995, Hemler et al. 1996)
[150](Levin et al. 1988)
[151](Jiang, Robb & Holton 1992)
[152](Taneja et al. 1994)
[153](van Herk & Kooy 1994)
[154](Kooy et al. 1994)
[155](Petti et al. 1994)
[156](Collignon et al. 1994)
[157](Hemler, van den Elsen, Sumanaweera, Napel, Drace & Adler 1995)
[158](Vandermeulen et al. 1995)
[159](Hill, Hawkes, Harrison & Ruff 1993)
[160](Collignon, Vandermeulen, Suetens & Marchal 1995)
[161](Collignon, Maes, Delaere, Vandermeulen, Suetens & Marchal 1995)
[162](Maes et al. 1996)
[163](Wells III et al. 1995, Wells III et al. 1996)
[164](West et al. 1996)

2.10.1.10 Multimodal applications: CT—PET

Rigid 3D transformations were performed by Alpert[165] using the images *principal axes* and center of gravity, by Chen[166] and Levin[167] using the head-hat method, and Pietrzyk[168], who used a fully *interactive* method. *Affine* registration was obtained by Wahl[169], employing user identified *anatomical landmarks* and *external markers*, and Maguire[170], who optimized cross-correlation around such user identified anatomical landmarks and external markers. The latter method is also used to supply an *elastic* transformation.

2.10.1.11 Multimodal applications: CT—SPECT

Maguire[171] also applied his method to CT—SPECT registration. The only other instance we found was van Herk[172], who used *rigid* Chamfer matching on *automatically* extracted surfaces.

2.10.1.12 Multimodal applications: DSA—MR

Hill[173] used *hand drawn* structures, combined with a distance minimization which incorporated use of anatomical knowledge to *rigidly* register the DSA vessel tree to the MR surface. Henri[174] performed *rigid* registration by least-squares fitting *user identified anatomical landmarks*. The landmarks identified in the MR where projected into the (DSA) plane, after applying the *rigid* transformation to the MR image.

2.10.1.13 Multimodal applications: PET—MR

Pietrzyk[175] performs *rigid* registration by using various graphical objects like edges and cut-planes in a a fully *interactive* manner. Ge[176] uses a more protocol-

[165](Alpert et al. 1990)
[166](Chen et al. 1987)
[167](Levin et al. 1988)
[168](Pietrzyk et al. 1994)
[169](Wahl et al. 1993)
[170](Maguire et al. 1991)
[171](Maguire et al. 1991)
[172](van Herk & Kooy 1994)
[173](Hill, Hawkes & Hardingham 1991)
[174](Henri et al. 1992)
[175](Pietrzyk et al. 1994)
[176](Ge et al. 1994)

ized method, where the user identifies planes, starting with the inter-hemispheric fissure (midsagittal plane) to provide a registration. Meyer[177] performs *affine* registration using *user identified* points, lines and planes simultaneously in a weighted way. His method uses –next to Simplex optimization– distance error minimization by the BFGS (Broyden-Fletcher-Goldfarb-Shanno) approach.

Neelin[178] finds a *rigid* transformation by means of *user identified anatomical landmarks*. Evans[179] also uses these, combined with a *foam mould* for patient immobilization. Later Evans[180] used *fiducial marks* provided by a fiducial band strapped to the head, to find an *affine* transformation. Maguire[181] used *user identified anatomical landmarks* and *external markers*, and found an *affine* or *curved* transformation by optimizing the cross-correlation locally in the identified areas. Wahl[182] uses the same points directly to find an *affine* transformation.

Rigid surface based methods were employed by Chen[183], Levin[184], and Staib[185] using the head-hat method. Turkington[186] used the same method, but *automated* the surface segmentation. Tsui[187] used the head-hat method, but computed the distance in 2D for more efficiency. Jiang[188] uses multi-resolution Chamfer matching. Ardekani[189] uses segmentation obtained by K-means clustering applied to the MR. *Rigid* registration is then performed by minimizing the PET grey value variance in each segment.

Kruggel[190] also uses Chamfer matching, but only as a pre-registration. The final transformation is *elastic* by locally finding the optimal shift minimizing the squared intensity differences. Other *full image content* based methods were implemented by Andersson, Miller, Woods, Collignon, Maes, and Wells: Andersson[191] performed *rigid* registration by simulating a PET image from the MR (by using a simple segmentation, and assigning a plausible radioactivity to each

[177](Meyer et al. 1995)
[178](Neelin et al. 1993)
[179](Evans et al. 1989, Evans, Collins, Neelin & Marrett 1996)
[180](Evans et al. 1991)
[181](Maguire et al. 1991)
[182](Wahl et al. 1993)
[183](Chen et al. 1987)
[184](Levin et al. 1988)
[185](Staib & Xianzhang 1994)
[186](Turkington et al. 1993, Turkington et al. 1995)
[187](Tsui et al. 1993)
[188](Jiang, Robb & Holton 1992)
[189](Ardekani et al. 1994, Ardekani et al. 1995)
[190](Kruggel & Bartenstein 1995)
[191](Andersson et al. 1995)

segment), and registering the simulated and real PET image using optimization of cross-correlation near edges, where the edges are obtained by thresholding a gradient image. Miller[192] performed *curved* registration using multi-valued MR images, (T1 weighted, T2 weighted, segment values, *etc.*) by minimizing the squared distance error and the elastic energy. Woods performed *rigid* registration by minimizing the standard deviation of the PET values corresponding to a single MR grey value. Collignon[193], Maes[194] and Wells[195] performed *rigid* registration by optimizing the mutual information contained in the joint image histogram.

Studholme, Strother, and West compared a large number of *rigid* registration methods: the former[196] used optimization of cross-correlation, minimization of intensity variance, minimization of joint histogram entropy and dispersion by means of the third order moment, and manually *anatomical landmark* registration. Strother[197], compared *frame* and *mould* based registration, head-hat *segmented surface* registration, *anatomical landmark* based methods, and ratios of voxel variance based methods. West[198] compared many (11) intrinsic methods to a registration based on *invasive fiducial markers*. Finally, Wang[199] investigated the use of registration in a clinical measurement study.

2.10.1.14 Multimodal applications: SPECT—MR

Rubinstein[200] and Malison[201] performed *rigid* registration *interactively* using *anatomical landmarks*. Maguire[202] also used *user identified anatomical landmarks*, or user identified external markers, but performed *affine* or *curved* registration by locally optimizing the cross-correlation in the identified areas. Kruggel[203] after an initial Chamfer match using segmented surfaces, performed *elastic* registration by minimizing the local squared intensity differences. Maintz[204]

[192](Miller et al. 1993)
[193](Collignon, Maes, Delaere, Vandermeulen, Suetens & Marchal 1995)
[194](Maes et al. 1996)
[195](Wells III et al. 1995, Wells III et al. 1996)
[196](Studholme et al. 1995*b*, Studholme et al. 1995*a*)
[197](Strother et al. 1994)
[198](West et al. 1996)
[199](Wang, Volkow, Levy, Fowler, Logan, Alexoff, Hitzemann & Schyler 1996)
[200](Rubinstein et al. 1996)
[201](Malison et al. 1993)
[202](Maguire et al. 1991)
[203](Kruggel & Bartenstein 1995)
[204](Maintz, van den Elsen & Viergever 1996*c*)

computed a *rigid* transformation by optimizing the cross-correlation of the "edgeness" of the skin, computed using morphological operators. The other reported methods are all *rigid* and *surface based:* Turkington[205] used the head-hat method with automated surface segmentation. Jiang[206] used multi-resolution Chamfer matching on semi-automatically segmented surfaces, as did Rizzo[207]. Finally Péria[208] performed registration using the facial surface. Since such a surface is absent in a detailed way in SPECT images, a calibrated laser range facial surface was used instead.

2.10.1.15 Multimodal applications: US or TMS—MR

Since both TMS and US transducers can be hand-held devices, registration is often obtained using *calibrated coordinate systems*, under the assumption that strict patient immobilization can be maintained. A registration based on calibrated coordinate system is by definition *rigid*. Ettinger[209] registered TMS to pre-TMS acquired MR via calibrating the TMS probe to a laser range scanner. The laser skin surface is then registered to the automatically segmented corresponding surface obtained from the MR. Erbe[210] registered intra-operative US to pre-operative MR via a pre-operative US calibrated to the intra-operative one. The pre-operative US (and hence, by calibration, the intra-operative one) is registered *rigidly* to the MR by means of *user identified anatomical landmarks*. Hata[211] calibrated 2D US to a 3D MR system, but refined the obtained rigid registration by local Chamfer matching on semi-automatically extracted contours and surfaces.

2.10.1.16 Multimodal applications: X-ray

Betting[212] registered MR (or CT) to X-ray images (*2D/3D*) by a "silhouette" method: *automatic* extraction of the external contours in all involved images, followed by *3D rigidly* transforming the MR, projecting the transformed contours onto the X-ray plane, and minimizing the contour distance using a variation of the

[205](Turkington et al. 1993)
[206](Jiang, Robb & Holton 1992)
[207](Rizzo et al. 1995)
[208](Péria et al. 1994)
[209](Ettinger et al. 1996)
[210](Erbe et al. 1996)
[211](Hata et al. 1994)
[212](Betting & Feldmar 1995)

ICP algorithm. Lavallée[213] registered a *3D* CT to *two* X-ray images, acquired at a known angle to one another. From the X-ray planes in 3D space, the (*segmented*) external contours are projected out of plane, creating a bundle. The intersection of the two X-ray bundles defines an interior into which the CT is *rigidly* placed, minimizing the distance of the CT external surface to the bundles.

Both Betting and Lavallée aim to use their methods in a *patient to modality* intra-operative setting, using the 2D X-ray images for intermediaries. Therefore, their methods also appear in the *patient to modality* section, if experiments have been conducted using real patient data.

In radiotherapy literature, three instances of *rigid 2D/2D* X-ray to portal image registration were found. Eilertsen[214] finds the radiation field edges by means of a Radon transform. The X-ray (simulator) image is then registered *automatically* to the portal images by aligning the field edge corners. Ding[215] also uses *landmarks*, either *geometrical* or *anatomical*, but *interactively* defined. Leszczynski[216] needs the field edges to be defined *interactively*, then performs Chamfer matching to find the correct transformation.

2.10.1.17 Modality to model registration

If models are obtained using statistics on different image data, the distinction between *modality to model* and *modality to atlas* registration is often vague. We subjectively draw the line between use of *fuzzy sets* (atlas) and *localized contours or surfaces* (models). The argument is that in the former case available information is used compounded, while in the latter case the information has been reduced to an average or modal model.

Modality to model registrations are nearly always *curved*. Bajcsy[217] performed elastic registration of a CT feature space (sub-images containing average intensity and edge information) to a model containing the brain and ventricular edges. Cuisenaire[218] also used the brain and ventricular edges, but obtained from MR images. They were extracted from the MR by segmentation using a morphological watershed and closing algorithm. The model was obtained from a brain atlas obtained from a number of cryosectioned brains, and registration

[213](Lavallée & Szeliski 1995, Lavallée, Szeliski & Brunie 1996)
[214](Eilertsen et al. 1994)
[215](Ding et al. 1993)
[216](Leszczynski et al. 1995)
[217](Bajcsy et al. 1983)
[218](Cuisenaire et al. 1996)

was performed by local Chamfer matching. Rizzo[219] registered the cortical surface, obtained *semi-automatically* using edge detection, in an *elastic* fashion to a compartment model. Registration was performed on a slice-by-slice basis, after an initial manual axial correction.

2.10.1.18 Patient to modality registration

Without exception, the reported methods provide *rigid* transformations. This is not surprising, considering that it is very hard to obtain more than surface information from the patient. Paradoxically, there is often a clinical need for curved transformation in the intra-operative occurrence of the registration problem.

Many authors report on using *probes* in solving the patient to modality registration problem. A probe is a device either optically or magnetically tracked, or mounted on a robot arm, so the spatial location of the probe tip is known accurately at all times. Bucholz[220] used CT, MR and PET images acquired with *skin markers*. After the image acquisition, the marker locations are marked with ink. During surgery, the patient wears a reference ring with LEDs clamped to the patient, which position is tracked optically. The ring is calibrated to the patient head position by probing the skin marker locations, hence the pre-operative images are calibrated to the patient. Edwards[221] used the probe in one of three registration approaches using a CT image. Either *anatomical landmarks* or *fiducials* where identified in the image and on the patient using the probe, or the skin surface was *segmented* from the CT and indicated on the patient by probing many surface points. The obtained spatial locations where subsequently registered using point or surface registration methods. The registration method using identifying *fiducials* and probing them during surgery is also used by Fuchs[222] who used *skin markers* and a CT image, and Maurer[223], who used an MR image and *invasive fiducials*. The method of registering a *segmented surface* from the CT image and a probed patient skin surface is also used by Henderson[224] using a CT image, and Ryan[225] and Wang[226] using an MR image.

[219](Rizzo et al. 1995)
[220](Bucholz et al. 1994)
[221](Edwards, Hill, Hawkes, Spink, Colchester, Strong & Gleeson 1995, Edwards, Hawkes, Hill, Jewell, Spink, Strong & Gleeson 1995)
[222](Fuchs et al. 1996)
[223](Maurer, Fitzpatrick, Galloway, Wang, Maciunas & Allen 1995)
[224](Henderson et al. 1994)
[225](Ryan et al. 1995)
[226](Wang, Toro, Zeffiro & Hallett 1994)

Approaches using *stereo video* images of the patient where proposed by Evans, Betting, and Henri. Evans[227] identified *anatomical landmarks* on a stereo video image as well as in pre-operatively acquired CT or MR images to obtain registration. Betting[228] and Henri[229] used the skin surface extracted from the video image and a pre-operative image to find the registration transformation. Betting used either CT or MR images, Henri MR images. The registration methods use either Chamfer matching or ICP.

The extraction of the surface from stereo video images is not an easy task, and many authors use the skin surface as obtained by *laser range scanning* to obtain this surface, and register it with the skin surface *segmented* from pre-operative images. Cuchet[230] used this method with MR images, Grimson[231] used both CT or MR, and Harmon[232] and Vassal[233] only CT. The last author uses the method in a radiotherapy setting instead of the surgical theater, and also describes a different method, which is to perform the registration of patient to pre-treatment 3D CT by means of two X-ray or two portal images acquired at a known angle during the treatment. From all of the images involved contours are segmented. From the CT image, DRRs (Digitally Reconstructed Radiographs) are created, and registered to the real X-ray or portal projection images using minimization of the contour distance. Similar methods which use two acquired intra-treatment projection images for registration to a pre-treatment CT image are described by Vassal[234], Gilhuijs[235], who uses bone ridges for contours, Gall[236], who does not use contours, but *user identified invasive markers* (tantalum screws), Leung Lam[237], who used implanted and surface *markers*, and Bainville[238], who reconstructs a surface from the two radiographs. Lemieux[239] uses a similar method, but in a surgical setting by optimizing the cross-correlation between two intra-operative X-ray images and two DRRs from pre-operative CT.

The only truly *2D/3D* method (all the other ones are intrinsically *3D/3D*) was

[227](Evans, Strong, Colchester, Zhao & Holton-Tainter 1996)
[228](Betting et al. 1995)
[229](Henri et al. 1995)
[230](Cuchet et al. 1995)
[231](Grimson, Lozano-Pérez, Wells, Ettinger, White & Kikinis 1994, Grimson, Lozano-Pérez, Wells III, Ettinger, White & Kikinis 1994*a*, Grimson, Lozano-Pérez, Wells III, Ettinger, White & Kikinis 1994*b*, Grimson et al. 1995, Grimson et al. 1996)
[232](Harmon et al. 1994)
[233](Vassal et al. 1995)
[234](Vassal et al. 1995)
[235](Gilhuijs et al. 1996)
[236](Gall & Verhey 1993)
[237](Leung Lam et al. 1993)
[238](Bainville et al. 1995)
[239](Lemieux, Jagoe, Fish, Kitchen & Thomas 1994)

proposed by Betting[240] who used the silhouette method described in section 2.10.1.16 for registration of a single X-ray to pre-operatively acquired CT or MR.

A number of the above described methods are reported on by Hamadeh[241], as used at a single site.

2.10.2 Registration of thoracic images

Registration of imaging of the thorax has three major application areas: *global*, *cardiac* and *breast*.

2.10.2.1 Registration of global thoracic images

Eberl[242] performed *3D rigid* registration of *monomodal* PET or SPECT images of the thorax by minimization of the SAD. In radiotherapy, two *2D* applications are reported. Moseley[243] performed *monomodal affine* portal image registration using a two-pass approach: local translation-only registration is performed in a number of user defined regions by optimizing the cross-correlation. Then, the local shifts are combined (by least squares fitting) into a global *affine* transformation. Wang[244] performed *rigid* registration of a portal to an X-ray (simulator) image by *moment* matching of the extracted radiation field edges. The edges were extracted automatically by using a morphological gradient and thresholding.

2.10.2.2 Registration of cardiac images

Cardiac image registration almost exclusively involves the use of *3D monomodal scintigraphic images*; we located only three exceptions. Tom[245] performed *2D curved automatic* registration on series of X-ray angiographic images, by matching the skeletons of segmented arteries. Savi[246] obtained *3D rigid* registration of US and PET images by aligning three *user defined anatomical landmarks*.

[240](Betting & Feldmar 1995)
[241](Hamadeh, Lavallée, Szeliski, Cinquin & Péria 1995)
[242](Eberl et al. 1996)
[243](Moseley & Munro 1994)
[244](Wang & Fallone 1994)
[245](Tom et al. 1994)
[246](Savi et al. 1995)

Thirion[247] performed *3D curved surface* registration on CT images using demons on segmented surfaces.

Thirion applies the same method to SPECT images. Other *curved* methods are reported by Goris and Lin. The former[248] accomplishes *automatic 3D curved* SPECT-SPECT registration by using an ICP variation on extracted Canny edges in a 3-step way: first globally rigid, then affine, and finally locally *curved* by using a spline representation. The latter obtains a *3D curved* transformation between two PET sets *automatically* by a *voxel based* method on image subcubes. The actual paradigm used is not reported.

A *2D rigid* method based on *geometrical landmarks* was proposed by He[249] for SPECT images. After the user selects the mid-ventricular slice, the algorithm finds the two local maxima along each image horizontal image line, and then locates the local minimum in between them. It then least-squares fits a line trough the minima, and the resultant models the left ventricular long axis. Registration is performed by aligning the found axes from two images.

3D automatic voxel property/full image content based methods are reported by Bacharach, Bettinardi, Eberl, Hoh, Perault, and Slomka. All but Slomka's method are *rigid*. Bacharach[250] performed PET-PET (emission) registration by optimizing the cross-correlation of the accompanying transmission scans[251]. He assumes the transmission and emission scans are internally registered. This is not always the case, as the patient is moved from the scanner bed after the transmission scan for tracer injection. Bettinardi[252] registers the PET transmission to the emission scan, by making a *second* transmission directly following the emission scan. He assumes the emission and second transmission scan registered, and can therefore register the first transmission to the emission scan by optimizing the cross correlation between the two transmission scans. Cross-correlation is also used for registering different PET (emission) scans by Perault[253], *i.e.*, rest and stress scans of one patient. Eberl[254] finds the optimal transformation between two SPECT or PET images by optimizing the SAD. Hoh[255] also uses the

[247](Thirion 1995)
[248](Goris et al. 1996)
[249](He et al. 1991)
[250](Bacharach et al. 1993)
[251]Many PET scanners come equipped with the possibility of transmission scanning prior to tracer injection and normal emission scanning. A radioactive line source is employed for this, and the resulting transmission image has a CT-like character and is used for a tissue attenuation map in the emission image reconstruction.
[252](Bettinardi et al. 1993)
[253](Perault et al. 1995)
[254](Eberl et al. 1996)
[255](Hoh et al. 1993)

SAD on PET images only, and compares the performance to optimizing the SSC. Finally, Slomka, performs *affine atlas* SPECT registration by minimization of the SAD, after an initial estimate using alignment of *principal axes*. His atlas is created by averaging a large number of normal SPECT scans registered in the same way.

Three authors report on *surface* based methods. Declerc[256] performs *affine or curved automatic* registration by a variation of ICP on two SPECT images using a surface based on pruned edges detected in a 3D polar map. Feldmar[257] also used an ICP variation on SPECT images. See section 2.10.1.2 for a description. Pallotta[258] obtained a *3D rigid* transformation between two (emission) PET scans by Chamfer matching of *surfaces* obtained by thresholding the accompanying transmission scans.

2.10.2.3 Registration of breast images

Consensus of registration of breast images seems to be that it is archetypal to the non-rigid registration problems. Perhaps the thus induced complexity is the reason that little attempt has been made to solve the registration problem. This makes Zuo's recent publication[259] all the more surprising, since it claims that serially acquired MR images (with and without a contrast agent) of a freely suspended breast imaged using a breast coil, display only *rigid* motion, if any at all. In this chapter, *3D* motion correction is performed using the *full image content* employing Woods' (1993) minimization of variance of intensity ratios. The only other publication found[260] performed *automatic 3D curved* registration on two MR images with and without contrast agent by minimizing the sum of squared intensity differences between the images. For a pre-registration, the same procedure was first applied in an *affine* manner.

2.10.3 Registration of abdominal images

Registration of abdominal images appears only as applied to renal or hepatic images in the literature.

[256](Declerc et al. 1996)
[257](Feldmar & Ayache 1994, Feldmar et al. 1996, Feldmar & Ayache 1996)
[258](Pallotta et al. 1995)
[259](Zuo et al. 1996)
[260](Kumar, Asmuth, Hanna & Bergen 1996)

Renal images: Venot[261] applied *2D automatic rigid* registration to DSA images of the kidney by minimizing the DSC criterion. In the same application of DSA images, Buzug[262] found a *2D automatic affine* transformation by combining local translations found in image subcubes by minimizing the entropy of the subtraction image. Péria[263] performed *non-image based 3D automatic rigid* registration of US and SPECT images by calibrating the US scanner to the SPECT coordinate system, and acquiring the US image while the patient is still on the SPECT gantry.

Hepatic images: Venot[264] applied the same DSC strategy mentioned above to SPECT images of the liver. Hoh[265] finds a *3D rigid automatic* registration in a similar way by minimizing the SAD or SSC criterion. Scott *3D rigidly* registers CT or MR images to SPECT images by using the head-hat method on *manually* drawn contours[266], or using CT external contours and contours obtained from an abdominal *fiduciary* band in SPECT[267].

2.10.4 Registration of pelvic images

Except for Venot and Studholme, all of the encountered papers appear in the context of radiotherapy. Venot[268] performed *2D rigid automatic* registration of DSA images of the iliac arteries by means of optimizing the DSC criterion. Studholme found a *3D rigid automatic* transformations between MR and PET images by optimization of the mutual information of the joint histogram.

The radiotherapy applications can be divided in *2D* applications, and *3D patient to modality* registration applications. *2D* applications where proposed by Dong, Ding, Eilertsen, Fritsch, Gilhuijs, and Wang. Dong registered portal images in a *2D affine automatic fashion* by optimization of the cross-correlation. Ding[269] registered X-ray to portal images by means of *user identified landmarks*. Eilertsen[270], in the same application, uses alignment of the corners of the field

[261](Venot & Leclerc 1984)
[262](Buzug & Weese 1996)
[263](Péria et al. 1995)
[264](Venot et al. 1983, Venot et al. 1984)
[265](Hoh et al. 1993)
[266](Scott et al. 1994)
[267](Scott et al. 1995)
[268](Venot & Leclerc 1984)
[269](Ding et al. 1993)
[270](Eilertsen et al. 1994)

edges, where the field edges are extracted using a Radon transform. Fritsch[271] registers portal images *rigidly* by minimizing the distance between their cores, *i.e.*, their multi-scale medial axes. Gilhuijs[272] finds a *2D affine automatic* transformation by Chamfer matching extracted edges from X-ray and portal images. Finally, Wang[273] does *2D* translation-only registration of portal images based on phase-only correlation in the Fourier domain.

3D patient to modality registration was done by Troccaz[274], who achieved this by *calibrating* a US probe to the radiotherapy system, and registering pre-treatment CT or MR to the US images by means of *user segmented* surfaces. Four other approaches to *3D patient to modality* were suggested, all of which involve the use of intra-treatment acquired portal or X-ray images. Bijhold[275] performed the registration by employing *user defined anatomical landmarks* in a pre-treatment CT image and the intra-treatment portal or X-ray images. Gall[276] used a similar technique with *invasive fiducial markers* and two X-ray images. Gilhuijs[277] found the transformation *automatically* using 2 X-ray or portal images using the technique described in 2.10.1.18. Vassal[278] used a similar technique for registration of pre-treatment CT or MR to the patient, using two portal or X-ray images, or one of two other techniques, namely a *calibrated* US probe, or *surface based* registration using a patient surface obtained by a *calibrated* laser range finder.

2.10.5 Registration of limb images

Registration of limb images is reported on almost exclusively in the context of orthopedic interventions, notably at the femur. Other application areas include the tibia, calcaneus and humerus, but there are usually few restrictions to adapt a certain registration method to another region. The transformations found are all *rigid*, as they concern mainly the displacement of bones. Hence, modalities always include CT or X-ray images. Since the bone contrast is very high, most methods, even those including segmentation tasks, can be automated.

[271](Fritsch 1993, Fritsch, Pizer, Morse, Eberly & Liu 1994, Fritsch, Pizer, Chaney, Liu, Raghavan & Shah 1994)
[272](Gilhuijs & van Herk 1993)
[273](Wang, Reinstein, Hanley & Meek 1996)
[274](Troccaz et al. 1995)
[275](Bijhold 1993)
[276](Gall & Verhey 1993)
[277](Gilhuijs et al. 1996)
[278](Vassal et al. 1995)

X-ray to CT registration was performed by Ellis and Gottesfeld Brown. Ellis[279] finds a *2D/3D* registration between an (X-ray) röntgenstereogrammetric analysis (RSA[280]) and a CT image, by using *invasive fiducial markers* attached to the bone surface of the tibia. Gottesfeld Brown[281] finds an *automatic 2D/3D* transformation by optimizing the cross-correlation between the X-ray and a DRR from the CT of the femur.

Monomodal 3D CT registration was done by Hemler[282] using surface registration on *manually* corrected, automatically segmented surfaces of calcaneus. Münch[283] performed an *automatic* registration by optimizing the cross-correlation of femural images. Jacq[284] performed *curved automatic* registration on images of the humerus by minimization of the local grey value differences.

Patient to CT modality registration was proposed by Lea, and Simon. Lea[285] gives an overview of current orthopedic methods, notably applied to the femur and tibia. Simon[286] compares *invasive fiducial* and *surface based* methods on femural images, and presents an *automatic* method on the same images using an ICP variation sped up by using Kd-trees[287].

Two other applications are reported on: Ault[288] registered US to CT images in an *automatic* fashion by means of *geometrical landmarks*, corners detected in the US and a surface model obtained from the CT. Finally, Amit[289] performed *2D curved automatic modality to model* registration on X-ray images of the hand by graph matching it to a model containing for nodes all anatomical flexion points.

2.10.6 Registration of spinal images

Except for van den Elsen, all of the reported algorithms are *surface based*. She[290] performs *3D rigid automatic* registration in a *full image content* based

[279](Ellis et al. 1996)
[280]Also known as stereophotogrammetry (SPG).
[281](Gottesfeld Brown & Boult 1996)
[282](Hemler, Sumanaweera, van den Elsen, Napel & Adler 1995)
[283](Münch & Rüegsegger 1993)
[284](Jacq & Roux 1995)
[285](Lea et al. 1994)
[286](Simon, O'Toole, Blackwell, Morgan, DiGioia & Kanade 1995)
[287](Simon, Hebert & Kanade 1995, Simon et al. 1994)
[288](Ault & Siegel 1995, Ault & Siegel 1994)
[289](Amit & Kong 1996)
[290](van den Elsen et al. 1994)

way by optimizing the cross-correlation between a CT and MR image, where the CT grey values are first remapped using localized linear transforms.

Burel and Bainville assume that the two spinal surfaces to be registered are given; no modality is named. The former[291] performs *3D* rotation-only registration by decomposing each surface into its spherical harmonics. Optimization is performed by using their special geometrical invariances. Bainville[292] found a local *curved* spline deformation using the local closest point of the surfaces combined with a regularization term.

Hemler[293] performs *3D rigid* registration of CT and MR images by means of an automatically extracted, user corrected surface. The surface is based on tracked Canny edges. Hamadeh[294] initially suggested the use of four *user identified anatomical landmarks* for *2D/3D* registration of X-ray to CT or MR images. This technique is only used for a pre-registration in later work[295], where *patient to modality* (CT) is performed using a calibrated X-ray in an intermediary step. In the pre-operative CT, a surface is segmented in a *semi-automated* way. From the intra-operative X-ray image contours are extracted by Canny-Deriche edge detection followed by hysteresis thresholding. The contour is then registered to the surface using Lavallée's "bundle" method described in section 2.10.1.16. Lavallée himself uses the very same method[296], but using *two* X-ray images, as described in section 2.10.1.16. In earlier work[297], pre-operative CT is registered to the patient by registering probed points to a surface segmented from the CT. In later work [298] the probed surface can also be replaced by an US image. Szeliski[299], finally, performed *3D curved* registration of CT images, given segmented surfaces, using local spline deformations, where the surface distance computation is simplified using a pre-computed octree distance map.

2.10.7 General papers

Papers that cannot or cannot easily be classified in specific *object* classes, are cited in this section. Typically, such papers contain overviews of methods, gen-

[291](Burel et al. 1995)
[292](Bainville et al. 1995)
[293](Hemler, Sumanaweera, Pichumani, van den Elsen, Napel & Adler 1994, Hemler, Sumanaweera, Pichumani, van den Elsen, Napel, Drace & Adler 1994, Hemler, Sumanaweera, van den Elsen, Napel & Adler 1995)
[294](Hamadeh, Sautot & Cinquin 1995)
[295](Hamadeh, Sautot, Lavallée & Cinquin 1995)
[296](Lavallée & Szeliski 1995, Lavallée 1996)
[297](Lavallée et al. 1994)
[298](Lavallée, Troccaz, Sautot, Mazier, Cinquin, Merloz & Chirossel 1996)
[299](Szelinsky & Lavallée 1994, Szeliski & Lavallée 1994, Szeliski & Lavallée 1996)

eral applicable registration approaches, or correspondences regarding aspects of some method.

2.10.7.1 Overviews

Overviews of papers concerning medical image registration were presented by Maurer[300], van den Elsen[301] and Viergever[302]. Overviews not primarily literature oriented were given by Barillot[303] and Hawkes[304]. Limited Overviews were presented by Collignon[305] (surface based methods), Lavallée[306] (computer aided surgery (CAS) methods), Lea[307] (CAS methods including a graph classification), and McInerney[308] (deformable models used in medical imaging).

2.10.7.2 General methods

The papers in this section are of such a diverse nature that any attempt to categorize them seems artificial. Table 2.1 shows a brief description of each paper.

[300](Maurer & Fitzpatrick 1993)
[301](van den Elsen, Pol & Viergever 1993)
[302](Viergever, Maintz, Stokking, van den Elsen & Zuiderveld 1995)
[303](Barillot, Lemoine, le Bricquer, Lachmann & Gibaud 1993, Barillot, Gibaud, Gee & Lemoine 1995)
[304](Hawkes et al. 1995)
[305](Collignon, Vandermeulen, Suetens & Marchal 1993)
[306](Lavallée 1996)
[307](Lea, Santos-munné & Peshkin 1995, Lea, Watkins, Mills, Peshkin, Kienzle III & Stulberg 1995)
[308](McInerney & Terzopoulos 1996)

Author	Contents
Arun[309]	Rigid landmark registration
Besl[310]	Introduction of the ICP
Bron[311]	Deformable models
Banerjee[312]	2D Cross correlation based control point registration
de Castro[313]	2D registration using Fourier transforms
Christensen[314]	General atlas concerns
Chua[315]	Surface based registration
Carlbom[316]	Physical interactive registration by a blink comparator
Christmas[317]	2D rigid graph matching
Cross[318]	2D rigid graph matching
Huang[319]	2D curve registration
Jain[320]	2D object registration using Bayesian methods
Kittler[321]	Graph matching
Little[322]	Deformable models: locally rigid or elastic
Li[323]	3D image to two 2D images registration
Metaxas[324]	Deformable models
Matas[325]	Color image registration
Péria[326]	CAS: calibrated images and tools
Pietrzyk[327]	Clinical examples of registration
Philips[328]	Point set registration using Voronoi diagrams
Qian[329]	Deformable model
Ravichandran[330]	2D rotation invariant filters using circular harmonic functions
Serra[331]	Elastic curve registration
Sull[332]	Registration by simultaneous use of points, lines, and regions
Shekarforoush[333]	2D Fourier based registration by polyphase decomposition
Taubin[334]	Elastic surface fitting
Uenohara[335]	Tracking of objects in image time series
Wang[336]	3D rigid registration of point sets

Table 2.1 General papers that cannot be classified according to object

2.10.7.3 Correspondences regarding existing methods

Improvements to existing surface based methods are suggested by Collignon[337]. Feldmar[338] proposes an extension to ICP to handle 2D/3D registration. Registration methods based on point sets are addressed by Kanatani[339], who proposes extensions to existing rotation only methods, and Krattenthaler[340], who suggests speed up techniques. Ways to speed up optimization of mutual information based registration are suggested by Pokrandt[341].

[309](Arun et al. 1987)
[310](Besl & McKay 1992)
[311](Bro-nielsen 1995)
[312](Banerjee & Toga 1994)
[313](de Castro & Morandi 1987)
[314](Christensen, Rabbitt, Miller, Joshi, Grenander, Coogan & van Essen 1995)
[315](Chua & Jarvis 1996)
[316](Carlbom, Terzopoulos & Harris 1994)
[317](Christmas et al. 1995)
[318](Cross et al. 1996)
[319](Huang & Cohen 1994)
[320](Jain et al. 1996)
[321](Kittler et al. 1993)
[322](Little et al. 1996)
[323](Li, Pelizzari & Chen 1994)
[324](Metaxas & Kakadiaris 1996)
[325](Matas, Marik & Kittler 1995)
[326](Péria et al. 1994)
[327](Pietrzyk, Herholz, Schuster, von Stockhausen, Lucht & Heiss 1996)
[328](Philips 1994)
[329](Qian et al. 1996)
[330](Ravichandran & Casasent 1994)
[331](Serra & Berthod 1994, Serra & Berthod 1995)
[332](Sull & Ahuja 1995)
[333](Shekarforoush et al. 1996)
[334](Taubin 1993)
[335](Uenohara & Kanade 1995)
[336](Wang, Cheng, Collins & Hanson 1996)
[337](Collignon, Géraud, Vandermeulen, Suetens & Marchal 1993)
[338](Feldmar et al. 1995)
[339](Kanatani 1994)
[340](Krattenthaler et al. 1994)
[341](Pokrandt 1996)

2.11 Related issues

2.11.1 How to use the registration

After a registration has been obtained, two questions appear paramount: *How accurate is the computed registration?* and *How can it be used?* The latter question presents us with an entire area of research of its own: the answer may be quite simple, *e.g.*, only some statistical property of the subtracted registered images is required, to highly complex, *e.g.*, a hybrid transparent stereo rendering that needs to be projected onto an operating microscope ocular is asked for. Such complex uses invariably require non-trivial visualizations in which segmentation must figure. This creates a paradox: on the one hand, many registration applications show how intertwined the problems of registration and segmentation can be, and hence the designer of the registration algorithm is tempted to draw on his own expertise in answering the question on how the registration is to be used; indeed, this question must have figured in the registration algorithm design, which should have started out with a clinical need for registration. On the other hand, once a registration is obtained, the problem of *How to use it?* poses interdisciplinary problems of a previously unencountered nature. Be that as it may, fact is that few registration papers attempt to follow up on the use of the registration, and likewise few papers in a vast plethora of visualization papers employ registered images for input[342]. The cause for this may be found in the fact that visualization solutions are often highly specific and problem dedicated, and the interdisciplinary nature of the problem. In other words: the areas of registration and visualization are still widely apart; not many registrations use state-of-the-art visualization, nor do many visualizations use registered input. Such solitary stances can be observed concerning other research areas too: registration and segmentation have many a common interest, yet are seldom integrated. Also, registration is rarely used in many clinical applications, even though such applications may benefit from registered images; in many cases the potential of image registration is still an unknown. This can be accredited to the fact that registration research is relatively young area where many applications are concerned, to the fact that registration often involves new visualizations that possibly come with a steep interpretation learning-curve, to the fact that registration accuracy is often very hard to quantify sufficiently, to the logistic problems involved in integrating digital (or even analog) data from different machines often departments apart, to the extra equipment and time needed, and

[342] Mostly the area of segmentation-free image *fusion* addresses this problem, but its applications to medical image problems are severely limited (Burt 1993, Chou, Chen, Sudakoff, Hoffmann, Chen & Dachman 1995, Li, Manjunath & Mitra 1994, Li, Manjunath & Mitra 1995, Pietrzyk et al. 1996, Wasserman, Rajapakse & Acharya 1994, Wasserman & Acharya 1995, Wahl et al. 1993, Zhou 1994).

to the interdisciplinary gap. The point of this long-winded periphrastic soliloquy is that the question *how can the registration be used* is for the most part still unanswered: even though the need for registration is born out of a clinical need, the track *after* obtaining the transformation parameters is still largely blank.

2.11.2 Validation

The other question concerning a computed registration entails the accuracy. The answer is non-trivial for the simple reason that a gold standard is lacking regarding clinical practice. We can usually only supply a measure of accuracy by reference to controlled phantom studies, simulations, or other registration methods. Such measures are often lacking as concerns clinical needs: not only does a thus obtained reference accuracy require the need for an accuracy *variability* measure –since the accuracy cannot be made local in a clinical example, and therefore needs to be supplied with reliability bounds–, but neither do such measures easily transfer to particular clinical cases, *e.g.*, instances of abnormally distortive pathology.

There is a widespread quest for measures that somehow quantify registration accuracy. In our opinion, such a task is paradoxical, because of the simple fact that if such measures existed, *they would be used for registration paradigms*[343] Which brings us to a positivistic statement on accuracy: *We cannot, with absolute certainty, quantify local registration errors. However, given that we can transfer error measures obtained by reference, we can eventually say that it is* unlikely *for the error to exceed a certain bound.*

For many applications, the phase where sufficiently small errors can be ascertained has not yet been reached. In many instances, proper accuracy studies are just starting. What is particularly hampering to giving any statistics on certain methods is not only the incomparability of accuracy experiments done on particular sites–images are often proprietary, implementation and circumstances site specific, circumstances are different *etc.* – but also the imprecise use of the terms *accuracy*, *precision*, and *robustness* in many studies. The notion that public databases of representative images are to be created, and validation protocols need to be assembled, is only now emerging. The involved logistics, cost, and effort, however, make prospects Utopian for many registration applications.

[343] As with many bold statements, this one is not entirely true, in the sense that we cannot simply use any paradigm, *e.g.*, since we are restricted in terms of computation time and convergence properties of the criterion used. Nevertheless, the gist of the statement holds.

2.11.2.1 Validation definitions

Validation of a registration embodies more than the accuracy verification. The list of items includes:

- Precision
- Accuracy
- Robustness/stability
- Reliability
- Resource requirements
- Algorithm complexity
- Assumption verification
- Clinical use

Except for the first two items (treated in the next paragraph), where the distinction is at times vague, unique definitions can be supplied. *Robustness* or *stability* refers to the basic requirement that small variations in the input should result in small variations in the output, *i.e.*, if input images are aligned in a slightly varied orientation, the algorithm should converge to approximately the same result. *Reliability* is the requirement that the algorithm should behave as expected, given a reasonable range of possible clinical input. *Resource requirements* concern the material and effort involved in the registration process. These should be reasonable relative to the clinical merit obtained from the registration. The *algorithm complexity* and related computation time should be adapted to the time and resource constraints of the clinical environment. Time can be a constraint in a two fold manner; either a single registration needs to be performed on-line because of direct clinical requirements, or multiple registrations appear in clinical *routine*, and need to be performed in a reasonable time frame so as not to cause lag in the clinical track. The *assumptions* on reality made in the paradigm and optimization modeling should be verified to hold up sufficiently in practice. Finally, the *clinical use* should be verified: does the registration provide in a clinical need, and does its use outweigh available alternatives? In ideal circumstances, all of the criteria should be satisfied. However, it is unrealistic to assume that all criteria can be met within one application; the weight attached to each criterion is application dependent, and a matter of judgment.

We have not yet defined *precision* or *accuracy*. For the problem at hand, we stray somewhat from conventional definitions. We define *precision* as the typical systematic error that can be obtained when the registration algorithm is supplied

with idealized input. For example, a simple one dimensional shift optimization algorithm that does exhaustive searching with a resolution of two pixels, is expected to perform with a precision of within two pixels when given ideal input, *e.g.,* two identical images. In a more complex vein, a local error measurement obtained at an invasive fiducial marker used in the registration process can be regarded as a precision measure. Precision measures can be obtained concerning the entire registration system, or applying to specific components, like the patient (movement, artifacts), the acquisition, the paradigm, and the optimization, although we are tempted to remove the patient from the list, as modeling and quantizations are hard here. *Accuracy* is a more direct measure, referring to the actual, "true" error occuring at a specific image location. Where precision is a system property, accuracy applies to specific registration instances. Accuracy will be the property that immediately concerns the clinician: for example, the surgeon can point at the screen and say "I must make an incision *here*. How accurate can this location be determined in the patient?". Accuracy can be divided into *qualitative* and *quantitative* accuracy. The former can usually be supplied using simple visualization tools and visual inspection, *e.g.,* when registering CT and MR brain images, overlaying the segmented bone contours onto MR slices supplies the clinician with a reasonable idea of accuracy. *Quantitative* accuracy, as pointed out before, needs a ground truth that is unavailable in clinical practice, and therefore needs to be emulated by reference to another measure.

Typically, evaluations of a registration method as concerns accuracy and precision (and other criteria) may occur at a number of levels: *synthetic*, *phantom*, *pre-clinical*, and *clinical*. The *synthetic* level is entirely software-based. The images used at this level can be controlled in every aspect. If images are *simulated* emulating the clinical acquisition, we speak of a *software phantom*. The merits of software phantoms include the availability of ground truth, and the fact that realistic image degrading factors can be controlled. The (physical) *phantom* level makes use of true image acquisitions, usually imaging anthropomorphic models. At this stage, ground truth is no longer available, but it can be approximated with high accuracy by introducing markers into the phantom, by using multiple acquisitions, and the fact that phantom movements can be controlled. The *pre-clinical* level involves using real patient (or volunteer) or cadaver data. Ground truth can again only be approximated at this level, although frequently accurately so by reference to a registration based on an established registration method. Cadaver studies offer good opportunities here, as patient movement is absent or fully controlled, and patient friendliness can be disregarded in obtaining the registration standard. Studies using real patient data should optimally employ images drawn from a database containing generic as well as acquisitionally and pathologically exceptional data. Finally, at the *clinical* level the registration method is used in the clinical routine, at the intended application

level. At this stage, a reference registration may or may not be available, and validation should primarily be turned over to the clinicians involved.

2.11.2.2 Validation: a survey

As mentioned before, validation studies are only now emerging. Many papers address some precision or accuracy validation at some level, but few extensively so, and even then is precision often restricted to the algorithmic level. Given the effort and time that needs to be expended in a complete validation study, this is not surprising, nor would it be a realistic expectation from authors presenting some new registration paradigm.

Those instances of validation we found are cited in this paragraph. We do not include robustness studies, nor precision studies not exceeding the algorithm level, *i.e.*, authors adding known transformations to input images to see if they can be recovered by the algorithm. Validation studies are frequently part of a paper presenting a new registration approach, but some papers are dedicated[344] entirely to validation.

Method validation by reference to external marker based methods can be found in[345]. Validation by comparison to registration based on probed points is found in[346], by comparison to manually identified anatomical landmark based registration in[347], and by comparison to frame based registration in[348]. Cross-method validation (reference to other intrinsic methods than the one principally used) is

[344] See, *e.g.*, (Holton, Taneja & Robb 1995, Holton et al. 1995, Lemieux, Kitchen, Hughes & Thomas 1994, Lemieux & Jagoe 1994, Maurer et al. 1993, Maurer et al. 1994, Neelin et al. 1993, Strother et al. 1994, Turkington et al. 1993, Taneja et al. 1994, Vassal et al. 1995)

[345] (Ardekani et al. 1995, Ayache et al. 1993, van den Elsen & Viergever 1993, van den Elsen et al. 1994, van den Elsen et al. 1995, Ge et al. 1996, Leslie et al. 1995, Maes et al. 1996, Maurer, Fitzpatrick, Galloway, Wang, Maciunas & Allen 1995, Maurer et al. 1993, Maurer et al. 1994, Maurer, Aboutanos, Dawant, Margolin, Maciunas & Fitzpatrick 1995, Maintz et al. 1994, Maintz, Beekman, de Bruin, van den Elsen, van Rijk & Viergever 1996, Simon, O'Toole, Blackwell, Morgan, DiGioia & Kanade 1995, Turkington et al. 1995, West et al. 1996, Zubal et al. 1991)

[346] (Evans, Strong, Colchester, Zhao & Holton-Tainter 1996, Ellis et al. 1996)

[347] (Andersson et al. 1995, Collins, Neelin, Peters & Evans 1994, Collins, Peters & Evans 1994, Evans et al. 1989, Gee et al. 1993, Gee, le Bricquer, Barillot, Haynor & Bajcsy 1995, Hill, Hawkes, Harrison & Ruff 1993, Leslie et al. 1995, Moseley & Munro 1994, Studholme et al. 1995*b*, Studholme et al. 1995*a*, Strother et al. 1994)

[348] (Collignon, Maes, Delaere, Vandermeulen, Suetens & Marchal 1995, Collignon, Vandermeulen, Suetens & Marchal 1995, Ge et al. 1994, Henri et al. 1992, Lemieux, Kitchen, Hughes & Thomas 1994, Lemieux & Jagoe 1994, Strother et al. 1994, Woods et al. 1993)

reported in[349]. Most popular validation techniques employ a physical phantom, possibly with controlled movement, and possibly with marking devices inserted or attached. Examples are found in[350]. Simulator studies, *i.e.*, studies were one modality is simulated from the other to obtain a registration standard, is found in[351]. Intra- and/or interobserver studies are performed in[352]. Finally, Hemler[353] performed cadaver studies using inserted markers for reference.

2.12 Discussion

What trends can be observed from the current literature? There is a definite shift in research from extrinsic to intrinsic methods, although clinically used methods are often still extrinsic. Of the intrinsic methods, the surface based methods appear most frequently, closely followed by "full image content" voxel property based methods. Instances of the latter type are slowly setting the standard for registration accuracy, a place formerly reserved for frame and invasive fiducial based registrations. The application of full image content voxel property based methods is however still largely limited in the extensive application field of intra-operative registration and radiotherapy treatment related registration (both requiring patient to modality registration). Especially in the area of intra-operative registration, surface based methods are dominant, and voxel based

[349](Andersson 1995, Collignon, Maes, Delaere, Vandermeulen, Suetens & Marchal 1995, Eberl et al. 1996, Hua & Fram 1993, Hoh et al. 1993, Lehmann et al. 1996, Leszczynski et al. 1995, Maurer, Aboutanos, Dawant, Margolin, Maciunas & Fitzpatrick 1995, Maintz, van den Elsen & Viergever 1996*b*, Maintz et al. 1995, Maintz, van den Elsen & Viergever 1996*a*, Simon, O'Toole, Blackwell, Morgan, DiGioia & Kanade 1995, Studholme et al. 1995*b*, Studholme et al. 1995*a*, Strother et al. 1994, West et al. 1996)

[350](Bijhold 1993, Betting & Feldmar 1995, Bettinardi et al. 1993, Chen et al. 1987, Dong & Boyer 1996, Ding et al. 1993, Eberl et al. 1996, Grimson, Lozano-Pérez, Wells, Ettinger, White & Kikinis 1994, Grimson, Lozano-Pérez, Wells III, Ettinger, White & Kikinis 1994*a*, Grimson, Lozano-Pérez, Wells III, Ettinger, White & Kikinis 1994*b*, Grimson et al. 1995, Grimson et al. 1996, Gottesfeld Brown & Boult 1996, Gluhchev & Shalev 1993, Gall & Verhey 1993, Holton et al. 1995, Holton-Tainter, Zhao & Colchester 1995, Lemieux, Jagoe, Fish, Kitchen & Thomas 1994, Lavallée et al. 1994, Lavallée & Szeliski 1995, Lavallée, Troccaz, Sautot, Mazier, Cinquin, Merloz & Chirossel 1996, Lavallée, Szeliski & Brunie 1996, Leung Lam et al. 1993, Maurer et al. 1993, McParland & Kumaradas 1995, Moseley & Munro 1994, Péria et al. 1994, Pallotta et al. 1995, Petti et al. 1994, Turkington et al. 1993, Taneja et al. 1994, Vassal et al. 1995)

[351](Cuchet et al. 1995, Evans, Collins, Neelin & Marrett 1996, Fritsch 1993, Fritsch, Pizer, Morse, Eberly & Liu 1994, Fritsch, Pizer, Chaney, Liu, Raghavan & Shah 1994, Neelin et al. 1993)

[352](Hill, Hawkes, Crossman, Gleeson, Cox, Bracey, Strong & Graves 1991, Malison et al. 1993, Pietrzyk et al. 1994, Stapleton et al. 1995)

[353](Hemler, Sumanaweera, Pichumani, van den Elsen, Napel & Adler 1994, Hemler, van den Elsen, Sumanaweera, Napel, Drace & Adler 1995, Hemler, Napel, Sumanaweera, Pichumani, van den Elsen, Martin, Drace & Adler 1995, Hemler et al. 1996)

methods almost absent. The reasons may be clear: it is relatively easy to obtain a surface from the patient, either using laser scanning, probes, 2D imagery, *etc.* , while obtaining reliable image information for voxel property based methods is more difficult: intra-operative imaging may not even be part of the normal surgical routine. If it is, images are usually 2D, and if 3D, of a relative poor quality given common equipment and acquisition sequence constraints in the operating theater. Moreover, surface based methods are, on the average, still faster than voxel property based methods. However, a problem with surface based methods is that they cannot cope with shift of relevant anatomy relative to the surface used in the registration, which may be severely restraining to intra-operative application. This problem may be solved using voxel based methods, but given the current state of affairs considering registration methods, surgical protocol, and intra-operative imaging, this will not be done in the very near future. In the case of radiotherapy treatment related registration (patient positioning, and patient position verification), the future will certainly include more of voxel based methods: imaging (X-ray simulator images and portal images) is already part of the common clinical treatment routine; radiotherapy relies almost exclusively on imaging for (tumor) localization, unlike surgery, where the visual impression is still the most important cue. It is not unlikely that this will change soon for a number of surgical applications, given the current trend of less and less invasive surgery that requires making use of advanced imaging techniques.

Many (but not all) *monomodal* registration problems appear to have been solved satisfactorily. We can accredit this to the fact that a registration paradigm can usually be relatively simple in the monomodal problem. Furthermore, given a computed transformation, many applications do not require complex visualization techniques, but can be adequately handled using subtraction techniques. *Multimodal* applications cannot be discussed in general terms, the applications are simply too diverse. It is tempting, but incorrect, to say registration results are somewhat more satisfying in methods involving scintigraphic imaging, perhaps because the relatively blurry nature of the images allows for a slightly larger displacement. In, *e.g.*, CT to MR registration, a displacement of a pixel can sometimes be obvious to the naked eye, and to obtain an accuracy in this order of magnitude, we cannot avoid to investigate precision at the acquisition level, (*e.g.*, the distortions induced by field inhomogeneity in MR images), which are of the same order of magnitude[354] However, the resolution of the images should not be used to formulate a clinically relevant level of accuracy: it is very well possible that a SPECT to MR registration requires a higher accuracy than some instance of CT to MR registration, even though it is likely that the smaller

[354]Distortion correcting algorithms have been proposed and are now available to a certain extent; scanners are calibrated better, and magnetic fields are adapted for minimum distortion.

error is more easily assessed by the naked eye in the latter case. The actual level of accuracy needed is in many applications still an unknown, and cannot accurately be quantified, even by the clinicians involved.

Intra-operative registration and methods on patient positioning in radiotherapy are in clinical use with apparent good results at a number of sites. On the *diagnostic use* of registration (modality to modality), much less information can be found. We suspect that, bearing in mind the possible clinical potential of diagnostic registration, it is actually used very little. The reasons for this are, probably, in essence of a logistic nature: unlike in the intra-operative scene (where all imaging and operations take place in the same room), in many multimodal diagnostic settings images are acquired at different places, –often even at different departments–, by different people, at different times, often transfered to different media, and frequently evaluated by different specialist diagnosticians. Besides these logistic reasons, it is also often unclear how a registration can optimally be used in the diagnostic process. It has already been pointed out that much research can still be done in this area.

Many methods can still be considered barred from meaningful clinical application by the fact that they are as yet improperly validated. Although the proper verification methods are known in most cases, and coarsely laid out in the previous section, for most applications the painstaking work of conducting the many experiments involved is only now starting.

Classification for medical registration methods

I. Dimensionality
- **a.** Spatial dimensions only:
  1. 2D/2D
  2. 2D/3D
  3. 3D/3D
- **b.** Time series (more than two images), with spatial dimensions:
  1. 2D/2D
  2. 2D/3D
  3. 3D/3D

II. Nature of registration basis
- **a.** Extrinsic
  1. Invasive
     - **A.** Stereotactic frame
     - **B.** Fiducials (screw markers)
  2. Non-invasive
     - **A.** Mould, frame, dental adapter, *etc.*
     - **B.** Fiducials (skin markers)
- **b.** Intrinsic
  1. Landmark based
     - **A.** Anatomical
     - **B.** Geometrical
  2. Segmentation based
     - **A.** Rigid models (points, curves, surfaces)
     - **B.** Deformable models (snakes, nets)
  3. Voxel property based
     - **A.** Reduction to scalars/vectors (moments, principal axes)
     - **B.** Using full image content
- **c.** Non-image based (calibrated coordinate systems)

III. Nature of transformation
- **a.** Rigid
- **b.** Affine
- **c.** Projective
- **d.** Curved

IV. Domain of transformation
- **a.** Local
- **b.** Global

V. Interaction
- **a.** Interactive
  1. Initialization supplied
  2. No initialization supplied
- **b.** Semi-automatic
  1. User initializing
  2. User steering/correcting
  3. Both
- **c.** Automatic

VI. Optimization procedure
- **a.** Parameters computed
- **b.** Parameters searched for

VII. Modalities involved
- **a.** Mono-modal
  1. Autoradiographic
  2. CT or CTA
  3. MR
  4. PET
  5. Portal
  6. SPECT
  7. US
  8. Video
  9. X-ray or DSA
- **b.** Multi-modal
  1. CT—MR
  2. CT—PET
  3. CT—SPECT
  4. DSA—MR
  5. PET—MR
  6. PET—US
  7. SPECT—MR
  8. SPECT—US
  9. TMS—MR
  10. US—CT
  11. US—MR
  12. X-ray—CT
  13. X-ray—MR
  14. X-ray—portal
  15. X-ray—US
  16. Video—CT
  17. Video—MR
- **c.** Modality to model
  1. CT
  2. MR
  3. SPECT
  4. X-ray
- **d.** Patient to modality
  1. CT
  2. MR
  3. PET
  4. Portal
  5. X-ray

VIII. Subject
- **a.** Intrasubject (1)
- **b.** Intersubject
- **c.** Atlas

IX. Object
- **a.** Head
  1. Brain or skull
  2. Eye
  3. Dental
- **b.** Thorax
  1. Entire
  2. Cardiac
  3. Breast
- **c.** Abdomen
  1. General
  2. Kidney
  3. Liver
- **d.** Pelvis and perineum
- **e.** Limbs (orthopedic)
  1. General
  2. Femur
  3. Humerus
  4. Hand
- **f.** Spine and vertebrae

- brief registration criterion description
- brief optimization procedure description
- validation (if any) used

Registration:
1. Problem statement (I,III,VII,VIII,IX)
2. Criterion (paradigm) (II,III,IV,V)
3. Optimization (V,VI)

Related:
- Validation
- Visualization/fusion

The ice falls! To that from the mountain's brow
Adown enormous ravines slope amain -
Torrents, methinks, that heard a mighty voice,
And stopped at once amid their maddest plunge!
Motionless torrents! Silent cataracts!
Samuel T. Coleridge, *Hymn Before Sunrise in the Vale of Chamouni.*

Chapter 3

Evaluation of Ridge Seeking Operators for Multimodality Medical Image Matching

J.B. Antoine Maintz
Petra A. van den Elsen
Max A. Viergever (1996b),
IEEE Pattern Analysis and Machine Intelligence

Abstract

Ridge-like structures in digital images may be extracted by convolving the images with derivatives of Gaussians. The choice of the convolution operator and of the parameters involved defines a specific ridge image. In this paper, various ridge measures related to isophote curvature are constructed, reviewed, and evaluated with respect to their usability in CT/MRI matching of human brain scans. Construction is initially done using heuristics in two-dimensional images, and then established firmly in a mathematical framework. Attention is paid to the necessity of operator invariance, scale of the operator, extension to three-dimensional images, and relations to isophote and principal curvature. It will be shown that one of the ridge measures appears well suited for the purpose of matching, despite the fact that the measure fails to detect ridges in a number of stylized scenes.

3.1 Introduction

Human anatomy and physiology are frequently examined with the aid of several imaging techniques. Generally, different modalities – or multi-parametric images of a single modality – highlight different aspects of the image subject. In many cases the proper fusion of these streams of information is desired (van den Elsen, Pol & Viergever 1993). Examples include radiation therapy planning, where CT[1] and MRI[2] information is merged, and epilepsy surgery planning, where EEG[3], MRI, and SPECT[4]/PET[5] is combined (van den Elsen, Maintz & Viergever 1992, van den Elsen & Viergever 1994).

Image matching, i.e., bringing two images geometrically into agreement, can be accomplished by transforming (e.g., translating, rotating, scaling) one of the images in such a way that the similarity with the other image is maximized in some sense. The similarity may apply to the original grey value images, to feature images derived from these, or to objects defined in the initial images or in the derived feature images. Maximizing the similarity of the initial images will be useful in particular when two images of the same type are to be matched. In multimodality image matching, however, the physical realities of the two images may be quite different, which calls for feature based or object based matching. Features used in image matching are, for example, edges (Borgefors 1988) and ridges (Monga, Benayoun & Faugeras 1992, Guéziec & Ayache 1992, van den Elsen et al. 1995, van den Elsen 1993). Object based matching may, e.g., be based on surface definitions (Levin et al. 1988, Pelizzari et al. 1989). Object based image matching has the disadvantage that the objects must first be defined, which is a high-level image processing task that might prove quite difficult for complex images. The use of low-level differential geometric features for image matching is attractive, but requires the careful selection of features that show sufficient similarity between the multimodal images. The selection of such features for CT/MRI brain image matching is the subject of the present article.

We focus our efforts on ridge-like features, because these have been proven viable for the applications at hand (van den Elsen, Maintz & Viergever 1992, van den Elsen et al. 1995). If CT and MR brain images are depicted as intensity landscapes, the skull forms a ridge in the CT image, and a negative ridge (trough) in the MR image. Since the skull is a virtually undeformable structure, it is ideal

[1] Computed Tomography
[2] Magnetic Resonance Imaging
[3] Electro EncefaloGraphy
[4] Single Photon Emission Computed Tomography
[5] Positron Emission Tomography

for matching purposes. The purpose of this paper is the extraction of ridges, representative of the skull, for CT/MRI brain image matching. Various ridge definitions will be discussed and evaluated on artificial test images whose ridges are known. We emphasize that, although the ridges proposed are representative of the skull, our approach is a (low-level) feature based matching method, since it does not rely on the definition of the skull as an object.

Ridge images can be extracted by means of differential operators. Direct differentiation, however, is an ill-posed problem since we are dealing with digital, sampled images instead of smooth mathematical functions. Section two will deal with the regularisation of this problem. In section three we will define two ridgeness measuring differential operators, which will be evaluated in section four. Section five presents the application of the ridge measures to CT/MRI matching.

3.2 Differentiation of images

3.2.1 Invariants

Features extracted by differential operators should be independent of the choice of coordinate system. If the image was, e.g., rotated prior to applying the operator, the features extracted should be the same, rotated by the same angle. Hence *invariance* under the group of orthogonal transformations is demanded. An operator that conforms to this restriction is called an (orthogonal) *invariant*. It can be shown that any tensorial expression in which all indices are resolved by means of contraction (pure or by multiplication by the Kronecker tensor (δ)) or alternation (multiplication by the Lévi-civita tensor (ε)) is an invariant (Spivak 1970).

We employ the Einstein summation convention, in which any index occuring twice signifies a summation: for example, L_iL_i denotes $L_xL_x + L_yL_y$ in two-dimensional space. Furthermore the δ and ε tensors are defined by

$$\delta_{ij} = \begin{cases} 1 & i = j \\ 0 & i \neq j \end{cases}$$
$$\varepsilon_{ij} = \begin{cases} 0 & i = j \\ 1 & ij \text{ is a cyclic permutation} \\ -1 & ij \text{ is a non-cyclic permutation} \end{cases} \tag{3.1}$$

3.2.2 Scale space

Differentiation is an ill-posed problem when applied to digital, sampled signals as opposed to smooth mathematical functions. Florack *et al.* showed that well-posed differentiation is possible by convolving the image with derivatives of a Gaussian (Florack, ter Haar Romeny, Koenderink & Viergever 1992). The width of the Gaussian used introduces a new parameter, the *image scale*, σ, extending the image dimensionality by one. The extended image is usually termed the *scale space* (Witkin 1983, Koenderink 1984) of an image. Using scale space, we can take derivatives that are coupled to the scale (i.e., the locality or globality) of structures. The scale is naturally bounded by the *inner* scale, the finest possible scale, a lower bound for which is the resolution of the scanning device, and the *outer* scale, the largest possible scale, an upper bound for which is the size of the entire image.

In figure 3.1 a CT image is shown together with two 'intensity landscape' versions of it; one formed directly, and one slightly smoothed. In the intensity landscapes, the skull ridge is readily apparent. In the unsmoothed version, however, extraction of this ridge by means of straightforward differentiation is wellnigh impossible, since the ridge is locally very jagged, which will greatly influence local differentiation operations. To arrive at the smoothed version we applied Gaussian convolution with an increasing width, until a coherent and easily extractable skull ridge was apparent.

We can thus use smoothing to 'tune' differential operators to multilocal structures. It has been shown (Florack et al. 1992, Florack, ter Haar Romeny, Koenderink & Viergever 1994) that upon demanding shift-invariance, directional invariance (isotropy) and scale invariance, the Gaussian is the unique linear smoothing kernel. The scale space $L(x,\sigma)$ of an image $L_0(x)$ is the continuous (hyper)stack of smoothed images, with the smoothing factor σ increasing as we rise in the stack. The original image rests at the bottom of the stack. The scale space can be computed using

$$L(x,\sigma) = (L_0 * G)(x,\sigma), \tag{3.2}$$

where G is the Gaussian kernel, x is the coordinate vector, and σ is the smoothing factor, i.e., the width ('standard deviation') of the Gaussian.

Smoothing and differentiation are two closely entwined factors of a single process: to ensure a differential operator is tuned to a certain scale these steps *must* be combined. This is easily implemented, since the scaled derivative of an image can be computed by convolving it with a derivative of the Gaussian kernel:

$$(L_{i_1 \ldots i_n})(x,\sigma) = (L_0 * G_{i_1 \ldots i_n})(x,\sigma), \tag{3.3}$$

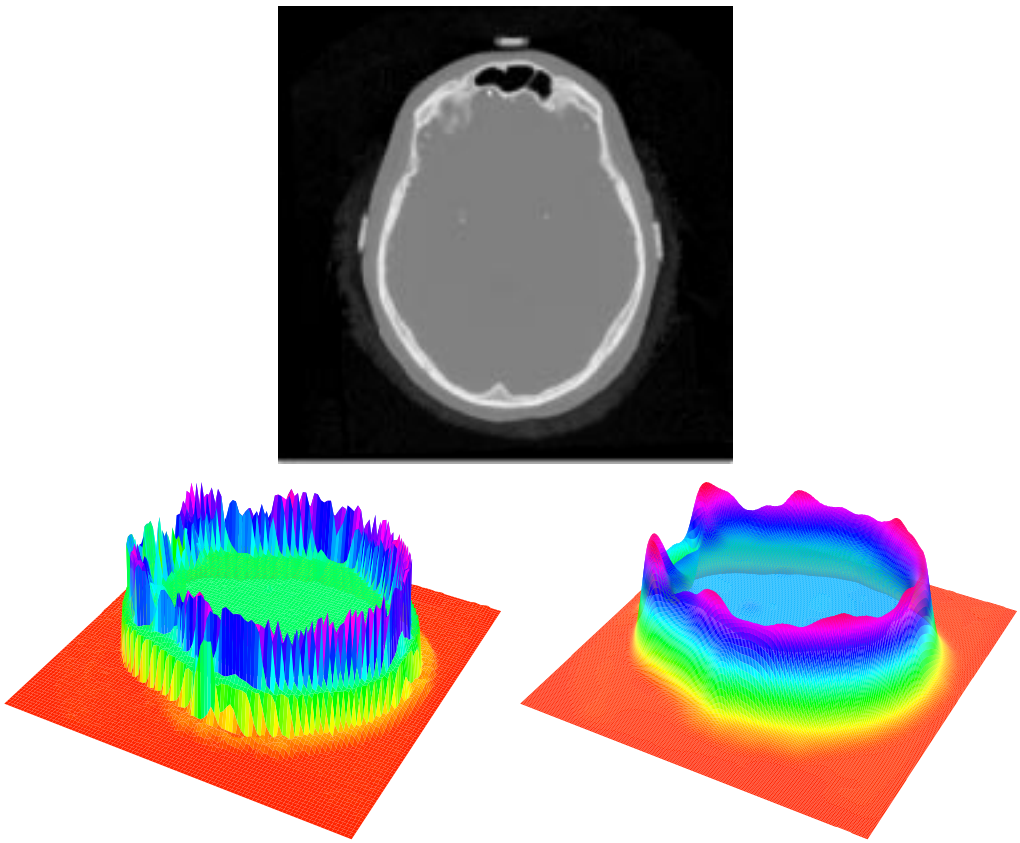

Figure 3.1 A transversal CT image slice and two 'intensity landscape' versions, the right one being smoothed by convolution with a Gaussian kernel. ($\sigma = 4$ mm)

where subscripts i_j denote the order of differentiation with respect to the spatial variables $i_j \in \{\mathbf{x}, \mathbf{y}, \mathbf{z}\}$, $n \in \mathbb{N}^+$, $j = 1 \ldots n$.

Note that -using this last formula- the numerical complexity of the computation of a differential image at a certain scale is reduced to mere multiplications, if we do all computations in the frequency domain:

$$(L_{i_1 \ldots i_n})(x, \sigma) = (\mathcal{F}^{-1}[\mathcal{L}_0 \cdot \mathcal{G} \cdot i^n \cdot \prod_j \omega_{i_j}])(x, \sigma), \tag{3.4}$$

where calligraphic letters ($\mathcal{G}, \mathcal{L}$) denote Fourier transforms, $\mathcal{F}^{-1}$ the inverse Four-

ier transform, and ω_{i_j} represent the spatial frequencies.

3.3 Ridge measures

Definitions of ridge-like structures in terms of differential geometry can be found in mathematical literature dating back for more than a century, see for example (Maxwell 1859). Recent work can be found in (Pizer, Burbeck, Coggins, Fritsch & Morse 1992, Morse, Pizer & Liu 1993, Eberly, Gardner, Morse, Pizer & Scharlach 1994, Koenderink & van Doorn 1994). Perhaps paradoxically, the literature does not seem to converge to a unique description of a "ridge". Instead, each author seems to start from a different definition, therefore almost certainly ending up with a ridge description alien to most of the other authors' descriptions. Although some authors claim unique correct definitions on debatably valid grounds, we will hold no such claims, nor will we debate other definitions. Our goal was to establish a feasible ridge description, useful in specific applications, a goal we think to have reached.

We will try to convey what we mean by an 'intuitive ridge'. It can be thought of as the path you follow in the mountains, where there's always a drop both on your left and to your right hand. The idea of 'ridgeness' increases if the drops are steep and sheer. Consider figure 3.2. Here we see two rising surfaces, and the curve of intersection is the ridge. This curve is an easy one to detect, since it is a singular curve of just about any derivative. However, things change radically if the ridge is smoothed somewhat. Intuitively, the ridge curve is still clear, yet mathematical models will have to resort to smarter methods to find it.

The existence of a plethora of mathematical ridge definitions is not strange, considering there are multiple definitions in terms of language, all sounding correct, yet denoting very different structures. For an example, consider these definitions:

- Turn your intensity landscape upside-down, and let it rain. Now look where the rivers form. These are your ridges.
- Keep walking uphill in the intensity landscape. The point where you make a sharp turn is a ridge point.

It can be shown these definitions apply to a very different set of ridges. In this paper we will mainly adhere to ridges related to the latter definition, for largely pragmatic reasons: there exists no local operator to detect ridges of the first definition (Koenderink & van Doorn 1994).

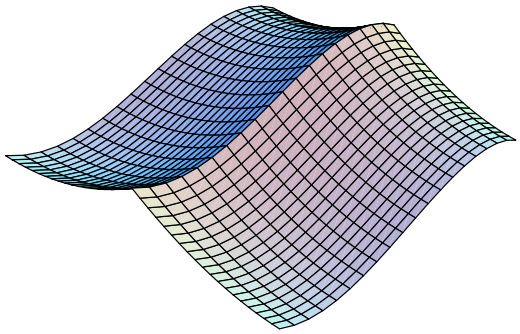

Figure 3.2 A clearly defined ridge: the meeting curve of two rising surfaces.

3.3.1 Ridge measures: L_{vv}

We define a gradient-based local coordinate system spanned by the gradient w and its right-handed normal v, so

$$v = \begin{pmatrix} L_y \\ -L_x \end{pmatrix} \quad and \quad w = \begin{pmatrix} L_x \\ L_y \end{pmatrix}, \tag{3.5}$$

or simply $w_i = L_i$, and $v_i = \varepsilon_{ij} L_j$ in tensor notation.

The gradient w points in the direction of steepest ascent if we represent our image as an intensity landscape. In figure 3.3, notice how the gradient in any point generally[6] points towards the ridge, except when the chosen point is actually on the ridge; in that case the gradient is aligned with the ridge[7]. As we move across a ridge, the gradient reverses its direction. On the ridge the v direction will be perpendicular to the ridge, and therefore the intensity profile along v in the neighbourhood of a ridge point will be very concave in comparison to profiles around non-ridge points. Therefore L_{vv}, the second derivative of the image intensity function in the v direction, will have a local minimum along v at ridge points. It will likewise have a local maximum along v at troughs. The L_{vv} feature images thus depict 'ridgeness' (Maintz 1992, van den Elsen et al. 1995, van den Elsen, Maintz & Viergever 1992). All this is illustrated in figure 3.3. Note that for matching we use the ridgeness images as such, and do not segment the image into ridge and non-ridge voxels.

[6] Exceptions will be illustrated later on.
[7] Only in the rare case of a perfectly horizontal ridge the gradient vanishes.

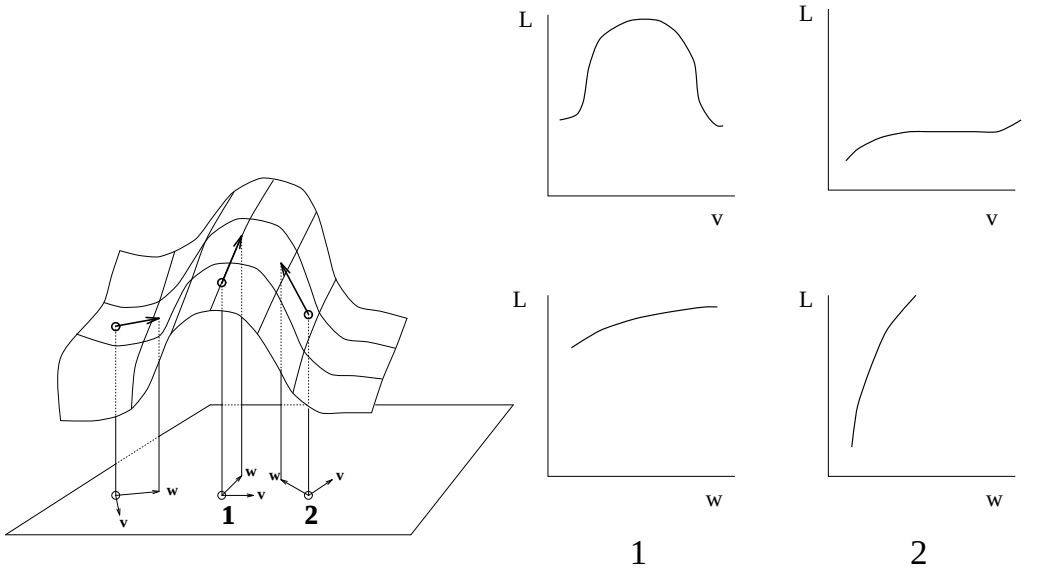

Figure 3.3 Intensity profiles in gradient (w) and normal, isophote tangent (v) directions of ridge points and non-ridge points. See text for details.

The value of L_{vv} can be computed using (Cartesian) local derivatives as follows:

$$\begin{aligned} L_{vv} &= \frac{1}{\|v\|^2}(v \cdot \nabla)^2 L \\ &= (L_y^2 L_{xx} - 2L_x L_y L_{xy} + L_x^2 L_{yy})(L_x^2 + L_y^2)^{-1}. \end{aligned} \tag{3.6}$$

L_{vv} is an invariant, since it equals a full alternation:

$$L_{vv} = \varepsilon_{jk}\varepsilon_{lm} L_j L_m L_{kl} (L_i L_i)^{-1}. \tag{3.7}$$

This invariance is also obvious since v itself is invariant.

In 2D the perpendicular v of the gradient is well defined. In 3D, however, there is an entire plane perpendicular to the gradient, making the 3D generalization of L_{vv} non-trivial. We constructed a ridge detector for surface-like ridges based on notions similar to those used with L_{vv}. As in the two-dimensional case, the gradient in 3D points towards the nearest ridge, and changes direction while moving across the ridge. On the ridge the gradient direction is along the ridge surface; the flowline bends at the ridge to flow with the ridge.

The intensity profile along a line perpendicular to the ridge is relatively concave. Thus in ridge points, there is a direction perpendicular to the local flowline with

a relatively strong concavity of its intensity profile. Our ridge measure is formulated as follows: the ridgeness (in each point) equals the second directional derivative of the intensity profile in the direction a, where a is (1) in the plane normal to the local gradient, and (2) the direction in this plane for which the second directional derivative is minimum. Troughs are detected by choosing the direction in which the second derivative is maximum. The direction a of maximum concavity (minimum convexity) can be found by solving the following system of equations:

$$\text{minimize } \frac{1}{\|a\|^2}(a \cdot \nabla)^2 L, \tag{3.8}$$

under the constraint $\nabla L \cdot a = 0$, $a \neq \vec{0}$.

The solution of this two-dimensional problem is given in appendix A. The solution vector p, and the solution vector q of the system if we maximize instead of minimize, equal the local principal curvature directions. The three-dimensional ridge and trough measures are L_{pp} and L_{qq} respectively. Note that if we apply L_{pp} (or possibly L_{qq}) to a certain image, a single slice will look similar to L_{vv} applied to the original slice, except that L_{pp} takes the full 3D geometry into account, and therefore usually produces better output. The similarity, i.e., the extraction of the same features in both 2D and 3D was exactly what we aimed for in the construction of the 3D operators. The major implication of this is that ridges in 3D in our definition are *surfaces* rather than lines.

3.3.2 Ridge measures: Isophote curvature

In two-dimensional images, the observation (see figure 3.3) that the gradient changes direction when crossing a ridge, gives rise to an alternative definition ridges: the rate by which the gradient direction changes in the v direction.

Let the two-dimensional gradient orientation be denoted by $\theta = \arctan(\frac{L_y}{L_x})$. The ridge measure then is ($\frac{\partial}{\partial \underline{v}}$ means derivation in the direction of v)

$$\frac{\partial \theta}{\partial \underline{v}} = \frac{1}{\|v\|}(v \cdot \nabla)\theta = \frac{2L_x L_y L_{xy} - L_y^2 L_{xx} - L_x^2 L_{yy}}{(L_x^2 + L_y^2)^{\frac{3}{2}}}. \tag{3.9}$$

Notice that $\frac{\partial \theta}{\partial \underline{v}} \equiv -\frac{L_{vv}}{L_w}$, so in fact the only difference with L_{vv} is a negation and a normalization with respect to the gradient magnitude. In tensor notation,

$$-\frac{L_{vv}}{L_w} = \varepsilon_{jk}\varepsilon_{lm} L_j L_m L_{kl} (L_i L_i)^{-3/2},$$

which is a full alternation, so $-\frac{L_{vv}}{L_w}$ is an invariant. $-\frac{L_{vv}}{L_w}$ is known in literature as the *isophote curvature*, often denoted by κ. The 3D equivalent of κ can be derived analogously to the 3D equivalent of L_{vv}. Depending on whether we maximize or minimize, we arrive at the maximum or minimum local principal curvature.

The normalization of κ with respect to the gradient magnitude causes it to react more than L_{vv} in relatively flat areas. Both L_{vv} and $L_{vv}L_w^{-1}$ have been identified as possible ridge detectors. More generally, $L_{vv}L_w^{\alpha}$ can be considered, with α ranging from -1 to 0, or even beyond these values.

3.4 Review: performance of the ridge measures

In this section we will show –using a number of illustrative examples– when, and when not, the L_{vv} (and κ) measure detect the 'intuitive' ridge we wish to find.

Consider the function $z = f(x, y) = -(\alpha x^2 + y^2)$, with $\alpha > 0$, so the iso-z lines are elliptic. $f_{vv}(x, y) = -2 + \frac{2y^2(1-\alpha)}{\alpha^2 x^2 + y^2}$. So, f_{vv} has a minimum along $x = 0$ if $\alpha > 1$ and a minimum along $y = 0$ if $0 < \alpha < 1$. If $\alpha = 1$ then $f_{vv} = -2$. This is exactly as may be expected: if $\alpha = 1$, then f is a strict (rotation-symmetric) paraboloid, so no ridge should be detected. If $\alpha > 1$ the paraboloid is elongated in the y-direction, and $x = 0$ equals the ridge. Likewise, if $0 < \alpha < 1$, then the elongation is in the x-direction, and $y = 0$ defines the ridge. Only at the point $(0, 0)$ the detection fails, since v vanishes there, and f_{vv} is singular. An example can be seen in figure 3.4. Notice that the detection would also fail if $\alpha = 0$, because then v vanishes at any point of the ridge ($y = 0$).

We next discuss the hyperbolic counterpart of the above example with elliptic isocurves. Consider $z = f(x, y) = \alpha x^2 - y^2$, (elongated saddle) with $\alpha > 0$, so the isocurves are hyperbolic. $f_{vv}(x, y) = -2 + \frac{2y^2(1+\alpha)}{\alpha^2 x^2 + y^2}$ (see figure 3.5). So, f_{vv} has a maximum along $x = 0$ (f has a trough) if $\alpha > 1$, and a minimum along $y = 0$ (f has a ridge) if $0 < \alpha < 1$. Both the minimum and the maximum occur if $\alpha = 1$. There is always a singular point at (0,0), because v vanishes there. Likewise, if $\alpha = 0$ the entire detection fails, because v vanishes along the entire ridge $y = 0$.

Actually, the above paragraph oversimplifies matters somewhat: the trough and ridge are both always present, as long as $\alpha > 0$. However, if α differs sufficiently from 1, one is much stronger than the other.

Consider now the function $z = f(x, y) = x^2 - y$ (see figure 3.6). In this case, the isocurves are parabolas. $f_{vv}(x, y) = f_{vv}(x) = \frac{2}{1+4x^2}$. As expected, f_{vv} has a maximum along $x = 0$.

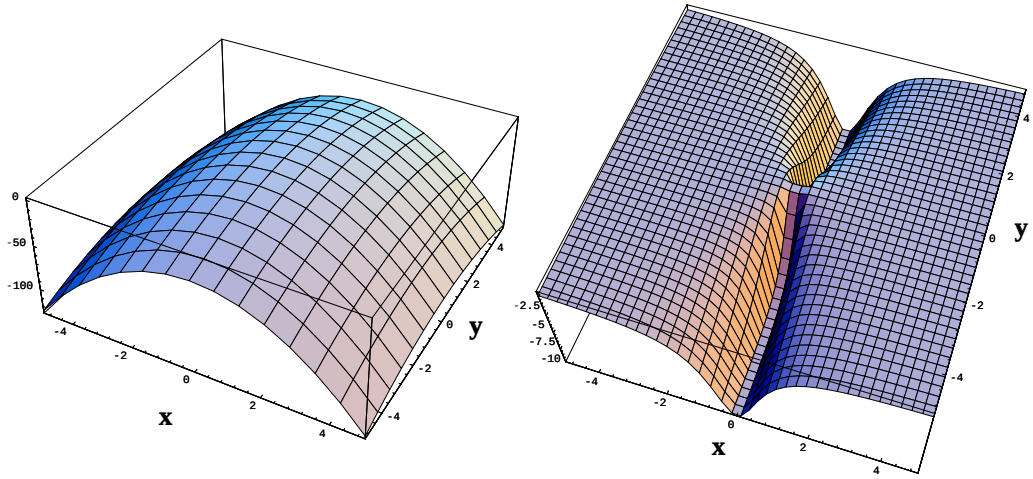

Figure 3.4 An example of ridge detection on an 'elongated' paraboloid, with equation $f(x, y) = -(\alpha x^2 + y^2)$ (left). In the picture $\alpha = 4$. On the right the f_{vv} function can be seen. There is a string of minima along $x = 0$, as expected. Only at $(0, 0)$ there is a singularity, because v vanishes there. As we move away from $x = 0$, f_{vv} approaches the value -2, which would equal the curvature measure if f were a strict paraboloid, i.e., $\alpha = 1$.

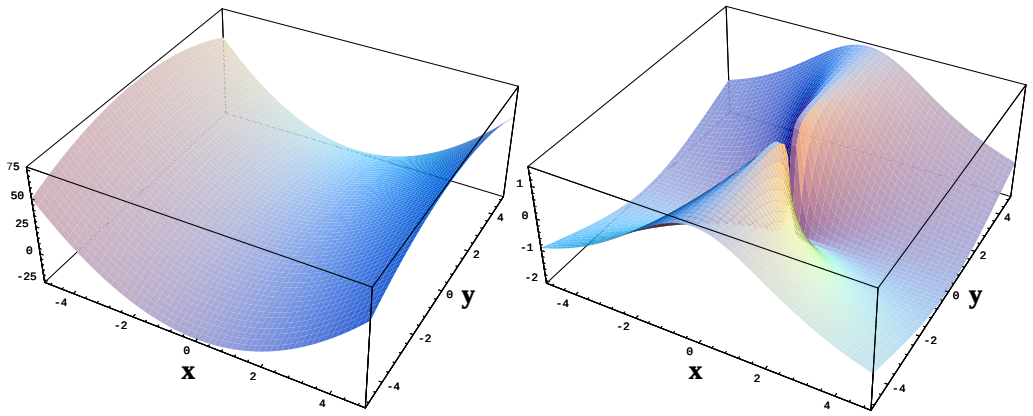

Figure 3.5 An example of ridge detection on an 'elongated' saddle, with equation $f(x, y) = \alpha x^2 - y^2$ (left.) In the picture $\alpha = 3$. To the right, the f_{vv} function. There is a string of maxima along $x = 0$, as expected. Only at $(0, 0)$ there is a singularity.

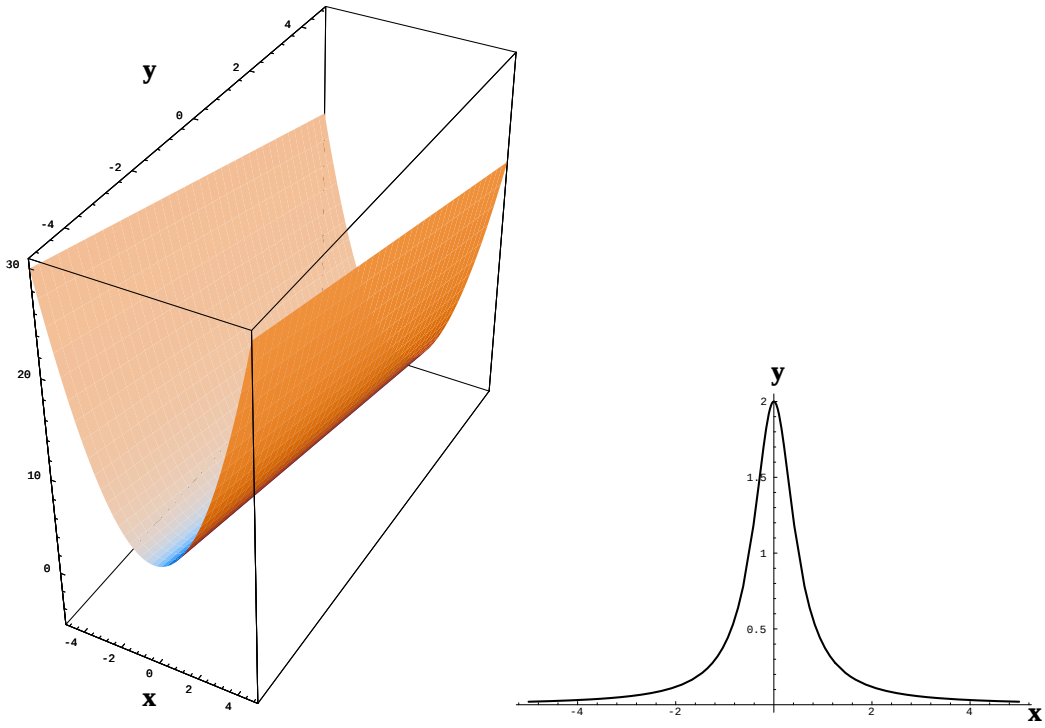

Figure 3.6 The function $f(x,y) = x^2 - y$ (left), which has parabolic isocurves. The f_{vv} function (right) is only dependent on x, so only a cross-section is shown. Clearly, the correct trough at $x = 0$ is found.

In all of the above cases, the ridges are detected as expected. However, cases where the L_{vv} detector fails are easily constructed. Since L_{vv} is closely related to the isophote curvature, we may expect trouble if the isophotes have constant curvature, i.e., the isophotes are circles or circle sectors, so any point of a certain isophote satisfies $(x-a)^2 + (y-b)^2 = r^2$, where a,b, and r are arbitrary functions of z. If we choose $a = z$, $b = 0$, and $r = 1$, we get a 'circular gutter'-function. Koenderink and van Doorn (1994) used this function to show the difference between isophote curvature based ridges and 'water courses'. L_{vv} indeed fails here: take $f(x,y) = x - \sqrt{1-y^2}$, (see figure 3.7). The isophotes are circular. $f_{vv} = \frac{1}{\sqrt{1-y^2}} \equiv f_w$, so the isophote curvature $\kappa_f \equiv -1$. Needless to say, no trough is detected by κ_f. Even worse, the f_{vv} function has a *minimum* along $y = 0$, suggesting a ridge.

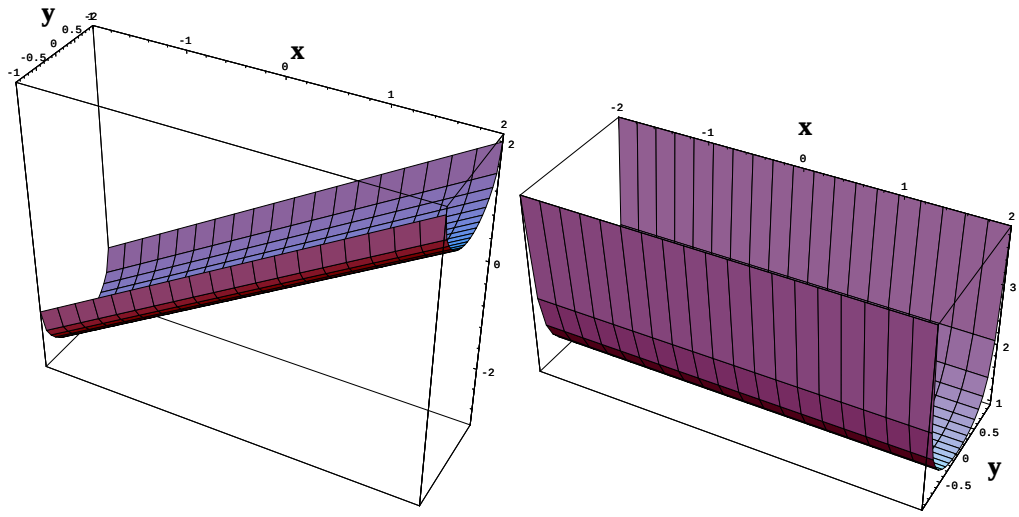

Figure 3.7 The function $f(x,y) = x - \sqrt{(1-y^2)}$ (top), which has circular isocurves. Since the isophote curvature is constant, the v vectors do not flip direction when passing the trough, as in general cases. Here, the f_{vv} function (right) fails as a trough detector.

The effect shown above is not the only unexpected event for circular isophotes. Suppose z is only a function of radius r, $z = z(r)$, then z_{vv} simplifies to

$$z_{vv}(r) = \frac{z_r}{r}. \tag{3.10}$$

This last formula shows that, in general cases of $z = z(r)$, there is a singularity at $r = 0$. This is because the curvature of the (circular) isophote κ equals $1/r = -\frac{z_{vv}}{z_w}$, and approaches infinity if r approaches zero. It also shows that the intuitive (horizontal) ridges and troughs now occur at the zero crossings (!) of z_{vv}. (Because the intuitive ridges and troughs are local minima / maxima of $z = z(r)$ here, and these occur when $z_r = 0$, which are also zero crossings of z_{vv}, as (3.10) shows.)

When defining our ridges and troughs by means of κ, we assumed that the intuitive ridges and troughs occured at the locus of maximal isophote curvature. This is not necessarily true, as the next example shows: Take $f(x,y) = x(x-1)(x-2) - y$, the tilted extension of $x(x-1)(x-2)$, which has zero crossings at 0,1, and 2. The intuitive ridge and trough occur at the maximum and minimum of $x(x-1)(x-2)$, so at $x = 1 \mp \frac{1}{3}\sqrt{3} (\approx (0.42, 1.58))$. However, $f_{vv} = \frac{6(x-1)}{1+(3x^2-6x+2)^2}$, so its minimum and maximum occur at $1 \mp \frac{1}{3}\sqrt{1+\sqrt{7}} (\approx (0.36, 1.64))$. The $\frac{f_{vv}}{f_w}$ measure

does slightly better in this case: it has a maximum/minimum at $1 \mp \frac{\sqrt{2+\sqrt{14}}}{\sqrt{15}} (\approx (0.38, 1.62))$.

In the above example, we needed a tilt ("$-y$") to find the ridge and trough, as explained below.

Vanishing of the gradient also causes the f_{vv} measure to fail, as has already been demonstrated in some of the above examples, where singularities occured at single points. The gradient may also vanish along the entire ridge or trough. Take, for instance, the function $f(x, y) = x^2$, a simple straight trough. (So, automatically, *not* a course line, since water will not flow there) The v-vector field is $v(x, y) = (0, -2x)^T$, and simply vanishes as we approach the trough $x = 0$. The v-vectors do not turn around at any point, so obviously isophote curvature related measures fail. This is also immediately clear if we consider that the isophotes are (pairs of) straight lines, and thus have zero curvature everywhere. If we 'tilt' the function, e.g., $x^2 - y$, we get parabolic isophotes, (see example function in figure 3.6), and the trough is readily detected.

Even in the light of all of the above examples, it is sometimes hard to predict the behavior of the f_{vv} measure, as can be seen in the next example. We take $f(r, \varphi) = \alpha r(1 - r)\varphi$. This function and its isophotes ($r = \frac{1}{2} \pm \sqrt{1 - \frac{4z}{\varphi\alpha}}$) can be seen in figure 3.8. The intuitive ridge occurs at $r = \frac{1}{2}$. This function suffers from two of the effects mentioned above: ridges occuring at zero-crossings of f_{vv} and ridges being detected somewhat displaced from the intuitive location. In figure 3.9 we see some cross-sections of f_{vv} as a function of r, at eight equidistant values of φ. Clearly, the ridge is detected for some values of φ only (in these cases, the minimum occurs at or near $r = 0.5$). At other values, $r = \frac{1}{2}$ is a zero-crossing of f_{vv}.

All examples considered, L_{vv} and κ might come out as questionable ridge detectors. However, test results on medical images (which will be shown below) and on other real world images indicate that the special cases in which L_{vv} and κ fail or are inaccurate do not seem to occur, or only occur very locally, in everyday practice.

3.5 Application of ridge measures to CT/MRI matching

We will now show some examples of ridges in CT/MR brain images. Figure 3.10 shows the L_{vv}-image of the CT-slice of figure 3.1, at a scale of 4 pixels (approximately 4 mm) to best detect the skull ridge. The result in the same slice

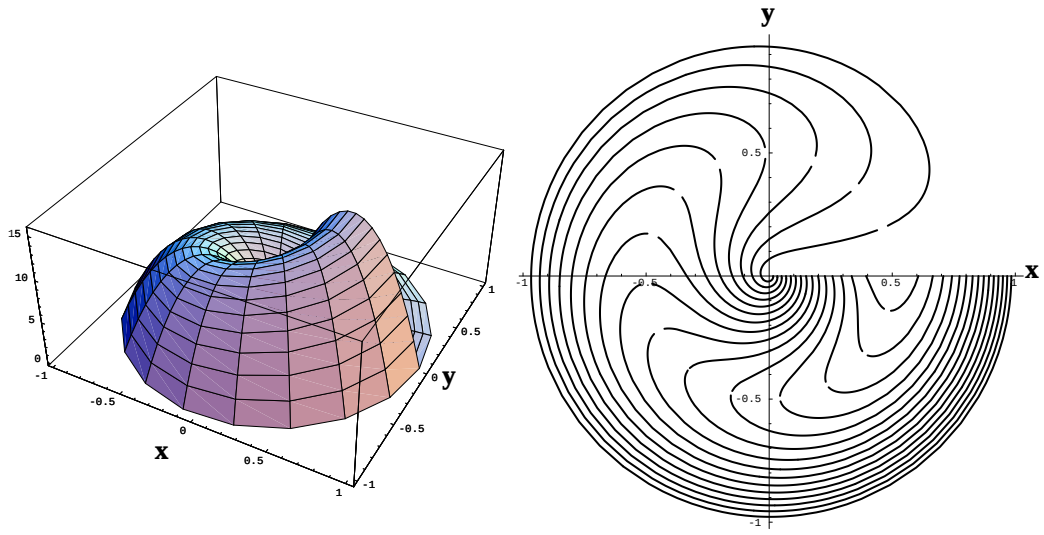

Figure 3.8 The function $f(r,\varphi) = \alpha r(1-r)\varphi$ (left) and its isophotes $r = \frac{1}{2} \pm \frac{1}{2}\sqrt{(1-\frac{4z}{\varphi\alpha})}$. In the figure $\alpha = 10$.

after applying the '3D-L_{vv}' operator on the 3D dataset is also shown. Notice the increase in quality: the ridge curves are much more continuous.

Figure 3.11 shows a result of the $\frac{L_{vv}}{L_w}$ operator and the 3D$-\frac{L_{vv}}{L_w}$ operator on the same CT image.

Figure 3.12 shows some variation of the ridgeness images of an MR image as we vary α in the 3D-$L_{vv}L_w^\alpha$ detector from 0 to -1, thus 'moving' from the 3D-L_{vv} to the 3D-$\frac{L_{vv}}{L_w}$ detector.

A number of observations can be made as α moves from 0 to -1:

- There is less "blobbing" at the end points of ridges. An explanation for this might be that when α changes from 0 to -1, the detector less resembles the corner detector $L_{vv}L_w^2$ (when $\alpha = 2$)

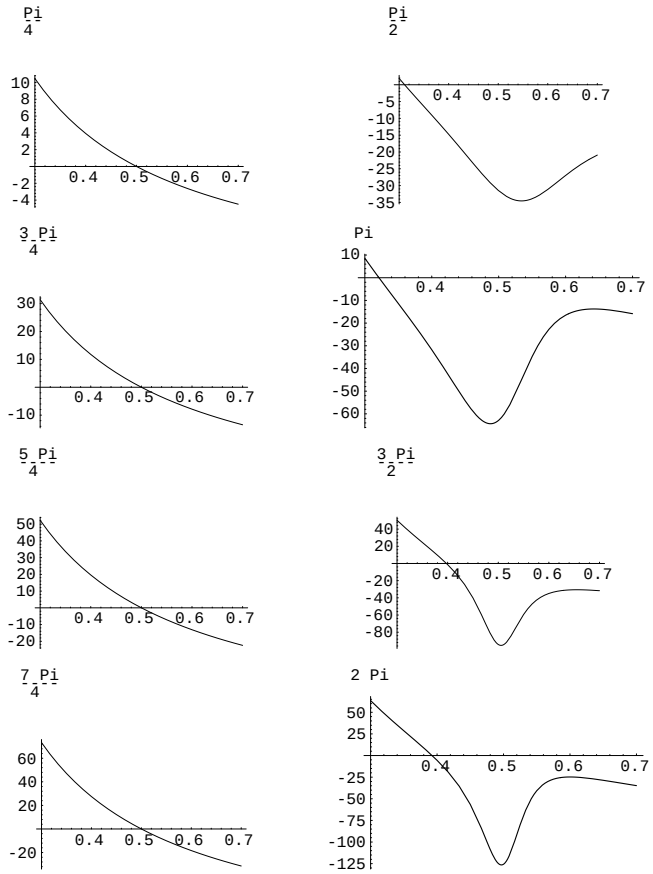

Figure 3.9 Some cross-sections of the f_{vv} function from the function f in the previous figure. The functions are functions of r, at eight equidistant values of φ. The corresponding value of φ is printed above the graph. Clearly, the minima of f_{vv} occur sometimes at (or near) $r = 0.5$, which is the correct ridge location, and sometimes $r = 0.5$ is a zero crossing of f_{vv}.

- Background ridges appear. This is because for $\alpha = -1$, the gradient magnitude in the denominator normalizes for 'unflatness'.
- When using the 2D operators, the ridges are thicker when $\alpha = 0$ than when $\alpha = -1$. With 3D operators, such a difference cannot be noticed.
- The range of real values of the ridge measure gets smaller.

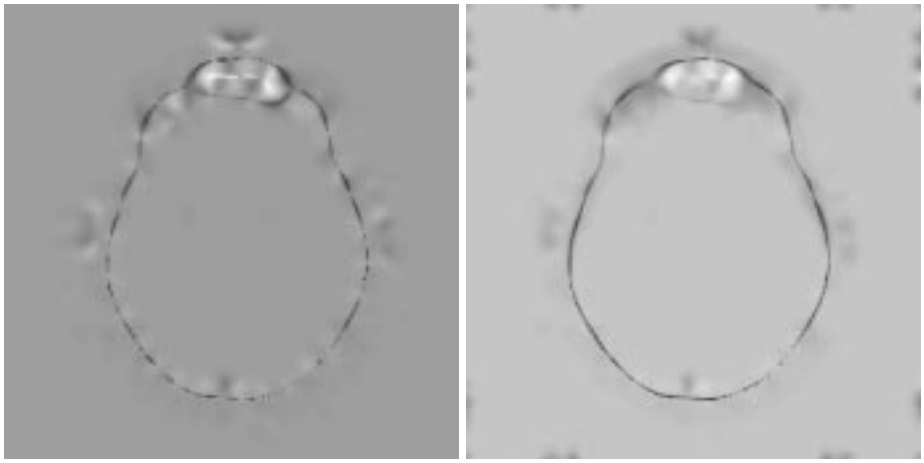

Figure 3.10 The result of the L_{vv} and 3D-L_{vv} operators on the CT image shown in figure 1.

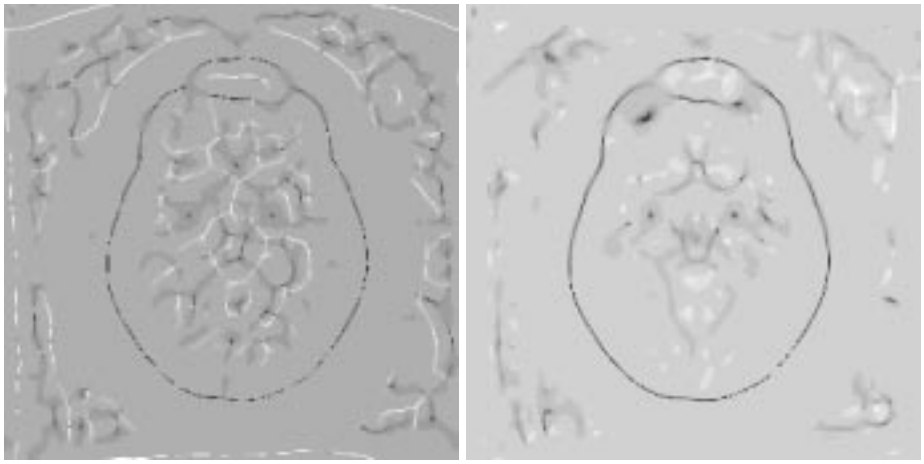

Figure 3.11 The result of the $\frac{L_{vv}}{L_w}$ and the 3D-$\frac{L_{vv}}{L_w}$ operators on the CT image shown in figure 1.

- The position of the ridge in which we are particularly interested for matching purposes, *viz.* the skull ridge, changes very little when α changes. In the cases examined, this position is excellent; the ridge is located in the middle of the skull area, both for CT and MRI.

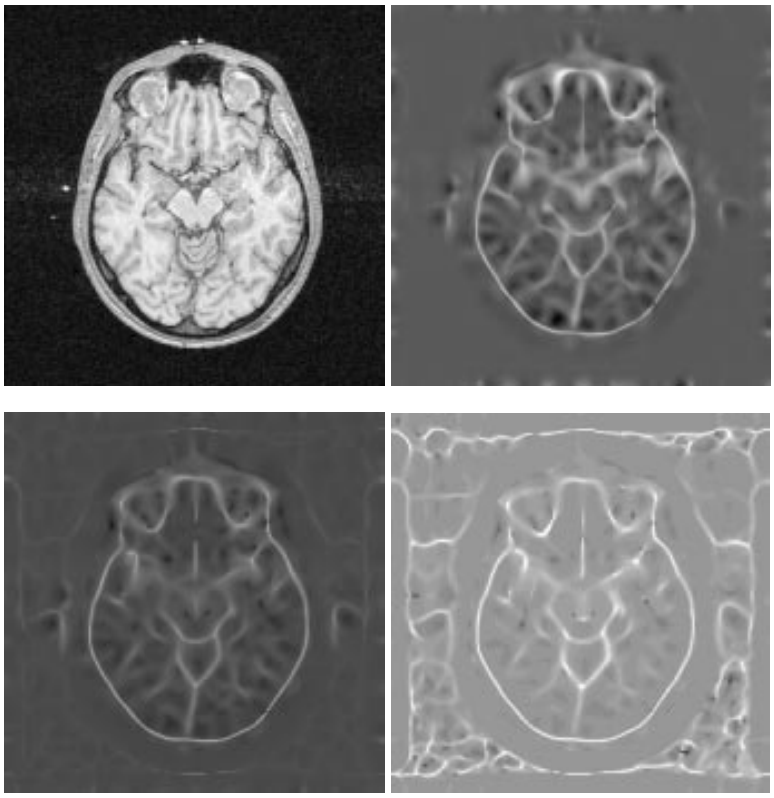

Figure 3.12 On the top left, a slice from an MR dataset is shown. In the top right picture a result obtained with the 3D-L_{vv} operator can be seen, and in the bottom left one a result obtained with the 3D-$L_{vv}L_w^{-0.5}$ operator. At the bottom right a result obtained with the 3D-$L_{vv}L_w^{-1}$ operator is shown. All ridgeness images were made at a scale of 4 pixels (approximately 4 mm). The gray scale of the ridgeness images was adjusted for display purposes.

A good ridge location, is of course of crucial importance for a correct match using these ridges. Experiments have shown accurate ridge position in areas where the skull is a neatly isolated structure. A certain radial symmetry (symmetry of the intensity profile when crossing the skull area normally) and little variation in thickness of the skull is of importance to avoid moving of the ridge locus when scaling the images. This approximate radial symmetry is present both in CT and in (most protocols of) MRI: medium intense brain matter to highly intense skull to medium intense skin in CT and medium intense brain matter to

hypo intense skull to medium intense skin in MRI. Sometimes, this symmetry is disturbed, causing erratic ridge measurements. Examples include transverse slices through the base of the brain, and external influences like headholder devices.

Owing to the different imaging characteristics of CT and MRI, extracted ridge images exhibit differences. In some MRI protocols not only the bone is black, but spinal fluid also. We can only extract the valley of this entire dark area, which is then likely to slightly mismatch the skull-only ridge extracted from the CT image. Another example is the area around the frontal sinus. Here the CT image shows black air surrounded by white bone: the extracted skull ridge will bifurcate and follow the bony parts. The MRI image again shows a black area only, and the detected valley will pass directly through the center of the sinus (van den Elsen et al. 1995).

We tested the ridge measures on images acquired by various CT and MRI protocols. The detection works best, of course, when the resolution is high in all dimensions (e.g., 128 slices of a 256x256 matrix), but the results are certainly acceptable when the z-resolution is lower (e.g., a 14 slice 256x256 matrix MR dataset). A scale of 4 mm is usually a good choice for detecting the skull ridges. The only case where we failed to detect a skull valley is in MR images of protocols where the bone marrow shows up too brightly in the dark skull area. In this case, however, we extracted the marrow ridge (at a scale of 1 to 2 mm), which also runs centrally through the skull bone. Note that the actual scale used (the σ of the Gaussian) will usually have to be corrected for anisotropic voxel dimensions, i.e., the σ in each direction is inversely proportional to the voxel dimension in that direction.

The resultant ridgeness images were employed in a matching approach using a hierarchical correlation technique (van den Elsen 1993, van den Elsen et al. 1995), which minimizes the correlation value $c(t)$ over all rigid (translations and rotations) transformations t:

$$c(t) = \sum_{(x,y,z)\in L_1} L_1(x,y,z)L_2(t(x,y,z)), \tag{3.11}$$

where L_1 and L_2 are the ridgeness images of the images to be matched.

The images were not preprocessed. After applying the operators, the image gray scales were adjusted linearly and quantified to integers to speed up computations. If necessary, outlyers that could disrupt this quantification were filtered out first.

3.5.1 2D matching results

We applied three ridge measuring operators (L_{vv}, $L_{vv}/\sqrt{L_w}$, and L_{vv}/L_w) on a 256x256x180 sampled T1 weighted FFE MR brain scan with contiguous slices, with cubic ($1mm^3$) voxels, and on a matched CT scan, (match furnished by a marker based method (van den Elsen & Viergever 1994)) originally 256x256x180 sampled, with contiguous slices, with pixel size of approximately 0.9 mm and slice thickness 1.5 mm. Both 2D and 3D operators were used; the 2D operators were applied to six representative slices, the 3D operators were applied to the entire sets.

3.5.1.1 2D ridge and trough operators

The 2D tests were performed on 7 different scales, ranging from $\sigma = 1$ pixel to $\sigma = 7$ pixels, so the total number of 2D experiments equals 126 (6 slices, 3 operators, 7 scales). The results concerning the topmost slice were discarded, on account of the failure of the algorithm to accomplish an accurate match. Apparently, the 2D feature information available is too little to furnish a match conforming with the original 3D marker based match, which was used as a standard for comparison[8]. To interpret the large amount of matching results, on the remaining five slices, these results were categorised into classes of increasing matching accuracy. These classes were subsequently indexed, '1' for the sub-pixel accuracy class, to '0' for the class of failed matches. The accumulated results can be seen in figure 3.13.

It is hard to draw any generally valid conclusions from these results. In our experiments, the matches are best at a scale of 3 or 4 mm, corroborating the visual impression of best visibility of the skull ridge at a scale of 4 mm. At this scale, there is a slight preference for L_{vv}, which renders better matches, to the other operators.

[8]The marker based matching technique used is described in (van den Elsen & Viergever 1994, van den Elsen 1993). It basically employs three V-shaped fiducial markers each marking a single well chosen point in the patient's anatomy, thus establishing a unique coordinate frame in each of the images to be matched. The V-shape of the markers allows for sub-pixel accurate determination of the location of the point marked. The subsequent match is therefore likely to be very accurate. Even so, the match was checked visually, and compared with matches slightly perturbed. The conclusion was that the marker based match was very well acceptable as a gold standard.

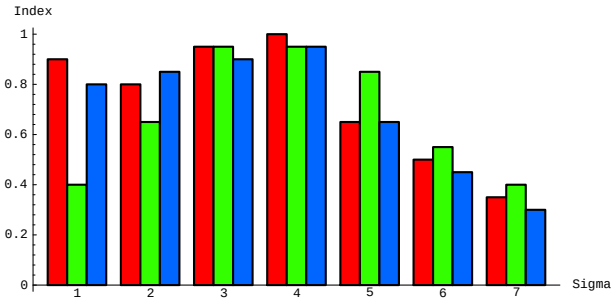

Figure 3.13 The results of the 2D matches, accumulated over 5 slices. The higher the bar, the more accurate a match is, up until the maximum 1, which represents a sub-pixel difference with the marker based gold standard. The left bar of each group represents the results obtained with the L_{vv} operator, the center bar the $L_{vv}/\sqrt{(L_w)}$ operator, and the right bar the L_{vv}/L_w operator.

3.5.1.2 3D ridge and trough operators

The results of 2D matchings after applying the 3D differential operators are in table 3.1. Only two operators (L_{vv} and L_{vv}/L_w) at one sigma were tried in these tests, because of the labour intensiveness of the feature extraction.

All matchings now have a sub-pixel error compared to the marker based gold standard, with the exception of slices 65 and 140. Slice 65 is a slice trough the base of the brain, where the ridge differences between CT and MR are larger. The skull ridge is less well defined. Even so, although the global correlation minimum supplies us with a bad match, there is a local correlation minimum near that *does* furnish a sub-pixel accurate match. Slice 140 is near the top of the brain: the rotation symmetry makes a good match nearly impossible. This problem vanishes when matching in 3D.

3.5.2 3D matching results

We tested and assessed the ridge matching (3D-L_{vv} and 3D-L_{vv}/L_w operators) on two pairs of unmatched CT and MRI brain scans. The first pair is the same as the one used in the previously described experiments, however the original

operator	slice	result	isolated
L_{vv}	65	$-$	
L_{vv}	73	$++$	•
L_{vv}	94	$++$	•
L_{vv}	108	$++$	•
L_{vv}	119	$++$	•
L_{vv}	140	$+$	•
L_{vv}/L_w	65	$++$	•
L_{vv}/L_w	73	$++$	•
L_{vv}/L_w	94	$++$	•
L_{vv}/L_w	108	$++$	•
L_{vv}/L_w	119	$++$	•
L_{vv}/L_w	140	$+$	•

Table 3.1 The results of the 2D matches, with 3D differential operators used. The results are categorized as follows: $++$ means the matching error is within one pixel translation and one degree rotation, $+$ means the error is within 2 pixels and 2 degrees, $-$ means the solution found was a false one (any solution farther away than 5 pixels and 5 degrees). There is a mark in the last column if the found minimum was well isolated, i.e., there is no other solution near.

MR is used instead of the marker matched version. The second pair consists of a T1 FFE MR image, sampled 256x256x100, with pixel size approximately 0.9 mm and slice thickness 1.5 mm, with contiguous slices, and a CT image sampled 256x256x128, with pixel size approximately 0.7 mm and 1.5 mm contiguous slices.

The matching results were assessed visually by extracting an ample number of sagittal, transversal and coronal slices from the matched images, then overlaying well defined bone contours[9] from the CT slice onto the MR slice, and visually evaluate the 'goodness of fit'. The fit was compared to the fit obtained by a marker matching method (van den Elsen & Viergever 1994, van den Elsen 1993), which was already in itself termed good enough for clinical purposes. The conclusion was that both ridge-correlation matches were even better than the marker-based match, as is illustrated in figure 3.14 , where the marker-based and the L_{vv}-ridge-based match are compared. The L_{vv} and L_{vv}/L_w ridge-based methods furnished matches so close to each other, that deciding on the better one was an impossibility.

3.6 Conclusion and discussion

We have constructed two- and three-dimensional ridge detecting differential operators, strongly related to isophote curvature. Review shows that numerous

[9] Bone contours can be extracted from CT very well using simple thresholding techniques.

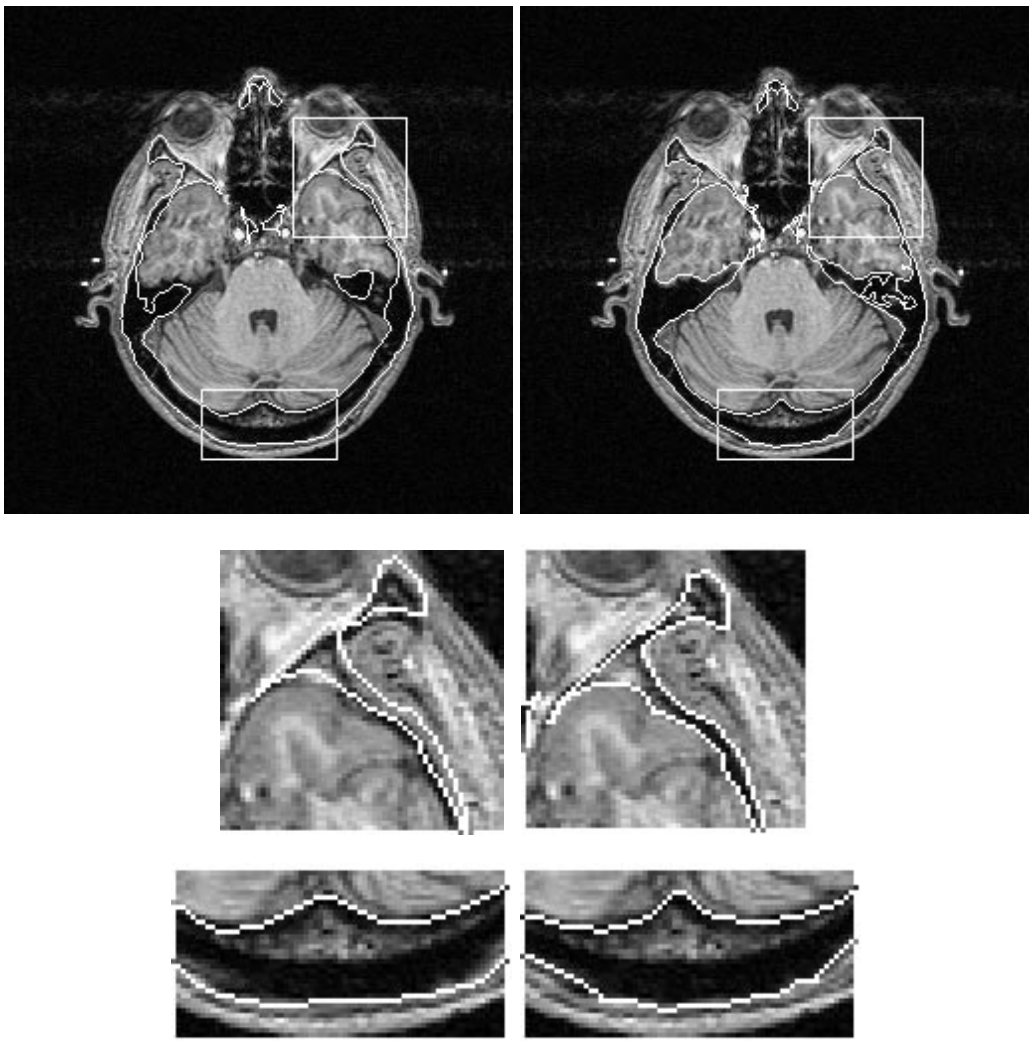

Figure 3.14 CT bone contours overlayed on matched MR slices. The rectangles indicate the magnified areas below. The left two magnified areas and the top picture show overlays obtained from the marker-based matching, the right two magnified areas and the second picture show overlays obtained from the ridge-based matching. The middle row shows a magnified part where the ridge-based matching results are visually superior to the marker-based results. The bottom row shows the magnification of a part which seems equally good for both methods.

mathematical examples can be constructed where these operators fail to find what is intuitively named the 'ridge'. However, experiments on 'real-life' medical images emphatically show the robustness of the operators in extracting ridge-like structures.

The ridge images of CT and MR images of the human head were used to find the matching transformation between the original images. This transformation was found by minimizing the correlation value between the ridge images. Both of the tested ridge detectors performed well on two pairs of sampled CT/MR images. The extraction of the ridge images and the matching process can be done *fully automatically*, once imaging protocol dependent variables have been determined. Visual evaluation of the obtained matches, by overlaying CT bone contours on to the matched MR images, shows the method to be very accurate.

As yet, we can provide no solid criterion for selecting one of the 3D ridge operators for matching purposes. The number of computer operations needed to compute different ridgeness images is (virtually) the same for all operators presented. The L_{vv} and L_{vv}/L_w operators both performed well in our experiments. Both operators have distinct advantages of which the impact on (correlation) matching has yet to be assessed. For example, L_{vv}/L_w is insensitive to general intensity transformations of the original image, which makes it the more robust operator in applications where this invariance is essential. L_{vv}, however, ignores spurious structure in the image background, which is a distinct advantage in the correlation matching process. In further research, the comparison between these two operators will be continued. Topics which have not been properly addressed are the influence of distortion owing to the image modality, or owing to disease or surgery. Local geometric distortion of 1 to 2 voxels is possible in MR. In our experiments, however, this does not have a significant impact on the global transformation found. Deformation of the brain may be a serious problem if it occurs between the imaging of the modalities to be matched. Such an event may call for a local matching approach. Deformation of the brain surface may locally disturb the proper detection of the skull ridge in MR images, possibly to the extent of causing the matching to fail. The marrow ridge however, is unlikely to be influenced. Such topics are still to be properly investigated. Also, we will study other operators, specifically edge detectors, and compare the resultant matches, as well as investigate overall performance in more general matching problems.

Appendices

3.A Solution to equation (3.8)

The form of equation (3.8) best represents its character as a minimal second directional derivative. We could also have written

$$\text{minimize } a_i H_{ij} a_j, \tag{3.12}$$

(where H is the Hessian matrix), under the constraint $L_i a_i = 0$, which gives a tensorial representation. We will use the latter form for conciseness.

We can remove the superfluous third dimension from our problem by rotating the coordinate system until the plane spanned by the x and y axes is parallel to our search plane. So, upon defining $a_i^{(r)} = R_{ij} a_j$, (the rotation matrix R is defined below) and $H_{ij}^{(r)} = R_{ik} H_{kl} R_{jl}$, we may write (3.8) as:

$$\text{minimize } a_i^{(r)} H_{ij}^{(r)} a_j^{(r)} \tag{3.13}$$

under the constraint $a^{(r)}[z] = 0$, (where $a^{(r)}[z]$ is the z-element of $a^{(r)}$), and $a^{(r)}[x]$ and $a^{(r)}[y]$ are not both zero. Since only the direction of a, and not its length, is important, the constraint $\|a\| = \sqrt{a_i a_i} = 1$ is added to further simplify the problem. In the above, R_{ij} is a rotation matrix satisfying

$$R_{ji} R_{jk} = \delta_{ik} \quad \text{and} \quad R_{ij} w_j = \begin{pmatrix} 0 \\ 0 \\ \sqrt{w_k w_k} \end{pmatrix} . \tag{3.14}$$

System (3.13) is basically two-dimensional. A possible R_{poss} (it is not unique) is

$$R_{poss} = \mathbf{diag}(n_1\ n_2\ n_3) \begin{pmatrix} L_x L_z & L_y L_z & -L_x^2 - L_y^2 \\ -L_y & L_x & 0 \\ L_x & L_y & L_z \end{pmatrix} . \tag{3.15}$$

The vector $(n_1\ n_2\ n_3)$ has entries equaling the inverse of the norms of the first, second and third row of the matrix respectively. The rows of R then form an orthonormal basis and system (3.13) transforms to $\alpha(a^{(r)}[x])^2 + \beta(a^{(r)}[x])(a^{(r)}[y]) + \gamma(a^{(r)}[y])^2$, to be minimized with $(a_i^{(r)} a_i^{(r)})^{1/2} = 1$. Here $\alpha = H^{(r)}[x,x]$, $\beta = H^{(r)}[y,x] + H^{(r)}[x,y]$, and $\gamma = H^{(r)}[y,y]$. This is solved easiest using polar coordinates

($a^{(r)}[x] = r\cos\varphi, a^{(r)}[y] = r\sin\varphi$). Since $r \equiv 1$, the system transforms to a single equation in φ to be minimized:

$$(\alpha - \gamma)\sin 2\varphi = \beta\cos 2\varphi \tag{3.16}$$

or, in the original coordinates

$$\beta((a^{(r)}[x])^2 - (a^{(r)}[y])^2) + 2(a^{(r)}[x])(a^{(r)}[y])(\gamma - \alpha) = 0 \tag{3.17}$$

Substituting

$$(a^{(r)}[y])^2 = 1 - (a^{(r)}[x])^2, \tag{3.18}$$

we are left with

$$4(a^{(r)}[x])^4 - 4(a^{(r)}[x])^2 + \frac{\beta^2}{\beta^2 + (\alpha - \gamma)^2} = 0 \tag{3.19}$$

and an analoguous expression in $a^{(r)}[y]$. This yields two solutions $(a^{(r)}[x], a^{(r)}[y])$, one minimizing (ridge measure) and one maximizing (trough measure) equation (3.13). These solutions p and q (note that $p \perp q$) equal the directions of principal curvature on the surface defined by the local gradient w. We now have effectively defined a local coordinate system (w, p, q), with L_{pp} being the ridge measure and L_{qq} being the trough measure.

3.B Implementation of L_{pp} and L_{qq}

This section describes briefly how the 3D ridge measures in this paper were computed. For each pixel,

1. compute the first order derivatives (L_x, L_y, and L_z), and the Hessian (H), using scaled derivatives
2. compute the rotation matrix (R) from (3.15)
3. compute the rotated Hessian $H^{(r)}$, and determine α, β, and γ from its entries.
4. solve $a^{(r)}[x]$ and $a^{(r)}[y]$ from (3.19) and (3.18). There are two solutions, the ridge detecting direction, and the trough detecting one.
5. compute the ridge measure and the trough measure by substituting the found solutions in $a_i^{(r)} H_{ij}^{(r)} a_j^{(r)}$.

The computational cost is considerable. The larger part of the required operations is located in the computation of the derivatives, which consists of

1. Fourier transforming the original image
2. creating the nine required derivatives of Gaussians directly in the Fourier domain
3. multiplying each of the nine derivatives with the Fourier transform of the original image
4. transforming each result back to the spatial domain.

In all, ten Fourier transforms are needed. The further computation of the ridge measure in each voxel is based only on the nine derivative values computed for the voxel and takes relatively few computer cycles. It is the Fourier transform that requires the major part of the operations necessary, and should –if possible– be carried out using a hardware implementation. Also, since typically large image volumes are used for input data, some attention must be paid to proper memory management, to avoid the excessive swapping of data. The speed of the algorithm will drop dramatically if operations cannot be performed entirely in core memory.

Acknowledgments

This research was supported in part by the industrial companies Philips Medical Systems, KEMA, and Shell Research, as well as by the Netherlands ministries of Education & Science and Economic Affairs through a SPIN grant, and by the Netherlands Organization for Scientific Research (NWO), through a TALENT fellowship. The volumetric MRI shown in the figures was acquired in the hospital "Medisch Spectrum" in Enschede, courtesy of Dr G. Wilts. We furthermore thank L.M. Ramos, Dr P.F.G.M. van Waes and Dr F.W. Zonneveld for their efforts to supply the other images. Dr Evert-Jan D. Pol is gratefully acknowledged for his contribution to the development of the 3D L_{vv} detector and his comments on earlier versions of the manuscript. The valuable discussions with Dr Bart ter Haar Romeny are greatly appreciated.

[On getting theory and practice straight:]
Wagner's music is much better than it sounds.
Mark Twain.

Chapter 4

Comparison of Edge-based and Ridge-based Registration of CT and MR Brain Images.

J.B. Antoine Maintz
Petra A. van den Elsen
Max A. Viergever (1996a),
Medical Image Analysis,
slightly modified

Abstract

In modern medicine, several different imaging techniques are frequently employed in the study of a single patient. This is useful, since different images show complementary information on the functionality and/or structure of the anatomy examined. This very difference between modalities, however, complicates the problem of proper registration of the images involved, and rules out the most basic approaches –like direct grey value correlation– to achieve registration. The observation that some common structures will always exist is supportive of the statement that registration may be feasible using edges or ridges present in the images. The existence of such structures defined in the binary sense is questionable, however, and their extraction from images requires a segmentation by definition. In this paper we propose to use fuzzy edgeness *and* ridgeness *images, thus avoiding the need for segmentation and using more of the available information from the original images. We will show that such fuzzy images can be used to achieve accurate registration. Several ridgeness and edgeness computing operators were compared. The best registration results were obtained using a gradient magnitude operator.*

4.1 Introduction

Medical imaging techniques in common use today show very different aspects of the anatomy examined. For example, CT[1] shows mostly information on dense matter, while MRI[2] shows information on softer tissue types. Both modalities clearly show anatomical morphology, while SPECT[3] and PET[4] show functional aspects of the anatomy. When several imaging modalities are used in a single patient's case, correct *registration*, i.e., determining the transformation to bring one of the acquired images into agreement with the other(s), may facilitate correct diagnosis and/or treatment. Registration often is the first of two steps of an integration process, the second being image *fusion* (integrated or combined display), which mainly concerns the proper visualization of useful image information. In this paper we concentrate on the registration step. In particular, we focus on the registration of CT and MR brain images. This type of registration is useful, for example, in radiation therapy planning, where CT is used for dose calculations, while the lesion to be treated is often best seen on MR images (Chen & Pelizzari 1989). Another example for its use is skull base surgery. The delicacy of this type of surgery requires maximum knowledge of the anatomy involved, which can be supplied by integrating CT bone structures and MR soft tissue contrast images (Ruff, Hill, Robinson & Hawkes 1993).

Medical image registration can be divided into extrinsic registration methods based on artificial marking devices, and intrinsic registration methods using patient related image properties (van den Elsen, Pol & Viergever 1993, Viergever, van den Elsen & Stokking 1992). The method described here falls into the latter category. Registration algorithms using patient related image properties maximize a similarity measure between two images. This similarity may apply directly to the original grey value images (van den Elsen et al. 1994), to statistical voxel similarity measures, to feature images derived from the original images, or to objects defined in the initial or the derived feature images. Maximizing the similarity of the initial images will be useful in particular when two images of the same modality are to be registered. In multi-modality image registration, however, the physical realities of the two images can be quite different, which may call for statistical similarity based (Collignon, Vandermeulen, Suetens & Marchal 1995, Collignon, Maes, Delaere, Vandermeulen, Suetens & Marchal 1995, Studholme et al. 1995*b*, Woods et al. 1993, Hill et al. 1994),

[1] Computed Tomography
[2] Magnetic Resonance Imaging
[3] Single Photon Emission Computed Tomography
[4] Positron Emission Tomography

feature based or object based registration. Features used in image registration are, for example, edges (Borgefors 1988) and ridges (Monga et al. 1992, Guéziec & Ayache 1992, van den Elsen, Maintz & Viergever 1992, van den Elsen 1993, Thirion 1994, Liu et al. 1994). Object based registration may, e.g., be based on surface definitions (Levin et al. 1988, Pelizzari et al. 1989, Hemler, Sumanaweera, van den Elsen, Napel & Adler 1995) or anatomical landmarks (Maguire et al. 1991, Hill, Hawkes, Crossman, Gleeson, Cox, Bracey, Strong & Graves 1991, Lemoine, Barillot, Gibaud & Pasqualini 1991). Object based image registration has the disadvantage that the objects must be defined first, which is a high-level image processing task that often proves difficult, and may introduce errors for complex images. The use of low-level differential geometric features for image registration is attractive, but requires the careful choice of operators that produce sufficiently similar feature images when applied to multi-modal images. Note that such a similarity (within this context) is not always immediately obvious by visually comparing images. The optimal similarity with respect to specific computer vision measures does not necessarily coincide with the 'visual' optimum, as shown in our experiments.

When CT and MR brain images are depicted as intensity landscapes, the skull forms a ridge in the CT image, and a negative ridge (trough) in the MR image. If a 'ridgeness' extracting operator is applied to these images, the resultant feature images show remarkable similarity when compared visually (van den Elsen, Maintz & Viergever 1992). Moreover, since the skull is a virtually undeformable structure, its ridge/trough is ideally suited for registration purposes. Edgeness images of CT and MRI brain scans often have less visual similarity than ridgeness images, because the edge extraction generally produces a number of structures in either image which are not matched by similar structures in the companion image. Enough similarity, however, is present to furnish a good registration, as will be shown. It is the aim of this paper to compare the quality of registration using ridgeness and edgeness operators, combined with grey value cross-correlation of the feature images for registration.

Feature images can be extracted by means of differential operators. Conventional differentiation is ill-posed in the sense of Hadamard since we are dealing with digital, sampled images rather than smooth mathematical functions. Well-posed differentiation is possible, however, by convolving images with derivatives of Gaussians, as is explained in section two. This section also deals with the necessity of the operators being invariant under rigid transformations. In section three we define ridgeness and edgeness measuring differential operators, and include some examples of ridgeness and edgeness images. A cross-correlation based hierarchical registration algorithm is proposed in section four. In section five, the operators are applied to CT/MRI registration algorithm proposed,

and the results are reviewed. In section 6 the results are discussed, and some conclusions are drawn.

4.2 Differentiation of images

4.2.1 Invariants

Image features obtained by means of differential operators should be independent of the choice of coordinate system; the position and orientation of the image should have no impact on the features extracted. Hence invariance under the group of orthogonal transformations (translations, rotations, reflections) is demanded. An operator that conforms to this restriction is called an orthogonal *invariant*.

We will denote by L the image luminance as a function of spatial coordinates. Subscripts denote derivation with respect to some spatial variable. We employ the Einstein summation convention, *i.e.*, the expression is summed over any index occuring twice by letting the particular index assume all spatial dimensions, e.g., $L_i L_i$ denotes $L_x L_x + L_y L_y$ in two-dimensional space. Any tensorial expression in which all indices are resolved by means of contraction (pure or by multiplication by the Kronecker tensor, δ_{ij}) or alternation (multiplication by the Lévi-civita tensor,ε_{ij}) is an invariant (Spivak 1970). All operators presented in this paper satisfy this requirement.

4.2.2 Scale space

The differentiation of any sampled signal (e.g., an image) is ill-posed in the sense of Hadamard as opposed to the generally well-posed differentiation of smooth mathematical functions. Well-posed differentiation is possible by convolving the image with derivatives of a Gaussian (Florack et al. 1992). The width of the Gaussian used introduces a new parameter, the *image scale*, σ, which extends the image dimensionality by one. The thus defined image is usually referred to as the *scale space* of the original image (Witkin 1983, Koenderink 1984). By convolving an image with derivatives of Gaussians, we can compute image derivatives that correspond to the scale of structures. The scale is naturally bounded by the *inner* scale, the finest possible resolution, usually determined

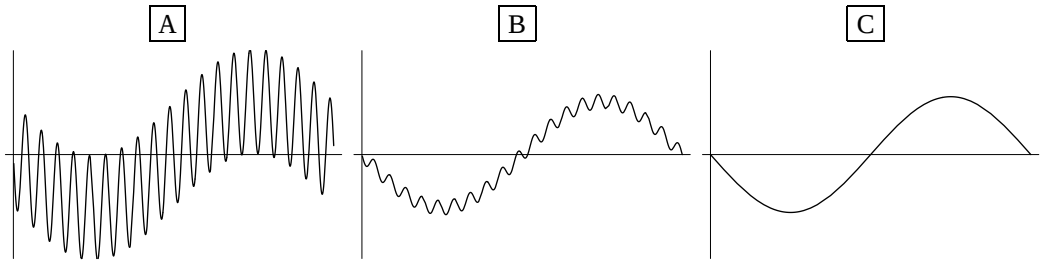

Figure 4.1 A function with distinct low scale and high scale features (A) is shown. Two convolutions of A with Gaussians of increasing width are also shown (B and C). Note that in the final picture only the large scale features of the original function remain.

by the aperture of the scanning device, and the *outer* scale, the largest possible scale, determined by the size of the entire image.

The use of the Gaussian as a convolution kernel is not mandatory. In fact, we can use any smoothing kernel to 'tune' differential operators to multi-local structures (local structures of certain spatial extent). However, upon demanding shift invariance, directional invariance (isotropy) and scale invariance, the Gaussian is the unique linear smoothing kernel (Florack et al. 1992, Florack et al. 1994). The (Gaussian) scale space $L(x, \sigma)$ of an image $L_0(x)$ is the continuous (hyper)stack of smoothed images, with the smoothing factor σ increasing as we rise in the stack. The original image rests at the bottom of the stack. The scale space can be computed using

$$L(x, \sigma) = (L_0 * G)(x, \sigma), \tag{4.1}$$

with

$$G(x, \sigma) = (2\pi\sigma^2)^{-\frac{d}{2}} \; e^{-\frac{x^2}{2\sigma^2}},$$

where G is the Gaussian kernel, x is the coordinate vector, σ is the smoothing factor, i.e., the scale, and d the number of spatial dimensions.

In figure 4.1 the notion of scale is illustrated. We show a function with a bimodal spectrum. ($f(x) = \sin(x) + \sin(20x)$, on a domain of $[0, 2\pi]$.) At a low scale, this function has 20 maxima and 20 minima –precluding boundary extrema– in the domain depicted. At a sufficiently high scale, the function has one maximum and one minimum). The use of the Gaussian (or, in fact, any smoothing kernel) for extracting these high scale extrema or to act as a low-pass filter is widely known and used. Scaling *and* differentiation however, are fused into a single operation within scale space: computing a derivative of L is equivalent to replacing

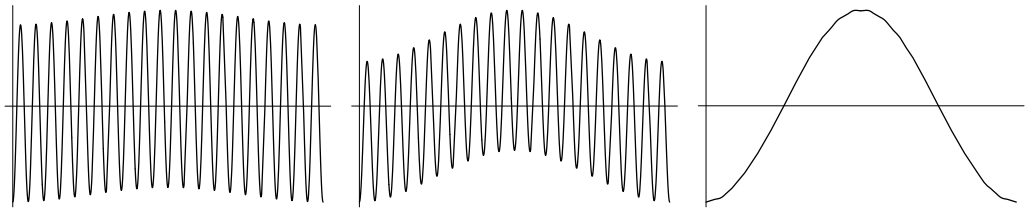

Figure 4.2 Three scaled first derivatives with increasing scale of the function in the previous figure. Note that in the final picture only the large scale features of the original function determine the resultant derivative. (Because the amplitude of the images varies largely, the images have been rescaled for display purposes.)

the Gaussian G with its appropriate derivative in the convolution operation:

$$(L_{i_1 \ldots i_n})(x,\sigma) = (L_0 * G_{i_1 \ldots i_n})(x,\sigma), \tag{4.2}$$

where subscripts i_j denote the order of derivation with respect to the spatial variables; $i_j \in \{\mathbf{x},\mathbf{y},\mathbf{z}\}$, $n \in \mathbb{N}^+$, $j = 1 \ldots n$. This property is easily verified: suppose $f = f(x)$, where f represents a sampled signal on a bounded domain (say, $f(x) = \text{Ш}(x)f'(x)$, Ш being the Shah or replicating symbol, and f' the actual signal) with the Fourier transform defined in the limiting case, and suppose $g = g(x)$, where g is some well-behaved smooth kernel, and consider $\frac{d}{dx}(f * g)$. In theory, this last expression equals $\frac{df}{dx} * g$ as well as $f * \frac{dg}{dx}$, since the Fourier transform of all three equals $i2\pi s\mathcal{F}(s)\mathcal{G}(s)$,where calligraphic letters $(\mathcal{F},\mathcal{G})$ denote Fourier transforms. The latter form is the only one well-posed, however. Figure 4.2 illustrates scaled differentiation.

The numerical complexity of the computation of a differential image at a certain scale is reduced to mere multiplications, when all computations are done in the frequency domain:

$$(L_{i_1 \ldots i_n})(x,\sigma) = (\mathcal{F}^{-1}[\mathcal{L}_0 \cdot \mathcal{G} \cdot i^n \cdot \prod_j \omega_{i_j}])(x,\sigma), \tag{4.3}$$

where $\mathcal{F}^{-1}$ denotes the inverse Fourier transform, and ω_{i_j} represent the spatial frequencies.

4.3 Feature measures

4.3.1 Ridgeness measures

For the differential-geometrical detection of ridge-like structures, many different schemes and mathematical ridge definitions have been proposed, some dating back for well over a century (Maxwell 1859). Koenderink showed that for some popular definitions based on the water drainage pattern of a landscape, a local ridge detector does not exist (Koenderink & van Doorn 1994). However, there are a number of geometrical invariants that approximate ridges well in a wide variety of images (Eberly et al. 1994). We have selected the so-called L_{vv} and closely related operators (van den Elsen, Maintz, Pol & Viergever 1992, van den Elsen, Maintz & Viergever 1993). A comparison with other ridge operators can be found in (Maintz, van den Elsen & Viergever 1996*b*), which also illustrates known shortcomings of this local operator.

$\boldsymbol{L_{vv}}$: The ridgeness operators used in this paper are derived from the L_{vv} operator. In this formula v is defined in a local gradient based coordinate system (v, w): $w_i = L_i$, and $v_i = \varepsilon_{ij} L_j$ in tensor notation. Therefore L_{vv} represents the second order derivative in the direction perpendicular to the local gradient. The value of L_{vv} can be computed using (Cartesian) local derivatives:

$$L_{vv} = \frac{1}{\|v\|^2}(v \cdot \nabla)^2 L = (L_y^2 L_{xx} - 2L_x L_y L_{xy} + L_x^2 L_{yy})(L_x^2 + L_y^2)^{-1}. \qquad (4.4)$$

The generalization to 3D can be found in (Maintz, van den Elsen & Viergever 1996*b*). This generalization is non-trivial, since in 3D the v direction as being perpendicular to the local gradient, needs another constraint to be properly defined.

$\boldsymbol{L_{vv}/L_w}$: L_{vv}/L_w Can also be considered a ridgeness measuring operator. This formula derives from the observation that in two dimensional images, the local gradient changes direction when crossing a ridge. Consequently, an alternative definition of ridgeness is the rate by which the gradient direction changes when moving along the v direction. Let the two-dimensional gradient orientation be denoted by $\theta = \arctan(\frac{L_y}{L_x})$. The new ridge measure then is

$$\frac{\partial \theta}{\partial v} = \frac{1}{\|v\|}(v \cdot \nabla)\theta = \frac{1}{\|v\|}(L_y \frac{\partial \theta}{\partial x} - L_x \frac{\partial \theta}{\partial y}) = \frac{2L_x L_y L_{xy} - L_y^2 L_{xx} - L_x^2 L_{yy}}{(L_x^2 + L_y^2)^{\frac{3}{2}}}, \qquad (4.5)$$

Notice that $\frac{\partial \theta}{\partial v} \equiv -\frac{L_{vv}}{L_w}$, so in fact the only difference with L_{vv} is a negation and a normalization with respect to the gradient magnitude. $-\frac{L_{vv}}{L_w}$ Often appears in

literature as the *isophote curvature*, frequently denoted by κ. The normalization of L_{vv} with respect to the gradient magnitude ($\frac{L_{vv}}{L_w}$) causes it to react stronger than L_{vv} in areas of the image where the variation in image intensity is relatively small, i.e., relatively flat areas in the intensity landscape.

$\boldsymbol{L_{vv}L_w^{\alpha}}$: Both L_{vv} and $L_{vv}L_w^{-1}$ have been identified as ridgeness measures. The notion of L_{vv} and L_{vv}/L_w as ridgeness measures can be readily expanded towards the more general formula $L_{vv}L_w^{\alpha}$, where α is bounded. The ridgeness operators used in this paper can be written in this form, with $\alpha \in \{-1, -0.5, 0\}$, although other values for α could be considered as well.

4.3.2 Edgeness measures

Well known edge measures are the gradient magnitude (L_w), and the Laplacian (L_{ii}). L_w measures the local 'steepness' of the intensity landscape, which presumably has a local maximum at an edge. It is a good detector for step edges. When edges get less steep, use of the Laplacian often gives better results. For example, in the 1D case of an edge, the Laplacian has a positive response in the convex part of the edge flank, and a negative response in the concave part. The edge locus is presumed to be at the zero crossing between these two parts.

4.3.3 Miscellaneous measures

Besides edge and ridge measures, we employed some other invariant measures, which are briefly mentioned here. Cartesian expressions are given in their 2D form.

$\boldsymbol{L_{vv}L_w^2}$: $L_{vv}L_w^2$ is a cornerness measure based on the work of Kitchen and Rosenfeld (Kitchen & Rosenfeld 1982) and Blom (Blom 1992). Note that it equals the (negated) isophote curvature times the gradient magnitude cubed: $L_{vv}L_w^2 = \frac{L_{vv}}{L_w}L_w^3$. The idea behind this detector is that the isophote curvature is extremely high at corners. As the isophote curvature reacts equally strong at 'background' structures and 'real' objects, and has a response at ridges, it is multiplied by a power of the gradient magnitude, to avoid phantom responses. This also solves the faulty detection of corners at local extrema (where $L_w = 0$). In the strictest sense, $L_{vv}L_w^2$ is categorized in our class of ridge detectors $L_{vv}L_w^{\alpha}$. However, valid values for α are bounded, and —although the exact bounds are subjective– 'cornerness measure' is a better description of $L_{vv}L_w^2$ than 'ridgeness

measure': the strong response at corners relatively suppresses the response at ridges. Some ridgeness information can be extracted from $L_{vv}L_w^2$ images by windowed display, or by enhancing the response at ridges by re-mapping the operator as $(L_{vv}L_w^2)^{(1/n)}$, where $n > 1$. Experiments have shown $n = 3$ to be a satisfying choice. In Cartesian notation, $L_{vv}L_w^2$ equals the numerator of the Cartesian expression of L_{vv}: $L_{vv}L_w^2 = L_y^2L_{xx} - 2L_xL_yL_{xy} + L_x^2L_{yy}$.

$\boldsymbol{L_{vw}}$: As $-\frac{L_{vv}}{L_w}$ equals the isophote curvature, $\frac{L_{vw}}{L_w}$ equals the flowline curvature, where the flowline is defined as the integral curve of the gradient. In each point of an image, the local flowline and isophote are perpendicular by definition. We employ L_{vw}, obtained by multiplying the flowline curvature with the gradient magnitude, thus diminishing its response in uninteresting areas. The Cartesian expression of L_{vw} equals $(L_xL_y(L_{yy} - L_{xx}) + L_{xy}(L_x^2 - L_y^2))/(L_x^2 + L_y^2)$.

$\boldsymbol{L_{ww}}$: $\frac{L_{ww}}{L_w}$ is a measure for isophote density. As with the previous expressions, we use the expression L_{ww} to reduce uninteresting responses. L_{ww} is closely connected to the Laplacian and L_{vv} ridgeness by the relation $L_{ww} = L_{ii} - L_{vv}$. The Cartesian expression of L_{ww} equals $(L_{xx}L_x^2 + 2L_{xy}L_xL_y + L_{yy}L_y^2)/(L_x^2 + L_y^2))$.

umbilicity, $\boldsymbol{L_{ij}L_{ji}}$: The umbilicity of a point can be determined by computing $\varepsilon_{ij}\varepsilon_{kl}\frac{L_{ik}L_{jl}}{L_{mn}L_{nm}} = \frac{L_{ii}L_{jj} - L_{ij}L_{ji}}{L_{kl}L_{lk}}$. The numerator equals twice the determinant of the Hessian $\det L_{ij}$, which is a measure for local ellipticity (positive value) or hyperbolicity (negative value) of a surface patch. A zero value of this determinant indicates a parabolic or planar patch. The denominator normalizes the umbilicity measure so as to be bounded by -1 and 1, which is most obvious when examining the form containing the ε tensors. The denominator can therefore be regarded as an 'unflatness'-measure. The Cartesian expression of umbilicity equals $2(L_{xx}L_{yy} - L_{xy}^2)/(L_{xx}^2 + 2L_{xy}^2 + L_{yy}^2)$.

checkerboard detector, Y-junction detector: The third and fourth order binary forms L_3 and L_4 of an image L at coordinates $\vec{x}$ are $\frac{1}{3!}L_{ijk}x_ix_jx_k$ and $\frac{1}{4!}L_{ijkl}x_ix_jx_kx_l$ respectively. The discriminants D_3 and D_4 of these forms can serve to detect Y-junctions and 'checkerboard' patterns respectively. The reader interested in a theoretical expansion of these expressions is referred to (Florack, ter Haar Romeny, Koenderink & Viergever 1993, ter Haar Romeny, Florack, Koenderink & Viergever 1991). The Cartesian expressions are: $D_3 = 6L_{xyy}^2L_{xxy}^2 - 2L_{xxx}^2L_{yyy}^2 - 8L_{yyy}L_{xxy}^3 - 8L_{xyy}^3L_{xxx} + 12L_{yyy}L_{xyy}L_{xxy}L_{xxx}$ and $D_4 = (L_{xxxx}L_{yyyy} - 4Lxxxy L_{xyyy} + 3L_{xxyy}L_{xxyy})^3 - 27(L_{xxxy}(L_{xxxy}L_{yyyy} - L_{xyyy}L_{xxyy}) + L_{xxyy}(L_{xxxy}L_{xyyy} - L_{xxyy}L_{xxyy}))^2$.

4.4 Registration method

The purpose of this paper is to register CT and MR brain images by means of geometrical image features. After having determined feature images as discussed in section 3 , we need to register the feature volumes or slices. The method we use to this end is cross-correlation of grey values. By using the grey values directly we avoid segmentation of our feature images. We seek the global optimum of the correlation value $c(t)$ of the CT feature volume L_1 and the MR feature volume L_2 over all rigid transformations t, where $c(t)$ is defined

$$c(t) = \sum_{(x,y,z)\in L_1} L_1(x,y,z)L_2(t(x,y,z)).$$

A brute force approach in which all possible values of t are investigated is computationally infeasible. We therefore resort to a multi-resolution method and a number of assumptions on the behavior of $c(t)$ to find the optimal t within an acceptable number of computational operations. A multi-resolution pyramid is created, with the original image at its bottom. The next level is formed by maximizing or minimizing each group of up to eight neighboring voxels into one voxel. The choice between maximizing and minimizing is based on the sign of the relevant response. Some operators change sign at interesting voxels, e.g., L_{ii}, and here an often arbitrary choice between maximizing and minimizing has to be made. New pyramid levels are formed as long as the largest image structures are clearly discernible. Typically, the pyramid will consist of four levels. Between the (very low resolution) top levels of the feature pyramids the optimal registration is found by optimizing the correlation value using an exhaustive search. Local extrema within a certain percentage of the strongest extremum found are passed on as search seeds to the next pyramid level, where new searches are started. As we progress further down the pyramid, the absolute search range of t (i.e., the actual range in parameter space in terms of millimeters and degrees around a certain origin) diminishes, as do the step sizes. By keeping the search range small, the number of values for t to test remain computationally feasible. To avoid the risk of a search range around a seed being too small, and a correlation optimum being missed, a hill-climbing operation may be performed after the search for a local optimum. Details on the procedure are furnished in (van den Elsen, Maintz & Viergever 1993, van den Elsen 1993). These references also explain in more detail the advantages of the correlation method over e.g. surface based methods (Levin et al. 1988, Pelizzari et al. 1989), which are computationally more attractive. These advantages include the absence of a segmentation step and decreased sensitivity to differences in the structures used for registration.

4.5 Application of feature measures to CT/MRI registration

4.5.1 Similarity of feature volumes

The edge (L_w and L_{ii}) and ridge operators (L_{vv}, $L_{vv}/\sqrt{(L_w)}$, and L_{vv}/L_w) all have a high degree of similarity when comparing CT and MR feature images of the brain (see figure 4.3). Of the ridge operators, (when grey values are scaled equally) L_{vv} looks most appealing because it shows less background response than the other operators. All ridge operators show a clearly visible ridge at the center of the skull. The L_w operator shows a high degree of similarity, notably the skin and skull edges. L_{ii} also shows this similarity, however, the CT pattern at the skin edge matches that of the MRI, whereas the pattern at the skull edge is reversed. Since both positive and negative responses are interesting (and occur coupled at edges), the building of the resolution pyramids can be done arbitrarily by maximizing or minimizing, as long as both pyramids are constructed the same way, and either feature image is reversed beforehand. We can then optimize the value of the correlation $c(t)$, which is maximal if the structures at the bone edge are properly aligned. It must be noted that the simultaneously occuring alignment of the skin edge has the adverse effect of lowering the correlation value. Fortunately, we have not seen this to disrupt finding the correct registration.

L_{ww} has the same ambiguity of patterns occuring both matched and reversed. It shows both edge and –at higher scales– ridge structures, and also looks promising. $L_{ij}L_{ji}$ is hard to assess visually, as it produces 'double-edge'-like structures which tend to interfere with each other. L_{vw} also poses difficulties. There is a definite similarity to the human eye, but its rapid sign changes at ridge structures makes the matching behavior hard to predict. The checkerboard, Y-junction, $L_{vv}L_w^2$ (corner), and umbilicity images show very little similarity to the human eye.

Regardless of the above observations on similarity, all operators were tested in the registration scheme described in section 4. We emphasize that we can only draw conclusions concerning the registration quality of invariant operators for our particular use of cross-correlation registration, not for integration regardless of the registration paradigm.

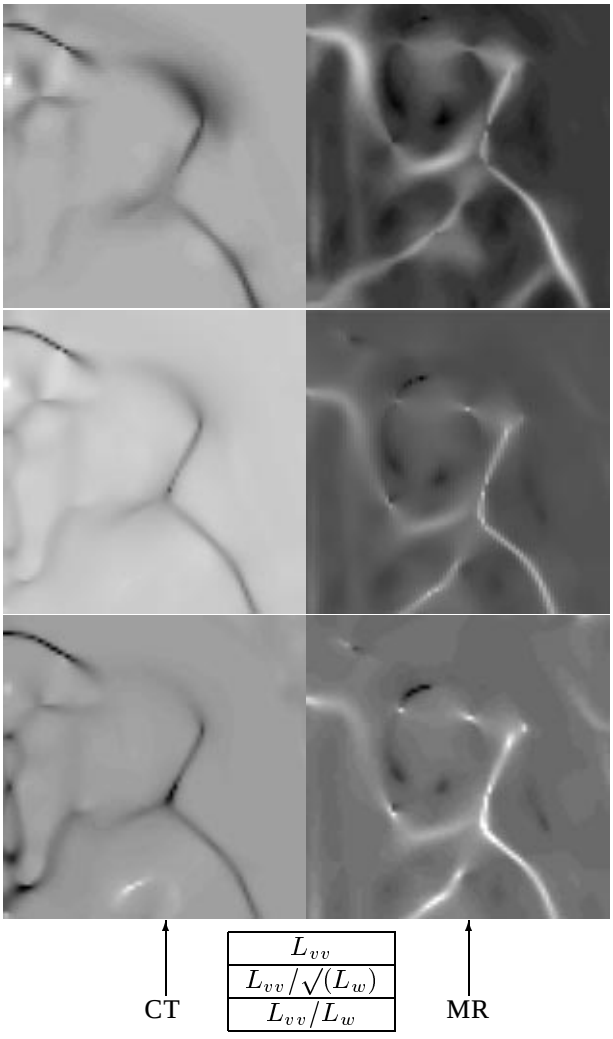

Figure 4.3 Visual comparison of the edge and ridge feature operators applied to an MR image and a registered CT image. Various scales were employed. The images show a zoom of the feature images around the right eye socket. The actual area depicted may differ between images to allow the inclusion of some interesting features. Of some images the grey values have been linearly re-mapped for display purposes.

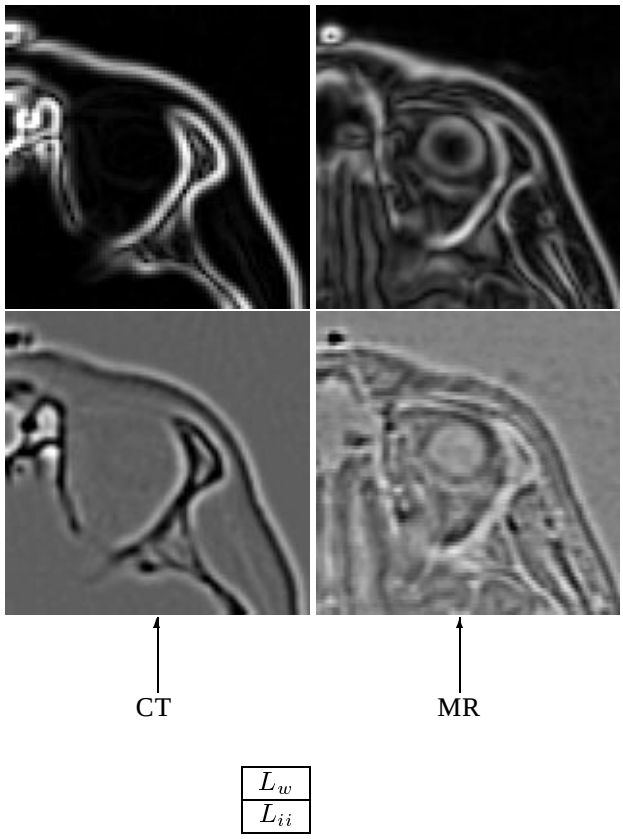

Figure 4.3 (Continued.)

4.5.2 2D registration experiments

To test the registration performance of all of the operators described, five representative registered pairs of CT and MRI transverse slices were chosen. These slices were chosen from volumes registered using skin markers (van den Elsen & Viergever 1994).

Each of the 5 operators was tested by registering the 5 slice pairs, at scales ranging from 1 to 7 mm, using 4 different artificially induced initial transformations

	initial transformation		initial maiming	
#	translation (mm)	rotation (deg)	#	power loss
1	(0,0)	0	1	0%
2	(10,10)	0	2	15.6%
3	(0,0)	15	3	55.9%
4	(15,15)	15	4	64.2%

Table 4.1 The initial transformations and initial 'maimings' of the images used in the 2D registration experiments. The last column shows the percentage of image power loss when applying the maiming, to give an indication of the severity of the maiming.

of one of the images of the registration pair, ranging from no transformation to 15 mm translations and 15 degrees rotation (see table 4.1).

After artificial transformation of the CT image of a pair, the feature operator in question was applied to both the images to be registered, and the resultant feature images were registered. Since some operators can suffer from boundary artifacts, additional experiments were performed to ensure these had no influence on the registration outcome. Ideally, the registration transformation found equals the inverse of the applied initial transformation, since the images were taken from sets registered beforehand. We must be careful to accept this transformation as a gold standard however, since the original registration will inevitably have a (small) error. Moreover, the original registration was based on 3D information, while we now register using the 2D slice information only. To make sure the original registration is an acceptable standard, it was re-assessed visually within the 2D slice, and compared visually to typical transformations found in the experiments. The original registration was visually found to be an excellent standard for all experiments.

Based on this run of experiments, the checkerboard, Y-junction, umbilicity, L_{vw}, L_{ww}, and $L_{ij}L_{ji}$ operators were discarded: in none or only very few cases a correlation optimum was found at the ideal matching transformation. The registration results based on the edge and ridge operators were very good[5] in almost all of the experiments. The L_{vv}/L_w was not used in further experiments, however, since there often were many local registration optima near the value of the optimum obtained at the correct registration transformation. Since all of these optima will have to be investigated by the registration program, the runtime increases dramatically. Because the $L_{vv}/\sqrt{(L_w)}$ and L_{vv} operator had no such problems, the L_{vv}/L_w operator was discarded.

[5] 'Very good' meaning here that shifting the registered images by a single pixel (or rotating the image so that there was a single pixel shift at the edge of the region of interest) worsened the registration when assessed visually.

deviation	index
$0 \leq . \leq 1$	1
$1 < . \leq 2$	0.75
$2 < . \leq 5$	0.5
$5 < . \leq 10$	0.25
$10 < .$	0
indeterminable	0

Table 4.2 Index values assigned to registations with a certain deviation from the reference match.

The remaining operators (L_{vv}, $L_{vv}/\sqrt{(L_w)}$, L_{ii}, and L_w) were tested further in three experiment runs, comprising 1680 experiments. Each run is similar to the initial run of experiments, except we now 'maim' the CT image before the start of the experiments (by cutting away specific parts of it), making correct registration harder, because there is less information available to base it on. The particular image loss induced by each 'maiming' is shown in table 4.1. To interpret the large amount of experimental results, each registration result was categorized as belonging to one of six classes of increasing registration accuracy. These classes were subsequently indexed, where the index ranged from '0' for the class of failed registrations (more than 10 pixels or degrees deviation, or no registration transformation found at all), to '1' for the class of registrations with less than 1 pixel or degree deviation from the original marker registration, as shown in table 4.2.

For each operator, the average experimental index was computed. Note that specific values of this index have no quantitative interpretation (in a sense like '0.5' means 50% of the registrations were registered adequately). Within one slice pair it can be used to compare operators though, since a higher index can be interpreted as a better registration performance. The overall performance index for each operator as a function of scale is shown in figure 4.4.

The best performance index and the scale at which this index occured is given in the table included in figure 4.4.

Evidently, L_w has the best overall performance. The edgeness detectors (L_w, L_{ii}) perform slightly better than the ridgeness detectors on their respective optimal scales. L_w is the least sensitive to changes in scale, as the graph shows. The maximum of the edge operators is a boundary maximum, which suggests that the actual maximum may occur at a scale lower than 1 mm. As computing derivatives at such low scales is infeasible on most image volumes since these scales are undersampled, scales lower than 1 mm cannot be properly examined.

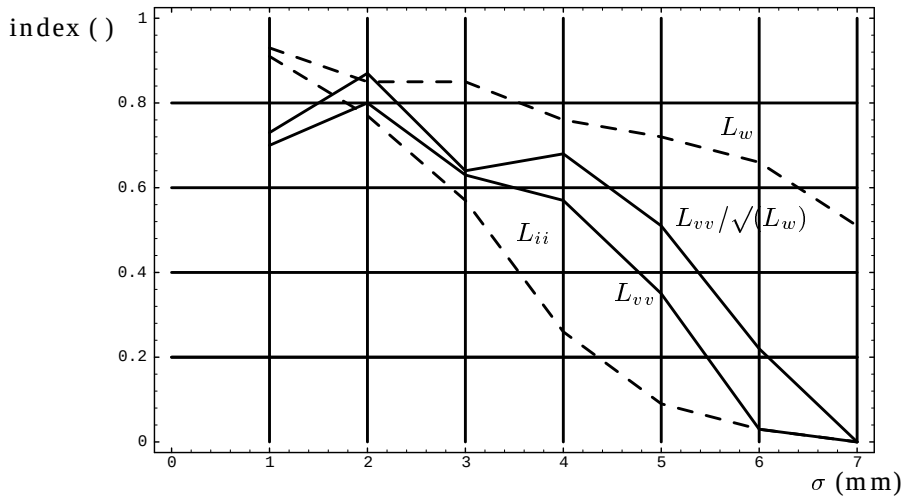

operator	best index	scale
L_w	0.93	1
L_{ii}	0.91	1
$L_{vv}/\sqrt{(L_w)}$	0.87	2
L_{vv}	0.80	2

Figure 4.4 Performance index of the four feature operators as a function of scale (top), and the value of the best index that occured for each operator (bottom). In the graph, edge operators are represented by dashed lines, and ridge operators as solid lines.

4.5.3 3D registration experiments

The 3D experiments comprised correlation registrations of the L_{vv}, $L_{vv}/\sqrt{(L_w)}$, L_{ii}, and L_w feature images of high resolution 3D CT and MR brain images[6]. The optimum operator scale was derived from the 2D experiments. The registration transformation found was compared to a previously established registration based on marker methods (van den Elsen & Viergever 1994). Additionally, the same experiments were carried out on volumes of lower transverse resolution. These volumes were generated from the high resolution sets by averaging each 2 (CT) or 3 (MR) slices into one slice, thus simulating 3 mm slices. We use simulated sets instead of directly acquired sets, because an accurate registration reference standard is needed, which is difficult to check visually for low-resolution

[6]The MR data set is a transverse T1 weighted 3D/FFE set, TR=30 msec, TE=9 msec, containing 180 slices, no gap, with cubic voxels of approx. $1mm^3$, obtained on a 1.5 Tesla Philips Gyroscan S15/ACS. The CT data set is a contiguous 100 slice set, pixel size approx. 0.9 mm, slice thickness 1.5 mm, obtained on a Philips Tomoscan 350, set to 120 kV and 120 mA.

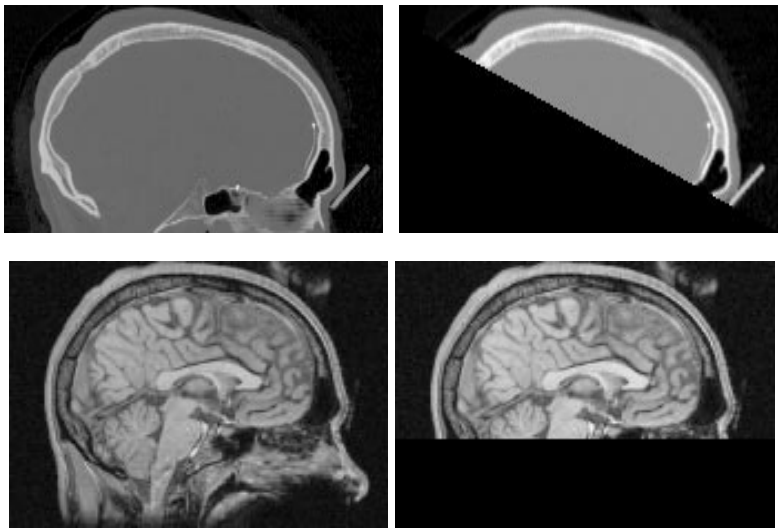

Figure 4.5 The midsagittal planes from the volumes used in the 3D registration experiments (top CT, bottom MRI). The right frames show the corresponding maimed images.

sets. Finally, we repeated all of the above described experiments on maimed sets. Both the CT and MR volumes were maimed, as indicated in figure 4.5. The power loss is 27.1% in the case of the MR volume, and 56.9% in case of the CT volume.

The results are summarized in the tables 4.3 and 4.4.

We increased the scale of the edge operator when using the low resolution sets, to maintain an appropriate scale relative to the slice thickness. If the scale were not increased, the operator is asked to supply information on an under-sampled level of detail. Table 4.3 shows the results of the 3D registration experiments.

The resultant registration transformation furthest from the reference registration was selected from the high resolution experiments (the L_{vv} registration), and subsequently applied to the original datasets. The thus found registration was compared visually to the original reference registration. This comparison was done by segmenting the bone contours –by grey value thresholding– from various transversal and sagitally and coronally reformatted slices from the registered CT volume, and overlaying these contours onto the corresponding MR slices (Maintz, van den Elsen & Viergever 1996*b*, van den Elsen, Maintz & Viergever 1992, van den Elsen, Maintz & Viergever 1993). Two independent observers concluded that the reference registration is inferior to the newly found

operator	σ	high res	maim	result						miss	#
				translation			rotation				
				x	y	z	x	y	z		
L_w	1	•		-0.02	0.04	0.44	0.45	-0.62	2.04		1
L_w	2			0.22	-0.20	-0.39	0.68	-0.17	1.37		1
L_w	1	•	•	0.22	0.98	0.44	0.00	0.28	1.37		6
L_w	2		•	0.45	0.27	-3.61	-0.22	1.17	2.04		0
L_{ii}	1	•		-0.02	0.04	1.22	0.45	-0.39	2.04		11
L_{ii}	2			0.22	0.04	1.16	0.68	0.05	2.94		0
L_{ii}	1	•	•	0.22	0.74	0.84	0.00	0.05	2.04		15
L_{ii}	2		•	0.45	0.98	-1.19	-0.44	0.05	2.04		1
L_{vv}	2	•		-0.25	0.04	1.60	0.45	-0.39	2.27		0
L_{vv}	2			-0.25	0.04	1.20	0.45	-0.17	2.04		0
L_{vv}	2	•	•	-0.25	0.04	1.60	0.45	-0.39	2.27		0
L_{vv}	2		•	∞	∞	∞	∞	∞	∞	•	(97)
$L_{vv}/\sqrt{(L_w)}$	2	•		-0.48	0.98	1.60	0.68	-0.17	2.04		0
$L_{vv}/\sqrt{(L_w)}$	2			0.45	-0.66	-1.20	1.35	0.73	4.28		1
$L_{vv}/\sqrt{(L_w)}$	2	•	•	0.22	0.98	0.83	0.23	0.05	1.82		4
$L_{vv}/\sqrt{(L_w)}$	2		•	0.22	1.21	-4.34	-0.44	0.50	0.92		16

Table 4.3 The results of the 3D registration experiments. The 'result' column shows the difference between the transformation found by feature registration and the reference transformation obtained by marker registration. The figures show the translation and rotation of the center CT volume voxel. All values mentioned are in millimeters or degrees. The obvious mismatches have a mark in the 'miss' column. The last column shows the number of extra local minima examined. If this number is bracketed, convergence of the particular correlation was too slow, and the number of minima to be examined was reduced manually.

	$\frac{L_{vv}}{\sqrt{L_w}}$	L_{vv}	L_{ii}	L_w
marker	5.27	6.00	4.21	3.97
L_w	2.29	2.33	1.18	
L_{ii}	1.46	1.89		
L_{vv}	2.66			

	$\frac{L_{vv}}{\sqrt{L_w}}$	L_{vv}	L_{ii}
L_w	6.24	2.23	3.57
L_{ii}	5.05	2.13	
L_{vv}	6.74		

Table 4.4 The maximal distances (in mm) between two corresponding voxels when transformed according to the different registration parameters found in the experiments. The distance was computed considering all voxels within a diameter of 20cm from the image center. The found value is an upper bound for the actual distance between any 2 corresponding voxels in the images. The left table shows the maximal distances between corresponding voxels for each of the edge or ridge based registrations and the marker registration. For example the '1.18' in the L_{ii} column and L_w row means that if you take a voxel from the set as transformed according to the parameters obtained from the L_{ii} based registration, it is never more than $1.18mm$ apart from the set as transformed according to the L_w based registration parameters. The right table shows the distances between the low-resolution registrations.

L_{vv} correlation registration. (This suggests that feature based registration is better than marker based registration. However, this mere observation of a few observers does not justify a definitive conclusion as regards the relative accuracy of feature based and marker based registration.) When visually comparing all high resolution/no maiming registrations in the table in the same manner, no conclusion could be drawn regarding the best registration. We may conclude that –even though owing to the inevitable intrinsic distortion of the MR image, *the* perfect rigid registration does not exist– these four registrations are clearly good approximations, and seem to be equally accurate. This is supported by table 4.4, which shows the same voxels from the high resolution sets to be never more than $2.33mm$ apart.

Table 4.3 shows that for both the low resolution sets and the maimed sets, the performance of all operators is still accurate. In the table, the last column shows the number of additional local minima examined (i.e., besides the absolute minimum found on each pyramid level) by the algorithm. This number is bracketed when the algorithm showed no or too slow convergence, e.g., too much incorrect minima remained to be examined on the high resolution pyramid levels. In this case, after the algorithm had run for a certain amount of time, all results but the best were removed from the list of minima to be examined, and the algorithm was continued. The final result is shown in the table.

When maimed low resolution sets are used, the performance of almost all operators diminishes. For the L_{vv} operator, the registration algorithm fails to converge on a single minimum. The other operators provide registrations with a less accurate z-translation. Given the poor z-resolution and the very severe maiming of the CT volume, these cannot be called poor results.

We verified the 3D results on similar datasets from two other patients. The registration results were almost identical.

4.6 Conclusion and discussion

We have tested and compared the registration of CT and MR brain images by correlation of image features, notably edge and ridge features. In 2D experiments, the registration merit of the feature operators was established using brute force experiments. Both edge and ridge operators showed good performance, with the edge operators having a slight advantage. Four operators and their optimal scale were selected for 3D registration experiments, the edge operators L_w (the gradient magnitude), and L_{ii} (the Laplacian), and the ridge operators L_{vv} and

$L_{vv}/\sqrt{(L_w)}$. The 3D registration results were accurate, visually even more accurate than the marker based results used as a reference. All operators showed proper convergence. Only when severely maimed low resolution images were employed, the L_{vv} registration failed, and the L_w and L_{ii} registrations were less accurate. The maiming of the volumes used borders the limits of normal protocol scope, however. Based on both the 2D and 3D experiments, the gradient magnitude L_w seems to be the best choice of the originally proposed operators. In the 2D experiments, it produced accurate registration results, and appeared robust under changes in scale, initial transformation and maiming of the original CT and MR images. In the 3D experiments, it led to accurate results when realistic initial CT and MR images were used. Moreover, of all operators mentioned, L_w is the fastest to compute, since only the three first order derivatives are needed.

For the registration of 3D CT and MR brain images, we propose a registration scheme using scaled L_w feature images in a hierarchical correlation algorithm. This scheme requires no interaction, and is therefore devoid of human subjectivity. Only patient-related geometrical features are used for the registration, so registration can be performed even if pre-acquisition registration accommodations have not been made. The use of patient-related features is also more patient friendly than the use of external features, since no marking devices are required to be attached to the patient's head. In this paper, the proposed scheme was shown to produce accurate registration results with the limited number of datasets employed. In future work, we hope to extend the scope of the scheme by testing it on more brain imaging protocols, and move on to other modalities, as well as images of other parts of the body. We would also like to reduce the number of computer operations required, in order to improve the clinical applicability.

4.7 Acknowledgments

This research was supported in part by the industrial companies Philips Medical Systems, KEMA, Shell Research, and ADAC, as well as by the Netherlands ministries of Education & Science and Economic Affairs through a SPIN grant, by the Murray Foundation, and by the Netherlands Organization for Scientific Research (NWO), through a travel grant. We wish to thank Dr G. Wilts, Dr L.M. Ramos, Dr P.F.G.M. van Waes and Dr F.W. Zonneveld for their efforts to supply the images. The help of Dr K.J. Zuiderveld and Dr B.M. ter Haar Romeny in the course of this work are also greatly appreciated. C. Bouma, W. Niessen, R. Stokking, and Dr Evert-Jan D. Pol are thanked for their comments on early manuscript versions.

Vision is the art of seeing things invisible.
Jonathan Swift.

Chapter 5

Automatic Registration and Intensity Scaling of SPECT Brain Images

Abstract

Many diagnostic applications may benefit from 3D subtractive ^{99m}Tc-HMPAO SPECT images. Before such difference images can be computed, the studies involved need to be accurately registered and count-normalized. In this paper we present a fully automated approach to accurate registration by correlation of grey values, and to intensity normalization using the stochastic sign change (SSC) criterion. The registration results are verified by visual inspection and by comparison to registration results based on fiducial markers. Finally, an interactive display environment for examining subtraction images is presented.

5.1 Introduction

Nowadays, ^{99m}Tc-HMPAO is widely used as a tracer for SPECT brain perfusion imaging. The comparison of two HMPAO studies of the same patient is diagnostically useful in a variety of applications. Such applications include the comparison of rest and activation state of regional cerebral blood flow (Woods, Hegeman, Zubal, Krystal, Koster, Smith, Heninger & Hoffer 1991, Devous 1992, Barber et al. 1995), the comparison of ictal and interictal cerebral blood flow with epilepsy patients (Zubal et al. 1995), and the comparison of perfusion *pre* and *post* administering a perfusion influencing agent, such as CO_2, which induces vasodilatation. Decrease of the CO_2 pressure is also used in conjunction with hyperventilation activation studies (Kraaier, van Huffelen & Wieneke 1988). All of these applications benefit from using subtractive imaging. Subtraction is only meaningful, however, if the studies involved are accurately registered –*i.e.*, spatially aligned– and normalized with respect to photon counts.

The registration can be accomplished in various ways, such as immobilizing the patient's head, using fiducial markers (van den Elsen & Viergever 1991, van den Elsen & Viergever 1994), or using only the clinical image data (intrinsic registration) in combination with some registration criterion (Levin et al. 1988, Pelizzari et al. 1989, van den Elsen et al. 1995, Woods et al. 1993, Hill et al. 1994, Maintz, van den Elsen & Viergever 1996*b*, Collignon, Maes, Delaere, Vandermeulen, Suetens & Marchal 1995, Studholme et al. 1995*b*, Viola & Wells III 1995, West et al. 1996). Immobilization of the head is generally unpractical and patient unfriendly. For some applications and patients it is not even a feasible option. Registration based on fiducial markers is not usually prohibited by circumstances, but it can only be as accurate as the placement of the markers. With markers attached to the skin, there is always room for some marker shift owing to skin movement. Markers screwed rigidly into the outer skull table are available, but are much less patient friendly, thus unacceptable in the diagnostic setting. Moreover, if the time period between subsequent SPECT studies is more than a few hours, the markers usually need to be replaced, thus increasing the placement uncertainty factor. Both immobilization and markers are prospective methods, *i.e.*, they require extra operations in the image acquisition process. Therefore, the use of an accurate retrospective (*i.e.*, no additional pre- or intra-acquisition operations are required) intrinsic registration method is preferable.

In this paper, we present an automatic registration algorithm based on optimizing the cross-correlation value (van den Elsen et al. 1995, Maintz, van den Elsen & Viergever 1996*b*, Maintz, van den Elsen & Viergever 1996*a*) with respect

to rigid (*i.e.*, limited to three-dimensional translation and rotation) transformations of one of the input images. The registration accuracy is validated by visual inspection and by comparison to registration based on fiducial markers. All experiments were carried out using actual clinical data of 13 volunteers and patients.

After the registration has been performed, the registered sets need to be count-normalized before they can be subtracted. To simply scale the intensity values of one of the images until the total number of counts in both images match would be erroneous, since it ignores the fact that the two acquired images are different, not just scaled versions of one image. Instead we scale the intensity of one of the images so as to optimize the stochastic sign change (SSC) criterion (Venot et al. 1983, Venot et al. 1984, Perault et al. 1995), which allows for differences between the two images without inducing an averaging effect on the scaling factor as in the case of simple count-matching.

After count-normalization of the registered images, they can be subtracted meaningfully. Typically, application-dependent processing of the subtraction image is then applied. For visualization purposes, this may be a statistical filter for, *e.g.*, highlighting significant hot and cold spots, or a spatial filter such as low pass filtering to reduce noise while retaining global structures. When statistical measures on count differences in larger regions are to be measured, such filters are not commonly used, but even then the data is usually split into positive and negative differences, and/or absolute and relative differences. We will present a software visualization tool able to encompass all these post-processing steps, as well as supply the opportunity to link subtraction images to anatomy by means of, *e.g.*, overlaying contours obtained from one of the original SPECT studies, or, possibly, from a registered MR study. We emphasize that it is *not* the purpose of this paper to review the merits and drawbacks of application-specific filters, but to present a general framework for brain SPECT subtractive imaging, including automated registration, automated intensity scaling, and a comprehensive visualization tool to handle the results.

In section 5.2 the registration methods –both intensity and marker-based– will be discussed, as well as the registration validation procedure. Section 5.3 will cover the intensity scaling algorithm. The visualization procedure is presented in section 5.4, and in the final section we conclude with a discussion of the entire system as presented in this paper.

5.2 Registration

In section 5.2.1 we describe our registration method based on optimization of the cross-correlation of grey values between the images to be registered. By using the grey values directly we avoid the need for segmentation or other preprocessing of the input images, and the need for attaching markers to the patient in the acquisition stage. Section 5.2.2 describes our marker based registration method, which is used solely as a verificative method for the intensity-based registration.

5.2.1 Intensity based registration

In previous work (van den Elsen et al. 1995, Maintz, van den Elsen & Viergever 1996*b*, Maintz, van den Elsen & Viergever 1996*a*, Maintz, van den Elsen & Viergever 1996*c*), we investigated the use of the grey-value cross-correlation measure as a registration criterion for multimodality medical image matching. The measure was applied to feature images extracted from the original modalities, and appeared well suited to the registration task. Cross-correlation has also successfully been applied to monomodality registration tasks such as SPECT-to-SPECT or PET-to-PET registration (Junck et al. 1990, Douglas, Bacharach & Kalkowski 1992, Bacharach et al. 1993, Bettinardi et al. 1993, Perault et al. 1995). The next section will describe the actual algorithm. It is fully automated, hence it requires no user interaction or preprocessing of the images.

The cross-correlation registration measure $c(t)$ is defined as

$$c(t) = \sum_{(x,y,z)\in L_1} L_1(x,y,z)L_2(t(x,y,z)),$$

where L_1 and L_2 are the SPECT volumes to be registered. The registration problem is to find the correct rigid transformation t maximizing $c(t)$. t Is a vector with six entries describing all parameters associated with a rigid transformation, *e.g.*, three parameters describing translation along the axes of a 3D coordinate frame, and three parameters describing rotation around the same axes. The choice of restricting the parameter space to rigid transformations is not only beneficial from the point of view of numerical complexity, but is also justified by the relative rigidity of all relevant structures in the human head. Unless severe trauma has occured or large changes have been induced by, *e.g.*, surgery between the acquisition of the involved SPECT studies, the limitation to rigid transformations is valid. The parameter space to examine is, however, still large. For example,

for input images with dimensions $128 \times 128 \times 50$ voxels, and a finest registration step size of, for instance, quarters of voxels and quarters of degrees, the number of parameter space locations to evaluate if an exhaustive search were performed is in the order of 10^{17}. At this point, we are not certain of the behavior of the cross-correlation value in the parameter space. If it is well-behaved, *i.e.*, convex, the size of the parameter space is not much of a problem since cheap and fast optimization strategies (*e.g.*, Powell's method, gradient descent) can be employed. For now, we will use a more robust method using a multi-resolution approach (van den Elsen 1993, van den Elsen et al. 1995).

From each of the SPECT input images a three-level pyramid is formed with the original image at the bottom level. The middle and top levels are formed by maximizing each group of eight neighboring voxels in the level below into one voxel. The number of voxels in the top level is therefore a factor of 64 smaller than in the original image, while the structure of the image (*i.e.*, the head) is still visible to the human eye. Between the top levels of the two pyramids the optimal registration is found by optimization of the correlation value using a quasi-exhaustive search of a reasonable search space (*e.g.* no rotations larger than 45^o degrees or shifts larger than half the diameter of the head). For each parameter about 7 equidistant values are selected, forming a 6-dimensional grid in the parameter space. The correlation value is evaluated at each grid position, and the global optimum and promising –*i.e.*, within 90% of the global optimum– local optima are retained in a list. Then finer-spaced grids are created and examined around the optima in the list, and the same search procedure is applied. The resulting list of optima is then passed to the next (higher resolution) pyramid level, where the optima are again used as seeds around which search grids are created. This process is continued, the grids getting increasingly localized and with ever decreasing step-sizes, until the original level is reached with grid step sizes of a quarter voxel in translation and a quarter degree in rotation. These values seem appropriate for the application at hand, but can be easily decreased further if necessary.

5.2.2 Marker based registration

For verification of the intensity-based registration algorithm we constructed a marker-based algorithm to provide a reference registration. Additionally, the registrations were checked by visual inspection.

The reference registration is based on three ^{57}Co source fiducial markers (see figure 5.1), which were attached to the skin near the temporomandibular joints

and near the nasion, by means of thin double-sided tape. The markers themselves are perspex blocks (see figure 5.2) of $11.5 \times 11.5 \times 5mm$. 4 Indentations are made to the sides that serve as nooks for making small marks with ink on the patient's skin, in case the marker needs to be removed and replaced later. A small hole is drilled in the center of the block and infused with the ^{57}Co source. The hole is then sealed with a cap to avoid leakage of radioactive material.

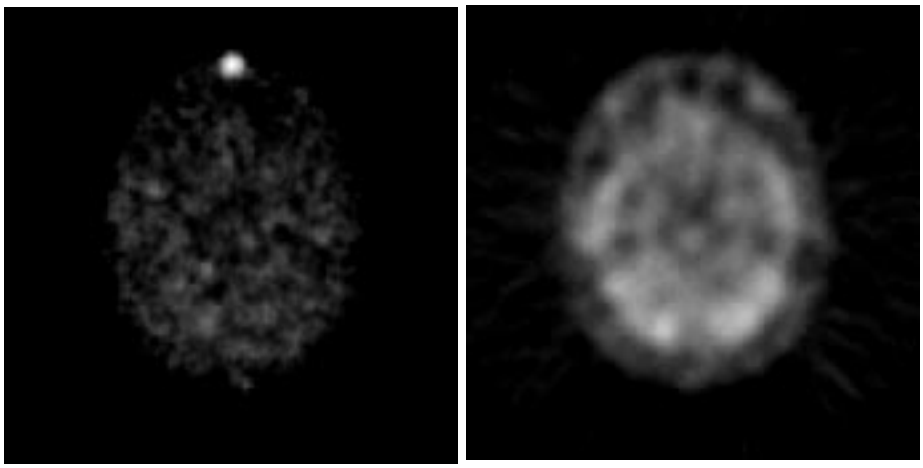

Figure 5.1 Example of the ^{57}Co marker image (left) accompanying the ^{99m}Tc image (right). The Co image does not influence the clinical data, and the Tc image does not interfere with the automatic marker detection.

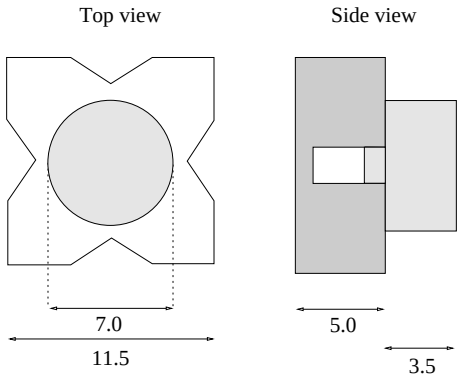

Figure 5.2 ^{57}Co Marker design. All numbers are in millimeters. See text for details.

The SPECT acquisition protocol for studies with markers is a dual window one: the first window is the 'normal' ^{99m}Tc window (centered at $140keV$, with a 15% window width) for acquisition of the clinical data, and the second window is centered around the ^{57}Co photo peak (at $122keV$, also with a 15% window width. In this study, all images were obtained using a Picker PRISM 3000[1]. Since this system does not allow for overlapping windows, both windows were slightly assymetrical. Pre-filtering of the ^{57}Co projections was done using a high order Metz filter. The ^{99m}Tc projections were pre-filtered using a Wiener filter with multiplier 1.0. Transaxial reconstruction of both the ^{57}Co and the ^{99m}Tc image was done simultaneously using a ramp backprojection filter. In previous work, we used ^{99m}Tc activated markers and a normal single window acquisition technique (van den Elsen & Viergever 1994). The present approach using ^{57}Co markers has several advantages. Firstly, the clinical data and the marker data are no longer combined in a single window, making automatic and accurate detection of the markers easier. Secondly, the markers do not interfere with the clinical data, nor are they in any way apparent in the ^{99m}Tc images, which is preferred by the nuclear physician. Thirdly, the intensity-based registration is not influenced by the presence of the markers. Finally, the ^{57}Co markers are easier in use since they are semi-permanent –with a half life of 271.8 days, they can be used for half a year or even longer– while the ^{99m}Tc markers need to be prepared anew for each study. A disadvantage is that the ^{57}Co markers are more expensive to make.

As can be seen in figure 5.1, the markers are easily detected in an image reconstructed from the ^{57}Co photo peak data. Automatic detection of the three marked points can be performed by moving –with step sizes of one voxel– a $15 \times 15 \times 15$voxels window across the Co image, keeping track of the number of counts in the window, and retaining those three window locations that contain the three maximum count values found. The $15 \times 15 \times 15$voxels window is then relocated at each of the three maxima positions, and the local center of gravity is computed. We assume this center of gravity to coincide with the actual point marked. Figure 5.3 gives a typical example of an automatically detected marked point.

After the three marker points in both of the SPECT images have been located, the actual registration is easily accomplished by aligning (in the least squares sense) the two sets of marker points in 3D space.

[1] Set to step-and-shoot mode, with a matrix size of 128, a 3^o angular step, $60s$ per frame, 360^o orbit. An ultra high resolution fan beam collimator was used.

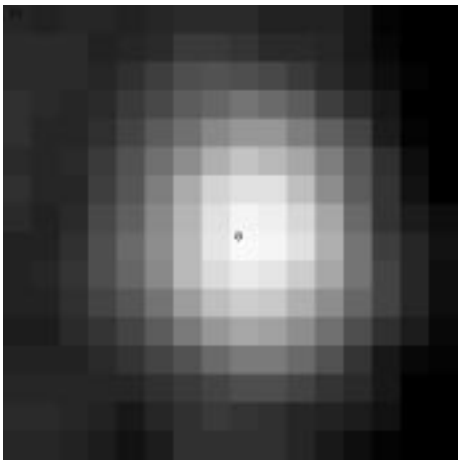

Figure 5.3 Example of the area around a marker in a ^{57}Co image. The dot indicates the automatically located marker point. Note that this presentation is not complete since we only present one slice of many.

5.2.3 Validation of intensity-based registration

Both the intensity and marker-based registration technique were applied to 13 different double ^{99m}-Tc HMPAO patient studies, each with dimensions $128 \times 128 \times n$ (n varies from 44 to 55) voxels of $1.95 \times 1.95 \times 3.56mm$. The reference match by means of markers provides us with a quantitative measure of accuracy of the intensity-based registration. For each patient, we compared the rigid transformations as obtained by the marker-based registration and the intensity-based registration, and computed the maximum distance between a voxel as transformed by the former and as transformed by the latter. This maximum distance was computed considering all voxels within a sphere encompassing the entire head, so the found maximum distance is actually an overestimation of the *true* maximum error. The average of the maximum distances of each study was $4.76mm$ with a standard deviation of $1.61mm$.

All registration results were checked by visual inspection: contours were extracted (by simple thresholding) from one of the images, and overlayed onto the registered second image. The result was then visually inspected with the original image beside it for reference. For each patient study, this method was applied to several transversal slices, as well as the median sagital and median coronal reformatted slice. In some cases, the intensity-based registration clearly outperforms the marker-based registration. In the remaining cases, there is no

pronounced preference for either one. When also considering that uncertainties as described in the introduction apply to the marker-based registration, we must be careful not to interpret the distance measures as computed from the reference registration as *error* measures, *i.e.* accept the marker-based registration for a gold standard. Rather, a small computed distance serves to increase the likelihood of *both* registrations being close to correct.

A typical registration example can be seen in the figures 5.4 and 5.5, where most observers will prefer the intensity-based registration over the marker-based one.

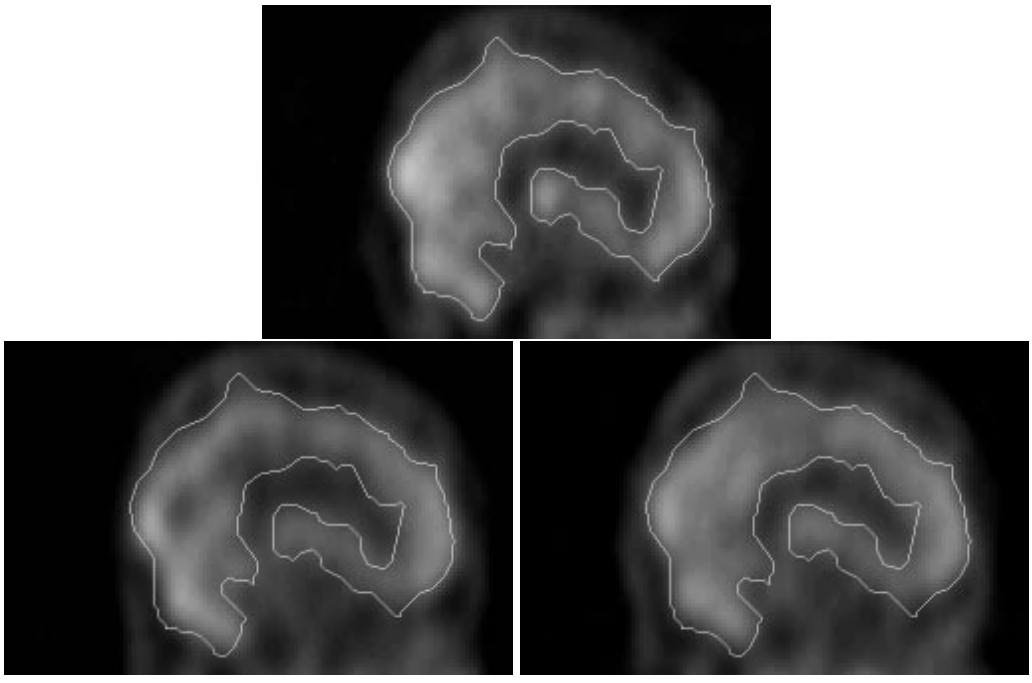

Figure 5.4 Top: The median sagital slice from an original SPECT dataset with a contour obtained by thresholding. **Bottom left:** The corresponding slice from the second SPECT dataset as registered by markers. The contour from the top image is overlayed to show how well the set is registered. **Bottom right:** The corresponding slice from the second SPECT dataset as registered by correlation. Again the same contour is overlayed to show the registration quality.

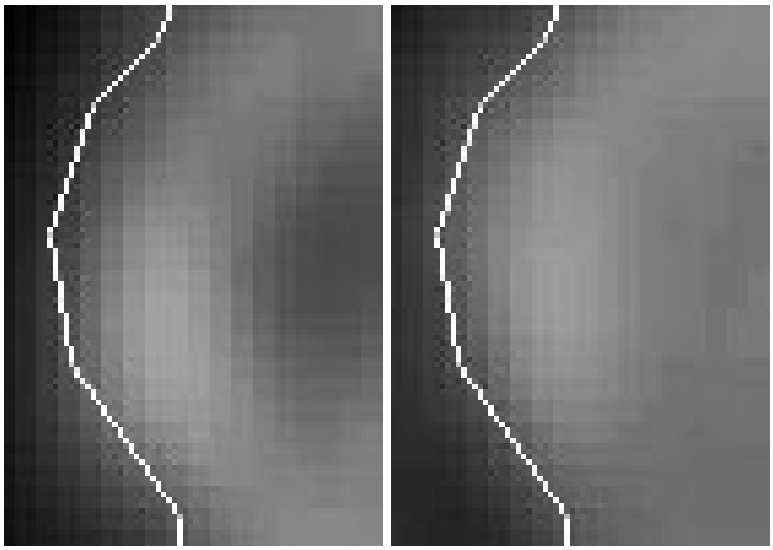

Figure 5.5 Posterior zoom of the marker based registration **(left)** and the correlation based registration **(right)**.

5.3 Intensity scaling

The registered SPECT studies still need to be count-normalized before they can be properly subtracted. We chose a normalization procedure purely based on the SPECT count values, since methods based on injected dose are prone to measurement errors, and moreover, because of biological influences –like activity retaining in tissue and not reaching the area of measurement at all– the relationship between injected dose and actual concentration of the isotope in the blood is not well defined. In our normalization method, we make the following assumption: in those regions that show no difference in perfusion, *i.e.*, in activity, between the two SPECT studies involved, the relation between the number of counts in those regions is multiplicative. Disregarding noise, $u(x) = fv(x)$, where u and v are the two SPECT studies, and x is any voxel coordinate vector in a region with no change in perfusion. With this assumption, we can find the optimal value of f with respect to the Stochastic Sign Change (SSC) criterion (Venot et al. 1983, Venot et al. 1984). The SSC is defined as the number of zero crossings in the difference image $u - fv$. A simplified 1D example can be seen in figure 5.6. Obviously, the SSC criterion is only meaningful in the presence of noise, as the difference signal as seen in figure 5.6C would otherwise be flat and have no zero crossings.

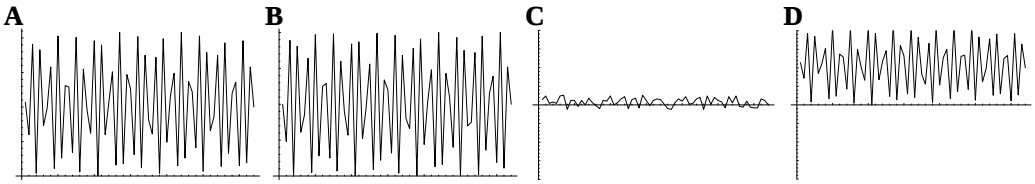

Figure 5.6 1D example of the SSC: the number of zero crossings in a difference signal. Here, the signals u (**A**) and v (**B**) are chosen identical but for noise. Of all difference signals $u - fv$, the difference signal $u - v$ (**C**) has a maximum number of zero crossings, while, *e.g.*, $u - 0.5 \cdot v$ (**D**) has none.

The intensity scaling optimization problem is much simpler than the registration problem, as the number of parameters involved is only one (f) instead of six. Since the SSC is rather well-behaved (*i.e.*, convex), a simple optimization strategy suffices. Here, the well known Brent algorithm (Press et al. 1992) is used with an initial bracket on f of $[0.5, 2]$.

In principle, the SSC criterion can be used to solve both the registration and normalization problem in one pass, *i.e.*, it is also suitable as a registration criterion. However, since the two problems of registration and scaling are disjunct in this case, this would unnecessarily complicate the parameter space.

5.4 Visualizing subtraction images

After the registration and count-normalization have been performed, the resulting images can be subtracted. Typically, the subtraction image is then processed in an application dependent way. For instance, based on fact whether differences are expected to occur spread out over large areas or localized in hot or cold spots. Since it is our purpose to present a general subtraction framework here, we will not discuss such *ad hoc* processing here. The actual visualization, however, contains elements that can be used for any subtraction application.

Our proposed visualization tool has two main windows, an overview and a subtraction windows, which can be used together, or either one can be hidden from view. The overview window simply presents all slices next to each other. Either one of the original SPECT images or the subtraction image can be viewed. This window is used mainly for selecting interesting slices. Such slices can then be displayed in the second main window; the subtraction window, which has

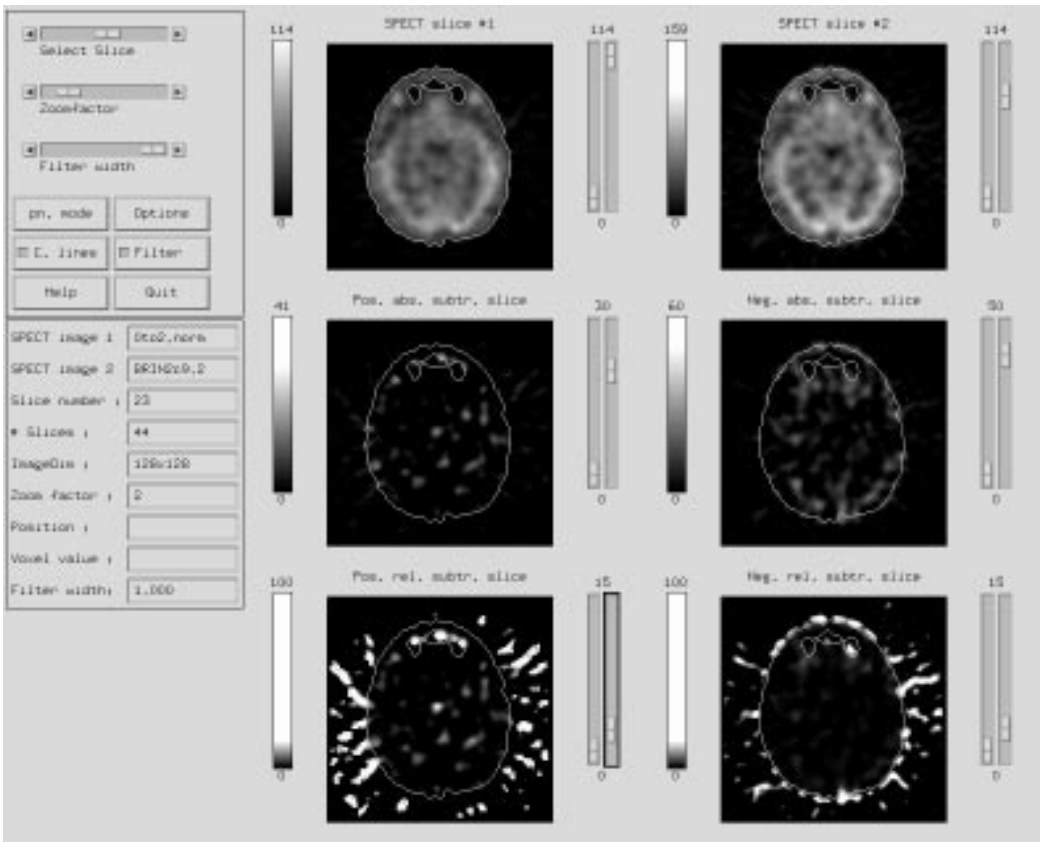

Figure 5.7 Example of a subtraction window. See text for explanation.

versatile viewing options. An example of the subtraction window can be seen in figure 5.7. Here, the window is shown in one of its most extensive modes: registered slices from both SPECT input images are shown (top row), the absolute positive and negative difference image (middle row) and the relative positive and negative difference image (bottom row). Windows that are not interesting to a particular application can be removed using the control buttons on the left. Each window's grey or color scale can be modified individually by using the slide bars next to them, and intensity bars are displayed for reference. The slide bars on the top left can be used to select a particular slice, control the displayed size of the images, and steer any filtering applied to the difference images. Contours are automatically extracted from the original SPECT slices and displayed in all windows to give a frame of reference to the difference images. In the example in

the figure, most of the differences occuring are probably meaningless artifacts. This is easily perceived by referencing them to the overlayed contour. We prefer this kind of visualization over a mask or a statistical filter to remove artifacts, because it gives more control to the user. However, if the user prefers otherwise, masking can be introduced at the click of a button. The buttons furthermore enable contours to be added, deleted, modified or removed entirely. If a registered MR image is available, this can also be included with a SPECT subtraction image for an overlay. Anatomical reference can furthermore be provided using a linked cursor, *i.e.*, when the mouse cursor is moved into a picture window, it appears at the corresponding location in all of the picture windows. This linked cursor can be used to draw regions on which various statistical operations can be performed, *e.g.*, an anatomically significant region can be outlined on the original SPECT slice, and the number and variance of counts of that region can be instantaneously computed in the subtraction image and the corresponding original images.

5.5 Discussion

The SSC criterion was introduced in the context of combined registration and scaling of scintigraphic images 13 years ago (Venot et al. 1983). However, there is a significant difference with our method. If the SSC criterion is used to solve both the registration and intensity scaling problem, *these two problems can no longer be separated*, *i.e.*, in the optimization process the registration parameters are dependent on the scaling parameters, and vice versa. By considering the registration and scaling problems separately using correlation and the SSC criterion, the complexity of the parameter space is reduced, and the scaling problem becomes a simple 1D optimization problem. Moreover, with the registration problem the optimization behavior using cross-correlation of grey values was shown to be very well behaved. There are also claims (Douglas et al. 1992) that correlation outperforms the SSC criterion in registration of nuclear images.

Correlation is a well-established technique for registration tasks. Optimizing the cross-correlation of 3D grey-valued images in a 6D parameter space, while in principle straightforward, has a considerable numerical complexity. Using a multi-resolution approach this complexity has been greatly reduced, while the optimization process still displayed a remarkably robust behavior in the convergence to the correct optimum. This very robust behavior indicates that we can probably slacken the now relatively severe parameter settings and optimization strategy if we would need to speed up the registration algorithm.

The choice of grey-value correlation has considerable advantages when compared to many current methods using surface based registration, such as the method described by Pellizari *et al.* (Pelizzari et al. 1989). Although these methods have exhibited good registration results and have less data overhead and computational cost, their accuracy is limited to the accuracy of the surface segmentation. By using cross-correlation of the grey values directly, the entire image content is taken into account, and no segmentation is necessary.

A classical problem of clinical registration algorithms is the absence of a gold standard as regards accuracy. However, when comparing the registrations of 13 clinical studies based on intensity correlation and on fiducial markers, the average of 13 sets of the *largest* difference occuring between the two registration algorithms for each set was $4.76mm$. When evaluated by nuclear physicians, there was a preference for the correlation based registration, which was deemed sufficiently accurate for clinical purposes.

In this paper, we constructed a general ^{99m}Tc HMPAO SPECT subtraction framework, usable in a variety of applications of perfusion imaging. The necessary preprocessing steps, registration and count-normalization, were outlined using fully automated algorithms. A possible visualization tool for the actual subtraction images was presented, which accommodates for many of the general visualization options associated with the problem at hand.

A realist lets circumstances decide which end of the telescope to look through. (Anon.)

Chapter 6

Registration of 3D Medical Images using Simple Morphological Tools

Abstract

Multimodal medical images are often of too different a nature to be registered on the basis of the image grey values only. It is the purpose of this chapter to construct operators that extract similar structures from these images that will enable registration by simple grey value based methods, such as optimization of cross-correlation. These operators can be constructed using only basic morphological tools such as erosion and dilation. Simple versions of these operators are easily implemented on any computer system, and are very fast. We will show that accurate registration images of various modalities (MR, CT, SPECT and PET) can be obtained using this approach.

6.1 Introduction

Registration and hybrid visualization of 3D medical images has received ample attention from researchers in the past few years. The reasons for this may be clear: there are numerous applications in diagnostic as well as treatment settings, benefitting from integrating the complementary character of multimodal images. Notable application fields include neurosurgery (Ruff et al. 1993) and radiation therapy planning (Chen & Pelizzari 1989). For example, in the latter field, dose calculation is done best using a CT image, while often the target area can best be identified in an MR image. A second important reason is the recent availibility of computing power and computer architecture that can handle the entire bulk of 3D data –eventhough the images at hand have also grown in size considerably– while older methods often required data reduction of the images to, *e.g.*, a limited point set, surface, or abstract representation. Such computing power gives access to a class of so called *voxel based* methods, that are in most cases preferable to previous methods.

Existing 3D rigid –*i.e.*, restricted to translational and rotational transformations– registration methods can be divided into extrinsic (external attachment based) and intrinsic (patient related) approaches (van den Elsen, Pol & Viergever 1993). Examples of extrinsic registration methods include methods based on fiducial markers (van den Elsen & Viergever 1994), a facial mould (Schad et al. 1987) or a stereotactic frame (Vandermeulen 1991). Compared to these methods, voxel based methods (Woods et al. 1993, Hill et al. 1994, Maintz et al. 1994, Maintz et al. 1995, Studholme et al. 1995*b*, Viola & Wells III 1995, van den Elsen et al. 1995, Maintz, van den Elsen & Viergever 1996*b*) are more patient friendly, and show higher reproducibility. Moreover, retrospective registration is now possible, as are extensions to allow for non-rigid registration. Examples of intrinsic registration approaches other than voxel based methods are landmark registration (Evans et al. 1989, Hill, Hawkes, Crossman, Gleeson, Cox, Bracey, Strong & Graves 1991), surface based registration (Levin et al. 1988, Pelizzari et al. 1989), and hybrids of these techniques. Compared to these methods voxel based methods are better reproducible, and less labour intensive. Voxel based methods are considered extremely promising with respect to accuracy (Viergever et al. 1995).

In this chapter, we investigate the use of certain morphological operators for voxel based registration. Multimodal medical images are often of too different a nature to be registered directly on the basis of the image grey values only. It is the purpose of this chapter to construct operators that extract similar structures from these images that will enable registration by optimization of the cross-correlation. The methods constrcuted are related to conventional surface based

methods. However, instead of binary-valued surfaces we employ real-valued 'surfaceness' images obtained from the original images, thus employing more of the available image content. The operators involved can be constructed using only concatenations of basic image operations such as computing the maximum or minimum of a small region. We will show that accurate registration of various different modalities (MR, CT, SPECT and PET) can be obtained using this approach.

6.2 Methods

In section 6.2.1 we outline the morphological operators featuring in our registration approach. The features extracted from the images by these operators can be used for registration by optimizing the cross-correlation value. Section 6.2.2 details the cross-correlation optimization algorithm. The next sections describe the morphological operator compounds that can be employed in three specific applications: CT-MR registration (6.2.3), MR-SPECT registration (6.2.4), and MR-PET registration (6.2.5). The final section (6.2.7) describes verification methods for the registrations obtained. Registration results of the developed methods will be shown in the following *results* section.

6.2.1 Morphological operations

The operators used in this chapter stem from the field of mathematical morphology (Serra 1982, Haralick, Sternberg & Zhuang 1987, Serra 1988); all are well known and frequently used there. They are simple in the sense that they usually have an intuitive geometrical interpretation, and that they allow straightforward implementations on a computer platform, although fast and elegant approaches require quite some sophistication. The basic structure upon which morphological operations are defined is a so called *complete lattice*, a set whose elements meet the requirements of partial ordering and existence of supremum and infimum:

- partial ordering:
  $x \leq x$
  $x \leq y \wedge y \leq x \Rightarrow x = y$
  $x \leq y \wedge y \leq z \Rightarrow x \leq z$

- for each subset there exists an infimum (maximum lower bound) and a supremum (minimum upper bound).

For digital images, the ordering boils down to the usual ordering of integer (or real) numbers. For two images A and B with the same image domain the relation $A \leq B$ holds if for all image elements (pixels or voxels) x, the inequality $A(x) \leq B(x)$ is obeyed. Since digital images have a countable numbers of pixels, the 'supremum' in the above can be replaced by a maximum, and likewise the 'infimum' by a minimum. Morphological image operations can therefore be constructed from maxima and minima operations defined on subsets of the image. In practical applications, these subsets are more often than not simple regions like squares and circles. For sets, the ordering is defined by the usual subset relation ($A \leq B \Leftrightarrow A \subset B$). The supremum and infimum operations are defined by the union and the intersection respectively. The intuitive relation between images (or functions in general) and sets is given by the image *subgraph* (or *umbra*), which we will explain in more detail later.

The fundamental structure of the lattice (ordering relation, supremum and infimum) dictates which morphological operations are useful: those preserving the ordering relation *(increasing operations)*, those commuting with the supremum *(dilations)*, and those commuting with the infimum *(erosions)*.

6.2.1.1 Erosion and dilation

The erosion ε of a set A by a symmetrical[1] structuring element B is defined by:

$$\varepsilon(A) = \{x | \forall b \in B, x + b \in A\}.$$

In words: the union of the centers of all the B-s that fit completely inside A. For an example, see figure 6.1.

The set-definition of erosion can be transfered to functions (and hence, images) by viewing a function $f(x)$ as a stack of sets $F(c)$; each set defined by a constant value c: $F(c) = \{x | f(x) \geq c\}$, see figure 6.2. There is a one-to-one relationship, as $f(x) = \sup\{c | x \in F(c)\}$. The union of all sets $F(c)$ is called the *umbra* or *subgraph* of the function.

The set-definition of erosion is now transferred to functions by applying the erosion to all of the sets $F(c)$ that make up the function $f(x)$. Note that this

[1] By using a symmetrical structuring element, we avoid problems with formal definitions requiring transposition of the structuring element

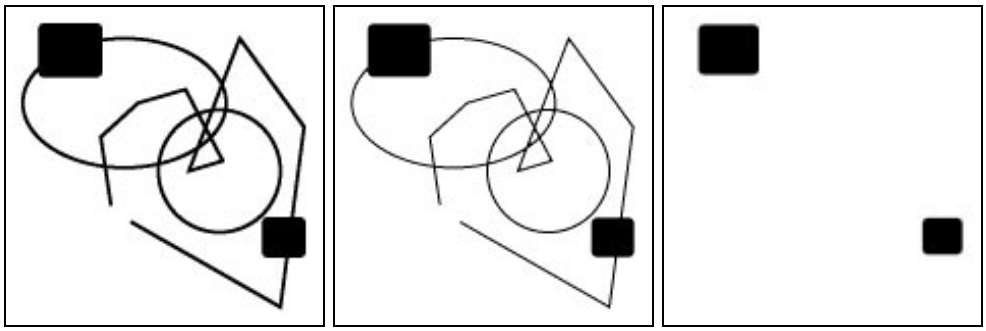

Figure 6.1 Example of erosion by a square structuring element on a set. To the left is the original set, in the middle and to the right erosions with a square of increasing size.

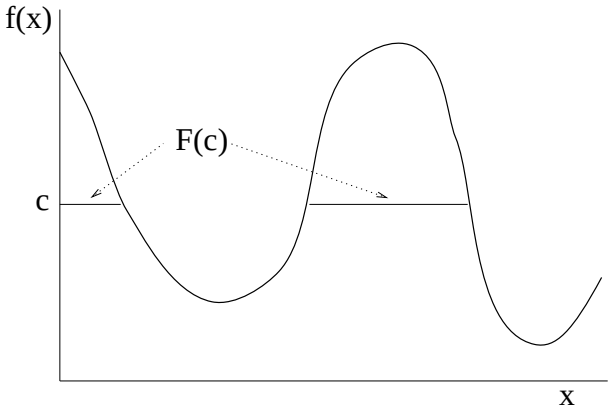

Figure 6.2 Example of a figure regarded as a stack of sets. The function $f(x)$ can be viewed as a collection of sets $F(c)$.

is not restricted to 1D functions; x can be non-scalar. After some calculations, it follows that the erosion for functions by a symmetrical planar structuring element B can be written as

$$\varepsilon(f)(x) = \inf_{b \in B}(f(x-b)).$$

An example can be seen in figure 6.3. B is a *planar* or flat structuring element if it is a simple set, *e.g.*, $B = [-1, 1]$. It is non-flat if B is a function which is not uniformly zero on its domain D_B. In the case of non-flat structuring elements,

the erosion definition is extended to

$$\varepsilon(f)(x) = \inf_{b \in D_B} (f(x-b) - B(b)).$$

The use of non-flat structuring elements adds the possibility to add weights to different parts of the structuring element. However, we will only use flat structuring elements in this chapter.

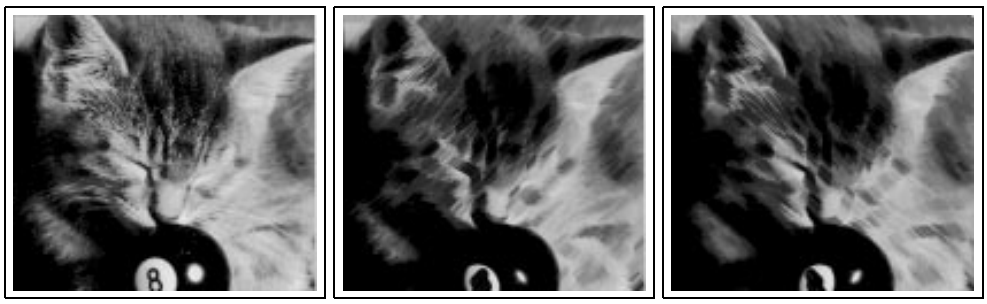

Figure 6.3 Example of grey valued erosion by a linear structuring element on a grey valued image. On the left is the original image. In the middle image the structuring element is directed to the upper right, and in the right image to the upper left.

The dual operation of erosion is called *dilation*. The dilation δ of a set A by a symmetrical planar structuring element B is defined as

$$\delta(A) = \{x + b | x \in A \wedge b \in B\},$$

or in words: the union of the centers of all B-s that have a non-empty intersection with A. Using the same reasoning as above with erosion, the definition for functions is

$$\delta(f)(x) = \sup_{b \in B}(f(x-b)),$$

where B is again a symmetrical planar structuring element. An example for dilation on a set can be seen in figure 6.4, one for a grey valued image in figure 6.5. The effects of the erosion and dilation operations will be intuitively clear: erosion will "eat away", abrade the boundary of objects, whereas dilation will expand objects at the boundary.

6.2.1.2 Opening and closing

Erosion and dilation are dual operations, *i.e.*, erosion of A equals dilation of the complement of A. They are not inverses, owing to the non-linear character of

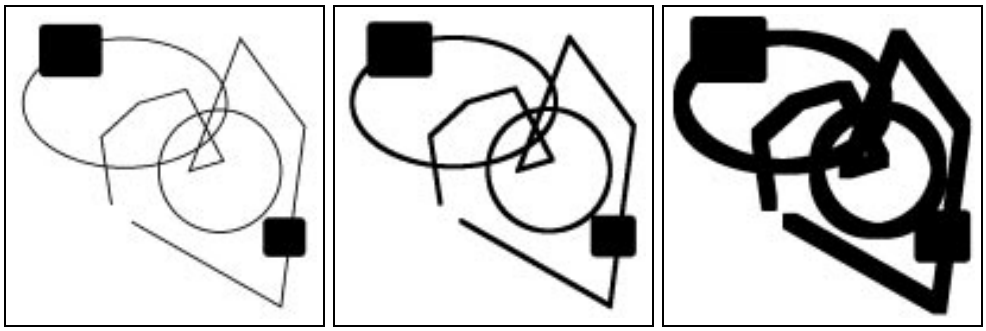

Figure 6.4 Example of dilation on a set. To the left is the original image, in the middle and to the right a dilation with a square structuring element of increasing size.

Figure 6.5 Example of dilation on a grey valued image. To the left is the original image, in the middle and to the right a dilation with a square structuring element of increasing size.

the operations; there are multiple input images that produce the same result when eroded. The smallest pseudo-inverse, *i.e.*, the composition of erosion and dilation, has some interesting properties. The morphological *opening* γ is defined as the composition of erosion and dilation, the morphological *closing* φ is defined as the composition of dilation and erosion:

$$\begin{aligned} \gamma &= \delta\varepsilon \\ \varphi &= \varepsilon\delta. \end{aligned}$$

Imagine the closing applied to a set: the dilation will expand object boundaries, which will be partly undone by the following erosion. Small, (*i.e.*, smaller than the structuring element) holes and thin tube-like structures in the interior or at the boundaries of objects will be filled up by the dilation, and not reconstructed by the erosion, inasmuch as these structures no longer have a boundary for the

erosion to act upon. In this sense the term 'closing' is a well chosen one, as the operation removes holes and thin cavities. In the same sense the opening opens up holes that are near (with respect to the size of the structuring element) a boundary, and removes small object protuberances. Examples of opening and closing can be seen in the figures 6.6 and 6.7.

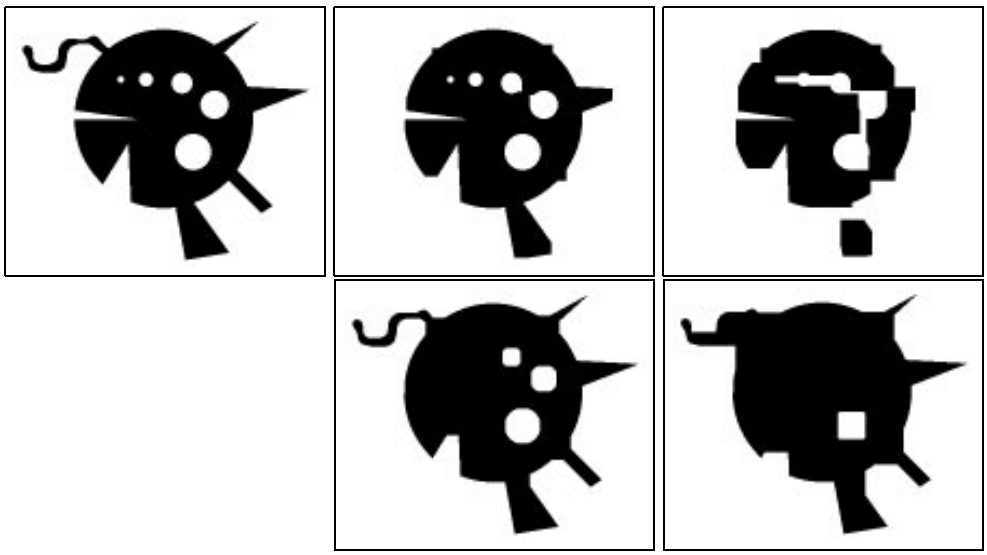

Figure 6.6 Example of opening and closing on a set. The top row shows the original, and two openings with a square structuring element of increasing size. The bottom rows shows the corresponding closings.

6.2.1.3 The morphological gradient

It has already been mentioned that, for sets, the erosion and dilation operations act on the edges of the sets. This is also true for functions, although this means stretching the definition of edge somewhat. Since the input is only modified at the edges, the *differences* between the eroded, the dilated and the original images bring out edge information of the original. The *morphological gradient* g is defined as the difference between a dilated and an eroded image:

$$g(f) = \delta(f) - \varepsilon(f).$$

See figure 6.8. This 'thick' gradient can be decomposed into two 'half' gradients:

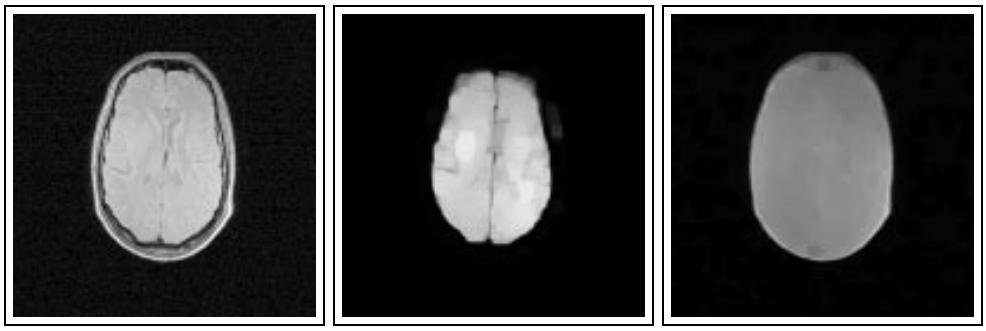

Figure 6.7 Example of opening and closing by a square structuring element on a grey valued MR image.

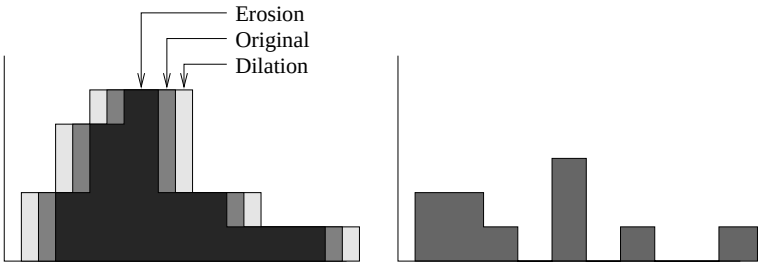

Figure 6.8 The morphological gradient: the difference between the dilation and the erosion. On the left the original function, a dilated version and an eroded version can be seen. On the right the morphological gradient is shown.

an 'inner' gradient g^- adhering to the inside of objects, *i.e.*, to the bright side of the edge, and an outer gradient g^+:

$$\begin{aligned} g^-(f) &= f - \varepsilon(f) \\ g^+(f) &= \delta(f) - f. \end{aligned}$$

For examples, see figures 6.9 and 6.10.

6.2.1.4 Deblurring

The ideas of erosion and dilation can also be employed for contrast enhancement and deblurring of grey valued images. The contrast can be enhanced by

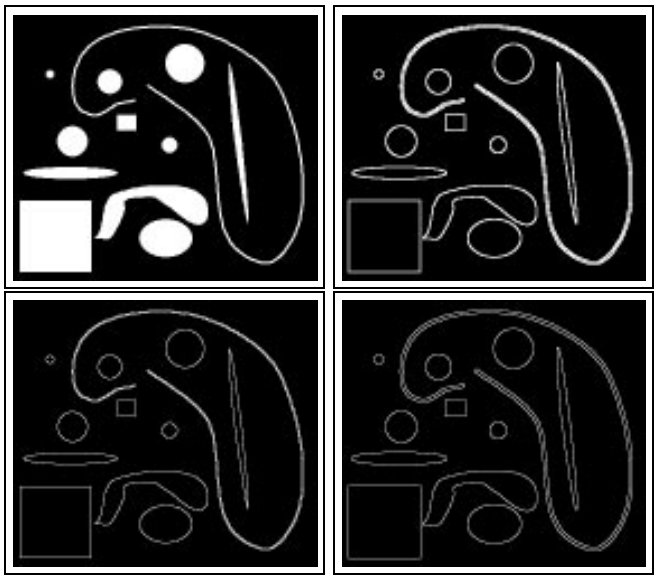

Figure 6.9 Example of 'half' gradients on sets. At the top the original (left) and the morphological gradient (right), at the bottom the inner (left) and outer (right) gradient.

Figure 6.10 Example of 'half' gradients on a grey valued image: original (left), morphological gradient (middle), and inner gradient (right).

replacing each pixel value by either the dilated or eroded value, whichever one was closer to the original value:

$$f_{\text{enh}} = \begin{cases} \delta(f) & \delta(f) - f \leq f - \varepsilon(f) \\ \varepsilon(f) & \text{otherwise.} \end{cases}$$

This technique can be shown to exactly reconstruct a convex homogeneous object that has been blurred by Gaussian convolution. This does not hold in the general case, but pleasing results can be obtained, as the figures 6.11 and 6.12 show. When iterating the deblurring operation, it always converges to a stable result (Kramer & Bruckner 1975).

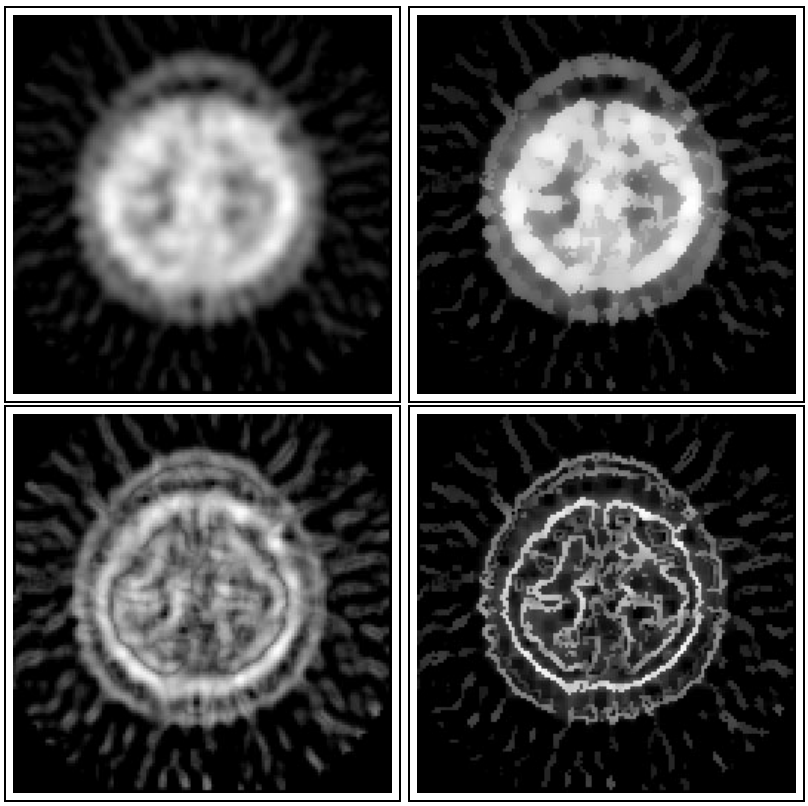

Figure 6.11 Example of deblurring applied to a SPECT image. At the top the original 128×128 SPECT image (left), and the image after a single step of deblurring with a 3×3 square (right). At the bottom the respective inner gradients can be seen.

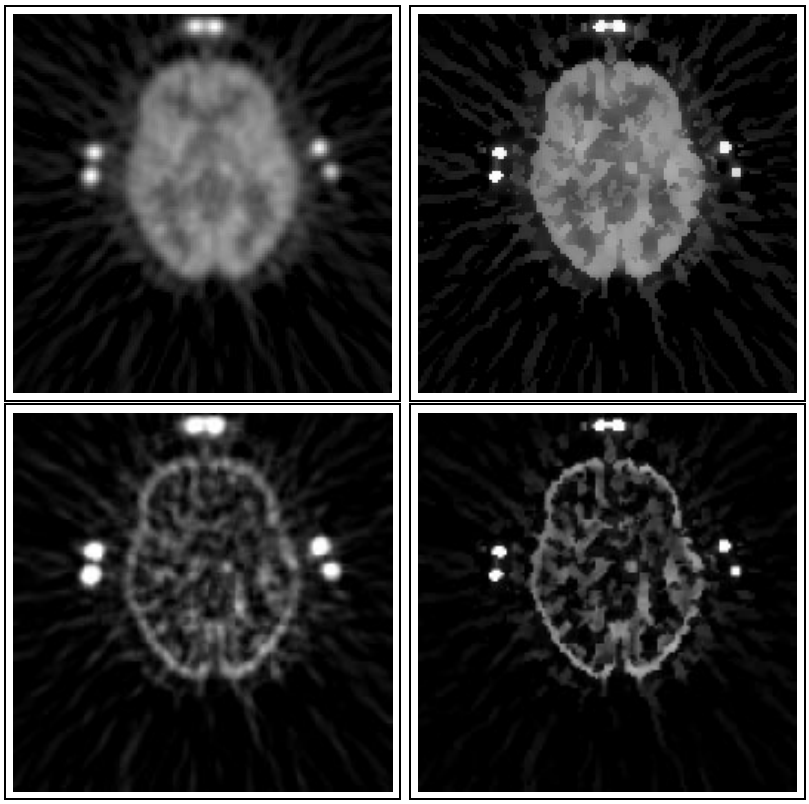

Figure 6.12 Example of deblurring applied to a PET image. At the top the original 128×128 PET image (left), and the image after a single step of deblurring with a 3×3 square (right). At the bottom the respective inner gradients can be seen.

6.2.1.5 Opening by reconstruction

It is often desirable to remove small objects from images, while keeping larger objects completely intact. The standard opening, as figure 6.6 shows, does not have the right properties to do this, because the shape of objects is not completely preserved. An approach to remedy this is to use *opening by reconstruction*. Before defining this, we need the concept of *geodesic dilation* δ_g:

$$\delta_g(f) = \min(\delta(f), g),$$

where g is a 'control' image: f is dilated in the usual way, but constrained so as to never be able to grow 'outside' of the control image g. If the geodesic dilation is iterated until stability is reached, it is called *reconstruction by dilation*.

The opening by reconstruction, finally, is the composition of erosion, and reconstruction by dilation. Here, the erosion removes small and thin objects, and the following reconstruction by dilation brings the remaining objects back to their original form. Examples can be seen in figure 6.13 and 6.14.

Figure 6.13 Example of opening by reconstruction on a set. On the left the original image can be seen, in the middle after erosion, and on the right after reconstruction of the erosion with the original image for a control image. Note that small segments are also easily segmented by taking the difference of the left and right images.

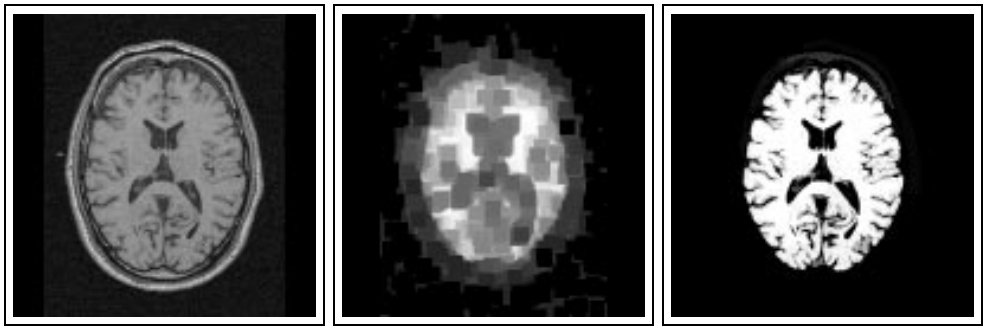

Figure 6.14 Example of opening by reconstruction of an MR image. To the left the original image can be seen, in the middle after erosion, and to the right after reconstruction and thresholding of the erosion with the original image for a control image.

6.2.2 Registration method

In our particular registration application we aim to obtain the rigid transformation that aligns one 3D medical image of a patient's head with another image of a

different modality of the same anatomy. In this chapter, we describe morphological operators that, when applied to the images to be registered, produce feature images that are similar to each other. With such operators, optimization of the cross correlation between the feature images with respect to feasible geometric transformations is expected to result in the desired registration transformation.

An exhaustive search of the 6-dimensional parameter space (three translations, three rotations), is not an option. For example, in the case of registering a large CT to a large MR image with an algorithm precision of, say, 0.25 voxels translation and 0.25 degrees rotation, the parameter space may contain over 10^{18} locations to be examined. We chose a *hierarchical* multi-resolution approach to handle this optimization problem. From each of the feature images to be registered a multi-resolution pyramid is created. The bottom layer of each pyramid equals the original image, and a number of layers are created by downsampling the layer directly below by a factor of eight. This downsampling is achieved by assigning to each downsampled voxel the maximum value of the cube of 8 neighbouring voxels associated with it in the layer below. Three (SPECT/PET) to five (high resolution CT) layers are created. On the top layer an exhaustive search of the parameter space is now feasible. We use the term 'exhaustive' loosely here, as we restrict the parameter space to realistic transformations: examining rotation angles of 90^o would be a waste of time. The global optimum found in the search, as well as local optima within a certain percentage of the global one are retained, and used as search seeds on the next pyramid layer. When progressing down the pyramid layers, we diminish the size of the search space (in terms of millimeters and degrees) around the search seeds, and the step sizes. The increasingly smaller search space ensures that the number of required operations remains within reasonable bounds. By decreasing the step sizes in parameter space, searches are coarse on the upper pyramid layers, yet accurate on the lowest levels, where accuracy is needed. The size of the search space on each layer and the coarseness of search in the layer directly above are narrowly adapted to one another to avoid failing to detect a local optimum. However, since the behavior of the correlation function in the parameter spaces of two subsequent pyramid layers is not always predictable, we included a fail safe mechanism by performing a hill-climbing operation in parameter space whenever the correlation optimum was not found in the interior of the parameter space.

6.2.3 Application: CT and MR registration

In previous work (Maintz et al. 1995, Maintz, van den Elsen & Viergever 1996*a*), we examined and compared a number of geometrically invariant features such

as 'edgeness', 'ridgeness', 'cornerness', and others, for use with registering CT and MR images of the head. An important conclusion was that edgeness, as computed by the gradient magnitude, performed best in the set registration tasks. In this research, much effort went into properly computing the necessary derivatives, *i.e.*, differentiation was done relative to a certain scale, and in a mathematically well-posed way, by convolving the original image with derivatives of Gaussians. We found that the optimal edgeness scale was very low, close to the image inner scale. Such low scale derivatives, however, can be accurately computed using local pixel operations, and do not require expensive operations like Gaussian convolution. In this chapter, therefore, we make use of relatively cheap morphological gradients.

Direct use of the morphological (inner) gradient often causes misregistration, especially where images with a large slice thickness are concerned. The reason for this is that various edges, notably the skull and skin edges, are frequently very close together, which causes the wrong edges to be aligned by the registration algorithm. We therefore extended the method to only use the skin edge. To detect this edge using a morphological inner gradient, we first need to remove all internal structures in the images, so the inner gradient acts upon an image containing only the skin edge. These internal structures can be removed by applying a closing for the removal of dark structures followed by an opening for the removal of bright structures. In the case of MRI, the nature of the images is such that the opening is not even necessary. The only parameters that need to be established are the sizes of the structuring elements used, which should be large enough to obtain the desired effect, while kept small to minimize distortion effects. The following operations were used for the feature extraction:

- CT: apply a
    1. Close (4mm), followed by an
    2. Open (8mm), followed by an
    3. Inner gradient.
- MR: apply a
    1. Close (4mm), followed by an
    2. Inner gradient.

In all cases, square structuring elements were used. The bracketed numbers indicate the structuring element half size, which is adapted to the approximate size of the anatomical object we wish to remove from the images. In the case of the inner gradients, the smallest possible structuring element is used. For

the CT images, the closing fills up dark areas (cavities, like, *e.g.*, the frontal sinus). The opening removes the bone, and we end up with a fairly homogeneous image of the head. The inner gradient will therefore only show the skin edge (see figure 6.15). The closing and opening have no significant bearing on the skin edge, as the figure shows. For the MR image, the closing will fill the gap between the cortex and the skin caused by bone which is dark in MR images, see figure 6.7. With poor quality initial images, both final edgeness images can still be improved (*i.e.* made more homogeneous) by applying a threshold. The actual threshold value does not appear to be critical, and we fixed it to 20% of the image maximum after processing. Figure 6.16 shows examples of the final feature images.

The above works well when T1 or PD weighted MR images are used. T2 weighted images are so different from these, that we use a different scheme:

- MR-T2: apply a
  1. Open (1mm), followed by a
  2. Threshold (low), followed by a
  3. Close (2mm), followed by an
  4. Inner gradient.

The threshold is necessary because the brighest edge in T2 images is at the cortex, while we are interested in the skin edge. By thresholding at a relatively low grey level, the large difference in brightness of skin and cortex edge is reduced. When thresholding at low grey levels, the image noise becomes more pronounced, which is why the open operation is included to remove noisy voxels. The close and inner gradient are used as with the T1 and PD weighted MR images.

It may seem –when looking at the final feature images– that the method reduces to surface based registration. The feature images, however, are not nearly binary, but have an extensive grey range, nor are the depicted structures thin. These very properties ensure proper convergence of the registration method.

6.2.4 Application: SPECT and MR-T1 registration

With SPECT[2] and MR-T1 registration, we use the same approach as with CT and MR registration: to avoid the risk of misregistration, *i.e.*, the alignment of

[2] In this application we use ^{99m}Tc-HMPAO perfusion SPECT images.

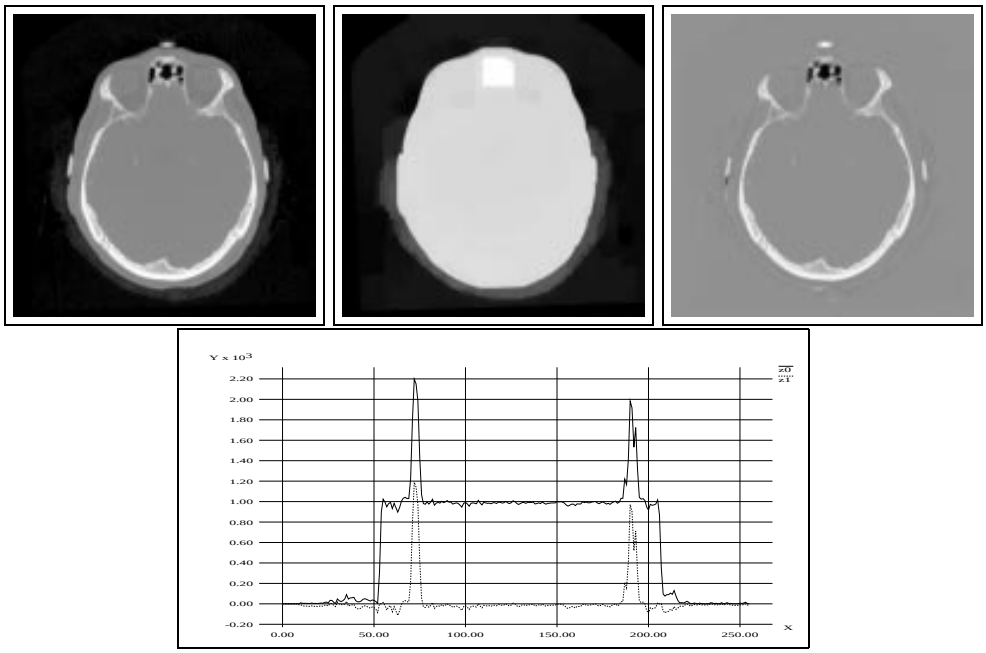

Figure 6.15 Computation of the CT feature image for CT/MR registration. At the top left is the original image. In the middle the image after closing and opening: a fairly homogeneous image of the head. At the right is the difference image of the original and the processed one. This shows that no noticeable artefacts are created at the skin edge by the process. Therefore the processed image may be used to compute the skin edge. This is further illustrated at the bottom, where horizontal cross sections of the original image (top graph) and the difference image (bottom graph) are shown: the bottom graph shows no artefacts at the location of the original skin edge.

anatomically non-corresponding edges upon using simple edgeness images, we use a morphological operator to select the skin edge from the MR. The edgeness is then computed both from MR and SPECT by applying a morphological inner gradient. The SPECT edgeness image can be improved upon by using morphological deblurring as a preprocessing step.

- MR: apply a
  1. Close (4mm), followed by an
  2. Inner gradient.
- SPECT: apply a

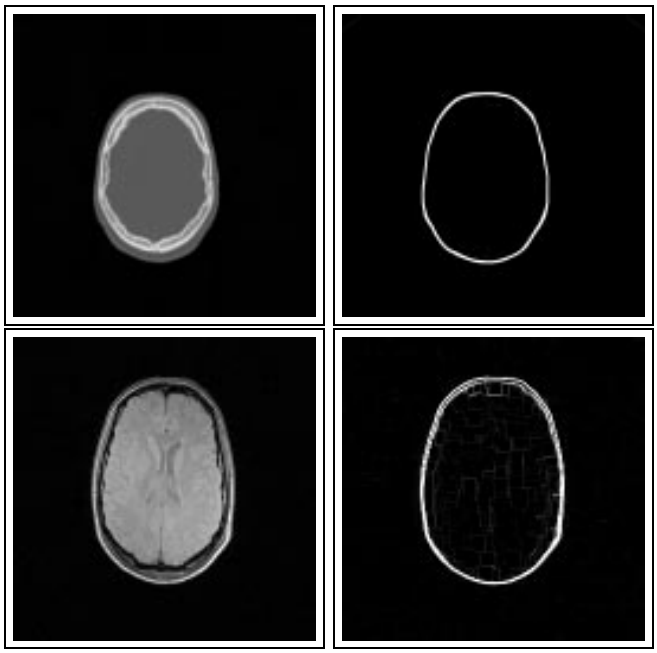

Figure 6.16 Examples of the original and edgeness feature images used in CT (top) to MR (bottom) registration.

1. Deblurring (1 iteration), followed by an
2. Inner gradient.

Examples of the SPECT feature images can be seen in figure 6.11 and of the MR feature image in figure 6.16.

6.2.5 Application: PET and MR registration

Registration of PET[3] and MR-T1 images based on the skin edge is not feasible, since the skin edge cannot be seen in a PET image like in a SPECT image (cf. figures 6.11 and 6.12). Our PET/MR registration is therefore based on the cortex edge, rather than the skin edge as with SPECT/MR registration.

[3]In this application we use FDG (fluorodeoxyglucose) or ethyl 8-fluoro-5,6-dihydro-5-methyl-6-oxo- H-imidazo [1,5-α]-[1,4] benzodiazepine-3-carboxylate (Flumazenil) PET images.

The extraction of the cortex edge from the PET image is relatively easy, since it is the dominant edge of the image. We improve the inner gradient image in much the same way as before (cf. CT and MR registration) by removing internal structures with a closing and an opening. In addition, since PET images are somewhat more blurry than MR images, we sharpen the image by a deblurring operation.

- PET: apply a
  1. Deblurring (1 iteration), followed by a
  2. Close (3mm), followed by an
  3. Open (3mm), followed by an
  4. Inner gradient.

In the MR image, we suppress the skin edge, and endeavor to 'select' only the cortex edge. We can achieve this by removing all structure outside of the cortex in the MR image, by applying an opening to it. This can either be a plain opening or an opening by reconstruction. While the latter produces less artefacts, it is also more time consuming to perform. Disadvantage of using an opening is that the cortex and the structures outside of it need to be well separated in the MR image in order for the opening to create the desired result. Although this holds for transverse image slices that depict areas above the eyes, it does not for slices near the base of the brain. A solution to this is to simply stop the reconstruction process after a number of iterations, instead of iterating until stability. Because the 'seed' of the reconstruction process is an eroded version of the original image (see figure 6.14), the first iterations will reconstruct the cortex, and only further iterations will allow the skin and other structures to 'grow back'. Since the size of the applied erosion is known, the number of iterations after which to stop the reconstruction is easily estimated.

- MR: apply a
  1. Open by reconstruction, followed by an
  2. Inner gradient.

The proposed PET feature images for registration can be seen in figure 6.17, and the MR feature images before computing the inner gradient in the figures 6.7 and 6.14.

For PET to MR-T2 registration, the above described method for PET to MR-T1 registration can be used. However, since the cortex edge is much brighter in T2

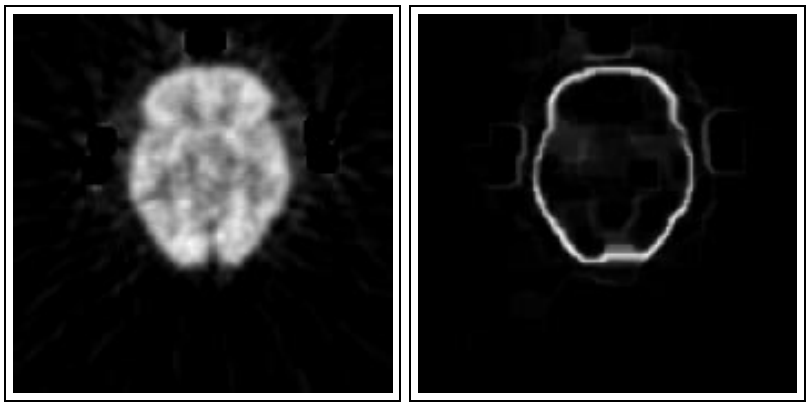

Figure 6.17 Example of a PET feature image (cortex edge) as used in PET to MR registration. On the left an original PET slice is shown, and on the right the corresponding slice from the feature volume can be seen.

weighted images than in T1 weighted MR images, we can suffice with a simpler feature extracting scheme for the MR image: an opening followed by a threshold and an inner gradient. MR-T2: apply a

1. Opening (4mm), followed by a
2. Threshold (low), followed by a
3. Inner gradient.

6.2.6 Summary of feature extractions

In table 6.1, the feature extracting schemes used in the various applications are summarized.

6.2.7 Accuracy verification of the registration

For an outline of accuracy verification methods, we refer the reader to section 2.11.2.1. In this chapter, we use the methods of visual inspection and comparison to registration based on fiducial skin markers in all of the applications. The visual inspection was performed by segmenting meaningful contours from a slice of one image, and overlaying them onto a corresponding slice from

From \ To	MR-T1	MR-T2
CT	CT: close(4), open(8), inner gradient	CT: close(4), open(8), inner gradient
	MR: close(4), inner gradient	MR: open(1), threshold(low), close(2), inner gradient
SPECT	SPECT: deblur, inner gradient	
	MR: close(4), inner gradient	
PET	PET: deblur, close(3), open(3), inner gradient	PET: deblur, close(3), open(3), inner gradient
	MR: open by reconstruction, inner gradient	MR: open(4), threshold(low), inner gradient

Table 6.1 Summary of morphological registration methods. Bracketed numbers indicate the structuring element half size used (in millimeters).

a registered image. This procedure is carried out using about four transversal slices, as well as the midsagittal and midcoronal slice from the MR image involved. The 'fit' of the contours is then assessed visually. In the case of CT to MR registration, we additionally used a cadaver study for validation, and also compared the registration results to those obtained by an earlier method: L_w *correlation*, a method which is based on optimizing the cross-correlation of edgeness images extracted from the original images involved by means of convolution with Gaussian derivatives, see chapter 4. Since this method was designed specifically for CT to MR registration, it could not be used to verify the registrations involving SPECT or PET. Finally, with PET to MR registration and CT to MR registration, 9 patients were implanted with four fixed markers, which were used to establish a comparative registration. The verification methods used are summarized in table 6.2.

	visual inspection	skin markers	fixed markers	comparison to L_w correlation	cadaver study
CT/MR	✓	✓	✓	✓	✓
PET/MR	✓	✓	✓	**np**	**np**
SPECT/MR	✓	✓	–	**np**	**np**

Table 6.2 Summary of verification methods used. Legend: ✓: method used, –: method not used, **np**: use of the method is not possible.

6.3 Results

6.3.1 Application: CT and MR registration

Within this application, our validation experiments can be divided into three categories according to the registration techniques to which the morphology based registration is compared:

1. Fiducial skin markers and L_w correlation (2 patient studies)
2. Implanted fixed fiducial markers (7 patient studies)
3. A specially prepared human cadaver (1 study)

In addition, visual inspection was employed in every case. The contours used in the inspection are CT skull contours, which can be readily obtained after thresholding the CT slice involved. The registration accuracy was subsequently assessed by an observer. To facilitate this, the contours were also presented slightly (in the order of one pixel) shifted, to see if this presented the observer with a better, worse, or equally accurate registration. In specific cases, contour deviations in the order of a pixel can be discerned. In other cases, it is hard to decide whether a registration improves or deteriorates, which can largely be accredited to factors such as slice thickness, presence of motion and other artefacts, and MR geometric distortion.

6.3.1.1 Studies validated by fiducial skin markers and L_w correlation

The patients involved in these studies were supplied with three markers glued to the skin just before image acquisition (van den Elsen, Viergever, van Huffelen, van der Meij & Wieneke 1991, van den Elsen & Viergever 1994). The markers are attached near the temporomandibular joints and at the nasion. The marked points can be located with subslice accuracy using near-automatic —two user-identified seed points are required for each marker— methods in each of the images involved. The marker based registration is then performed by aligning (in the least squares sense) the three points located in each of the images involved.

In previous work (Maintz et al. 1995, Maintz, van den Elsen & Viergever 1996*a*), we examined the use of edgeness images –as generated from CT and MR volumes by means of computing a scaled gradient magnitude– for registration purposes.

The edgeness computing operator, called L_w, appeared well suited for the task of CT to MR registration.

The two studies involved[4] were registered by means of the new morphologically based method, as well the above mentioned skin marker and L_w based methods. As a measure for the difference between the various registration results, we use the *maximum* and *mean* distance between two corresponding voxels as transformed by the different registration results. We compute these distances taking into account all voxels within a sphere containing the entire head, so these measures are in fact overstimates of the 'true' error, *i.e.* the error based only on patient related voxels. Table 6.3 shows the maximum and mean distances between all of the registrations. The results of the visual inspection was that shifting the registered contours did not improve the morphologically based registration, and that in a number of image areas there is a clear preference for the morphologically based match over the marker based registration. For an example, see figure 6.18.

	Study 1			Study 2		
		Morph.	L_w		Morph.	L_w
Maximum distance	Marker	6.8	3.3	Marker	4.2	6.0
	Morph.		4.3	Morph.		5.8
		Morph.	L_w		Morph.	L_w
Mean distance	Marker	3.9	1.9	Marker	2.8	3.4
	Morph.		2.6	Morph.		3.3

Table 6.3 Maximum and mean distances (in millimeters) between CT to MR registrations as obtained by marker based, L_w based, and morphologically based registrations.

[4] Study **I** contained a 256 matrix, 200-slice transversal T1-weighted FFE sequence MR image, with voxel dimensions of $0.98 \times 0.98 \times 1.0mm$, obtained on a 1.5 T Philips Gyroscan S15, and a 256 matrix, 100-slice transversal CT image, with voxel dimensions $0.94 \times 0.94 \times 1.55mm$, obtained on a Philips Tomoscan 350. Study **II** contained a 256 matrix, 100-slice transversal T1-weighted FFE sequence MR image, with voxel dimensions $0.9 \times 0.9 \times 1.55mm$, obtained on a Philips Gyroscan T5, and an 256 matrix, 128-slice transversal CT image, with voxel dimensions $0.7 \times 0.7 \times 1.5mm$, obtained on a philips Tomoscan LX. These images are –in terms of image quality– at the high end of current clinical practice.

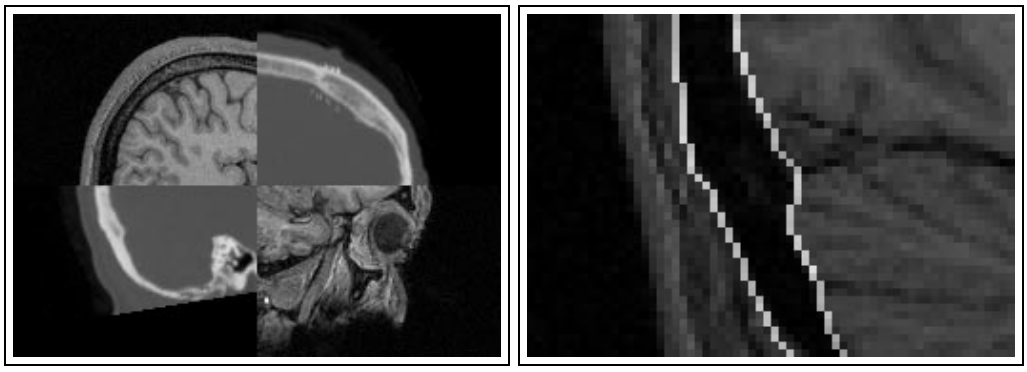

Figure 6.18 Example of a CT to MR registration as obtained by a morphological approach. **Left:** The top right and bottom left parts of the displayed MR image were replaced by their counterparts from the registered CT volume. Note the uncertainties introduced by deformation of the skin surface. **Right:** A zoom of the posterior part of the left image near the cerebellum showing the accuracy of the registration by overlaying CT bone contours onto the MR image.

6.3.1.2 Studies validated by fixed fiducial markers

The patient group involved here comprises seven patients, each implanted with four fixed fiducial markers, any trace of which was removed from the images before feature detection was applied. The reference registration was computed based on the fiducials. The validation of our morphologically based registration was done in a more elaborate way than in the previous study, namely by computing the maximum and median distance between the two registrations in ten small anatomically relevant volumes of interest, which were located in the MR image by clinical experts[5]. Per patient, six registrations were performed: the CT was registered to a proton density (PD) weighted MR image, a T1 weighted MR image, a T2 weighted MR image, and geometrically rectified (Chang & Fitzpatrick 1992) versions[6] of all of the MR images[7]. An advantage of this patient group is that the fixed markers are most likely more reliable than the

[5]The method of computing the maximum distance differs from the one used in the previous study, since this particular validation study was part of an off-site blinded registration validation protocol. This is also the reason why median distances are used in this validation study instead of mean distances.

[6]Except for patient 6, MR T1.

[7]The CT images were 512 matrix, approximately 30 tranversal slices, with voxel dimensions $0.65 \times 0.65 \times 4.0mm$, obtained on a Siemens Dr-H. The MR (PD, T1 and T2-weighted) images were 256 matrix, approximately 23 transversal slices, SE sequence, with voxel dimension $1.25 \times 1.25 \times 4.0mm$, obtained on a 1.5T Siemens SP.

skin markers used in the previous section. The image quality in this group is considerably poorer, but not unrealistically so with respect to today's clinical practice. The results can be viewed in table 6.4. Note that, in this particular study, the geometrical rectification of the MR sets did not significantly alter the registration results.

The results of the visual inspection were less good than in the previous section. Although the actual inspection is made more difficult by the relatively poor quality of the images and the thicker slices, it is obvious that, at least for a number of patients, the morphologically based registrations could be improved.

	Maximum distances	Study #						
		1	2	3	4	5	6	7
Modalities	CT-MR(PD)	4.7	11.0	19.0	6.8	8.2	9.9	4.7
	CT-MR(T1)	7.4	12.8	8.4	9.1	9.1	10.5	4.0
	CT-MR(T2)	4.2	3.4	6.1	5.1	6.0	6.3	5.0
	CT-MR(PD rect)	1.4	9.9	7.3	9.0	7.4	6.4	1.4
	CT-MR(T1 rect)	5.2	10.5	7.5	14.2	8.6	-	1.7
	CT-MR(T2 rect)	4.9	6.5	5.4	3.4	3.7	6.2	4.4
	Median distances	Study #						
		1	2	3	4	5	6	7
Modalities	CT-MR(PD)	4.0	5.5	8.9	2.7	4.0	4.5	3.7
	CT-MR(T1)	5.6	7.0	7.6	8.4	4.7	4.8	3.6
	CT-MR(T2)	3.4	3.2	5.3	4.8	4.6	4.0	4.4
	CT-MR(PD rect)	1.2	6.7	6.9	7.2	3.0	3.2	0.8
	CT-MR(T1 rect)	4.6	6.7	6.9	11.7	4.2	-	1.1
	CT-MR(T2 rect)	4.5	5.3	4.6	3.2	3.0	5.1	3.8

Table 6.4 Maximum and median distances (in millimeters) computed over 10 anatomically relevant volumes of interest, between our morphologically based registrations and a reference registration based on fixed fiducials. The dash indicates the rectified MR volume was not available.

6.3.1.3 Study validated by a cadaver study

One cadaver study[8] was included in the validation experiments. Cadaver based validation has several attractive properties: The images are free of motion artefacts, there is no need to pay heed to radiation dose with the CT acquisition, *i.e.*, the field-of-view can be chosen arbitrarily large, and external and internal markers can be attached and inserted without paying much attention to possible tissue damage. On the other hand, post-mortem changes in the anatomy could possibly make the data unrealistic.

The reference registration (Hemler, van den Elsen, Sumanaweera, Napel, Drace & Adler 1995) was obtained by inserting four glass hollow rods ($1.5/3.0mm$ inside/outside diameter) into the head of a human cadaver at different angles.

[8]The CT image was a 512 matrix, 180-slice transversal image, with voxel dimensions of $0.67 \times 0.67 \times 1.0mm$, obtained on a GE HiSpeed Advantage Helical CT. The MR image was a 256 matrix, 124-slice transversal 3D GRASS sequence image, with voxel dimensions $1.09 \times 1.09 \times 1mm$, obtained on a GE Signa 1.5T.

These tubes were filled with a contrast agent, and detected in each of the modalities. The center lines of the detected tubes were used to compute the maximum and mean distances. Before applying the morphologically based registration method, the tube structures were eliminated from the images.

Since the contained (scanned) volume of the head in the CT image is of a size seldom encountered in clinical practice, these data provide us with an opportunity to simulate more clinically relevant registration cases by selecting an appropriate volume from the CT image, while keeping the reference registration based on the entire scanned volume. Also, from the original volumes images with thicker slices were simulated. The morphologically based registration was applied to all of the original and simulated volumes separately, and the registration results were compared to the reference registration based on the entire high-resolution volumes. The maximum and mean distances are given in table 6.5. Note that this is an overestimation of the 'true' error. The results of the visual inspection were that the registrations were accurate, with the exception of the registration using only the lower part of the CT volume. In the latter case an error in the order of a few pixels could be observed in some image areas.

Images used	Maximum distance	Mean distance
original volumes	1.1	0.4
$3mm$ slices	2.5	1.0
$5mm$ slices	3.7	2.1
lower CT volume only	4.6	2.2
upper CT volume only	2.1	0.7

Table 6.5 The maximum and mean distances (in millimeters) between the morphologically based registrations and the reference registration of a cadaver study.

6.3.2 Application: SPECT and MR registration

In this application, ^{99m}Tc-HMPAO SPECT images were registered to T1-weighted MR images[9]. The patient group comprised five patients, and the reference registration was provided by means of fiducial skin markers. Initially, the patient group was much larger, but, owing to the cumbersome nature in terms of image acquisition –the group consisted of children with tics and concentrative

[9]The MR images were 256 matrix, 127 slice, FFE sequence T1-weighted transversal images, with voxel dimensions $0.78 \times 0.78 \times 1.25mm$, obtained on a Philips Gyroscan T5. The SPECT images were 64 matrix, with approximately 50 slices, ^{99m}Tc-HMPAO transversal images, with voxel dimensions $3.91 \times 3.91 \times 3.56mm$, obtained on a Picker PRISM 3000.

disorders– only in five cases could the markers be used succesfully. This in itself is already an argument in favor of retrospective registration techniques. The maximum and mean distances between the marker based (reference) registration and the morphologically based registration of the five remaining patients are listed and table 6.6. The visual inspection gives the impression of imprecise

	Study #				
	1	2	3	4	5
Maximum distance	15.6	7.8	6.2	12.6	10.9
Mean distance	8.3	3.9	3.0	6.5	8.5

Table 6.6 The maximum and mean distances (in millimeters) between the marker based (reference) registration and the morphologically based registrations of five SPECT to MR registrations.

results when viewing most of the marker based registrations. Two of the morphologically based registrations could also be improved upon. The inaccuracy is also reflected in the relatively large errors in the table. We suspect the sometimes severe motion artefacts in the images to hamper proper registrations. Examples of an accurate and a clearly mismatched registration can be seen in figure 6.19. For viewing purposes we used MR images without many motion artefacts here.

We can as yet not draw definite conclusions regarding the quality of the morphologically based registration, because of the poor quality of the images used, and the lack of precision in the marker based reference registation. More images need to be acquired for proper tuning and verification of the morphologically based registration method.

6.3.3 Application: PET and MR registration

Within this application, we used two types of validation: using fixed implanted fiducial markers, and using skin fiducial markers. In both cases visual inspection was also applied. The verification is the same as in the case of the CT to MR registration application: with the fixed markers, the median and maximum distances in ten anatomically relevant volumes of interest are computed, whereas with the skin markers the maximum and mean distances in a sphere containing the entire head are computed.

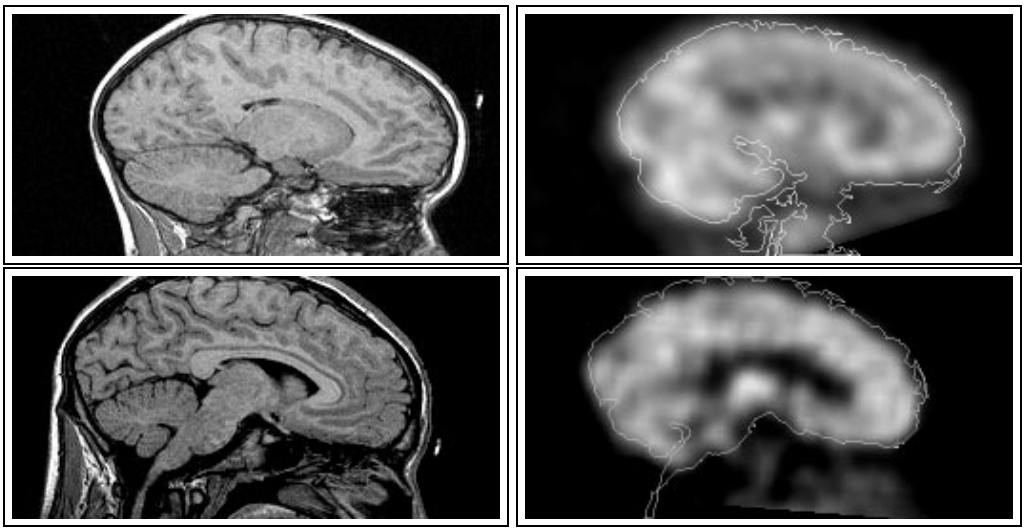

Figure 6.19 Example of an accurate (top) and a somewhat mismatched (bottom) registration of SPECT and MR images.

6.3.3.1 Studies validated by fixed fiducial markers

Seven patient studies were used in these experiments (of which five concern patients also used in the CT to MR registration as validated by fixed fiducials). Of each patient, three MR studies and a PET study were acquired[10]. Of five patients the MR studies were also geometrically corrected (Chang & Fitzpatrick 1992). The registration results can be seen in table 6.7. Visual inspection is hard compared to CT to MR inspection, owing to the relatively poor image quality, as is reflected in figure 6.20. The accuracy as assessed from visual inspection correlates well in a qualitative sense with the differences listed in table 6.7.

[10]The MR images were respectively PD, T1 and T2-weighted transversal SE sequence images, with a 256 matrix, containing approximately 23 slices, with voxel dimension $1.25 \times 1.25 \times 4.0mm$, obtained on a 1.5T Siemens SP. The PET image was a 128 matrix, 15 slice transversal FDG (^{18}F-fluorodeoxyglucose) image with voxel dimensions $2.59 \times 2.59 \times 8.0mm$, obtained on a Siemens/CTI ECAT 933/08-16.

	Maximum distances	Study # 1	2	3	4	5	6	7
Modalities	PET-MR(PD)	8.0	7.7	8.1	5.6	7.6	9.8	7.5
	PET-MR(T1)	5.5	10.6	3.8	3.9	5.9	5.1	4.0
	PET-MR(T2)	7.2	12.7	6.4	15.0	4.0	13.1	8.8
	PET-MR(PD rect)	5.4	6.9	5.2	6.6	9.2	-	-
	PET-MR(T1 rect)	6.2	4.4	4.5	-	7.7	-	-
	PET-MR(T2 rect)	5.4	9.0	4.1	10.9	3.6	-	-
	Median distances	Study # 1	2	3	4	5	6	7
Modalities	PET-MR(PD)	3.6	4.9	3.6	3.4	4.9	6.4	5.8
	PET-MR(T1)	2.6	8.6	2.3	2.5	4.8	3.7	3.3
	PET-MR(T2)	3.7	6.3	3.2	11.6	2.3	8.1	5.4
	PET-MR(PD rect)	3.6	6.6	3.6	4.3	5.9	-	-
	PET-MR(T1 rect)	4.5	3.2	3.7	-	5.1	-	-
	PET-MR(T2 rect)	3.9	7.7	3.4	10.6	2.2	-	-

Table 6.7 Maximum and Median distances (in millimeters) computed over 10 anatomically relevant volumes of interest, between our morphologically based registrations and a reference registration based on fixed fiducials. If there is a dash in the table, the rectified MR volume was not available.

6.3.3.2 Studies validated by skin fiducial markers

Four patient studies were involved in these experiments. Of three patients MR T1 weighted, MR T2 weighted, PET FDG, and PET Flumazenil images[11] were made. Of the fourth patient only an MR T1 weighted and a PET FDG study was made. For various logistic reasons, notably the short half life of the ^{11}C based Flumazenil, no markers were used in the Flumazenil studies. The markers in one of the FDG studies could not be detected properly because the used clinically relevant field-of-view did not allow for proper inclusion of one of the markers. The remaining maximum and mean distances between the marker based registrations and the morphologically based registrations are listed in table 6.8. The visual inspection reveals that the accurate marker detection is limited by the blurry nature of the PET images. The marker based registrations is therefore not the best of standards. The morphologically based registrations appear accurate in

[11] The T1 weighted MR images were 256 matrix, 127 slice FFE sequence images, with voxel dimensions $0.98 \times 0.98 \times 1.2mm$. The T2 weighted images were 256 matrix, 130 slice TSE sequence images, with voxel dimensions equal to the T1 weighted image. Both MR images were obtained on a Philips Gyroscan T5. The PET images, both Flumazenil and FDG studies, were 128 matrix, 31 slice images with voxel dimensions $2.35 \times 2.35 \times 3.38mm$, obtained on a Siemens/CTI ECAT 951/31R.

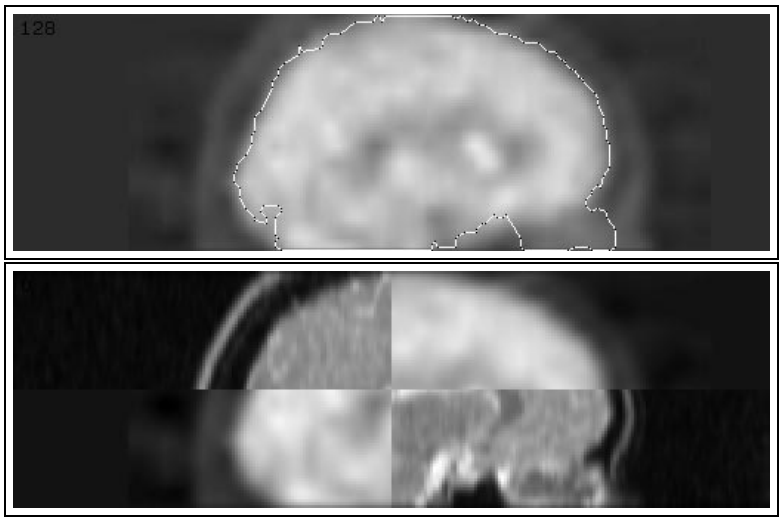

Figure 6.20 Example of a PET to MR (T2) registration. At the top the midsagittal slice of the registered PET volume is shown with a contour obtained from the MR image. At the bottom the same slice is shown as a hybrid of MR and registered PET slice.

Maximum distances	Study # 1	2	3	4	Mean distances	Study # 1	2	3	4
FDG-T1	-	7.5	4.6	8.8	FDG-T1	-	5.1	2.4	6.6
FDG-T2	-	11.7	13.8	-	FDG-T2	-	8.9	11.0	-

Table 6.8 The maximum and mean distances (in millimeters) between the marker based and morphologically based registrations of the FDG and MR studies involved.

most cases, but in some cases a visible mismatch can be perceived when viewing the midsagittal plane. There seems to be no difference between the quality of registrations involving FDG PET images and the ones using Flumazenil PET images. The registrations involving T1 weighted MR images seem more accurate than the ones using T2 weighted MR images.

6.4 Discussion

We have applied the morphologically based registration techniques on many more image pairs than addressed in this chapter. The ones reported here are

those pairs that come with a reference registration that can be used for at least some validative measure. The methods perform satisfactorily in all cases of CT to MR registration with images of regular clinical protocols, but –as the above sections showed– mismatches may still occur when functional images are involved. Generally, significant misregistrations can easily be perceived when inspecting the registration visually. It is not difficult to adapt the feature extraction procedure in these cases such that a satisfactory match is obtained. However, such interventions destroy the automatic nature of the whole registration process. As can be learned from West *et al.* (1996), our MR to PET registration accuracy measurements are in an order of magnitude comparable to most other registration algorithms, even though many methods in this study use manual intervention to optimize the registration.

In conclusion, simple morphological tools are capable of registering CT and MR images accurately and robustly, and provide acceptable PET to MR and SPECT to MR registrations in most cases. We have not found a simple procedure that adequately registers SPECT or PET with MRI in all cases considered; the variability in the data is too large to enable a fully robust registration paradigm.

A point we want to emphasize is that the reference registrations should not be regarded as a gold standard, *i.e.*, the distances in the tables should not be interpreted as errors. Such distances are at best *indicative* of the quality of the morphological registrations. In a number of cases, especially in the CT to MR application, it was clear from visual inspection that the morphologically based registration was of superior quality. Moreover, even with high resolution volumes (voxel volume $1mm^3$), experts sometimes could not distinguish between the quality of two matches, although the maximum distance between them exceeded $3mm$. This can have a number of causes, amongst which are local image distortion, the fact that the distance overestimates the 'true' error, the *rigid* transformation paradigm, the fact that a registration algorithm will perform better in those image areas dominant in the feature images (*i.e.*, at the edges used in the registration), *etc.*

In the opinion of these authors, voxel based registration methods will eventually outperform others. We are currently experimenting with mutual information based methods as developed by Collignon and co-workers (Collignon, Maes, Delaere, Vandermeulen, Suetens & Marchal 1995), which produces visually attractive results on *almost all* of the image pairs used in this chapter. However, these methods are as yet unsuitable for registration tasks that are severely time-constrained (such as intra-operative registration) or tasks that do not allow registration by means of a rigid transformation only (*e.g.* involving abdominal scans). Speed of the registration method is heavily dependant on the information content of the images involved. In this chapter, by applying morphological

operators, we have dramatically reduced the total information content of images, while simultaneously extraction feature information of corresponding anatomical structures. Also, we have shown that multi-resolution approaches can be used in the optimization procedure. Preliminary experiments corraborate that both the multi-resolution approach and the information reduction could be incorporated into mutual information based registration.

6.5 Acknowledgments

This research was supported in part by the industrial companies Philips Medical Systems, KEMA, Shell Industrial Exploration and Production, and ADAC Europe, as well as by the Netherlands ministries of Education & Science and Economic Affairs through a SPIN grant, and by the Netherlands Organization for Scientific Research (NWO), through a travel grant. Dr Paul Hemler and Dr Thilaka Sumanaweera are kindly acknowledged for their work on the cadaver study. Dr Jan Buitelaar and Alice van Dongen, MA are greatfully acknowledged for their assistance with the SPECT images. The images with implanted fixed markers used in the validation of the CT/MR and PET/MR registrations were acquired as part of the project "Evaluation of Retrospective Image Registration", NIH R01MS/CA 3392 6-01, coordinated by Dr Michael Fitzpatrick, Vanderbilt University. We are indebted to Jay West and Dr Michael Fitzpatrick for their help regarding these images. We also wish to thank Dr René Debets, Dr B. Sadzot and Christian Degueldre for their assistance in acquiring the PET images, and Dr Linda Meiners in helping out with the related MR protocol.

Bibliography

Alpert, N. M., Bradshaw, J. F., Kennedy, D. & Correia, J. A. (1990), 'The principal axis transformation–a method for image registration', *Journal of nuclear medicine* **31**, 1717–1722.

Amit, Y. & Kong, A. (1996), 'Graphical templates for model registration', *IEEE Transactions on pattern analysis and machine intelligence* **18**(3), 225–236.

Andersson, J. L. R. (1995), 'A rapid and accurate method to realign PET scans utilizing image edge information', *Journal of nuclear medicine* **36**, 657–669.

Andersson, J. L. R., Sundin, A. & Valind, S. (1995), 'A method for coregistration of PET and MR brain images', *Journal of nuclear medicine* **36**, 1307–1315.

Ardekani, B. A., Braun, M., Hutton, B. F., Kanno, I. & Ida, H. (1995), 'A fully automatic multimodality image registration algorithm', *Journal of computer assisted tomography* **19**(4), 615–623.

Ardekani, B. A., Braun, M., Kanno, I. & Hutton, B. F. (1994), 'Automatic detection of intradural spaces in MR images', *Journal of computer assisted tomography* **18**(6), 963–969.

Arun, K. S., Huang, T. S. & Blostein, S. D. (1987), 'Least-squares fitting of two 3-D point sets', *IEEE Transactions on pattern analysis and machine intelligence* **5**, 698–700.

Ault, T. & Siegel, M. W. (1994), Frameless patient registration using ultrasonic imaging, *in* 'Medical robotics and computer assisted surgery', pp. 74–81.

Ault, T. & Siegel, M. W. (1995), 'Frameless patient registration using ultrasonic imaging: a preliminary study', *Journal of image guided surgery* **1**, 94–102.

Ayache, N., Guéziec, A., Thirion, J., Gourdon, A. & Knoplioch, J. (1993), Evaluating 3D registration of CT-scan images using crest lines, *in* D. C. Wilson & J. N. Wilson, eds, 'Mathematical methods in medical imaging', Vol. 2035, SPIE Press, Bellingham, WA, pp. 60–71.

Bacharach, S. L., Douglas, M. A., Carson, R. E., Kalkowski, P. J., Freedman, N. M. T., Perrone-Filardi, P. & Bonow, R. O. (1993), 'Three-dimensional registration of cardiac positron emission tomography attenuation scans', *Journal of nuclear medicine* **34**(2), 311–321.

Bainville, E., Champledoux, G., Cinquin, P., Dessenne, V., Hamadeh, A., Troccaz, J., Lavallée, S., Péria, O., Sautot, P. & Szeliski, R. (1995), Anatomical surfaces based 3D/3D and 3D/2D registration for computer assisted medical interventions, *in* L. Beolchi & M. H. Kuhn, eds, 'Medical imaging: analysis of multimodality 2D/3D images', Vol. 19 of *Studies in health, technology and informatics*, IOS Press, Amsterdam, pp. 53–69.

Bajcsy, R., Lieberson, R. & Reivich, M. (1983), 'A computerized system for the elastic matching of deformed radiographic images to idealized atlas images', *Journal of computer assisted tomography* **7**(4), 618–625.

Bandari, E., Xiang, Q. S. & Little, J. (1994), Visual echo registration of magnetic resonance images, *in* 'Applications of computer vision in medical image processing', AAAI spring symposium series, pp. 38–41.

Banerjee, P. K. & Toga, A. W. (1994), 'Image alignment by integrated rotational and translational transformation matrix', *Physics in medicine and biology* **39**, 1969–1988.

Bani-Hashemi, A., Krishnan, A. & Samaddar, S. (1996), Warped matching for digital subtraction of CT-angiography studies, *in* M. H. Loew & K. M. Hanson, eds, 'Medical Imaging: Image processing', Vol. 2710, SPIE, Bellingham, WA, pp. 428–437.

Barber, D. C., Tindale, W. B., Hunt, E., Mayes, A. & Sagar, H. J. (1995), 'Automatic registration of SPECT images as an alternative to immobilization in neuroactivation studies', *Physics in medicine and biology* **40**, 449–463.

Barillot, C., Gibaud, B., Gee, J. C. & Lemoine, D. (1995), Segmentation and fusion of multimodality and multi-subjects data for the preparation of neurosurgical procedures, *in* L. Beolchi & M. H. Kuhn, eds, 'Medical imaging: analysis of multimodality 2D/3D images', Vol. 19 of *Studies in health, technology and informatics*, IOS Press, Amsterdam, pp. 70–82.

Barillot, C., Lemoine, D., le Bricquer, L., Lachmann, F. & Gibaud, B. (1993), 'Data fusion in medical imaging: merging multimodal and multipatient images, identification of structures and 3D display aspects', *European journal of radiology* **17**, 22–27.

Besl, P. J. & McKay, N. D. (1992), 'A method for registration of 3-D shapes', *IEEE Transactions on pattern analysis and machine intelligence* **14**(2), 239–256.

Bettinardi, V., Gilardi, M. C., Lucignani, G., Landoni, C., Rizzo, G., Striano, G. & Fazio, F. (1993), 'A procedure for patient repositioning and compensation for misalignment between transmission and emission data in PET heart studies', *Journal of nuclear medicine* **34**, 137–142.

Betting, F. & Feldmar, J. (1995), 3D-2D projective registration of anatomical surfaces with their projections, *in* Y. Bizais & C. Barillot, eds, 'Information processing in medical imaging', Kluwer, pp. 275–286.

Betting, F., Feldmar, J., Ayache, N. & Devernay, F. (1995), A new framework for fusing stereo images with volumetric medical images, *in* N. Ayache, ed., 'Computer vision, virtual reality, and robotics in medicine', Vol. 905 of *Lecture notes in computer science*, Springer-Verlag, Berlin, pp. 30–39.

Bijhold, J. (1993), 'Three-dimensional verification of patient placement during radiotherapy using portal images', *Medical physics* **20**(2), 347–356.

Blom, J. (1992), Topological and Geometrical Aspects of Image Structure, PhD thesis, Utrecht University, the Netherlands.

Borgefors, G. (1988), 'Hierarchical chamfer matching: a parametric edge matching algorithm', *IEEE Transactions on pattern analysis and machine intelligence* **10**, 849–865.

Bro-nielsen, M. (1995), Modelling elasticity in solids using active cubes – application to simulated operations, *in* N. Ayache, ed., 'Computer vision, virtual reality, and robotics in medicine', Vol. 905 of *Lecture notes in computer science*, Springer-Verlag, Berlin, pp. 535–541.

Bucholz, R. D., Smith, K. R., Henderson, J. & McDurmont, L. (1994), Intraoperative localization using a three dimensional optical digitizer, *in* 'Medical robotics and computer assisted surgery', pp. 283–290.

Burel, G., Henocq, H. & Catros, J. (1995), registration of 3D objects using linear algebra, *in* N. Ayache, ed., 'Computer vision, virtual reality, and robotics in medicine', Vol. 905 of *Lecture notes in computer science*, Springer-Verlag, Berlin, pp. 252–256.

Burt, P. J. (1993), Enhanced image capture trough fusion, *in* 'International conference on computer vision', IEEE computer society press, Los Alamitos, CA, pp. 173–182.

Buzug, T. & Weese, J. (1996), Improving DSA images with an automatic algorithm based om template matching and an entropy measure, *in* H. U. Lemke, M. W. Vannier, K. Inamura & A. G. Farman, eds, 'Computer assisted radiology', Vol. 1124 of *Excerpta medica - international congress series*, Elsevier, Amsterdam, pp. 145–150.

Carlbom, I., Terzopoulos, D. & Harris, K. M. (1994), 'Computer-assisted registration, segmentation, and 3D reconstruction from images of neuronal tissue sections', *IEEE Transactions on medical imaging* **13**(2), 351–362.

Chang, H. & Fitzpatrick, J. M. (1992), 'A technique for accurate magnetic resonance imaging in the presence of field inhomogeneities', *IEEE Transactions on medical imaging* **11**, 319–329.

Chen, C., Pelizzari, C. A., Chen, G. T. Y., Cooper, M. D. & Levin, D. N. (1987), Image analysis of PET data with the aid of CT and MR images, *in* 'Information processing in medical imaging', pp. 601–611.

Chen, G. T. Y. & Pelizzari, C. A. (1989), 'Image correlation techniques in radiation therapy planning', *Computerized medical imaging and graphics* **13**(3), 235 – 240.

Chen, Q. (1993), Image registration and its applications in medical imaging, PhD thesis, Vrije universiteit Brussel, Brussels, Belgium.

Chou, J., Chen, S., Sudakoff, G. S., Hoffmann, K. R., Chen, C. & Dachman, A. H. (1995), Image fusion for visualization of hepatic vasculature and tumors, *in* M. H. Loew, ed., 'Medical imaging: image processing', Vol. 2434, SPIE Press, Bellingham, WA, pp. 157–163.

Christensen, G. E., Kane, A. A., Marsh, J. L. & Vannier, M. W. (1996), Synthesis of an individual cranial atlas with dysmorphic shape, *in* 'Mathematical methods in biomedical image analysis', IEEE computer society press, Los Alamitos, CA, pp. 309–318.

Christensen, G. E., Miller, M. I., Marsh, J. L. & Vannier, M. W. (1995), Automatic analysis of medical images using a deformable textbook, *in* 'Computer assisted radiology', Springer-Verlag, Berlin, pp. 146–151.

Christensen, G. E., Rabbitt, R. D., Miller, M. I., Joshi, S. C., Grenander, U., Coogan, T. A. & van Essen, D. C. (1995), Topological properties of smooth anatomic maps, *in* Y. Bizais, C. Barillot & R. di Paola, eds, 'Information processing in medical imaging', Kluwer, the Netherlands, pp. 101–112.

Christmas, W. J., Kittler, J. & Petrou, M. (1995), 'Structural matching in computer vision using probabilistic relaxation', *IEEE Transactions on pattern analysis and machine intelligence* **17**(8), 749–764.

Chua, C. S. & Jarvis, R. (1996), '3D free-form surface registration and object recognition', *International journal of computer vision* **17**, 77–99.

Cideciyan, A. V. (1995), 'Registration of ocular fundus images', *IEEE Engineering in medicine and biology* **14**(1), 52–58.

Collignon, A., Géraud, T., Vandermeulen, D., Suetens, P. & Marchal, G. (1993), New high-performance 3D registration algorithms for 3D medical images, *in* M. H. Loew, ed., 'Medical imaging: image processing', Vol. 1898, SPIE Press, Bellingham, WA, pp. 779–788.

Collignon, A., Maes, F., Delaere, D., Vandermeulen, D., Suetens, P. & Marchal, G. (1995), Automated multimodality image registration using information theory, *in* Y. Bizais & C. Barillot, eds, 'Information Processing in Medical Imaging', Kluwer Academic Publishers, Dordrecht, pp. 263–274.

Collignon, A., Vandermeulen, D., Suetens, P. & Marchal, G. (1993), Surface based registration of 3D medical images, *in* M. H. Loew, ed., 'Medical imaging: image processing', Vol. 1898, SPIE Press, Bellingham, WA, pp. 32–42.

Collignon, A., Vandermeulen, D., Suetens, P. & Marchal, G. (1995), 3D multi-modality medical image registration using feature space clustering, *in* N. Ayache, ed., 'CVRMed', Vol. 905 of *Lecture notes in computer science*, Springer-verlag, Berlin, pp. 195–204.

Collignon, A., Vandermeulen, D., Suetens, P., Marchal, G., Baert, A. & Oosterlinck, A. (1994), Automatic registration of 3D images of the brain based on fuzzy objects, *in* M. H. Loew, ed., 'Medical imaging: image processing', Vol. 2167, SPIE Press, Bellingham, WA, pp. 162–175.

Collins, D. L., Evans, A. C., Holmes, C. & Peters, T. M. (1995), Automatic 3D segmentation of neuro-anatomical structures from MRI, *in* Y. Bizais, C. Barillot & R. di Paola, eds, 'Information processing in medical imaging', Kluwer, pp. 139–152.

Collins, D. L., Neelin, P., Peters, T. M. & Evans, A. C. (1994), 'automatic 3D intersubject registration of MR volumetric data in standardized Talairach space', *Journal of computer assisted tomography* **18**(2), 192–205.

Collins, D. L., Peters, T. M. & Evans, A. C. (1994), An automated 3D non-linear deformation procedure for determination of gross morphometric variability in human brain, *in* R. A. Robb, ed., 'Visualization in biomedical computing', Vol. 2359, SPIE Press, Bellingham, WA, pp. 180–190.

Cox, G. S. & de Jager, G. (1994), Automatic registration of temporal image pairs for digital subtraction angiography, *in* M. H. Loew, ed., 'Medical imaging: image processing', Vol. 2167, SPIE Press, Bellingham, WA, pp. 188–199.

Cross, A. D. J., Wilson, R. C. & Hancock, E. R. (1996), Genetic search for structural matching, *in* Bernard, Buxton, Roberto & Cipolla, eds, 'Computer vision - ECCV', Vol. 1064 of *Lecture notes in computer science*, Springer-Verlag, Berlin, pp. 514–525.

Cuchet, E., Knoplioch, J., Dormont, D. & Marsault, C. (1995), Registration in neurosurgery and neuroradiotherapy applications, *in* 'Medical Robotics and computer assisted surgery', Wiley, New York, pp. 31–38.

Cuisenaire, O., Thiran, J., Macq, B., Michel, C., de Volder, A. & Marquès, F. (1996), Automatic registration of 3D MR images with a computerized brain atlas, *in* M. H. Loew & K. M. Hanson, eds, 'Medical imaging', Vol. 2710, SPIE, pp. 438–448.

Davatzikos, C. (1996), Nonlinear registration of brain images using deformable models, *in* 'Mathematical methods in biomedical image analysis', IEEE computer society press, Los Alamitos, CA, pp. 94–103.

Davatzikos, C. & Prince, J. L. (1994), Brain image registration based on curve mapping, *in* 'IEEE workshop on biomedical image analysis', IEEE computer society press, Los Alamitos, CA, pp. 245–254.

Davatzikos, C., Prince, J. L. & Bryan, R. N. (1996), 'Image registration based on boundary mapping', *IEEE Transactions on medical imaging* **15**(1), 112–115.

de Castro, E. & Morandi, C. (1987), 'Registration of translated and rotated images using finite Fourier transforms', *IEEE Transactions on pattern analysis and machine intelligence* **5**, 700–703.

Declerc, J., Feldmar, J., Betting, F. & Goris, M. L. (1996), Automatic registration and alignment on a template of cardiac stress and rest SPECT images, *in* 'Mathematical methods in biomedical image analysis', IEEE computer society press, Los Alamitos, CA, pp. 212–221.

Devous, M. D. (1992), 'Comparison of SPECT applications in neurology and psychiatry', *Journal of clinical psychiatry* **53**(supp 11), 13–19.

Ding, G. X., Shalev, S. & Gluchev, G. (1993), 'A $\rho - \theta$ technique for treatment verification in radiotherapy and its clinical applications', *Medical physics* **20**(4), 1135–1143.

Dong, L. & Boyer, A. L. (1996), 'A portal image alignment and patient setup verification procedure using moments and correlation techniques', *Physics in medicine and biology* **41**, 697–723.

Douglas, M. A., Bacharach, S. L. & Kalkowski, P. J. (1992), Alignment of PET attenuation images., *in* 'Computer in radiology', IEEE computer society press, New York.

Eberl, S., Kanno, I., Fulton, R. R., Ryan, A., Hutton, B. F. & Fulham, M. J. (1996), 'Automated interstudy image registration technique for SPECT and PET', *Journal of nuclear medicine* **37**, 137–145.

Eberly, D., Gardner, R., Morse, B., Pizer, S. & Scharlach, C. (1994), 'Ridges for image analysis', *Mathematical Imaging and Vision* **4**, 353–373.

Edwards, P. J., Hawkes, D. J., Hill, D. L. G., Jewell, D., Spink, R., Strong, A. & Gleeson, M. (1995), Augmented reality in the stereo operating microscope for otolaryngology and neurosurgical guidance, *in* 'Medical robotics and computer assisted surgery', Wiley, pp. 8–15.

Edwards, P. J., Hill, D. L. G., Hawkes, D. J., Spink, R., Colchester, A. C. F., Strong, A. & Gleeson, M. (1995), Neurosurgical guidance using the stereo microscope, *in* N. Ayache, ed., 'Computer vision, virtual reality, and robotics in medicine', Vol. 905 of *Lecture notes in computer science*, Springer-Verlag, Berlin, pp. 555–564.

Eilertsen, K., Skretting, A. & Tennvassas (1994), 'Methods for fully automated verification of patient set-up in external beam radiotherapy with polygon shaped fields', *Physics in medicine and biology* **39**, 993–1012.

Ellis, R. E., Toksvig-Larsen, S., Marcacci, M., Caramella, D. & Fadda, M. (1996), A biocompatible fiducial marker for evaluating the accuracy of CT image registration, *in* H. U. Lemke, M. W. Vannier, K. Inamura & A. G. Farman, eds, 'Computer assisted radiology', Vol. 1124 of *Excerpta medica - international congress series*, Elsevier, Amsterdam, pp. 693–698.

Erbe, H., Kriete, A., Jödicke, A., Deinsberger, W. & Böker, D. (1996), 3D-ultrasonography and image matching for detection of brain shift during intracranial surgery, *in* H. U. Lemke, M. W. Vannier, K. Inamura & A. G. Farman, eds, 'Computer assisted radiology', Vol. 1124 of *Excerpta medica - international congress series*, Elsevier, Amsterdam, pp. 225–230.

Ettinger, G. J., Grimson, W. E. L., Leventon, M. E., Kikinis, R., Gugino, V., Cote, W., Karapelou, M., Aglio, L., Shenton, M., Potts, G. & Alexander, E. (1996), Non-invasive functional brain mapping using registered transcranial magnetic stimulation, *in* 'Mathematical methods in biomedical image analysis', IEEE computer society press, Los Alamitos, CA, pp. 332–41.

Ettinger, G. J., Grimson, W. E. L. & Lozano-Pérez, T. (1994), Automatic 3D image registration for medical change detection applications, *in* 'Applications of computer vision in medical image processing', AAAI spring symposium series, pp. 182–185.

Ettinger, G. J., Grimson, W. E. L., Lozano-Pérez, T., Wells III, W. M., White, S. J. & Kikinis, R. (1994), Automatic registration for multiple sclerosis change detection, *in* 'IEEE workshop on biomedical image analysis', IEEE computer society press, Los Alamitos, CA, pp. 297–306.

Evans, A. C., Collins, D. L., Neelin, P. & Marrett, T. S. (1996), Correlative analysis of three-dimensional brain images, *in* R. H. Taylor, S. Lavallée, G. C. Burdea & R. Mösges, eds, 'Computer-integrated surgery', Technology and clinical applications, MIT Press, Cambridge, MA, chapter 6, pp. 99–114.

Evans, A. C., Marrett, S., Collins, L. & Peters, T. M. (1989), Anatomical-functional correlative analysis of the human brain using three dimensional imaging systems, *in* R. Schneider, S. Dwyer III & R. Jost, eds, 'Medical imaging: image processing', Vol. 1092, SPIE press, Bellingham, WA, pp. 264–274.

Evans, A. C., Marrett, S., Torrescorzo, J., Ku, S. & Collins, L. (1991), 'MRI-PET correlation in three dimensions using a volume of interest (VOI) atlas', *Journal of cerebral blood flow and metabolism* **11**, A69–A78.

Evans, R. J., Strong, A. J., Colchester, A. C. F., Zhao, J. & Holton-Tainter, K. (1996), Clinical accuracy of the VISLAN surgical navigation and guidance system, *in* H. U. Lemke, M. W. Vannier, K. Inamura & A. G. Farman, eds, 'Computer assisted radiology', Vol. 1124 of *Excerpta medica - international congress series*, Elsevier, Amsterdam, pp. 799–804.

Fang, S., Raghavan, R. & Richtsmeier, J. T. (1996), Volume morphing methods for landmark based 3D image deformation, *in* M. H. Loew & K. M. Hanson, eds, 'Medical Imaging: Image processing', Vol. 2710, SPIE, Bellingham, WA, pp. 404–415.

Feldmar, J. & Ayache, N. (1994), Locally affine registration of free-form surfaces, *in* 'Computer vision and pattern recognition', IEEE Computer Society press, Los Alamitos, CA, pp. 496–501.

Feldmar, J. & Ayache, N. (1996), 'Rigid, affine and locally affine registration of free-form surfaces', *International journal of computer vision* **18**(2), 99–119.

Feldmar, J., Ayache, N. & Betting, F. (1995), 3D-2D projective registration of free-form curves and surfaces, *in* 'International conference on computer vision', IEEE computer society press, Los Alamitos, CA, pp. 549–556.

Feldmar, J., Malandain, G., Declerck, J. & Ayache, N. (1996), Extension of the ICP algorithm to non-rigid intensity-based registration of 3D volumes, *in* 'Mathematical methods in biomedical image analysis', IEEE computer society press, Los Alamitos, CA, pp. 84–93.

Florack, L. M. J., ter Haar Romeny, B. M., Koenderink, J. J. & Viergever, M. A. (1992), 'On scale and the differential structure of images', *Image & Vision Computing* **10**, 376–388.

Florack, L. M. J., ter Haar Romeny, B. M., Koenderink, J. J. & Viergever, M. A. (1993), 'Cartesian differential invariants in scale-space', *Journal of Mathematical Imaging and Vision* **3**, 327–348.

Florack, L. M. J., ter Haar Romeny, B. M., Koenderink, J. J. & Viergever, M. A. (1994), 'Linear scale-space', *Journal of Mathematical Imaging and Vision* **4**(4), 325–351.

Fontana, F., Crovetto, A., Bergognoni, M. & Casali, A. M. (1993), Multiresolution registration for volume reconstruction in microscopical applications, *in* M. H. Loew, ed., 'Medical imaging: image processing', Vol. 1898, SPIE Press, Bellingham, WA, pp. 55–60.

Fright, R. W. & Linney, A. D. (1993), 'Registration of 3-D head surfaces using multiple landmarks', *IEEE Transactions on medical imaging* **12**(3), 515–520.

Fritsch, D. F. (1993), Registration of radiotherapy images using multiscale medial descriptions of image structure, PhD thesis, University of North Carolina, Chapel Hill, NC.

Fritsch, D. F., Pizer, S. M., Chaney, E., Liu, A., Raghavan, S. & Shah, T. (1994), Cores for image registration, *in* 'Medical imaging', SPIE press.

Fritsch, D. F., Pizer, S. M., Morse, B. S., Eberly, D. H. & Liu, A. (1994), 'The multiscale medial axis and its applications in image registration', *Pattern recognition letters* **15**, 445–452.

Fuchs, M., Wischmann, H., Neumann, A., Weese, J., Zylka, W., Sabczynski, J., Kuhn, M. H., Buzug, T. M., Schmitz, G. & Gieles, P. M. C. (1996), Accuracy analysis for image-guided neurosurgery using fiducial skin markers, 3D CT imaging, and an optical localizer system, *in* H. U. Lemke, M. W. Vannier, K. Inamura & A. G. Farman, eds, 'Computer assisted radiology', Vol. 1124 of *Excerpta medica - international congress series*, Elsevier, Amsterdam, pp. 770–775.

Gall, K. P. & Verhey, L. J. (1993), 'Computer-assisted positioning of radiotherapy patients using implanted radioopaque fiducials', *Medical physics* **20**(4), 1152–1159.

Ge, Y., Fitzpatrick, J. M., Kessler, R. M., Jeske-Janicka, M. & Margolin, R. A. (1995), Intersubject brain image registration using both cortical and subcortical landmarks, *in* M. Loew, ed., 'Medical imaging', Vol. 2434, SPIE, Bellingham, WA, pp. 81–95.

Ge, Y., Fitzpatrick, J. M., Votaw, J. R., Gadamsetty, S., Maciunas, R. J., Kessler, R. M. & Margolin, R. A. (1994), 'Retrospective registration of PET and MR brain images: an algorithm and its stereotactic validation', *Journal of computer assisted tomography* **18**(5), 800–810.

Ge, Y., Maurer, C. R. & Fitzpatrick, J. M. (1996), Surface-based 3-D image registration using the iterative closest point algorithm with a closest point transform, *in* M. H. Loew & K. M. Hanson, eds, 'Medical Imaging: Image processing', Vol. 2710, SPIE, Bellingham, WA, pp. 358–367.

Gee, J. C., Barillot, C., le Bricquer, L., Haynor, D. R. & Bajcsy, R. (1994), Matching structural images of the human brain using statistical and geometrical image features, *in* 'Visualization in biomedical imaging', Vol. 2359, SPIE press, Bellingham, WA, pp. 191–204.

Gee, J. C. & Haynor, D. R. (1996), Rapid coarse-to-fine matching using scale-specific priors, *in* M. H. Loew & K. M. Hanson, eds, 'Medical Imaging: Image processing', Vol. 2710, SPIE, Bellingham, WA, pp. 416–427.

Gee, J. C., le Bricquer, L. & Barillot, C. (1995), Probabilistic matching of brain images, *in* Y. Bizais, C. Barillot & R. di Paola, eds, 'Information processing in medical imaging', Kluwer, pp. 113–125.

Gee, J. C., le Bricquer, L., Barillot, C., Haynor, D. R. & Bajcsy, R. (1995), Bayesian approach to the brain image matching problem, *in* M. H. Loew, ed., 'Medical imaging: image processing', Vol. 2434, SPIE Press, Bellingham, WA, pp. 145–156.

Gee, J. C., Reivicj, M. & Bajcsy, R. (1993), 'Elastically deforming 3D atlas to match anatomical brain images', *Journal of computer assisted tomography* **17**(2), 225–236.

Gilhuijs, K. G. A., van den Ven, P. J. H. & van Herk, M. (1996), 'Automatic three-dimensional inspection of patient setup in radiation therapy using portal images, simulator images, and computed tomography data', *Medical physics* **23**(3), 389–399.

Gilhuijs, K. G. A. & van Herk, M. (1993), 'Automatic on-line inspection of patient setup in radiation therapy using digital portal images', *Medical physics* **20**(3), 667–677.

Gluhchev, G. & Shalev, S. (1993), Robust registration in case of different scaling, *in* M. H. Loew, ed., 'Medical imaging: image processing', Vol. 1898, SPIE Press, Bellingham, WA, pp. 126–133.

Goris, M. L., Declerck, J., Feldmar, K. & Ayache, N. (1996), Elastic transformations in referential quantification of scintigraphic images, *in* H. U. Lemke, M. W. Vannier, K. Inamura & A. G. Farman, eds, 'Computer assisted radiology', Vol. 1124 of *Excerpta medica - international congress series*, Elsevier, Amsterdam, pp. 298–301.

Gottesfeld Brown, L. & Boult, T. E. (1996), Registration of planar film radiographs with computed tomography, *in* 'Mathematical methods in biomedical image analysis', IEEE computer society press, Los Alamitos, CA, pp. 42–51.

Greitz, T., Bergström, M., Boëthius, J., Kingsley, D. & Ribbe, T. (1980), 'Head fixation system for integration of radiodiagnostic and therapeutic procedures', *Neuroradiology* **19**, 1–6.

Grimson, E., Lozano-Pérez, T., Wells, W., Ettinger, G., White, S. & Kikinis, R. (1994), Automated registration for enhanced reality visualization in surgery, *in* 'Applications of computer vision in medical image processing', AAAI spring symposium series, pp. 26–29.

Grimson, W. E. L., Ettinger, G. J., White, S. J., Gleason, P. L., Lozano-Pérez, T., Wells III, W. M. & Kikinis, R. (1995), Evaluating and validating an automated registration system for enhanced reality visualization in surgery, *in* N. Ayache, ed., 'Computer vision, virtual reality, and robotics in medicine', Vol. 905 of *Lecture notes in computer science*, Springer-Verlag, Berlin, pp. 3–12.

Grimson, W. E. L., Ettinger, G. J., White, S. J., Lozano-Pérez, T., Wells III, W. M. & Kikinis, R. (1996), 'An automatic registration method for frameless stereotaxy, image guided surgery, and enhanced reality visualization', *IEEE Transactions on medical imaging* **15**(2), 129–140.

Grimson, W. E. L., Lozano-Pérez, T., Wells III, W. M., Ettinger, G. J., White, S. J. & Kikinis, R. (1994*a*), An automatic registration method for frameless stereotaxy, image guided surgery, and enhanced reality visualization, *in* 'Computer vision and pattern recognition', IEEE Computer Society press, Los Alamitos, CA, pp. 430–436.

Grimson, W. E. L., Lozano-Pérez, T., Wells III, W. M., Ettinger, G. J., White, S. J. & Kikinis, R. (1994*b*), Automated registration for enhanced reality visualization in surgery, *in* 'Medical robotics and computer assisted surgery', pp. 82–89.

Guéziec, A. (1993), Large deformable splines, crest lines and matching, *in* 'International conference on computer vision', IEEE computer society press, Los Alamitos, CA, pp. 650–657.

Guéziec, A. & Ayache, N. (1992), Smoothing and matching of 3-D space curves, *in* R. Robb, ed., 'Visualization in biomedical computing', Vol. 1808 of *Proc. SPIE*, SPIE Press, Bellingham, WA, pp. 259–273.

Hajnal, J. V., Saeed, N., Oatridge, A., Williams, E. J., Young, I. R. & Bydder, G. M. (1995), 'Detection of subtle brain changes using subvoxel registration and subtraction of serial MR images', *Journal of computer assisted tomography* **19**(5), 677–691.

Hajnal, J. V., Saeed, N., Soar, E. J., Oatridge, A., Young, I. R. & Bydder, G. M. (1995), 'A registration and interpolation procedure for subvoxel matching of serially acquired MR images', *Journal of computer assisted tomography* **19**(2), 289–296.

Haller, J. W., Christensen, G. E., Joshi, S. C., Newcomer, J. W., Miller, M. I., Csernansky, J. G. & Vannier, M. W. (1996), 'Hippocampal MR imaging morphometry by means of general pattern matching', *Radiology* **199**, 787–791.

Haller, J. W., Christensen, G. E., Joshi, S., Miller, M. I. & Vannier, M. W. (1995), Digital atlas-based segmentation of the hippocampus, *in* H. U. Lemke, K. Inamura, C. C. Jaffe & M. W. Vannier, eds, 'Computer assisted radiology', Springer-Verlag, Berlin, pp. 152–157.

Hamadeh, A., Lavallée, S., Szeliski, R., Cinquin, P. & Péria, O. (1995), Anatomy-based registration for computer-integrated surgery, *in* N. Ayache, ed., 'Computer vision, virtual reality, and robotics in medicine', Vol. 905 of *Lecture notes in computer science*, Springer-Verlag, Berlin, pp. 212–218.

Hamadeh, A., Sautot, P. & Cinquin, P. (1995), A unified approach to 3D-2D registration and 2D images segmentation, *in* H. U. Lemke, K. Inamura, C. C. Jaffe & M. W. Vannier, eds, 'Computer assisted radiology', Springer-Verlag, Berlin, pp. 1191–1196.

Hamadeh, A., Sautot, P., Lavallée, S. & Cinquin, P. (1995), Towards automatic registration between CT and X-ray images: cooperation between 3D/2D registration and 2D edge detection, *in* 'Medical robotics and computer assisted surgery', Wiley, pp. 39–46.

Haralick, R. M., Sternberg, S. R. & Zhuang, X. (1987), 'Image analysis using mathematical morphology', *IEEE transactions on pattern analysis and machine intelligence* **9**(4), 532–550.

Harmon, L., Vayda, A., Erlandson, E., Taren, J. & Ross, D. (1994), 3D laser scanning for image-guided neurosurgery, *in* 'Applications of computer vision in medical image processing', AAAI spring symposium series, pp. 106–109.

Hata, N., Suzuki, M., Dohi, T., Iseki, H., Takakura, K. & Hashimoto, D. (1994), Registration of ultrasound echography for intraoperative use: a newly developed multiproperty method, *in* R. A. Robb, ed., 'Visualization in biomedical computing', Vol. 2359, SPIE Press, Bellingham, WA, pp. 251–259.

Hawkes, D. J., Hill, D. L. G. & Bracey, E. C. M. L. (1992), Multi-modal data fusion to combine anatomical and physiological information in the head and heart, *in* J. H. C. Reiber & E. E. van der Wall, eds, 'Cardiovascular nuclear medicine and MRI', Kluwer, Dordrecht, the Netherlands, pp. 113–130.

Hawkes, D. J., Ruff, C. F., Hill, D. L. G., Studholme, C., Edwards, P. J. & Wong, W. L. (1995), 3D multimodal imaging in image guided interventions, *in* L. Beolchi & M. H. Kuhn, eds, 'Medical imaging: analysis of multimodality 2D/3D images', Vol. 19 of *Studies in health, technology and informatics*, IOS Press, Amsterdam, pp. 83–100.

He, Z., Maublant, J. C., Cauvin, J. C. & Veyre, A. (1991), 'Reorientation of the left ventricular long-axis on myocardial transaxial tomograms by a linear fitting method', *Journal of nuclear medicine* **32**, 1794–1800.

Hemler, P. F., Napel, S., Sumanaweera, T. S., Pichumani, R., van den Elsen, P. A., Martin, D., Drace, J. & Adler, J. R. (1995), 'Registration error quantification of a surface-based multimodality image fusion system', *Medical physics* **22**(7), 1049–1056.

Hemler, P. F., Sumanaweera, T., Pichumani, R., van den Elsen, P. A., Napel, S. & Adler, J. (1994), A system for multimodality image fusion, *in* 'IEEE symposium on computer-based medical systems', IEEE Computer Society Press, Los Alamitos, CA, pp. 335–340.

Hemler, P. F., Sumanaweera, T., Pichumani, R., van den Elsen, P. A., Napel, S., Drace, J. & Adler, J. (1994), A system for multimodality image fusion of the spine, *in* 'Applications of computer vision in medical image processing', AAAI spring symposium series, pp. 42–45.

Hemler, P. F., Sumanaweera, T. S., van den Elsen, P. A., Napel, S. & Adler, J. (1995), 'A versatile system for multimodality image fusion', *Journal of image guided surgery* **1**(1).

Hemler, P. F., Sumanaweera, T., van den Elsen, P. A., Napel, S. & Adler, J. R. (1996), Quantified registration error versus the accuracy of registered surfaces for a multimodality surface-based registration system, *in* M. H. Loew & K. M. Hanson, eds, 'Medical Imaging: Image processing', Vol. 2710, SPIE, Bellingham, WA, pp. 348–357.

Hemler, P. F., van den Elsen, P. A., Sumanaweera, T. S., Napel, S., Drace, J. & Adler, J. R. (1995), A quantitative comparison of residual error for three different multimodality registration techniques, *in* Y. Bizais, C. Barillot & R. di Paola, eds, 'Information processing in medical imaging', Kluwer, pp. 389–390.

Henderson, J. M., Smith, K. R. & Bucholz, R. D. (1994), 'An accurate and ergonomic method of registration for image-guided neurosurgery', *Computerized medical imaging and graphics* **18**(4), 273–277.

Henri, C. J., Colchester, A. C. F., Zhao, J., Hawkes, D. J., Hill, D. L. G. & Evans, R. L. (1995), Registration of 3-D surface data for intra-operative guidance and visualization in frameless stereotactic neurosurgery, *in* N. Ayache, ed., 'Computer vision, virtual reality, and robotics in medicine', Vol. 905 of *Lecture notes in computer science*, Springer-Verlag, Berlin, pp. 47–56.

Henri, C. J., Cukiert, A., Collins, D. L., Olivier, A. & Peters, T. M. (1992), Towards frameless stereotaxy: anatomical-vascular correlation and registration, *in* 'Visualization in biomedical computing', Vol. 1808, SPIE press, Bellingham, WA, pp. 214–224.

Hill, D. L. G. (1993), Combination of 3D medical images from multiple modalities, PhD thesis, University of London.

Hill, D. L. G. & Hawkes, D. J. (1994), Medical image registration using voxel similarity measures, *in* 'Applications of computer vision in medical image processing', AAAI spring symposium series, pp. 34–37.

Hill, D. L. G., Hawkes, D. J., Crossman, J. E., Gleeson, M. J., Cox, T. C. S., Bracey, E. C. M. L., Strong, A. J. & Graves, P. (1991), 'Registration of MR and CT images for skull base surgery using pointlike anatomical features', *British journal of radiology* **64**(767), 1030–1035.

Hill, D. L. G., Hawkes, D. J. & Hardingham, C. R. (1991), The use of anatomical knowledge to register 3D blood vessel data derived from DSA with MR images, *in* 'Medical imaging: image processing', Vol. 1445, SPIE press, Bellingham, WA, pp. 348–357.

Hill, D. L. G., Hawkes, D. J., Harrison, N. A. & Ruff, C. F. (1993), A strategy for automated multimodality image registration incorporating anatomical knowledge and imager characteristics, *in* H. H. Barrett & A. F. Gmitro, eds, 'Information processing in medical imaging', Vol. 687 of *Lecture notes in computer science*, Springer-Verlag, Berlin, pp. 182–196.

Hill, D. L. G., Hawkes, D. J., Hussain, Z., Green, S. E. M., Ruff, C. F. & Robinson, G. P. (1993), 'Accurate combination of CT and MR data of the head: validation and applications in surgical and therapy planning', *Computerized medical imaging and graphics* **17**(4/5), 357–363.

Hill, D. L. G., Studholme, C. & Hawkes, D. J. (1994), Voxel similarity measures for automated image registration, *in* R. Robb, ed., 'Visualization in biomedical computing', Vol. 2359, SPIE Press, Bellingham, WA, pp. 205–216.

Hoh, C. K., Dahlbom, M., Harris, G., Choi, Y., Hawkins, R. A., Phelps, M. E. & Maddahi, J. (1993), 'Automated iterative three-dimensional registration of positron emission tomography images', *Journal of nuclear medicine* **34**, 2009–2018.

Holton, K. S., Taneja, U. & Robb, R. A. (1995), Quantitative validation of 3D image registration techniques, *in* M. H. Loew, ed., 'Medical imaging: image processing', Vol. 2434, SPIE Press, Bellingham, WA, pp. 504–519.

Holton-Tainter, K., Zhao, J. & Colchester, A. C. F. (1995), Accuracy of the VISLAN intra-operative pointer in localising markers from pre-operative images, *in* 'Medical robotics and computer assisted surgery', Wiley, pp. 278–285.

Hristov, D. H. & Fallone, B. G. (1996), 'A grey-level alignment algorithm for registration of portal images and digitally reconstructed radiographs', *Medical physics* **23**(1), 75–84.

Hua, P. & Fram, I. (1993), Feature-based image registration for digital subtraction angiography, *in* M. H. Loew, ed., 'Medical imaging: image processing', Vol. 1898, SPIE Press, Bellingham, WA, pp. 24–31.

Huang, Z. & Cohen, F. S. (1994), Affine-invariant B-spline moments for curve matching, *in* 'Computer vision and pattern recognition', IEEE Computer Society press, Los Alamitos, CA, pp. 587–592.

Jacq, J. & Roux, C. (1995), Registration of non-segmented images using a genetic algorithm, *in* N. Ayache, ed., 'Computer vision, virtual reality, and robotics in medicine', Vol. 905 of *Lecture notes in computer science*, Springer-Verlag, Berlin, pp. 205–211.

Jain, A. K., Zhong, Y. & Lakshmanan, S. (1996), 'Object matching using deformable templates', *IEEE Transactions on pattern analysis and machine intelligence* **18**(3), 267–277.

Jiang, H., Holton, K. & Robb, R. (1992), Image registration of multimodality 3-D medical images by chamfer matching, Technical report, Dept of Physiology and Biophysics, Biomedical Imaging Resource, Mayo Foundation, Rochester, MN 55905.

Jiang, H., Robb, R. A. & Holton, K. S. (1992), A new approach to 3-D registration of multimodality medical images by surface matching, *in* 'Visualization in biomedical computing', Vol. 1808, SPIE press, Bellingham, WA, pp. 196–213.

Junck, L., Moen, J. G., Hutchins, G. D., Brown, M. B. & Kuhl, D. E. (1990), 'Correlation methods for the centering, rotation, and alignment of functional brain images', *Journal of nuclear medicine* **31**, 1220–1276.

Kanatani, K. (1994), 'Analysis of 3-D rotation fitting', *IEEE Transactions on pattern analysis and machine intelligence* **16**(5), 543–549.

Kitchen, L. & Rosenfeld, A. (1982), 'Gray-level corner detection', *Pattern Recognition Letters* **1**, 95–102.

Kittler, J., Christmas, W. J. & Petrou, M. (1993), Probabilistic relaxation for matching problems in computer vision, *in* 'International conference on computer vision', IEEE computer society press, Los Alamitos, CA, pp. 666–673.

Koenderink, J. J. (1984), 'The structure of images', *Biological Cybernetics* **50**, 363–370.

Koenderink, J. J. & van Doorn, A. J. (1994), 'Two-plus-one dimensional differential geometry', *Pattern Recognition Letters* **15**, 439–443.

Kooy, H. M., van Herk, M., Barnes, P. D., Alexander III, E., Dunbar, S. F., Tarbell, N. J., Mulkern, R. V., Holupka, E. J. & Loeffler, J. S. (1994), 'Image fusion for stereotactic radiotherapy and radiosurgery treatment planning', *International journal of radiation oncology* **28**(5), 1229–1234.

Kraaier, V., van Huffelen, A. C. & Wieneke, G. H. (1988), 'Changes in quantitative EEG and blood flow velocity due to standardized hyperventilation; a model of transient ischaemia in young human subjects', *Electroencephalography and clinical neurophysiology* **70**, 377–387.

Kramer, H. P. & Bruckner, J. B. (1975), 'Iterations of a non-linear transformation for enhancement of digital images', *Pattern recognition* **7**, 53–58.

Krattenthaler, W., Mayer, K. J. & Zeiler, M. (1994), Point correlation: a reduced-cost template matching technique, *in* 'International conference on image processing', IEEE computer society press, Los Alamitos, CA, pp. 208–212.

Kruggel, F. & Bartenstein, P. (1995), Automatical registration of brain volume datasets, *in* Y. Bizais, C. Barillot & R. di Paola, eds, 'Information processing in medical imaging', Kluwer, pp. 389–390.

Kumar, R., Asmuth, J. C., Hanna, K. & Bergen, J. (1996), Application of 3D registration for detecing lesions in magnetic resonance scans, *in* M. H. Loew & K. M. Hanson, eds, 'Medical Imaging: Image processing', Vol. 2710, SPIE, Bellingham, WA, pp. 646–656.

Laitinen, L. V., Liliequist, B., Fagerlund, M. & Eriksson, A. T. (1985), 'An adapter for computer tomography guided stereotaxis', *Surgical neurology* **23**, 559–566.

Lange, N., O'Tuama, L. A. & Treves, S. T. (1993), Statistical methods for paired comparisons of SPECT brain images, *in* D. C. Wilson & J. N. Wilson, eds, 'Mathematical methods in medical imaging', Vol. 2035, SPIE Press, Bellingham, WA, pp. 171–178.

Lavallée, S. (1996), Registration for computer-integrated surgery: methodology, state of the art, *in* R. H. Taylor, S. Lavallée, G. C. Burdea & R. Mösges, eds, 'Computer-integrated surgery', Technology and clinical applications, MIT Press, Cambridge, MA, chapter 5, pp. 77–97.

Lavallée, S., Sautot, P., Troccaz, J., Cinquin, P. & Merloz, P. (1994), Computer assisted spine surgery: a technique for accurate transpedicular screw fixation using CT data and a 3-D optical localizer, *in* 'Medical robotics and computer assisted surgery', pp. 315–322.

Lavallée, S. & Szeliski, R. (1995), 'Recovering the position and orientation of free-form objects', *IEEE Transactions on pattern analysis and machine intelligence* **17**(4), 378–390.

Lavallée, S., Szeliski, R. & Brunie, L. (1996), Anatomy-based registration of three-dimensional medical images, range images, X-ray projections, and three-dimensional models using octree-splines, *in* R. H. Taylor, S. Lavallée, G. C. Burdea & R. Mösges, eds, 'Computer-integrated surgery', Technology and clinical applications, MIT Press, Cambridge, MA, chapter 7, pp. 115–143.

Lavallée, S., Troccaz, J., Sautot, P., Mazier, B., Cinquin, P., Merloz, P. & Chirossel, J. (1996), Computer-assisted spinal surgery using anatomy-based registration, *in* R. H. Taylor, S. Lavallée, G. C. Burdea & R. Mösges, eds, 'Computer-integrated surgery', Technology and clinical applications, MIT Press, Cambridge, MA, chapter 32, pp. 425–449.

Lea, J. T., Santos-munné, J. J. & Peshkin, M. A. (1995), 'Diagramming registration connectivity and structure', *IEEE Engineering in medicine and biology* **14**(3), 271–278.

Lea, J. T., Watkins, D., Mills, A., Peshkin, M. A., Kienzle III, T. C. & Stulberg, S. D. (1994), Registration and immobilization for robot-assisted orthopaedic surgery, *in* 'Medical robotics and computer assisted surgery', pp. 63–68.

Lea, J. T., Watkins, D., Mills, A., Peshkin, M. A., Kienzle III, T. C. & Stulberg, S. D. (1995), 'Registration and immobilization in robot-assisted surgery', *Journal of image guided surgery* **1**, 80–87.

Leclerc, V. & Benchimol, C. (1987), Automatic elastic registration of DSA images, *in* 'Computer assisted radiology', pp. 719–723.

Lehmann, T., Goerke, C., Schmitt, W., Kaupp, A. & Repges, R. (1996), A rotation-extended cepstrum technique optimized by systematic analysis of various sets of X-ray images, *in* M. H. Loew & K. M. Hanson, eds, 'Medical Imaging: Image processing', Vol. 2710, SPIE, Bellingham, WA, pp. 390–401.

Lemieux, L. & Jagoe, R. (1994), 'Effect of fiducial marker localization on stereotactic target coordinate calculation in CT slices and radiographs', *Physics in medicine and biology* **39**, 1915–1928.

Lemieux, L., Jagoe, R., Fish, D. R., Kitchen, N. D. & Thomas, D. G. T. (1994), 'A patient-to-computed-tomography image registration method based on digitally reconstructed radiographs', *Medical physics* **21**(11), 1749–1760.

Lemieux, L., Kitchen, N. D., Hughes, S. W. & Thomas, D. G. T. (1994), 'Voxel-based localization in frame-based and frameless stereotaxy and its accuracy', *Medical physics* **21**(8), 1301–1310.

Lemoine, D., Barillot, C., Gibaud, B. & Pasqualini, E. (1991), An anatomical based 3d registration of multimodality and atlas data in neurosurgery, *in* A. C. F. Colchester & D. J. Hawkes, eds, 'Information Processing in Medical Imaging, Proceedings of the 12^{th} International Conference', Springer-Verlag, Berlin, pp. 154–164.

Leslie, W. D., Borys, A., McDonald, D., Dupont, J. O. & Peterdy, A. E. (1995), 'External reference markers for the correction of head rotation in brain single-photon emission tomography', *European journal of nuclear medicine* **22**(4), 351–355.

Leszczynski, K., Loose, S. & Dunscombe, P. (1995), 'Segmented chamfer matching for the registration of field borders in radiotherapy images', *Physics in medicine and biology* **40**, 83–94.

Leung Lam, K., ten Haken, R. K., McShan, D. L. & Thornton, A. F. (1993), 'Automated determination of patient setup errors in radiation therapy using spherical radio-opaque markers', *Medical physics* **20**(4), 1145–1152.

Levin, D. N., Pelizzari, C. A., Chen, G. T. Y., Chen, C. & Cooper, M. D. (1988), 'Retrospective geometric correlation of MR, CT, and PET images', *Radiology* **169**(3), 817–823.

Li, H., Manjunath, B. S. & Mitra, S. K. (1994), Multi-sensor image fusion using the wavelet transform, *in* 'International conference on image processing', IEEE computer society press, Los Alamitos, CA, pp. 51–55.

Li, H., Manjunath, B. S. & Mitra, S. K. (1995), 'Multisensor image fusion using the wavelet transform', *Graphical models and image processing* **57**(3), 235–245.

Li, S., Pelizzari, C. A. & Chen, G. T. Y. (1994), 'Unfolding patient motion with biplane radiographs', *Medical physics* **21**(9), 1427–1433.

Little, J. A., Hill, D. L. G. & Hawkes, D. J. (1996), Deformations incorporating rigid structures, *in* 'Mathematical methods in biomedical image analysis', IEEE computer society press, Los Alamitos, CA, pp. 104–113.

Liu, A., Pizer, S., Eberly, D., Morse, B., Rosenman, J., Chaney, E., Bullitt, E. & Carrasco, V. (1994), Volume registration using the 3D core, *in* R. A. Robb, ed., 'Visualization in biomedical computing', Vol. 2359, SPIE Press, Bellingham, WA, pp. 217–226.

Lunsford, L. D. (1988), *Modern stereotactic neurosurgery*, Martinus Nijhoff, Boston, MA.

MacDonald, D., Avis, D. & Evans, A. C. (1994), Multiple surface identification and matching in magnetic resonance images, *in* 'Visualization in biomedical computing', Vol. 2359, SPIE press, Bellingham, WA, pp. 160–169.

Maes, F., Collignon, A., Vandermeulen, D., Marchal, G. & Suetens, P. (1996), Multi-modality image registration by maximization of mutual information, *in* 'Mathematical methods in biomedical image analysis', IEEE computer society press, Los Alamitos, CA, pp. 14–22.

Maguire, G. Q., Noz, M., Rusinek, H., Jaeger, J., Kramer, E. L., Sanger, J. & Smith, G. (1991), 'Graphics applied to medical image registration', *IEEE Computer graphics and applications* **11**(2), 20–28.

Maintz, J. B. A. (1992), Matching of medical images using geometrical features, Master's thesis, Utrecht University, Report 3DCV 92-30.

Maintz, J. B. A., Beekman, F. J., de Bruin, W., van den Elsen, P. A., van Rijk, P. P. & Viergever, M. A. (1996), 'Automatic registration and intensity scaling of SPECT brain images', *Journal of nuclear medicine* **37**(5, supplement), 213P. abstract.

Maintz, J. B. A., van den Elsen, P. A. & Viergever, M. A. (1994), Using geometrical features to match CT and MR brain images, *in* L. Beolchi & M. Kuhn, eds, 'Medical imaging, analysis of multimodality 2D/3D images', Vol. 19 of *Studies in Health, Technology and Informatics*, IOS Press, Amsterdam, pp. 43–52.

Maintz, J. B. A., van den Elsen, P. A. & Viergever, M. A. (1995), Comparison of feature-based matching of CT and MR brain images, *in* N. Ayache, ed., 'Computer vision, virtual reality, and robotics in medicine', Vol. 905 of *Lecture notes in computer science*, Springer-Verlag, Berlin, pp. 219–228.

Maintz, J. B. A., van den Elsen, P. A. & Viergever, M. A. (1996*a*), 'Comparison of edge-based and ridge-based registration of CT and MR brain images', *Medical image analysis* **1**(2). in press.

Maintz, J. B. A., van den Elsen, P. A. & Viergever, M. A. (1996*b*), 'Evaluation of ridge seeking operators for multimodality medical image matching', *IEEE Transactions on pattern analysis and machine intelligence* **18**(4), 353–365.

Maintz, J. B. A., van den Elsen, P. A. & Viergever, M. A. (1996*c*), Registration of SPECT and MR brain images using a fuzzy surface, *in* M. H. Loew & K. M. Hanson, eds, 'Medical Imaging: Image processing', Vol. 2710, SPIE, Bellingham, WA, pp. 821–829.

Malison, R. T., Miller, E. G., Greene, R., McCarthy, G., Charney, D. S. & Innis, R. B. (1993), 'Computer-assisted coregistration of multislice SPECT and MR brain images by fixed external fiducials', *Journal of computer assisted tomography* **17**(6), 952–960.

Mangin, J., Tupin, V. F., Bloch, I., Rougetet, R., Régis, J. & López-krahe, J. (1995), Deformable topological models for segmentation of 3D medical images, *in* Y. Bizais, C. Barillot & R. di Paola, eds, 'Information processing in medical imaging', Kluwer, pp. 153–164.

Matas, J., Marik, R. & Kittler, J. (1995), On representing and matching of multi-coloured objects, *in* 'International conference on computer vision', IEEE computer society press, Los Alamitos, CA, pp. 726–732.

Maurer, C. R., Aboutanos, G. B., Dawant, B. M., Gadamsetty, S., Margolin, R. A., Maciunas, R. J. & Fitzpatrick, J. M. (1994), Effect of geometrical distortion correction in MR on image registration accuracy, *in* M. H. Loew, ed., 'Medical imaging: image processing', Vol. 2167, SPIE Press, Bellingham, WA, pp. 200–213.

Maurer, C. R., Aboutanos, G. B., Dawant, B. M., Margolin, R. A., Maciunas, R. J. & Fitzpatrick, J. M. (1995), Registration of CT and MR brain images using a combination of points and surfaces, *in* M. H. Loew, ed., 'Medical imaging: image processing', Vol. 2434, SPIE Press, Bellingham, WA, pp. 109–123.

Maurer, C. R. & Fitzpatrick, J. M. (1993), A review of medical image registration, *in* R. J. Maciunas, ed., 'Interactive image-guided neurosurgery', American Association of neurological surgeons, Park ridge, IL, pp. 17–44.

Maurer, C. R., Fitzpatrick, J. M., Galloway, R. L., Wang, M. Y., Maciunas, R. J. & Allen, G. S. (1995), The accuracy of image-guided neurosurgery using implantable fiducial markers, *in* H. U. Lemke, K. Inamura, C. C. Jaffe & M. W. Vannier, eds, 'Computer assisted radiology', Springer-Verlag, Berlin, pp. 1197–1202.

Maurer, C. R., McCrory, J. J. & Fitzpatrick, J. M. (1993), Estimation of accuracy in localizing externally attached markers in multimodal volume head images, *in* M. H. Loew, ed., 'Medical imaging: image processing', Vol. 1898, SPIE Press, Bellingham, WA, pp. 43–54.

Maxwell, J. C. (1859), 'On hills and dales', *The London, Edinburgh and Dublin Philosophical Magazine and Journal of Science* **40**, 421–425.

McInerney, T. & Terzopoulos, D. (1996), Deformable models in medical image analysis, *in* 'Mathematical methods in biomedical image analysis', IEEE computer society press, Los Alamitos, CA, pp. 171–180.

McParland, B. J. & Kumaradas, J. C. (1995), 'Digital portal image registration by sequential anatomical matchpoint and image correlations for real-time continuous field alignment verfication', *Medical physics* **22**(7), 1063–1075.

Mendonça, A. M., Campilho, A. & Nunes, J. M. R. (1994), A new similarity criterion for retinal image registration, *in* 'International conference on image processing', IEEE computer society press, Los Alamitos, CA, pp. 696–700.

Metaxas, D. & Kakadiaris, I. (1996), Elastically adaptive deformable models, *in* Bernard, Buxton, Roberto & Cipolla, eds, 'Computer vision - ECCV', Vol. 1064 of *Lecture notes in computer science*, Springer-Verlag, Berlin, pp. 550–559.

Meunier, J., Guimond, A., Janicki, C., Imbert, B. & Soucy, J. (1996), Automatic 3D registration of brain SPECT images, *in* H. U. Lemke, M. W. Vannier, K. Inamura & A. G. Farman, eds, 'Computer assisted radiology', Vol. 1124 of *Excerpta medica - international congress series*, Elsevier, Amsterdam, pp. 187–192.

Meyer, C. R., Leichtman, G. S., Brunberg, J. A., Wahl, R. L. & Quint, L. E. (1995), 'Simultaneous usage of homologous points, lines, and planes for optimal, 3-D, linear registration of multimodality imaging data', *IEEE Transactions on medical imaging* **14**(1), 1–11.

Miaux, Y., Guermazi, A., Gossot, D., Bourrier, P., Angoulvant, D., Kahiroune, A., Turki, C. & Bouché, E. (1995), 'Laser guidance system for CT-guided procedures', *Radiology* **194**, 282–284.

Miller, M. I., Christensen, G. E., Amit, Y. A. & Grenander, U. (1993), Mathematical textbook of deformable neuroanatomies, *in* 'National academy of sciences', Vol. 90 of *Medical sciences*, pp. 11944–11948.

Monga, O., Benayoun, S. & Faugeras, O. D. (1992), From partial derivatives of 3D density images to ridge lines, *in* R. A. Robb, ed., 'Visualization in biomedical computing', Vol. 1808 of *Proc. SPIE*, SPIE Press, Bellingham, WA, pp. 118–127.

Morris, E. D., Muswick, G. J., Ellert, E. S., Steagall, R. N., Goyer, P. F. & Semple, W. E. (1993), Computer-aided techniques for aligning interleaved sets of non-identical medical images, *in* M. H. Loew, ed., 'Medical imaging: image processing', Vol. 1898, SPIE Press, Bellingham, WA, pp. 146–157.

Morse, B. S., Pizer, S. M. & Liu, A. (1993), Multiscale medial analysis of medical images, Technical report, dep. of Computer Science, University of NC, Chapel Hill.

Moseley, J. & Munro, P. (1994), 'A semiautomatic method for registration of portal images', *Medical physics* **21**(4), 551–558.

Münch, B. & Rüegsegger (1993), '3-D repositioning and differential images of volumetric CT measurements', *IEEE Transactions on medical imaging* **12**(3), 509–514.

Nakazawa, Y. & Saito, T. (1994), Region extraction with brain atlas for analysis of MRI brain images, *in* 'International conference on image processing', IEEE computer society press, Los Alamitos, CA, pp. 387–391.

Neelin, P., Crossman, J., Hawkes, D. J., Ma, Y. & Evans, A. C. (1993), 'Validation of an MRI/PET landmark registration method using 3D simulated PET images and point simulations', *Computerized medical imaging and graphics* **17**(4/5), 351–356.

Pajdla, T. & van Gool, L. (1995), Matching of 3-D curves using semi-differential invariants, *in* 'International conference on computer vision', IEEE computer society press, Los Alamitos, CA, pp. 390–395.

Pallotta, S., Gilardi, M. C., Bettinardi, V., Rizzo, G., Landoni, C., Striano, G., Masi, R. & Fazio, F. (1995), 'Application of a surface matching image registration technique to the correlation of cardiac studies in positron emission tomography (PET) by transmission images', *Physics in medicine and biology* **40**, 1695–1708.

Pavía, J., Ros, D., Catafau, A. M., Lomeña, Huguet, M. & Setoain, J. (1994), 'Three-dimensional realignment of activation brain single-photon emission tomographic studies', *European journal of nuclear medicine* **21**(12), 1298–1302.

Pelizzari, C. A., Chen, G. T. Y., Spelbring, D. R., Weichselbaum, R. R. & Chen, C. T. (1989), 'Accurate three-dimensional registration of CT, PET, and/or MR images of the brain', *Computer assisted tomography* **13**(1), 20–26.

Pellot, C., Bloch, I., Sureda, F., Herment, A., Sigelle, M., Horain, P. & Long, A. (1995), Probabilistic fusion of angiographic and echographic images for the 3D reconstruction of vessels, *in* M. H. Loew, ed., 'Medical imaging: image processing', Vol. 2434, SPIE Press, Bellingham, WA, pp. 164–172.

Pennec, X. & Thirion, J. (1995), Validation of 3-D registration methods based on points and frames, *in* 'International conference on computer vision', IEEE computer society press, Los Alamitos, CA, pp. 557–562.

Perault, C., Wampach, H. & Liehn, J. (1995), Three dimensional SPECT myocardial rest-stress subtraction images after automated registration and normalization, *in* Y. Bizais, C. Barillot & R. di Paola, eds, 'Information processing in medical imaging', Kluwer, pp. 391–392.

Péria, O., Chevalier, L., François-Joubert, A., Caravel, J., Dalsoglio, S., Lavallée, S. & Cinquin, P. (1995), Using a 3D position sensor for registration of SPECT and US images of the kidney, *in* N. Ayache, ed., 'Computer vision, virtual reality, and robotics in medicine', Vol. 905 of *Lecture notes in computer science*, Springer-Verlag, Berlin, pp. 23–29.

Péria, O., François-Joubert, A., Lavallée, S., Champleboux, G., Cinquin, P. & Grand, S. (1994), Accurate registration of SPECT and MR brain images of patients suffering from epilepsy or tumor, *in* 'Medical robotics and computer assisted surgery', pp. 58–62.

Peters, T., Davey, B., Munger, P., Comeau, R., Evans, A. & Olivier, A. (1996), 'Three-dimensional multimodal image-guidance for neurosurgery', *IEEE Transactions on medical imaging* **15**(2), 121–128.

Petti, P. L., Kessler, M. L., Fleming, T. & Pitluck, S. (1994), 'An automated image-registration technique based on multiple structure matching', *Medical physics* **21**(9), 1419–1426.

Philips, P. J. (1994), Point set pattern matching using the procrustean metric, *in* F. L. Bookstein, J. S. Duncan, N. Lange & D. C. Wilson, eds, 'Mathematical methods in medical imaging', Vol. 2299, SPIE Press, Bellingham, WA, pp. 180–191.

Pietrzyk, U., Herholz, K., Fink, G., Jacobs, A., Mielke, R., Slansky, I., Würker, M. & Heis, W. (1994), 'An interactive technique for three-dimensional image registration: validation for PET, SPECT, MRI and CT brain studies', *Journal of nuclear medicine* **35**, 2011–2018.

Pietrzyk, U., Herholz, K., Schuster, A., von Stockhausen, H., Lucht, H. & Heiss, W. (1996), 'Clinical applications of registration and fusion of multimodality brain images from PET, SPECT, CT, and MRI', *European journal of radiology* **21**, 174–182.

Pizer, S. M., Burbeck, C. A., Coggins, J. M., Fritsch, D. S. & Morse, B. S. (1992), *Shape in Picture*, NATO-ASI series, Springer-Verlag, chapter Object Shape before Boundary Shape: Scale-space Medial Axes.

Pokrandt, P. (1996), Fast non-supervised matching: a probabilistic approach, *in* H. U. Lemke, M. W. Vannier, K. Inamura & A. G. Farman, eds, 'Computer assisted radiology', Vol. 1124 of *Excerpta medica - international congress series*, Elsevier, Amsterdam, pp. 306–310.

Potamianos, P., Davies, B. L. & Hibberd, R. D. (1995), Intra-operative registration for percutaneous surgery, *in* 'Medical robotics and computer assisted surgery', Wiley, pp. 156–164.

Press, W. H., Teukolsky, S. A., Vetterling, W. T. & Flannery, B. P. (1992), *Numerical recipes in C*, second edn, Cambridge university press.

Qian, J., Mitsa, T. & Hoffman, E. A. (1996), Contour/surface registration using a physically deformable model, *in* 'Mathematical methods in biomedical image analysis', IEEE computer society press, Los Alamitos, CA, pp. 114–122.

Radcliffe, T., Rajapakshe, R. & Shalev, S. (1993), Pseudocorrelation: a fast, robust, absolute, grey level image alignment algorithm, *in* M. H. Loew, ed., 'Medical imaging: image processing', Vol. 1898, SPIE Press, Bellingham, WA, pp. 134–145.

Radcliffe, T., Rajapakshe, R. & Shalev, S. (1994), 'Pseudocorrelation: a fast, robust, absolute, grey-level image alignment algorithm', *Medical physics* **21**(6), 761–769.

Ravichandran, G. & Casasent, D. (1994), 'Advanced in-plane rotation-invariant correlation filters', *IEEE Transactions on pattern analysis and machine intelligence* **16**(4), 415–420.

Rizzo, G., Gilardi, M. C., Prinster, A., Grassi, F., Scotti, G., Cerutti, S. & Fazio, F. (1995), 'An elastic computerized brain atlas for the analysis of clinical PET/SPET data', *European journal of nuclear medicine* **22**(11), 1313–1318.

Rubinstein, R., Karger, H., Pietrzyk, U., Siegal, T., Gomori, J. M. & Chisin, R. (1996), 'Use of ^{201}thallium brain SPECT, image registration, and semi-quantitative analysis in the follow-up of brain tumors', *European journal of radiology* **21**, 188–195.

Ruff, C. F., Hill, D. L. G., Robinson, G. P. & Hawkes, D. J. (1993), Volume Rendering of Multimodal Images for the Planning of Skull Base Surgery, *in* H. U. Lemke, ed., 'Computer Assisted Radiology '93', Springer-Verlag, pp. 574 – 579.

Rusinek, H., Tsui, W., Levy, A. V., Noz, M. E. & de Leon, M. J. (1993), 'Principal axes and surface fitting methods for three-dimensional image registration', *Journal of nuclear medicine* **34**, 2019–2024.

Ryan, M. J., Erickson, R. K., Levin, D. N., Pelizzari, C. A., MacDonald, R. L. & Dohrmann, G. J. (1995), Frameless stereotaxy with real-time tracking of patient head movement and retrospective patient-image registration, *in* 'Medical robotics and computer assisted surgery', Wiley, pp. 1–5.

Sandor, S. & Leahy, R. (1994), Matching deformable atlas models to preprocessed magnetic resonance brain images, *in* 'International conference on image processing', IEEE computer society press, Los Alamitos, CA, pp. 686–690.

Sandor, S. R. & Leahy, R. M. (1995), Towards automated labelling of the cerebral cortex using a deformable atlas, *in* Y. Bizais, C. Barillot & R. di Paola, eds, 'Information processing in medical imaging', Kluwer, pp. 127–138.

Savi, A., Gilardi, M. C., Rizzo, G., Pepi, M., Landoni, C., Rossetti, C., Lucignani, G., Bartorelli, A. & Fazio, F. (1995), 'Spatial registration of echocardiographic and positron emission tomographic heart studies', *European journal of nuclear medicine* **22**(3), 243–247.

Schad, L. R., Boesecke, R., Schlegel, W., Hartmann, G. H., Sturm, G. H., Strauss, L. G. & Lorenz, W. (1987), 'Three dimensional image correlation of CT, MR, and PET studies in radiotherapy treatment of brain tumors', *Computer assisted tomography* **11**, 948–954.

Scott, A. M., Macapinlac, H., Divgi, C. R., Zhang, J. J., Kalaigian, H., Pentlow, K., Hilton, S., Graham, M. C., Sgouros, G., Pelizzari, C., Chen, G., Schlom, J., Goldsmith, S. J. & Larson, S. M. (1994), 'Clinical validation of SPECT and CT/MRI image registration in radiolabeled monoclonal antibody studies of colorectal carcinoma', *Journal of nuclear medicine* **35**, 1976–1984.

Scott, A. M., Macapinlac, H., Zhang, J., Daghighian, F., Montemayor, N., Kalaigian, H., Sgouros, G., Graham, M. C., Kolbert, K., Yeh, S. D. J., Lai, E., Goldsmith, S. J. & Larson, S. M. (1995), 'Image registration of SPECT and CT images using an external fiduciary band and three-dimensional surface fitting in metastatic thyroid cancer', *Journal of nuclear medicine* **36**, 100–103.

Serra, B. & Berthod, M. (1994), Subpixel contour matching using continuous dynamic programming, *in* 'Computer vision and pattern recognition', IEEE Computer Society press, Los Alamitos, CA, pp. 202–207.

Serra, B. & Berthod, M. (1995), Optimal subpixel matching of contour chains and segments, *in* 'International conference on computer vision', IEEE computer society press, Los Alamitos, CA, pp. 402–407.

Serra, J. (1982), *Image analysis and mathematical morphology*, Academic press.

Serra, J. (1988), *Image analysis and mathematical morphology, volume 2: theoretical advances*, Academic press.

Shekarforoush, H., Berthod, M. & Zerubia, J. (1996), Subpixel image registration by estimating the polyphase decomposition of cross power spectrum, *in* 'Computer vision and pattern recognition', IEEE computer society press, Los Alamitos, CA, pp. 532–537.

Shields, K., Barber, D. C. & Sheriff, S. B. (1993), Image registration for the investigation of atherosclerotic plaque movement, *in* H. H. Barrett & A. F. Gmitro, eds, 'Information processing in medical imaging', Vol. 687 of *Lecture notes in computer science*, Springer-Verlag, Berlin, pp. 438–458.

Simon, D. A., Hebert, M. & Kanade, T. (1994), Techniques for fast and accurate intra-surgical registration, *in* A. M. DiGioia III, T. Kanade & R. Taylor, eds, 'Medical robotics and computer assisted surgery', pp. 90–97.

Simon, D. A., Hebert, M. & Kanade, T. (1995), 'Techniques for fast and accurate intra-surgical registration', *Journal of image guided surgery* **1**(1).

Simon, D. A., O'Toole, R. V., Blackwell, M., Morgan, F., DiGioia, A. M. & Kanade, T. (1995), Accuracy validation in image-guided orthopaedic surgery, *in* 'Medical robotics and computer assisted surgery', Wiley, pp. 185–192.

Slomka, P. J., Hurwitz, G. A., Stephenson, J. & Cradduck, T. (1995), 'Automated alignment and sizing of myocardial stress and rest scans to three-dimensional normal templates using an image registration algorithm', *Journal of nuclear medicine* **36**, 1115–1122.

Soltys, M., Beard, D. V., Carrasco, V., Mukherji, S. & Rosenman, J. (1995), FUSION: a tool for registration and visualization of multiple modality 3D medical data, *in* M. H. Loew, ed., 'Medical imaging: image processing', Vol. 2434, SPIE Press, Bellingham, WA, pp. 74–80.

Spivak, S. M. (1970), *A Comprehensive Introduction to Differential Geometry*, Publish or Perish Inc., Berkeley.

Staib, L. H. & Xianzhang, L. (1994), Intermodality 3D medical image registration with global search, *in* 'IEEE workshop on biomedical image analysis', IEEE computer society press, Los Alamitos, CA, pp. 225–234.

Stapleton, S. J., Caldwell, C. B., Ehrlich, L. E., Leonhardt, C. L., Black, S. E. & Yaffe, M. J. (1995), 'Effects on non-linear flow and spatial orientation on technetium-99m hexamethylpropylene amin oxime single-photon emission tomography', *European journal of nuclear medicine* **22**(9), 1009–1016.

Strother, S. C., Anderson, J. R., Xu, X., Liow, J., Bonar, D. C. & Rottenberg, D. A. (1994), 'Quantitative comparisons of image registration techniques based on high-resolution MRI of the brain', *Journal of computer assisted tomography* **18**(6), 954–962.

Studholme, C., Hill, D. L. G. & Hawkes, D. J. (1995*a*), Automated 3D MR and PET brain image registration, *in* Lemke, Imamura, Jaffe & Vannier, eds, 'Computer assisted radiology', pp. 248–253.

Studholme, C., Hill, D. L. G. & Hawkes, D. J. (1995*b*), Multi resolution voxel similarity measures for MR-PET registration, *in* Y. Bizais & C. Barillot, eds, 'Information Processing in Medical Imaging', Kluwer Academic Publishers, Dordrecht, pp. 287–298.

Studholme, C., Hill, D. L. G. & Hawkes, D. J. (1996), incorporating connected region labelling into automated image registration using mutual information, *in* 'Mathematical methods in biomedical image analysis', IEEE computer society press, Los Alamitos, CA, pp. 23–31.

Sull, S. & Ahuja, N. (1995), 'Integrated matching and segmentation of multiple features in two views', *Computer vision and image understanding* **62**(3), 279–297.

Szelinsky, R. & Lavallée, S. (1994), Matching 3-D anatomical surfaces with non-rigid volumetric deformations, *in* 'Applications of computer vision in medical image processing', AAAI spring symposium series, pp. 22–25.

Szeliski, R. & Lavallée, S. (1994), Matching 3-D anatomical surfaces with non-rigid deformations using octree-splines, *in* 'proceedings of the IEEE workshop on biomedical image analysis', IEEE computer society press, Los alamitos, CA, pp. 144–153.

Szeliski, R. & Lavallée, S. (1996), 'Matching 3-D anatomical surfaces with non-rigid deformations using octree-splines', *International journal of computer vision* **18**(2), 171–186.

Taneja, U., Holton, K. S., Camp, J. C. & Robb, R. A. (1994), Evaluating the accuracy of three-dimensional image registration algorithms used in multimodal image fusion, *in* 'Visualization in biomedical computing', Vol. 2359, SPIE press, Bellingham, WA, pp. 238–250.

Taubin, G. (1993), An improved algorithm for algebraic curve and surface fitting, *in* 'International conference on computer vision', IEEE computer society press, Los Alamitos, CA, pp. 658–665.

ter Haar Romeny, B. M., Florack, L. M. J., Koenderink, J. J. & Viergever, M. A. (1991), Scale-space: its natural operators and differential invariants, *in* A. Colchester & D. Hawkes, eds, 'Information Processing in Medical Imaging, Proceedings of the 12^{th} International Conference', Springer-Verlag, Berlin.

Thirion, J. (1994), Extremal points: definition and application to 3D image registration, *in* 'Computer vision and pattern recognition', IEEE Computer Society press, Los Alamitos, CA, pp. 587–592.

Thirion, J. (1995), Fast intensity-based non-rigid matching, *in* 'Medical robotics and computer assisted surgery', Wiley, pp. 47–54.

Thirion, J. (1996*a*), 'New feature points based on geometric invariants for 3D image registration', *International journal of computer vision* **18**(2), 121–137.

Thirion, J. (1996*b*), Non-rigid matching using demons, *in* 'Computer vision and pattern recognition', IEEE computer society press, Los Alamitos, CA, pp. 245–251.

Tom, B. C. S., Efstratiadis, S. N. & Katsaggelos, A. K. (1994), 'Motion estimation of skeletonized angiographic images using elastic registration', *IEEE Transactions on medical imaging* **13**(3), 450–460.

Troccaz, J., Laieb, N., Vassal, P., Menguy, Y., Cinquin, P., Bolla, M. & Giraud, J. Y. (1995), 'Patient setup optimization for external conformal radiotherapy', *Journal of image guided surgery* **1**, 113–120.

Tsui, W., Rusinek, H., van Gelder, P. & Lebedev, S. (1993), Fast surface-fitting algorithm for 3-D image registration, *in* M. H. Loew, ed., 'Medical imaging: image processing', Vol. 1898, SPIE Press, Bellingham, WA, pp. 14–23.

Turkington, T. G., Hoffman, J. M., Jaszczak, R. J., MacFall, J. R., Harris, C. C., Kilts, C. D., Pelizzari, C. A. & Coleman, R. E. (1995), 'Accuracy of surface fit registration for PET and MR brain images using full and incomplete brain surfaces', *Journal of computer assisted tomography* **19**(1), 117–124.

Turkington, T. G., Jaszczak, R. J., Pelizzari, C. A., Harris, C., MacFall, J. R., M., H. J. & Coleman, R. E. (1993), 'Accuracy of registration of PET, SPECT and MR images of a brain phantom', *Journal of nuclear medicine* **34**, 1587–1594.

Uenohara, M. & Kanade, T. (1995), Vision-based object registration for real-time image overlay, *in* N. Ayache, ed., 'Computer vision, virtual reality, and robotics in medicine', Vol. 905 of *Lecture notes in computer science*, Springer-Verlag, Berlin, pp. 13–22.

Unser, M., Thévenaz, P., Lee, C. & Ruttimann, U. E. (1995), 'Registration and statistical analysis of PET images using the wavelet transform', *IEEE Engineering in medicine and biology* **14**(5), 603–611.

van den Elsen, P. A., Maintz, J. B. A., Pol, E. & Viergever, M. A. (1995), 'Automatic registration of CT and MR brain images using correlation of geometrical features', *IEEE Transactions on medical images* **14**(2), 384–398.

van den Elsen, P. A. (1993), Multimodality matching of brain images, PhD thesis, Utrecht University, The Netherlands.

van den Elsen, P. A. (1994), Retrospective fusion of CT and MR brain images using mathematical operators, *in* 'AAAI symposium on medical applications of computer vision', pp. 30–33.

van den Elsen, P. A., Maintz, J. B. A., Pol, E. J. D. & Viergever, M. A. (1992), Image fusion using geometrical features, *in* R. A. Robb, ed., 'Visualization in Biomedical Computing', Vol. 1808 of *Proc. SPIE*, SPIE Press, Bellingham, WA, pp. 172–186.

van den Elsen, P. A., Maintz, J. B. A. & Viergever, M. A. (1992), 'Geometry driven multimodality matching of brain images', *Brain topography* **5**, 153–158.

van den Elsen, P. A., Maintz, J. B. A. & Viergever, M. A. (1993), Automated CT and MR brain image matching using correlation of geometrical "ridgeness" features, Technical Report 3DCV 93-07, Utrecht University. submitted for publication.

van den Elsen, P. A., Pol, E. J. D., Sumanaweera, T. S., Hemler, P., Napel, S. & Adler, J. (1994), Grey value correlation techniques used for automatic matching of CT and MR brain and spine images, *in* 'Visualization in Biomedical Computing', Vol. 2359 of *Proc. SPIE*, SPIE Press, Bellingham, WA, pp. 227–237.

van den Elsen, P. A., Pol, E. J. D. & Viergever, M. A. (1993), 'Medical image matching– a review with classification', *IEEE Engineering in medicine and biology* **12**(1), 26–39.

van den Elsen, P. A. & Viergever, M. A. (1991), Marker guided registration of electromagnetic dipole data with tomographic images, *in* A. C. F. Colchester & D. J. Hawkes, eds, 'Information processing in medical imaging', Springer-Verlag, Berlin, pp. 240–246.

van den Elsen, P. A. & Viergever, M. A. (1993), Automated CT and MR brain image registration using geometrical feature correlation, *in* 'Nuclear science symposium and medical imaging conference', IEEE, pp. 1827–1830.

van den Elsen, P. A. & Viergever, M. A. (1994), 'Marker guided multimodality matching of the brain', *European radiology* **4**, 45–51.

van den Elsen, P. A., Viergever, M. A., van Huffelen, A. C., van der Meij, W. & Wieneke, G. H. (1991), 'Accurate matching of electromagnetic dipole data with CT and MR images', *Brain topography* **3**(4), 425–432.

van Herk, M. & Kooy, H. M. (1994), 'Automatic three-dimensional correlation of CT-CT, CT-MRI, and CT-SPECT using chamfer matching', *Medical physics* **21**(7), 1163–1177.

Vandermeulen, D. (1991), Methods for registration, interpolation and interpretation of three-dimensional medical image data for use in 3-D display, 3-D modelling and therapy planning, PhD thesis, University of Leuven, Belgium.

Vandermeulen, D., Collignon, A., Michiels, J., Bosmans, H., Suetens, P., Marchal, G., Timmens, G., van den Elsen, P., Viergever, M., Ehricke, H., Hentschel, D. & Graumann, R. (1995), Multi-modality image registration within COVIRA, *in* L. Beolchi & M. H. Kuhn, eds, 'Medical imaging: analysis of multimodality 2D/3D images', Vol. 19 of *Studies in health, technology and informatics*, IOS Press, Amsterdam, pp. 29–42.

Vassal, P., Troccaz, J., Laieb, N., Cinquin, P., Bolla, M. & Berland, E. (1995), Introducing computer vision sensors in radiotherapy for accurate dose selivery, *in* 'Medical robotics and computer assisted surgery', Wiley, pp. 16–23.

Venot, A., Golmard, J. L., Lebruchec, J. F., Pronzato, L., Walter, E., Frij, G. & Roucayrol, J. C. (1983), Digital methods for change detection in medical images, *in* F. Deconinck, ed., 'Information processing in medical imaging', Nijhoff publ., Dordrecht, pp. 1–16.

Venot, A., Lebruchec, J. F. & Roucayrol, J. C. (1984), 'A new class of similarity measures for robust image registration', *Computer vision, graphics, and image processing* **28**, 176–184.

Venot, A. & Leclerc, V. (1984), 'Automated correction of patient motion and gray values to subtraction in digitized angiography', *IEEE Transactions on medical imaging* **3**(4), 179–186.

Venot, A., Pronzato, L. & Walter, E. (1994), 'Comments about the coincident bit counting (CBC) criterion for image registration', *IEEE Transactions on medical imaging* **13**(3), 565–566.

Viergever, M. A., Maintz, J. B. A., Stokking, R., van den Elsen, P. A. & Zuiderveld, K. J. (1995), Matching and integrated display of brain images from multiple modalities, *in* 'Medical Imaging', Vol. 2434, SPIE Press, Bellingham, WA, pp. 2–13.

Viergever, M., van den Elsen, P. & Stokking, R. (1992), 'Integrated presentation of multimodal brain images', *Brain topography* **5**, 135–145.

Viola, P. A. (1995), Alignment by maximization of mutual information, PhD thesis, Massachusetts institute of technology, artificial intelligence laboratory. A. I. technical report No. 1548.

Viola, P., Schraudolph, N. N. & Sejnowski, T. J. (1996), 'Empirical entropy manipulation for real-world problems', *Advances in neural information processing systems* **8**. In press.

Viola, P. & Wells III, W. (1995), Alignment by maximization of mutual information, *in* 'International conference on computer vision', IEEE computer society press, Los Alamitos, CA, pp. 16–23.

Wahl, R. L., Quint, L. E., Cieslak, R. D., Aisen, A. M., Koeppe, R. A. & Meyer, C. R. (1993), "'anametabolic" tumor imaging: fusion of FDG PET with CT or MRI to localize foci of increased activity', *Journal of nuclear medicine* **34**, 1190–1197.

Wang, B., Toro, C., Zeffiro, T. A. & Hallett, M. (1994), 'Head surface digitization and registration: a method for mapping positions on the head onto magnetic resonance images', *Brain topography* **6**(3), 185–192.

Wang, G., Volkow, N. D., Levy, A. V., Fowler, J. S., Logan, J., Alexoff, D., Hitzemann, R. J. & Schyler, D. J. (1996), 'MR-PET image coregistration for quantitation of striatal dopamine D_2 receptors', *Journal of computer assisted tomography* **20**(3), 423–428.

Wang, H. & Fallone, B. G. (1994), 'A robust morphological algorithm for automatic radiation field extraction and correlation of portal images', *Medical physics* **21**(2), 237–244.

Wang, J., Reinstein, L. E., Hanley, J. & Meek, A. G. (1996), 'Investigation of a phase-only correlation technique for anatomical alignment of portal images in radiation therapy', *Physics in medicine and biology* **41**, 1045–1058.

Wang, M. Y., Fitzpatrick, J. M. & Maurer, C. R. (1995), Design of fiducials for accurate registration of CT and MR volume images, *in* M. Loew, ed., 'Medical imaging', Vol. 2434, SPIE, pp. 96–108.

Wang, M. Y., Fitzpatrick, J. M., Maurer, C. R. & Maciunas, R. J. (1994), An automatic technique for localizing externally attached markers in MR and CT volume images of the head, *in* M. H. Loew, ed., 'Medical imaging: image processing', Vol. 2167, SPIE Press, Bellingham, WA, pp. 214–224.

Wang, X., Cheng, Y., Collins, R. T. & Hanson, A. R. (1996), Determining correspondences and rigid motion of 3-D point sets with missing data, *in* 'Computer vision and pattern recognition', IEEE computer society press, Los Alamitos, CA, pp. 252–257.

Wasserman, R. & Acharya, R. (1995), Multimodality tumor delineation via fuzzy fusion and deformable modelling, *in* M. H. Loew, ed., 'Medical imaging: image processing', Vol. 2434, SPIE Press, Bellingham, WA, pp. 133–144.

Wasserman, R., Rajapakse, J. C. & Acharya, R. (1994), Multimodality medical imaging for radiotherapy treatment planning, *in* 'IEEE workshop on biomedical image analysis', IEEE computer society press, Los alamitos, CA, pp. 235–244.

Wells III, W. M., Viola, P., Atsumi, H., Nakajima, S. & Kikinis, R. (1996), 'Multi-modal volume registration by maximization of mutual information', *Medical image analysis* **1**. In press.

Wells III, W. M., Viola, P. & Kikinis, R. (1995), Multi-modal volume registration by maximization of mutual information, *in* 'Medical robotics and computer assisted surgery', Wiley, pp. 55–62.

West et al., J. (1996), Comparison and evaluation of retrospective intermodality image registration techniques, *in* M. H. Loew & K. M. Hanson, eds, 'SPIE proc MI', Vol. 2710, pp. 332–347.

Witkin, A. (1983), Scale space filtering, *in* 'Proceedings of the 7th International Confernece on Artificial Intelligence', Karlsruhe, pp. 1019–1021.

Woods, R., Maziotta, J. & Cherry, S. (1993), 'MRI-PET registration with automated algorithm', *journal of computer assisted tomography* **17**(4), 536–546.

Woods, S. W., Hegeman, I. M., Zubal, G., Krystal, J. H., Koster, K., Smith, E. O., Heninger, G. T. & Hoffer, P. B. (1991), 'Visual stimulation increases technetium-99m-HMPAO distribution in human visual cortex', *Journal of nuclear medicine* **32**, 210–215.

Xiao, H. & Jackson, I. T. (1995), Surface matching: application in post-surgical/post-treatment evaluation, *in* H. U. Lemke, K. Inamura, C. C. Jaffe & M. W. Vannier, eds, 'Computer assisted radiology', Springer-Verlag, Berlin, pp. 804–811.

Yeung, M. M., Yeo, B., Liou, S. & Bani-Hashemi, A. (1994), Three-dimensional image registration for spiral CT angiography, *in* 'Computer vision and pattern recognition', IEEE Computer Society press, Los Alamitos, CA, pp. 423–429.

Zhao, W., Young, T. Y. & Ginsberg, M. D. (1993), 'Registration and three-dimensional reconstruction of autoradiographic images by the disparity analysis method', *IEEE Transactions on medical imaging* **12**(4), 782–791.

Zhou, Y. T. (1994), Multi-sensor image fusion, *in* 'International conference on image processing', IEEE computer society press, Los Alamitos, CA, pp. 193–197.

Zubal, G. Tagare, H., Zhang, L. & Duncan, J. (1991), 3-D registration of intermodality medical images, *in* 'proceedings of the annual international conference of the IEEE engineering in medicine and biology society', Vol. 13, pp. 293–294.

Zubal, I. G., Spencer, S. S., Khurseed Imam, J. S., Smith, E. O., Wisniewski, G. & Hoffer, P. B. (1995), 'Difference images calculated from ictal and interictal technetium-99m-HMPAO SPECT scans of epilepsy', *Journal of nuclear medicine* **36**(4), 684–689.

Zuk, T., Atkins, S. & Booth, K. (1994), Approaches to registration using 3D surfaces, *in* M. H. Loew, ed., 'Medical imaging: image processing', Vol. 2167, SPIE Press, Bellingham, WA, pp. 176–187.

Zuo, C. S., Jiang, A., Buff, B. L., Mahon, T. G. & Wong, T. Z. (1996), 'Automatic motion correction for breast MR imaging', *Radiology* **198**(3), 903–906.

Publications

Papers in international journals

J. B. A. Maintz, P. A. van den Elsen, & M. A. Viergever (1996), 'Evaluation of ridge seeking operators for multimodality medical image matching', *IEEE Transactions on pattern analysis and machine intelligence*, **18**(4):353-365.

J. B. A. Maintz, P. A. van den Elsen, & M. A Viergever (1996), 'Comparison of edge-based and ridge-based registration of CT and MR brain images', *Medical image analysis*, **1**(2), in press.

P. A. van den Elsen, J. B. A. Maintz, E.J.D. Pol, & M. A. Viergever (1995), 'Automatic registration of CT and MR brain images using correlation of geometrical features', *IEEE Transactions on medical images*, **14**(2):384-398.

P. A. van den Elsen, J. B. A. Maintz, & M. A. Viergever (1992), 'Geometry driven multimodality matching of brain images', *Brain topography*, **5**:153-158.

M. A. Viergever, J. B. A. Maintz, R. Stokking, P. A. van den Elsen, & K. J. Zuiderveld (1997), 'Integration of functional and anatomical brain images', *Biophysical chemistry*, invited paper, in preparation.

K. J. Zuiderveld, A. H. J. Koning, R. Stokking, J. B. A. Maintz, F. J. R. Appelman, & M. A. Viergever (1996), 'Multimodality visualization of medical volume data', *Computer and graphics*, **20**(6), in press.

Full papers in conference proceedings

J. B. A. Maintz, P. A. van den Elsen, & M. A. Viergever (1993), Extraction of invariant ridgelike features for CT and MR brain image matching, *in* M. A. Viergever, ed., 'International conference on volume image processing (VIP'93)', SCVR, Utrecht, pp. 129-132.

J. B. A. Maintz, P. A. van den Elsen, & M. A. Viergever (1995), Comparison of feature-based matching of CT and MR brain images, *in* N. Ayache, ed., 'CVRMed', vol. 905 of *Lecture notes in computer science*, Springer-verlag, Berlin, pp. 219-228.

J. B. A. Maintz, P. A. van den Elsen, & M. A. Viergever (1996), Registration of SPECT and MR brain images using a fuzzy surface, *in* M. H. Loew and K. M. Hanson, eds., 'Medical imaging '96 - Image processing', vol. 2710, SPIE Press, Bellingham, WA, pp. 821-829.

P. A. van den Elsen, J. B. A. Maintz, E. J. D. Pol, & M. A. Viergever (1992), Image fusion using geometrical features, *in* R. A. Robb, ed., 'Visualization in biomedical computing', vol 1808 of *Proc. SPIE*, SPIE Press, Bellingham, WA, pp. 172-186.

P. A. van den Elsen, J. B. A. Maintz, & M. A. Viergever (1993), Automated CT and MR brain image matching using correlation of geometrical 'ridgeness' features, *in* M.A. Viergever, ed., 'International conference on volume image processing (VIP'93)', SCVR, Utrecht, pp. 31-34.

M.A. Viergever, J.B.A. Maintz, R. Stokking, P.A. van den Elsen, & K.J. Zuiderveld (1995), Matching and integrated display of brain images from multiple modalities, *in* 'Medical imaging', vol. 2434, SPIE Press, Bellingham, WA, pp. 2-13.

Published chapters in books

J. B. A. Maintz, P. A. van den Elsen, & M. A. Viergever (1994), Using geometrical features to match CT and MR brain images, *in* L. Beolchi and M. Kuhn, eds., 'Medical imaging, analysis of multimodality 2D/3D images', vol. 19 of *Studies in Health, Technology and Informatics*, IOS Press, Amsterdam, pp. 43-52.

Published abstracts

J.B.A. Maintz (1995), Registration of medical images, *in* L.J. van Vliet and I.T. Young, eds., 'ASCI Imaging workshop 1995', ASCI, pp. 40-41.

J. B. A. Maintz, F. J. Beekman, W. de Bruin, P. A. van den Elsen, P. P. van Rijk, & M. A. Viergever, (1996), 'Automatic registration and intensity scaling of SPECT brain images', *Journal of nuclear medicine*, **37**(5, supplement):213P.

Submitted for journal publication

J. B. A. Maintz, F. J. Beekman, A. J. van Dongen, P. A. van den Elsen, M. T. J. G. Groenewegen, P. P. van Rijk, & M. A. Viergever, 'Automatic registration and intensity scaling of SPECT brain images'.

J. West, J. M. Fitzpatrick, M. Y. Wang, B. M. Dawant, C. R. Maurer Jr., R. M. Kessler, R. J. Maciunas, C. Barillot, D. Lemoine, A. Collignon, F. Maes, P. Suetens, D. Vandermeulen, P. A. van den Elsen, S. Napel, T. Sumanaweera, B. Harkness, P. F. Hemler, D. L. G. Hill, C. Studholme, J. B. A. Maintz, M. A. Viergever, G. Malandain, X. Pennec, M. E. Noz, G. Q. Maguire Jr., M. Pollack, C. A. Pelizzari, R. A. Robb, & D. Hanson. 'Comparison and evaluation of retrospective intermodality image registration techniques'.

Dankwoord

Het schrijven van een dankwoord is bepaald geen makkelijke opgave. Er zijn zoveel mensen die mij, direct of indirect, hebben geholpen met het tot stand brengen van dit boekje, dat het risico van iemand vergeten te vermelden als een levensgroot zwaard van Damocles boven mijn hoofd hangt[16]. Dat wordt niet makkelijker gemaakt door het feit dat de grootste dank verschuldigd zou moeten zijn aan diegenen die mij de afgelopen maanden weinig hebben gezien; ik heb me aan een groot aantal sociale en andere verplichtingen weten te onttrekken: “Nee, hoofdstuk vijf is nog niet af...” of “Sorry, maar de spaties in de inhoudsopgave zijn nog steeds fout”. Daarom aan *iedereen* die geholpen heeft mijn hartelijke dank!

Jij, Renate, mijn vriendin en beste vriendin, hebt het meeste gemerkt wat het betekent om een proefschrift naar tevredenheid te schrijven. Tot ver in augustus zijn er dagen, weken, geweest waarop we elkaar nauwelijks zagen, of hooguit even telefoneerden. Je hebt er niets van gezegd, en dat zal ik niet gauw vergeten. Ook mijn ouders hebben me de soms wekenlange stiltes uit Utrecht niet verweten. Pa en ma**ma**, jullie hebben me altijd de vrijheid gelaten die ik nodig had om te komen waar ik nu ben.

Petra, begeleidster, co-promotor en confidante, jouw begeleiding was op zijn zachtst gezegd bijzonder, met negen uur tijdsverschil tussen onze bureaus. Je hebt me altijd mijn eigen gang laten gang in ons onderzoek, en ik hoop dat nog vele coproducties zullen volgen. Bedankt, Medoc, voor de Californische bezoekjes, en de *miata* ritjes tussen de Redwoods.

Max, jij bent één van de mensen voor wie ik veel respect heb, en dat wil in mijn geval veel zeggen. Bedankt voor je begeleiding en je vriendschap (en het mij

[16] Zoals de tabel aan het eind van deze sectie, jaartal 1916, aangeeft kunnen omissies desastreus zijn.

meeslepen naar de Sushi bar in Newport Beach). Je vermogen om de hele groep te leiden terwijl je er tegelijkertijd in slaagt de afstand tussen baas en werknemer weg te nemen is bijna eng. Dat verklaart wel waarom we elke keer weer bereid waren om papers, dia's en subsidieaanvragen met slaapderving en veel koffie zo'n 45 seconden voor de extended deadline af te krijgen. Laten we duidelijk zijn dat dit niet zo'n akelig slijmstukje is. Zo staat me nog helder voor de geest dat je plotseling verdwenen was op de conferentie in Nice, en -nadat ik een doodsaaie middag had doorstaan- weer opdook en met een grijns rapporteerde dat je *een postzegel* had gekocht. Nou ja. Gelukkig hebben we dat 's avonds rechtgezet; ik geloof niet dat die speciale fles ooit Nederland heeft gehaald[17].

Romhild "ik bent bij dûh entee" Hoogeveen, als vriend, mede-winbin en medemister Unsupported, maar vooral als kamergenoot heb je het zwaar gehad met iemand tegenover je die constant met zijn CD's meefluit. En nog vals ook. Bedankt voor alle praatjes en gezelschap, soms tot diep in de nacht. Koen "Kampungspülle" Vincken, de man die mij alle kneepjes van het "praatjesmaker annex regelneef"-vak heeft geleerd, óók bedankt voor het niet willen delen van het bed in Nice, en het navigeren op de zonnestand om Brussel aan de goede kant uit te rijden. Bart "scale space" ter Haar Romeny: mijn dank voor je altijd grote en aanstekelijke enthousiasme, onze trip naar Cambridge en een prima (©) erwtensoepje. Karel "frequent redesign" Zuiderveld, je C++ en LaTeX 2_ε hulp waren onmisbaar, maar ik sluit geen weddenschappen meer met je af. Margo "pc-tobberd" Agterberg: bedankt voor het af en toe gooien van een woordenboek naar Ger (of mikte je op Koen?), voor je snoeppot en het aanhoren van mijn prekoffie gebrabbel. Bart "kan het per mail?" Muyzer: het is geen eenvoudige taak om iedere dag weer het systeem overeind te houden onder een waar gebruikersbeleg, honderd kleine dingetjes te doen, en genoeg fruit voor een half weeshuis te eten[18], maar het lukt toch altijd weer. Klasse!

Alfons Salden, je hebt de zeldzame gave mij binnen dertig seconden volledig in de war te brengen. Dat is een compliment, denk ik. Carolien Bouma ("this is the animal, and this is Kerrolein Boema"), als enige groepslid dat af en toe haar witte jas vies maakt, vinden we je een beetje eng. Maar je heldere kijk is af en toe verkwikkend, en je koffie niet te weerstaan. Chris Kamphuis, ik ben je nog steeds dankbaar voor het op het juiste moment nicen van de ISRA-s. En nou niet meer zoveel tegelijk opstarten... Estia en Evert-Jan ("eitjes"), bij het volgende proefschrift kom ik wel verven. Dan wil ik wel dat Evert-Jan erbij is, want hij kan *wel* pleisters plakken. Erik Meijering en Theo van Walsum, jullie ken ik eigenlijk nog niet, maar jullie moeten in ieder geval meer koffie zetten.

[17] Maar dat is meer Koen's schuld.

[18] Als je bij hem binnenkomt heeft hij óf een banaan, óf de telefoon in zijn hand. Ik wacht op de dag dat hij per ongeluk een hap uit de hoorn neemt.

Fred Appelman, bedankt voor al de programmeerhulp en weetjes de afgelopen jaren. Je krijgt nog steeds een ijsje van me. Freek Beekman, eigenwijze donder, bedankt voor je hulp bij het SPECT registratieonderzoek. (Heeft U door dat ik op alfabet werk? Ik probeer onpartijdig te zijn.) Joachim Weickert en Stiliyan Kalitzin, jullie hebben in een fenomenaal tempo Nederlands geleerd. Het is een genoegen om met zulke slimme mensen in één groep te zitten. (Now give me your software.) Manon "kluitje" Kluytmans, ondanks het spoor van destructie dat je achterlaat –een dozijn onderzoekers, aan de gammafitness ten onder gegaan– was je een zeer aangename kamergenoot. Ik heb nog geprobeerd om niet al te geschokt te reageren op je neusbel ("∗slik∗ ja leuk"), maar het is niet helemaal gelukt. Maurits "zes truien en een kilo aardappels, graag" Konings, bedankt voor je muzikaliteit en je scherpe blik op zaken. Onno Wink, je C tips waren nuttig, en je koffiemonitoring wordt al beter... Rik Stokking, jij en Ger waren vaak de enigen die er ook dwaze werktijden op na hielden, en dat maakte de maaltijden en het werk 's avonds een stuk minder eenzaam. Ger Timmens, je vele scripts, programmaatjes en hulp de afgelopen jaren waren van groot nut. Robert "Am∗dam" Maas, je naam lijkt fonetisch niet eens op hoe jij hem uitspreekt. Nu ik je een beetje begrijp en je van ons de telefoon mag aannemen, blijk je een heel aardige jongen te zijn. Kom maar gauw terug uit Denemarken. Sandra "culinair" Boeijink, het is jammer dat we (met Manon), geen kamer meer delen (sorry Rommel, prioriteiten en zo), het was altijd erg informatief... Als ze je nog eens secretaresse noemen, doe ik er wat aan. Wiro "hoe bedoelt hij, dorpsgek?" Niessen, ik ken weinig mensen met een groter gevoel voor humor. Bedankt voor alle hulp en voor *GAAF*. Tenslotte wil ik "mijn" studenten bedanken voor het uitstaan van hun knorrige en drukke begeleider: Josien Pluim en Martin Groenewegen, dat jullie het nog ver mogen schoppen.

En dan zijn er nog zoveel meer mensen die ik wil bedanken, maar die ik noodgedwongen op een alfabetische hoop moet gaan gooien. De mensen die onze groep inmiddels hebben verlaten: Luc Florack, Kees de Graaf, Sipko Hensen, André Koster, Richard Kraan, Anton "carapacious fountains" Koning en Ronald van Loon. Iedereen van het AZU die mij geholpen heeft: Cees Haring, Chris Bakker, Dries van Engelen, dhr Duiveman, Emiel Polman, Eric Tetteroo, Frans Zonneveld, Hilleke Hulshoff Pol, Hugo Schnack, Jan Lagendijk, Jan de Groot, Linda Meiners, Marcel Metselaar, Martje van Leuven, René Debets, Shira de Bie, Tineke Kievit (de ideale secretaresse!), Willeke Rauw, prof. Jan Buitelaar, prof. Mali, prof. van Huffelen, en prof. van Veelen. En natuurlijk iedereen van Nucleaire Geneeskunde, de afdeling die toch een beetje als de mijne voelt, met name Alice van Dongen, Anne Hoekstra, Els Jurg, Hans van Isselt, Peter Anema, Peter van Rijk en Ron Jonk.

Een aantal mensen van buiten de Universiteit of het AZU verdient het speciaal

vermeld te worden: Ik wil Evert-Jan Pol bedanken voor zijn wiskundige hulp bij de definitie van de ridge operatoren. *Je veux remercier dr B. Sadzot et Christian Degueuldre pour leur aide avec l'acquisition des images tomoscintigraphique. I would like to thank Sandy Napel for allowing my stay at Stanford University, and Thilaka Sumanaweera and Paul Hemler for their aid while I was there. I am grateful to Steve Pizer for the discussions while he was at our group, for arranging my stay at UNC, and for the (too few) clarinet duets we played. Special thanks go to Dave and Shelly Eberly. Guys, you really made my trip to North Carolina a joy!*

Tenslotte wil ik mijn afstudeerhoogleraar, prof. Hermans, bedanken, en de overige leden van de promotiecommissie voor het lezen van dit proefschrift.

A Brief History of Scholarly Publishing (extract)

50.000 BC Stone age publisher demands that all manuscripts be double-spaced, and hacked on one side of stone only.

1483 Invention of *ibid*.

1507 First use of circumlocution.

1859 "without whom" is used for the first time in list of acknowledgments.

1916 First succesful divorce case based on failure of author to thank his wife, in the foreword of his book, for typing the manuscript.

1928 Early use of ambiguous rejection letter, beginning, "while we have many good things to say about your manuscript, we feel that we are not now in position..."

1962 Copy editors' anthem "Revise or Delete" is first sung at national convention. Quarrel over hyphenation in second stanza delays officical acceptance.

D.D. Jackson (1986), The journal of irreproducible results.

About the author

Twan Maintz was born in Doetinchem, the Netherlands, on June 18, 1969. Shortly after, he moved to Dordrecht, where he lived until he was 22 years old. He and his girlfriend, two cats, and lots of fish now live in Utrecht. They cooperate in perfect unison to generally make a mess of things.

The author received his *Atheneum* diploma in 1987 from the *Titus Brandsmacollege* in Dordrecht. In the same year, he started his study of mathematics at the *Technische Universiteit Delft*. After three years, he decided to change things a bit, and dropped his regular courses for a while. He took a course on high school teaching of mathematics, spent a few months in Budapest designing a mathematical model and software for measuring the solidity of car roofs at the local college for engineering, and a few months writing a paper on the philosophies of scientific realism. After exactly one year, he picked up his regular study of mathematics. Shortly after, he joined the *Computer Vision Research Group* (3DCV) at the University Hospital Utrecht/Utrecht University for his final project, which was on (indeed) medical image registration. Thirteen months after, he received his *Master of Science* ("ingenieur") degree. He stayed at the 3DCV group continuing the registration project as a PhD student ("AIO"), and generally enjoyed himself. Occasionally, he wrote a paper or went to a conference. During his research, he spent a brief period at the *Stanford University School of Medicine*, and a few months at the Computer Science Department of the *University of North Carolina at Chapel Hill*, where he tried to improve his physical condition by cycling up aforementioned hill each day. At 27, he will continue his research of medical image registration as a post-doctoral fellow at the *Imaging Center Utrecht*, focusing on registration associated with neurosurgery of epileptic patients.

In his spare time, the author is a fervent clarinet player and classical music lover. He has written numerous arrangements and orchestrations for chamber orchestra, wind band, vocal accompaniments, and symphony orchestra; and

conducted his own chamber orchestra. A great admirer of the orchestrations of the romantic age, he would like to study further the art of orchestration. Together with his girlfriend, he would like to learn to play the French horn, a wish long forestalled. If only the day had more hours...

Figure A.1 Excerpt from an early publication.

Die liebe Erde allüberall
Blüht auf im Lenz und grünt aufs neu!
Allüberall und ewig
blauen licht die Fernen!
Ewig... ewig...

Gustav Mahler, *Das Lied von der Erde*,
after Mong-Kao-Yen en Wang-Wei.